

Role of c-Met in Abnormal Bone Homeostasis Leading to Fracture Non-union

by

Guoju Hong

A thesis submitted in partial fulfillment of the requirements for the degree of

Doctor of Philosophy

Department of Surgery

University of Alberta

© Guoju Hong, 2022

## Abstract

Fracture healing involves a fragile continuum from inflammation to repair and finally ends in bone reestablishment. Fractures that fail to heal progress to a state of nonunion, causing substantial morbidity for the individual. Nonunion is one of the most serious complications of fracture. In an updated investigation, the incidence of nonunion in fractures was found to be 1.9%; however, the value can be as high as 9% in specific fracture types, such as tibial and clavicular fractures. Nonunion results in major living and economic burdens on patients and seriously affects their mobility. Currently, no effective medical treatments are available to promote fracture repair, and the mainstay of fracture nonunion management is surgery. Infection, ageing, and poor blood supply have been implicated in nonunion. However, the exact mechanism of fracture nonunion is unknown.

In recent studies, it has been shown that HGF/c-Met are closely related to the differentiation of osteoblasts and osteoclasts, which are the prominent cells responsible for callus formation and bone remodelling during fracture repair. Furthermore, hypoxia caused by poor vascularization in fracture healing interrupted osteogenesis *in vivo* and impaired osteoblast and osteoclast differentiation *in vitro*. There is also evidence that hypoxia regulates c-Met in many cell types. We hypothesized that hypoxia modulates osteoblast and osteoclast differentiation via c-Met and ultimately causes fracture nonunion.

To validate our hypothesis, we performed three types of experiments. First, human bone samples obtained from participants with fracture union and nonunion were collected to determine the expression of c-MET. The results show that c-MET expression is downregulated in fracture nonunion tissues such as callus and the greater trochanter. In serum and bone samples

of patients with fracture nonunion, key osteoblastic and osteoclastic markers were also suppressed.

To further explore the mechanism of c-Met in the regulation of osteoblasts and osteoclasts, we generated *c-Met*<sup>fl/fl</sup> mice possessing loxP sites flanking exon 16 of the *c-Met* sequence. Removing exon 16 results in the loss of the c-Met catalytic domain and the mice are thus knockout mice. We then crossed the *c-Met*<sup>fl/fl</sup> mice with *Prx1*<sup>cre</sup> mice (to target expression in osteoblast progenitors) or *Ctsk*<sup>cre</sup> mice (to target expression in osteoclast precursors) and investigated differences in fracture healing following a proximal femur osteotomy. Our findings suggest that conditional knockout of c-Met in both cell lines does not cause abnormal bone development. However, we observed impaired osteoblast and osteoclast differentiation after birth, subsequently leading to osteopenia (*Prx1*<sup>cre</sup> *c-Met*<sup>fl/fl</sup>) and increased bone formation (*Ctsk*<sup>cre</sup> *c-Met*<sup>fl/fl</sup>). Knockout of c-Met also delayed the process of fracture healing in the gene-edited mice following fracture surgery.

Finally, cell models were established to explore if c-Met regulates osteogenesis under hypoxic conditions or following treatment with cabozantinib (a c-Met kinase activity inhibitor). Our findings show that hypoxia increases c-Met phosphorylation during the differentiation of MC3T3 (osteoblast progenitors) and RAW264.7 (osteoclast precursors) cells. However, the differentiation of neither cell type was affected after treatment with cabozantinib. Thus we conclude that enhanced phosphorylation of c-Met in hypoxia is not related to the inhibition of osteoblast and osteoclast differentiation.

To summarize, our findings indicate that c-Met is a molecular driver of osteoblast and osteoclast differentiation and that the knockout of c-Met results in delayed fracture union in

mice. In addition, we did not find evidence to link c-Met and hypoxia from tissue ischaemia to impaired fracture repair.

## Preface

This thesis is an original work by Guoju Hong. The clinical section (Chapter 2), including subject recruitment and sample collection, received research ethics approval from the clinical ethics board of the University of Alberta (ID: Pro00109397) and the First Affiliated Hospital of Guangzhou University of Chinese Medicine (ID: ZYYECK[2020]078). The animal model section (Chapter 3) received research ethics approval from the animal ethics board of Guangzhou University of Chinese Medicine (ID: GZTCM485772). Experimental protocols for these two sections were approved by the above relevant ethics boards.

With the exception explained below, the study was designed and carried out by Guoju Hong under the supervision of Dr. Peter Kannu. In Chapter 2 entitled “c-Met Expression Patterns in Human Fracture Healing” and Chapter 3 entitled "The Phenotypes and Expression Changes of c-Met in a Fracture Mouse Model Made by Conditional Knockout of c-Met", Dr. Zhenqiu Chen and his surgery and research team contributed to subject recruitment, hip arthroplasty surgeries, clinical information collection, mouse feeding and sample detection.

In Chapter 3, the *c-Met*<sup>fl/fl</sup> mice were created by Shanghai Model Organisms Center, Inc. The *Prx1*<sup>Cre</sup> mice were purchased from the Jackson Laboratory, and the *Ctsk*<sup>cre</sup> mice were provided by Shanghai Model Organisms Center, Inc. The crossbreeding between the *c-Met*<sup>fl/fl</sup> mice and two types of Cre mice was carried out by Shanghai Model Organisms Center, Inc.

In Chapter 4 entitled "The Roles of c-Met in the Regulation of Osteoclastogenesis and Osteoblastogenesis Under Hypoxic Conditions", Dr. Fred Berry donated the MC3T3 cell lines for the tissue culture experiments. Dr. Carrie-lynn Soltys provided technical support for the tissue culture work. The committee members Dr. Fred Berry and Dr. Zhixiang Wang provided comments and suggestions for research and writing.

## Acknowledge

As an orthopaedic surgeon, I am not only seeking to improve my surgical techniques. My curiosity about emerging surgical problems related to bone healing prompted me to conduct research to provide new data and develop new techniques. This aim led me to Canada and my PhD program, where I have been ever since.

I would like to express gratitude to my supervisor, Dr. Peter Kannu, who was supportive of my research work and actively provided me with valuable guidance to achieve my goals. I also thank Dr. Fred Berry for encouraging and supporting me at a very difficult time, as well as assisting me in my subsequent research. My sincere thanks go to my committee member, Dr. Zhixiang Wang, for his expertise and guidance, which helped me finish and polish this thesis, and to my thesis examiners, Dr. Daniel Graf and Dr. Frank Beier, for their advice and patience in reviewing my thesis. I would like to thank my candidacy examiners, Dr. Daniel Graf and Dr. Monica Gibson, for taking part in my candidacy exam and providing valuable insights.

Mrs. Carrie-lynn Soltys is to be sincerely thanked for her strong support for my experiments and my life. Moreover, I would like to thank my colleagues and friends Dr. Karina da Costa Silveira, Dr. Asghar Fallah, Liliana Vertel Morales, Parker Wengryn, Connor Oborn, Saima Ghafour, Daria Antoszko, and Alex Beke. Having the opportunity to work with all of you during the past years was wonderful.

I wish to acknowledge the financial support by the Chinese Scholarship Council, Canadian Institutes of Health Research, Alberta Innovates Research Funding, and China Institute Student Research Grant.

Finally, I am grateful to my parents and my lovely daughter, Youmi Hong. I am grateful for my wife, Xiaorui Han, for her unfailing assistance and support with my life and study.

# Table of Contents

<b>CHAPTER 1 INTRODUCTION.....</b>	<b>1</b>
1.1 CURRENT CONCEPT, AETIOLOGY, EPIDEMIOLOGY AND CHALLENGES OF FRACTURE NONUNION	2
1.2 BIOLOGICAL BASIS OF FRACTURE HEALING.....	3
1.3 OSTEOBLAST AND OSTEOCLAST-MEDIATED BONE REMODELING IN FRACTURE HEALING.....	5
1.4 SIGNALING AND CYTOKINES INVOLVING IN OSTEOBLAST AND OSTEOCLAST DIFFERENTIATION	7
1.5 C-MET SIGNALING AND ITS ROLE IN OSTEOBLASTOGENESIS AND OSTEOCLASTOGENESIS ...	10
1.5.1 <i>c-Met signaling and its single legend HGF</i> .....	10
1.5.2 <i>HGF/c-Met signaling in osteoblast and osteoclast differentiation</i> .....	11
1.6 ISCHEMIA-INDUCED HYPOXIA DISRUPTED FRACTURE HEALING VIA OSTEOBLASTS AND OSTEOCLASTS.....	14
1.7 KNOWLEDGE GAPS, RESEARCH HYPOTHESES AND GENERAL AIMS.....	15
<b>CHAPTER 2 C-MET EXPRESSION PATTERNS IN HUMAN FRACTURE HEALING.....</b>	<b>24</b>
2.1 ABSTRACT .....	25
2.2 INTRODUCTION .....	25
2.3 METHODS AND MATERIALS .....	28
2.3.1 <i>Ethical approval</i> .....	28
2.3.2 <i>Subject enrollment</i> .....	28
2.3.3 <i>Inclusion and exclusion criteria</i> .....	28
2.3.4 <i>Group assignment</i> .....	29
2.3.5 <i>Pre-surgical data collection</i> .....	29

2.3.6	<i>Sample collection</i> .....	29
2.3.7	<i>ELISA assay</i> .....	29
2.3.8	<i>Histomorphometric analysis</i> .....	30
2.3.9	<i>Immunofluorescence</i> .....	30
2.3.10	<i>Micro-CT</i> .....	31
2.3.11	<i>Western blotting assay</i> .....	31
2.3.12	<i>RT-qPCR</i> .....	31
2.3.13	<i>Statistical analysis</i> .....	32
2.4	RESULTS .....	32
2.4.1	<i>Osteoblastic and osteoclastic activities in serum are suppressed in fracture nonunion</i> 32	
2.4.2	<i>Failure of endochondral ossification, osteogenesis and resorption activity in human nonunion bone samples</i> .....	33
2.4.3	<i>Osteoblastic and osteoclastic activities in serum and bones are suppressed in fracture nonunion</i> .....	34
2.4.4	<i>c-Met and HGF are down-regulated in the human nonunion bone samples</i> .....	34
2.5	DISCUSSION .....	35
<b>CHAPTER 3 THE PHENOTYPES AND EXPRESSION CHANGES OF C-MET IN FRACTURE MODEL MADE BY CONDITIONAL KNOCKOUT C-MET MICE .....</b>		
<b>50</b>		
3.1	ABSTRACT .....	51
3.2	INTRODUCTION .....	51
3.3	METHODS AND MATERIALS .....	53
3.3.1	<i>Subgroup analysis</i> .....	53
3.3.2	<i>RT-qPCR</i> .....	54



3.3.3	<i>Generation of c-Met<sup>fl/fl</sup>, Prx1<sup>cre</sup> mice and c-Met<sup>fl/fl</sup>, Ctsk<sup>cre</sup> mice and phenotype identification</i>	54
3.3.4	<i>Proximal femur osteotomy</i>	55
3.3.5	<i>Alcian Blue-Alizarin Red staining</i>	55
3.3.6	<i>Histological analysis</i>	55
3.3.7	<i>Micro-CT</i>	56
3.3.8	<i>Cell line and tissue culture</i>	56
3.3.9	<i>Group setting for Alizarin Red staining and ALP staining</i>	57
3.3.10	<i>MTT assay</i>	57
3.3.11	<i>Statistical analysis</i>	57
3.4	<b>RESULTS</b>	58
3.4.1	<i>c-Met is expressed in the endosteum and highly activated in adult male mice.</i>	58
3.4.2	<i>Osteoblastic c-Met deficiency resulted in exhaustion of osteoblast differentiation</i>	58
3.4.3	<i>Osteoclastic c-Met deficiency resulted in osteoclast suppression and osteopetrosis.</i>	60
3.4.4	<i>C-Met ablation in osteoblast progenitor and osteoclast progenitor impair fracture healing</i>	60
3.5	<b>DISCUSSION</b>	61
<p style="text-align: center;"><b>CHAPTER 4 THE ROLES OF C-MET IN REGULATION OF OSTEOCLASTO-GENESIS AND OSTEOBLASTOGENESIS UNDER THE HYPOXIC CONDITION .. 94</b></p>		
4.1	<b>ABSTRACT</b>	95
4.2	<b>INTRODUCTION</b>	95
4.3	<b>MATERIALS AND METHODS</b>	98
4.3.1	<i>Cell lines and tissue culture</i>	98
4.3.2	<i>Hypoxic incubation and cabozantinib usage</i>	98
4.3.3	<i>Alizarin Red staining and ALP staining</i>	98

4.3.4	<i>TRAcP staining</i> .....	99
4.3.5	<i>Western blot</i> .....	99
4.3.6	<i>RT-qPCR</i> .....	100
4.3.7	<i>ELISA assay</i> .....	100
4.3.8	<i>Statistical analysis</i> .....	101
4.4	RESULTS .....	101
4.4.1	<i>Hypoxia suppresses osteoblast differentiation and increases c-Met phosphorylation</i> .....	101
4.4.2	<i>Hypoxia inhibits osteoclast differentiation and promotes c-Met phosphorylation</i> .....	102
4.4.3	<i>Cabozatinib doesn't reverse the suppression of osteoblastogenesis and osteoclastogenesis under hypoxia</i> .....	103
4.5	DISCUSSION .....	104
	<b>CHAPTER 5 SUMMARY AND GENERAL DISCUSSION</b> .....	<b>127</b>

## **List of Table**

Table 1. Demographic characteristic of unions and non-unions.....	48
---	----

## List of Figures

Figure 1. The procedure of osteoblast differentiation from mesenchymal stem cell to osteoblast progenitor, immature osteoblast, finally differentiating into mature osteoblast .....	17
Figure 2. The procedure of osteoclast differentiation from bone marrow precursor to preosteoclast, subsequently differentiating into activated osteoclast .....	18
Figure 3. (A) the molecular structure of c-Met. (B) the Hgf/c-Met system as well as its known downstream signaling pathways.....	19
Figure 4. HGF/c-Met signaling in regulation of osteoblast differentiation. ....	20
Figure 5. Types of c-Met inhibitors in regulating osteoblast differentiation.....	21
Figure 6. HGF/c-Met system in mature osteoblast regulation.....	22
Figure 7. HGF/c-Met system in osteoclast differentiation. ....	23
Figure 8. Group assignment of samples from control volunteers and subjects with nonunion. ...	38
Figure 9. Samples were collected from control volunteers and patients with nonunion. ....	39
Figure 10. Morphological changes in fracture calli and control bone cubes obtained from the union group and nonunion group. ....	41
Figure 11. Safranin O/fast green staining, Masson's trichrome staining and TRAcP staining of fracture calli and bone cubes obtained from the union group and nonunion group. ....	43
Figure 12. Osteoblastic and osteoclastic markers and genes expressed in the serum and bone samples of the union group and nonunion group. ....	45
Figure 13. c-MET and HGF expression in bone samples of the union group and nonunion group. ....	46
Figure 14. Protein expression of c-Met, HGF and the downstream signaling factors in fracture calluses and bone cubes of the union group and nonunion group.....	48
Figure 15. The strategy of CRISPR/Cas9 editing for conditional knockout of <i>c-Met</i> .....	66

Figure 16. The strategy of mouse breeding for generating <i>c-Met<sup>fl/fl</sup></i> , <i>Prx1<sup>cre</sup></i> mice and <i>c-Met<sup>fl/fl</sup></i> , <i>Ctsk<sup>cre</sup></i> mice.....	67
Figure 17. The surgical strategy of proximal femur fracture in mice. ....	68
Figure 18. c-Met and HGF expression in the skeleton and viscera of wild-type mice.....	70
Figure 19. The distribution of c-Met and Hgf expression in the tibia of wild-type mice.....	72
Figure 20. Phenotype of the <i>c-Met<sup>fl/fl</sup></i> , <i>Prx1<sup>cre</sup></i> mice and the control mice. ....	74
Figure 21. Osteoblast and osteoclast activities of the <i>c-Met<sup>fl/fl</sup></i> , <i>Prx1<sup>cre</sup></i> mice and the control mice of different ages.....	76
Figure 22. Viscera of the <i>c-Met<sup>fl/fl</sup></i> , <i>Prx1<sup>cre</sup></i> mice and the control mice.....	77
Figure 23. c-Met kinase activity inhibitor cabozantinib promotes osteogenic differentiation but suppresses proliferation of osteoblast progenitor MC3T3 cell lines.....	79
Figure 24. Phenotype of the <i>c-Met<sup>fl/fl</sup></i> , <i>Ctsk<sup>cre</sup></i> mice and the control mice.....	81
Figure 25. Osteoblast and osteoclast activities of <i>c-Met<sup>fl/fl</sup></i> , <i>Ctsk<sup>cre</sup></i> mice of different ages and control mice.....	83
Figure 26. Viscera of the <i>c-Met<sup>fl/fl</sup></i> , <i>Ctsk<sup>cre</sup></i> mice and control mice. ....	84
Figure 27. Micro-CT and H&E staining of the <i>c-Met<sup>fl/fl</sup></i> , <i>Prx1<sup>cre</sup></i> mice and the control mice.....	86
Figure 28. Safranin O/fast green staining, Masson's trichrome staining, TRAcP staining and ALP immunohistochemistry of the <i>c-Met<sup>fl/fl</sup></i> , <i>Prx1<sup>cre</sup></i> mice and the control mice. ....	88
Figure 29. Fracture healing and callus formation of the <i>c-Met<sup>fl/fl</sup></i> , <i>Ctsk<sup>cre</sup></i> mice and the control mice. ....	89
Figure 30. Safranin O/fast green staining, Masson's trichrome staining, TRAcP staining and ALP immunohistochemistry of the <i>c-Met<sup>fl/fl</sup></i> , <i>Ctsk<sup>cre</sup></i> mice and the control mice. ....	91
Figure 31. Summary of trends of bone matrix, ALP expression, number of osteoblasts and osteoclasts in <i>c-Met<sup>fl/fl</sup></i> , <i>Prx1<sup>cre</sup></i> mice and <i>c-Met<sup>fl/fl</sup></i> , <i>Ctsk<sup>cre</sup></i> mice from 3-week to 25-week-old.....	92
Figure 32. Stages of fracture healing in normal mice, <i>c-Met<sup>fl/fl</sup></i> , <i>Prx1<sup>cre</sup></i> mice and <i>c-Met<sup>fl/fl</sup></i> , <i>Ctsk<sup>cre</sup></i> mice after osteotomy. ....	93

Figure 33. Hypoxia regulates osteoblast differentiation and c-Met/HGF expression. ....	107
Figure 34. Hypoxia regulates RUNX2 and $\beta$ -catenin in osteoblast differentiation.....	109
Figure 35. Hypoxia regulates MAPK/Erk signalling in osteoblast differentiation.....	110
Figure 36. Hypoxia regulates PI3K/AKT signalling in osteoblast differentiation. ....	111
Figure 37. Hypoxia regulates c-Met and osteoblast-related genes during osteoblast differentia- tion.....	112
Figure 38. Hypoxia regulates osteoclast differentiation and c-Met/HGF expression.....	113
Figure 39. Hypoxia regulates NFAT1, CTSK and AKT in osteoclast differentiation. ....	115
Figure 40. Hypoxia regulates JNK and p38 in osteoclast differentiation. ....	117
Figure 41. Hypoxia regulates c-Met and osteoclast-related genes during osteoclast differentia- tion.....	118
Figure 42. Cabozantinib regulates osteoblast differentiation and c-Met expression. ....	119
Figure 43. Cabozantinib regulates RUNX2 and $\beta$ -catenin in osteoblast differentiation. ....	120
Figure 44. Cabozantinib regulates the phosphorylation of AKT and PI3K and ERK1/2 signalling in osteoblast differentiation. ....	121
Figure 45. Cabozantinib regulates the phosphorylation of MAPK signalling (JNK and p38) in osteoblast differentiation. ....	122
Figure 46. Hypoxia regulates osteoclast differentiation and c-Met protein expression. ....	123
Figure 47. Cabozantinib regulates NFATc1, CTSK and AKT signalling in osteoclast differenti- ation. ....	124
Figure 48. Cabozantinib regulates MAPK signalling (JNK and p38) in osteoclast differentiation. .....	126

## Table of Abbreviation

A	ALP	alkaline phosphatase
	Akt	protein kinase B
B	BALP	bone alkaline phosphatase
	BMP2	bone morphogenetic proteins 2
	BSP	bone lipoprotein
	BRU	bone remodelling unit
	BV/TV	bone volume per tissue volume
C	c-Fms	colony stimulating factor 1 receptor
	c-Met	tyrosine protein kinase Met
	COLL-1	collagen type I
	Conn.Dn	connectivity density
	c-Src	proto-oncogene tyrosine-protein kinase Src
	CT	computed tomography
	CTX	c-terminal telopeptide
D	DKK1	dickkopf-1
E	ELISA	enzyme-linked immunosorbent assay
	ERK	extracellular signal-regulated kinase

H	H&E	haematoxylin & eosin
	HGF	hepatocyte growth factor
	HGFR	hepatocyte growth factor receptor
I	IHC	immunohistochemistry
M	MAPK	mitogen-activated protein kinase
	M-CSF	Macrophage colony-stimulating factor
	MMLV	Moloney murine leukaemia virus
	MSC	mesenchymal stem cell
N	NF- $\kappa$ B	nuclear factor kappa-light-chain enhancer of activated B cells
	NFATc1	nuclear factor of activated T cells 1
	NTX	type I collagen N-telopeptide
O	OA	osteoarthritis
	OC	osteocalcin
	OPG	ostoprotegerin
	OPN	osteopontin
	OSE	osteogenic-specific cis-element
	OSX	osterix
P	PI3K	phosphoinositide 3-kinase
	PICP	pro-collagen I C-terminal propeptide



	PFA	paraformaldehyde
	PPAR $\gamma$	peroxisome proliferator-activated receptor $\gamma$
	PVP	polyvinylpyrrolidone
R	RANKL	receptor activator of nuclear factor kappa-B ligand
	ROI	region of interest
	RT-qPCR	quantitative reverse transcription polymerase chain reaction
	Runx2	runt-related transcription factor 2
S	siRNA	small interfering RNA
	SDS	sodium dodecyl sulphate
T	Tb.N	number of trabeculae
	Tb.Th	trabecular thickness
	TRAcP	tartrate-resistant acid phosphatase
	TRAF6	TNF receptor-associated factor 6

# **CHAPTER 1**

## **Introduction**

## 1.1 Current concept, aetiology, epidemiology and challenges of fracture nonunion

In terms of bone regeneration, skeletons are capable of regenerating at an extraordinary rate<sup>1</sup>. How bones heal after a fracture can be modulated by both mechanical and biological factors<sup>2</sup>. Functional fracture repair can only be achieved if there is a well-balanced combination of mechanical and biological factors<sup>3,4</sup>. A fracture that does not heal, also known as fracture nonunion, can result from the impairment of one or more of these factors<sup>5</sup>.

Nonunion is an abnormal bone healing process in which absolutely no healing occurs<sup>2,6</sup>. Diagnosis of non-union depends on a combination of clinical, pathological, and radiological signs<sup>7</sup>. Generally, nonunion occurs when a fracture does not heal nine months after the injury. Nonunion is suspected if a fracture does not appear to heal three months after an injury<sup>5</sup>. In the assessment and diagnosis of nonunion, bone movement or pain at the fracture site indicate that the fracture is not healing properly<sup>7</sup>. Radiologically, nonunion is defined as bridging callus present in three of the four bone cortices<sup>8</sup>. Nonunion is often determined by only one of these parameters, and a lack of a consistent definition contributes to the clinical subjectivity of the diagnosis<sup>9</sup>.

Nonunions are influenced by multiple factors, including the severity and location of the fracture, the patients' overall medical condition and concurrent medication usage<sup>6</sup>. Other significant factors include i) *Fracture mechanism*. A high-energy injury that results in an open fracture (fracture which has an open wound at the skin) and complex fracture (multiple breaks in the bone) is most likely to result in nonunion causing significant morbidity<sup>10</sup>; ii) *Age and sex*. In general, the likelihood of nonunion is higher among men than among women<sup>7,5</sup>. Males younger than 40 years are more likely to sustain trauma from high-energy injuries, whereas osteoporosis predisposing to fracture equally among both genders<sup>7</sup>; iii) *Smoking*. Nicotine causes blood vessel constriction impairing bone development<sup>5</sup>. In fact, nicotine is one of the most common risk factors for non-union. Smoking further increases the incidence of nonunion in ischaemic, open and complex fractures<sup>11</sup>; iv) *Drug side effects*. The use of anti-inflammatory drugs, such as nonsteroidal anti-inflammatory medication (NSAIDs), impair fracture union by inhibiting inflammation which is crucial to the initial stages of bone healing<sup>12</sup>. Additionally, drugs such as antibiotics, anticoagulants, analgesics, tranquilizers, and glucocorticoids, lead to more severe fractures that are less likely to heal<sup>13,14</sup>; v) *Chronic illness*. Obesity has been shown

to slow the healing of fractures mainly in the lower limbs<sup>11,15,16</sup>. Diabetes contributes to non-union by contributing to microangiopathy and a disruption of blood flow to the fracture<sup>17</sup>. Osteoporosis results in reduced bone regrowth potential<sup>18</sup>.

Generally, the incidence of fracture nonunion varies from region to region depending on the quality of the local healthcare system<sup>8,11</sup>. Access to appropriate diagnosis and treatment has kept the incidence of fracture non-union low in developed countries. However, fracture nonunion remains a major complication after fracture surgery, particularly in developing countries<sup>5,19</sup>. The estimated worldwide incidence of fracture nonunion is 5% to 10%<sup>20</sup>. Among 309,330 fractures of 18 bones in the United States, the fracture nonunion rate was 4.9%<sup>11</sup>. A meta-analysis found that in China, the nonunion rate was 4.93%<sup>21</sup>. The incidence of nonunion is closely tied to the fracture site. Nonunions are more likely to occur in the tibia due to a lack of muscle coverage and blood supply. The femur is the second most common bone affected<sup>8</sup>. The current epidemiology of fracture nonunion is hampered by a lack of good quality data and scattered studies<sup>5</sup>. Nonunion causes the individual substantial physical, psychological, and financial distress. In particular, fracture non-union has the potential to severely curtail a patients' functional activities through a restriction of mobility and pain<sup>5,7</sup>.

Fracture nonunion requires lengthy treatment, and complete healing is difficult<sup>2,7</sup>. Currently, surgeons advocate aggressive interventional treatment as well as preventing the onset of nonunion through the modification of risk factors, such as smoking, diabetes control, and obesity<sup>9</sup>. Surgeons focus more on perioperative management, such as periosteal protection, adequate bone fixation, and rehabilitation, to promote fracture end healing. Preventive measures also incorporate close follow-up and the radiological tracking of fracture repair<sup>22</sup>.

Despite the current improvements in clinical outcomes, there is still a lot unknown about the basic biological mechanisms contributing to fracture nonunion<sup>3</sup>. By bridging this gap, we will gain a deeper understanding of fracture nonunion biology paving the way for innovative new treatment measures.

## **1.2 Biological basis of fracture healing**

Fractures heal via two distinct mechanisms: intramembranous and endochondral ossification<sup>23,2</sup>. In intramembranous repair, a callus does not develop because of rigid bone fixation, and the bone naturally heals without any connective tissue or callus<sup>24</sup>. Bones which are attached to

each other naturally by physiological compression (gap less than 400  $\mu\text{m}$ ) heal without any need for an external callus<sup>25</sup>. In contrast, callus formation following a fracture is the most common method of fracture repair<sup>26</sup>. The callus is a form of preossified cartilage that forms as a result of restricted movement at the fracture site. The process involves haematoma formation and inflammation, soft callus, hard callus, and reconstruction or remodelling of the callus<sup>27</sup>.

*Haematoma and granulation tissue formation.* A haematoma develops at the site of trauma when the integrity and circulation of bone are disrupted by external injury<sup>28</sup>. Fracture results in a loss of bone tensile strength, a depletion of nutrients and oxygen, and the release of platelet derived cytokines<sup>29</sup>. The fracture site is then infiltrated by macrophages, immune cells, and inflammatory cells<sup>18</sup>. The trauma of the fracture makes the remaining surviving cells nearby the fracture site reactive and heightened to more efficiently recognize and respond to external stimuli, such as vessel growing or cytokine invasion<sup>30</sup>. This procedure peaks within 24 h but lasts for approximately seven days<sup>18</sup>.

*Soft callus development.* Cells within the haematoma are activated in the inflammatory stage to promote blood vessel growth, fibroblast formation, and tissue regeneration<sup>31</sup>. Fibrin-rich granulation tissue then replaces the haematoma<sup>29</sup>. Next, fibrocartilage forms reinforcing and fixing the ends of the bones. Soft callus growth begins seven to ten days after fracture, and is characterized by the enhanced synthesis of type II collagen and proteoglycan<sup>31,32</sup>.

*Hard callus development.* Upon forming a soft callus, the fibrocartilage is gradually replaced by bone via endochondral ossification<sup>26</sup>. Periosteal bone deposition is induced by osteoblasts, which leads to the growth of the hard callus<sup>33,18</sup>. The calcified cartilage template is removed and substituted with woven bone<sup>34</sup>. Key markers of this process include type I collagen, alkaline phosphatase (ALP), and osteocalcin. Hard callus development typically peaks approximately 14 days after fracture<sup>35</sup>. Interestingly, intramembranous ossification at the periphery of the bone injury can also cause hard callus formation<sup>4,25</sup>.

*Bone remodelling.* Through bone remodelling, woven bone is gradually transformed to lamellar bone at the final stage of fracture repair<sup>32,36</sup>. Osteoclasts resorb the hard callus and osteoblasts form lamellar bone to reconstruct the morphology of the damaged bone. Pressure loading of the bone is important for this process to successfully occur<sup>27</sup>. The fracture heals in

three to four weeks, but the original structure may not be restored until years later<sup>34</sup>. However, most individuals do not regain the original anatomic structure or strength following a fracture<sup>20</sup>.

Bone fractures heal if the structural stability of fracture sites is maintained by bridging the interrupted gap with new bone before the final shaping occurs. Healthy fracture repair requires abundant blood flow, nutrients, oxygen supply and physical stability<sup>1</sup>. Nonunion results when these processes are disrupted. Generally, fractures with nonunion are categorized as hypertrophic or atrophic. Fracture sites with inadequate blood supply usually develop atrophic nonunion, in which no callus is formed. Conversely, hypertrophic nonunion manifests as nonhealing bone due to insufficient mobility but abundant vascularization and cartilage formation, which leads to pseudoarthrosis<sup>5</sup>.

### **1.3 Osteoblast and osteoclast-mediated bone remodeling in fracture healing**

A healthy bone environment is dependent on osteoclast-mediated bone resorption and osteoblast-mediated bone formation. The mechanisms that regulate osteoclast interaction with osteoblasts are therefore critical for fracture healing<sup>32</sup>. After a fracture, osteoblasts and osteoclasts become active during the healing process. Both cell types are necessary for fracture healing<sup>3</sup>.

Osteoblasts are differentiated mesenchymal stem cells that exhibit specialized functions<sup>37</sup>. Osteoblasts are responsible for generating dense, crosslinked collagen and specific proteins that are responsible for forming the bone's extracellular matrix<sup>38</sup>. Osteoclasts are multinuclear, large cells that dissolve and absorb bone<sup>39</sup>. Osteoclast formation is dependent upon the activation of receptor activator of nuclear factor kappa-B ligand (RANKL) and the activation of macrophage colony-stimulating factor (M-CSF)<sup>40</sup>. It is believed that these membrane-bound proteins are secreted from adjacent progenitor cells and osteoblasts; therefore, the contact of osteoclast precursors with these cells is necessary<sup>41</sup>.

Specifically, in fracture healing, osteoblasts and osteoclasts develop during the early inflammation stage. In the reparative stage, vessels penetrate hyaline cartilage (the cartilage modelling template), promoting the migration of mesenchymal progenitors that develop into osteoblasts and of monocytes that transform into osteoclasts<sup>33</sup>. Additionally, chondrocytes in fracture healing can undergo transdifferentiation to osteoblasts<sup>26</sup>. Osteoclasts, in contrast, are derived from haemopoietic cells of bone marrow<sup>3,25</sup>. As osteoblasts and osteoclasts are the dominant

cells in the reparative and remodelling stages, failure of osteoblast or osteoclast differentiation can directly lead to fracture nonunion<sup>32,42</sup>.

i) *Limited potential of osteogenic progenitor cells.* Osteoblasts from the periosteum distal to the fracture gap start forming woven bone seven days after a fracture when the calcified cartilage is resorbed. The woven bone gradually accumulates and transforms into a new mass of heterogeneous tissue called a fracture callus, which bridges the fracture gap<sup>43</sup>. Osteoblasts are also involved in the substitution of woven bone by forming lamellar bone<sup>44</sup>. Lamellar bone begins to form shortly after the collagen matrix of woven bone becomes mineralized<sup>45</sup>. The microvasculature penetrates the mineralized matrix and brings along osteoblasts. Osteoblasts form new lamellar bones consisting of trabeculae over the exposed mineralized matrix.<sup>25,36</sup>

Therefore, impaired fracture healing can result from limited activity of osteogenic progenitor cells, meaning that suppression of osteoblast differentiation results in failure of woven bone and lamellar bone formation. It has been shown that fractures caused by severe soft tissue trauma are more likely to suffer nonunion because the thin membrane on the outside of bones (periosteum) contains progenitor cells that facilitate bone healing<sup>35</sup>. Additionally, osteogenic differentiation is low in cells from patients with nonunion, indicating that a deficiency in cellular properties might negatively affect bone healing<sup>30</sup>. In the case of nonunion, osteogenic progenitor cells and osteoblasts may be negatively affected by the patient's advanced age, sex, concurrent illness, and drug treatment<sup>46</sup>.

ii) *Impaired bone remodelling by osteoclasts.* As mentioned before, remodelling is mainly mediated by osteoclasts and starts the moment bone is formed, taking up to several years to complete<sup>1,25</sup>. Initially, the trabecular bone is resorbed by osteoclasts, resulting in a superficial bone resorption pit. Following this, osteoblasts deposit compact bone to change bone appearance<sup>36</sup>. Eventually, the fracture callus becomes remodelled to resemble the original shape of the bone with similar strength. The precise role of osteoclasts is to ensure the transition from trabecular bone to compact bone. Accordingly, suppression of bone resorption delays the decomposition of endochondral tissue and regeneration of diaphyseal bone<sup>42</sup>. Older patients undergoing osteoclast-inhibiting bisphosphonate therapy after fracture show a significant increase in the incidence of nonunion compared with patients who did not receive bisphosphonates<sup>47</sup>.

## 1.4 Signaling and cytokines involving in osteoblast and osteoclast differentiation

Mature osteoblasts differentiated from mesenchymal stem cells (MSCs) drive osteogenesis<sup>48</sup>. Since MSCs can differentiate into osteoblasts, adipocytes, chondrocytes, etc, specific signalling pathways and cytokines direct the differentiation of MSCs into osteoblasts and later mature osteoblasts<sup>49</sup> (**Figure 1**).

1) *Runx2 and Osterix*. Runt-related transcription factor 2 (*Runx2*), also known as *Cbfa1*, belongs to the Runt structural domain gene family<sup>50</sup>. This molecule is important for osteogenic differentiation, as shown by its critical role in osteoblast maturation and its ability to inhibit MSC differentiation into adipocytes<sup>50,37</sup>. *Runx2* knockout mice demonstrate dysfunctional osteogenesis<sup>51</sup>. *Runx2* regulates the expression of key osteogenic differentiation factors, such as alkaline phosphatase (ALP), osteocalcin (OC), collagen type I (COLL-1), bone sialoprotein (BSP) and osteopontin (OPN). *Runx2* binds to osteogenic-specific cis-elements (OSEs) in the promoter sequences of these genes, thereby activating their expression<sup>52</sup>. Similarly, *Osterix* (*Osx*) is a transcription factor associated with the differentiation of osteoblasts<sup>38,53</sup>. Knocking out the mouse *Osx* gene impaired the development of cortical and trabecular bone<sup>54</sup>. *Osx* was not expressed in mice lacking *Runx2*, indicating that the expression of *Osx* is regulated by *Runx2* and that *Osx* lies downstream of *Runx2*<sup>55</sup>. The human disease cleidocranial dysplasia is due to loss of function variants in *RUNX2* and is associated with the hypoplastic development of the clavicles. Biallelic variants in *Osx* are associated with the brittle bone disease osteogenesis imperfecta<sup>55</sup>.

2) *The Wnt/ $\beta$ -catenin pathway*. Wnt signalling pathways are classified as canonical and noncanonical<sup>56</sup>. In the canonical Wnt signalling pathway (the Wnt/ $\beta$ -catenin pathway), Wnt ligand and its receptors interact along with intracellular signalling molecules to initiate osteoblast differentiation<sup>57</sup>. The Wnt/ $\beta$ -catenin signalling pathway is activated by Wnt ligand binding to the Frizzled receptor and inhibiting GSK3 $\beta$  activity through the LRP5/6 receptor<sup>57,58</sup>. As a result,  $\beta$ -catenin phosphorylation is blocked, while  $\beta$ -catenin protein stability is maintained. Unphosphorylated  $\beta$ -catenin is thus transferred into the nucleus and interacts with TCF/LEF, thereby promoting the expression of osteogenic genes<sup>38,59</sup>.



Wnt signalling induces osteogenesis and inhibits adipogenesis, as shown in numerous cell models. For example, in the 3T3-L1 cell line (murine preadipocytes), the Wnt/ $\beta$ -catenin signalling pathway interacts with peroxisome proliferator-activated receptor  $\gamma$  (PPAR $\gamma$ ) to regulate the differentiation of cells towards adipogenesis or osteogenesis<sup>60</sup>. One of the Wnt family members, Wnt3a, enhances osteogenic differentiation in bone marrow MSCs and C3H10T1/2 cells (murine mesenchymal stem cell line), whereas it inhibits adipocyte differentiation<sup>61</sup>. In contrast, addition of Dickkopf-1 (DKK1), a secreted inhibitor of Wnt signalling, enhanced 3T3-L1 cell differentiation into adipocytes<sup>62</sup>. After knockout of *Dkk1*, MSCs lost their adipogenic differentiation ability, whereas MC3T3-E1 cells and MSCs exhibited increased osteogenic differentiation<sup>63</sup>. The Runx2 terminus is the point at which the Wnt/ $\beta$ -catenin pathway controls osteoblast differentiation and bone formation<sup>64</sup>. To initiate Runx2 expression,  $\beta$ -catenin binds to a TCF site of the Runx2 promoter, which in turn regulates ALP and OCN, which are involved in osteogenic differentiation<sup>65</sup>.

Several human disorders in which bone is compromised arise from different variants in the WNT pathway. Heterozygous and biallelic variants in WNT10 result in tooth agenesis; biallelic variants in LRP5 cause osteoporosis; a high-bone-mass phenotype is caused by gain-of-function mutations in *LRP5* whereas a reduction in expression or activity of the extracellular soluble Wnt antagonist *SOST* leads to van Buchem disease and sclerostosis. There is also evidence to support a role for the regulation of  $\beta$ -catenin in the development of tibial pseudoarthrosis secondary to Neurofibromatosis type 1. Pseudoarthrosis starts as anterolateral bowing of the tibia, culminating in fracture nonunion. While the etiology of a tibial pseudoarthrosis remains unknown, it is hypothesized that the fracture nonunion is due to a lack of blood supply to the periosteum.

3) *Bone morphogenetic proteins (BMPs)*. BMPs are cytokines and metabologens belonging to the TGF- $\beta$  superfamily<sup>66</sup>. Initially recognized by their ability to stimulate skeletal and cartilage development, BMPs are currently believed to be key morphogenetic factors, modulating tissue structure<sup>67</sup>. During osteoblast differentiation, BMPs contribute more to the late stage than to the early stage of differentiation<sup>68</sup>.

BMPs activate the BMP/Smad pathway by binding to specific BMP receptors on the cell membrane<sup>66</sup>. In this way, downstream Smad proteins (such as Smad1 and Smad5) are phosphorylated, and the transcription of osteoblast-specific transcription factor genes (such as Runx2, Osx, etc.) is initiated. Consequently, this change enhances osteoblast differentiation and bone formation<sup>69</sup>. A key regulatory function of the ubiquitin proteasome is to control the BMP/Smad signalling pathway, particularly Smurf1, which is an E3 ubiquitin ligase<sup>70</sup>. Smurf1 can recognize and bind Runx2 and Smad1 to promote their degradation via the ubiquitin proteasome pathway, thus inhibiting osteoblast differentiation and bone formation mediated by BMP/Smad signalling<sup>71</sup>. USP34, a ubiquitin-specific protease, stabilizes Smad1 and Runx2 by deactivating Smurf1-mediated ubiquitination, thereby improving osteoblast differentiation and bone formation<sup>72</sup>.

Osteoclasts are multinucleated giant cells derived from the mononuclear macrophage precursors of haematopoietic stem cells that circulate in the peripheral blood<sup>73</sup>. In response to factors such as M-CSF and RANKL, osteoclast precursor cells gather in bone remodelling units (BRUs) and develop into osteoclasts<sup>41</sup> (**Figure 2**).

1) M-CSF. M-CSF is a homodimeric glycoprotein synthesized by fibroblasts, osteoblasts, and epithelial cells<sup>74</sup>. The colony stimulating factor 1 receptor (c-Fms) is a tyrosine kinase superfamily member that targets M-CSF<sup>75</sup>. In the initial stage of monocyte differentiation, the transcription factor PU.1 promotes the expression of c-Fms in bone marrow haematopoietic stem cells<sup>76</sup>. M-CSF and c-Fms can be combined to activate the phosphorylation of c-Fms through tyrosine kinase activity<sup>75</sup>. Following this, Grb-2 together with c-Fms activates extracellular signal-regulated kinase (ERK), while phosphoinositide 3-kinase (PI3K) activates protein kinase B (Akt), thereby promoting osteoclast precursor survival<sup>77</sup>. Furthermore, M-CSF can induce bone marrow cells to express the RANK receptor, which then interacts with RANKL to induce osteoclast differentiation<sup>78</sup>. M-CSF can also interact with RANKL by activating the Akt, c-Fos, and ERK signalling pathways and then participate in late osteoclast formation<sup>74</sup>.

2) RANKL. RANKL is a protein that in humans is encoded by *TNFSF11*<sup>79</sup>. This membrane-bound protein can be cleaved into soluble molecules by metalloproteinases<sup>80</sup>. Its receptor RANK belongs to the tumour necrosis factor superfamily. A lack of endogenous enzyme activity of RANK's intracellular domain necessitates TRAF6 recruitment for activation<sup>81</sup>.

The interaction between RANKL and RANK directly recruits TNF receptor-associated factor 6 (TRAF6) and activates a series of intracellular molecular events, which involve nuclear factor kappa-light-chain enhancer of activated B cells (NF- $\kappa$ B) and mitogen-activated protein kinase (MAPK), which in turn stimulate the expression of osteoclast-related downstream factors, such as nuclear factor of activated T cells 1 (NFATc1)<sup>40,79,81</sup>. Biallelic variants in RANKL result in a human dense bone disease called osteopetrosis<sup>81</sup>. i) The NF- $\kappa$ B pathway is predominantly involved in initial osteoclastic differentiation and is known to precede c-Fos induction and the induction of NFATc1<sup>82</sup>. Induction of NF- $\kappa$ B by TNF- $\alpha$  is regulated by redox-driven modulation of dynein light chain LC8<sup>83</sup>. In a murine model, NF- $\kappa$ B deficiency resulted in impaired differentiation of osteoclasts<sup>84</sup>. ii) MAPK proteins, such as ERK, p38, and JNK, are proline-mediated serine proteins<sup>85</sup>. These molecules are crucial in the intracellular pathway of osteoclast precursors and modulate osteoclastogenic properties, especially proliferation, morphogenesis, and differentiation<sup>86</sup>. ERK signalling helps extend osteoclast lifespan by enhancing the transcription of c-Fos<sup>87</sup>. Both phosphorylated JNK and p38 can induce the differentiation, fusion, and activation of osteoclasts<sup>88</sup>. Alternatively, blockade of JNK and p38 phosphorylation resulted in decreased osteoclast maturation<sup>89</sup>. iii) RANKL-induced signal transduction is also mediated by NFATc1, a pivotal factor in osteoclast development and survival<sup>90</sup>. Additionally, NFATc1 modulates the mRNA levels of osteoclast-related genes driven by various specific promoters, such as *Acp5*, *Cathepsin K*, *Atp6v0d2*, *Nfact1*, *c-Fos*, and *Mmp9*, which are essential for osteoclast formation<sup>91</sup>.

## **1.5 c-Met signaling and its role in osteoblastogenesis and osteoclastogenesis**

### **1.5.1 c-Met signaling and its single legend HGF**

Beyond the above molecular mechanisms involving osteoblasts and osteoclasts, c-Met has been shown to play a crucial role in bone metabolism and bone repair, making it an interesting research subject. c-Met, also known as tyrosine protein kinase Met or hepatocyte growth factor receptor (HGFR), is a protein encoded by the MET gene in humans<sup>92</sup>. This primary single chain precursor protein c-Met is cleaved into its alpha and beta subunits during post-translational processing; these subunits are linked by disulfide bonds to form the mature receptor. Hepatocyte growth factor (HGF) is the only ligand for c-Met<sup>93</sup>. C-Met functions as a single-pass tyrosine kinase receptor in embryogenesis, tissue growth and repair. The role of the c-Met receptor in cellular activity and cancer progression is well documented<sup>94</sup>.

Upon interaction of HGF and its receptor c-Met, a cascade of downstream signaling occurs that establishes a multiplicity of biological effects through a multitude of pathways<sup>95</sup>. In response to HGF binding to c-Met, there are two potential immediate effects: phosphorylation of key residues in the receptor and activation of downstream signaling pathways. The tyrosine kinase domain of the c-Met receptor transduces its signal by autophosphorylating the tyrosine residues Y1234 and Y1235 (**Figure 4**). Downstream signaling is in turn induced by phosphorylating the tyrosine residues Y1349 and Y1356<sup>96</sup>. The initiation of the c-Met receptor and subsequent pathway activation depends on the cell type. The receptor is important in regulating cell migration, cellular differentiation and proliferation in stem cells<sup>97</sup>. Proteases specific to c-Met degrade c-Met after it is activated. The juxtamembrane domain of the c-Met receptor also negatively regulates the c-Met signal by targeting the receptor for ubiquitination upon phosphorylation of the Y1003 residue. Ubiquitination and degradation of c-Met via Cbl prevents the continuous signalling of the receptor<sup>98</sup>. Cancer cells tend to become more motile and invasive due to constitutive activation of c-Met caused by dysregulated degradation (mutations affecting Y1003) or c-Met overexpression<sup>95,96</sup>. ERK1/2, PI3K/Akt and p38-MAPK are the primary downstream signalling pathways in the HGF/c-Met network<sup>99,100</sup>.

### **1.5.2 HGF/c-Met signaling in osteoblast and osteoclast differentiation**

1) *The HGF/c-Met signalling pathway in osteoblast progenitors (Figures 4 and 5)*. In osteoblast progenitor cells, exogenous HGF regulates cellular differentiation and proliferation in a dose-dependent manner. Low concentrations of exogenous HGF plus an osteogenic inducer stimulate osteogenic differentiation of mesenchymal stem cells by upregulating c-Met activity, Akt pathway activation and Runx2, Osx and p27 expression<sup>101-103</sup>. In contrast, a high concentration of exogenous HGF dramatically induced cellular proliferation through the activation of the ERK1/2 signal transduction pathway. HGF at high concentrations blocked the initiation and progression of BMP-induced osteoblastogenesis *in vitro* and suppressed Runx2 and Osx expression in response to BMP-2<sup>104</sup>. HGF prior to BMP-2 stimulation induced osteoblast progenitor cellular proliferation but did not affect BMP-2-induced osteoblast differentiation<sup>102</sup>. This suggests that the actions of exogenous HGF may vary depending on the maturity of the differentiation progenitors.

With regard to endogenous HGF, elimination of HGF secretion by knockdown of HGF mRNA *in vitro* led to augmentation of BMP-2-induced ALP expression in myoblasts<sup>102</sup>. Alternatively, infection with a recombinant adenovirus carrying the HGF gene (rAd-HGF) enhanced the secretion of HGF and proliferation of bone MSCs. Osteogenesis is also accelerated by stimulating the deposition of calcium nodules with the addition of endogenous HGF<sup>103</sup>. Collectively, exogenous and endogenous HGF competes with BMP-2 for osteogenesis, although the intrinsic mechanism is not known.

Intriguingly, HGF antagonists and c-Met inhibitors suppress BMP-2-stimulated HGF production in myoblasts (embryonic precursors of myocytes that can also transform into osteoblasts) but increased Runx2, ALP, and OC expression<sup>105</sup>. Similarly, osteoblast precursors showed the same behaviour when treated with a c-Met inhibitor<sup>106</sup>. Furthermore, treatment with BMS-777607, a c-Met inhibitor, significantly suppressed cell proliferation<sup>107</sup>. Evidently, c-Met inhibitors do not behave as expected; that is, blocking c-Met attenuated downstream signalling, prevented osteogenic differentiation and suppressed cellular proliferation<sup>106</sup>. In order to explain these contradictory findings, the following model has been proposed. In a published model cell system, the c-Met-Mek-ERK-Smad and c-Met-PI3K-Akt-Smad signalling pathways were shown to increase osteogenesis, while c-Met signalling decreased osteogenesis in a Met-ERK-Smad and PI3K-Akt-Smad independent manner<sup>105</sup>.

Intracellular c-Met function is highly determined by endogenous HGF secreted by the cells. C-Met inhibition promotes the effects of rAd-HGF infection (increased endogenous HGF secretion) on hBMSC osteogenesis. When cells were infected with rAd-Ctrl (normal endogenous HGF secretion), treatment with SU11274 (c-Met inhibitor) promoted osteogenesis. Since BMSCs self-secrete HGF, this result suggested that the regulatory effects of c-Met was responsive to low levels of HGF<sup>103</sup>.

2) *The HGF/c-Met signalling pathway in osteoblasts (Figure 6)*. Human osteoblasts express osteopontin (OPN) by the addition of exogenous HGF, but the effects can be attenuated via the use of c-Met inhibitors or silencing RNA (siRNA). Osteoblasts stimulated with HGF activate PI3K, Akt, and c-Src<sup>97</sup>. Human osteoblasts overexpressed BMP-2 in response to exogenous HGF, which was attenuated by c-Met inhibitors or siRNA<sup>108</sup>.

Currently, only one study has focused on the role of endogenous HGF in mature osteoblasts. The results indicated that the expression of endogenous HGF was greater in osteoblasts from patients with osteoarthritis (OA) than in healthy osteoblasts. Normal osteoblasts are stimulated by BMP-2, whereas osteoblasts from patients with OA are inhibited. Treatment with siRNA against HGF reversed the osteoarthritic osteoblast response to BMP-2 and restored their response to HGF. With HGF inhibitor treatment, the reduction in Smad1/5/8 phosphorylation in OA osteoblasts in response to BMP-2 was abrogated. Therefore, it has been hypothesized that endogenous HGF can block the function of BMP-2 in osteoblasts<sup>109</sup>. Interestingly, through overexpression of c-Met, it was possible to convert primary human osteoblasts into osteosarcoma cells *in vitro*, displaying the characteristic phenotype of human osteosarcoma<sup>110</sup>.

3) *The HGF/c-Met signalling pathway in osteoclasts (Figure 7)*. C-Met is expressed on monocytes of peripheral mononuclear cells<sup>111</sup>. The formation of numerous vitronectin-positive multinucleated tartrate-resistant osteoclasts indicates that HGF promotes osteoclastic differentiation in the presence of RANKL<sup>112</sup>. The addition of a neutralizing antibody to M-CSF did not inhibit osteoclast differentiation. It is well established that HGF promotes the survival and proliferation of monocytes and osteoclasts in a similar way to M-CSF in viability assays and live/dead staining<sup>113</sup>.

HGF increased osteoclastic motility and spreading. In addition to recruiting osteoclasts to bone resorption sites, HGF may suppress resorptive functions during migration. Osteoblastic cells modulate osteoclast responses to HGF, thus enhancing osteoclast activity at resorptive sites<sup>114</sup>. Osteoclasts activated by HGF (2.5 ng/mL) receptors exhibit increased intracellular calcium concentrations and activated pp60 kinases. HGF (5 ng/mL) induces changes in osteoclast shape and stimulates DNA replication as well as chemotactic migration. Osteoclasts make and secrete biologically active HGF<sup>111</sup>. Osteoclastic differentiation and bone resorption activity were significantly inhibited by cabozantinib (a c-Met inhibitor). Cabozantinib decreased the expression of osteoclast marker genes, increased osteoprotegerin mRNA and protein levels and inhibited RANKL<sup>115</sup>.

## 1.6 Ischemia-induced hypoxia disrupted fracture healing via osteoblasts and osteoclasts

A sufficient supply of oxygen is essential for maintaining normal cellular and physiological functions<sup>116</sup>. Without enough oxygen provided, organism is generally forced to make adaptations to survive<sup>117</sup>. A definition for hypoxia in biologic context can be found at the oxygen concentration threshold where normal cellular functions become limited<sup>118</sup>. Usually, the physiological hypoxia response is triggered by depressed ambient oxygen partial pressure, insufficient oxygen diffusion and perfusion<sup>119</sup>. As demonstrated by the previous data, there is approximately 20% oxygen in the atmosphere, but only around 5% of it is found in the tissues. Consequently, tiny changes in oxygen tension can induce cellular oxygen stress, which activates the hypoxia pathway<sup>120</sup>.

HIF, or hypoxia-inducible factor, is a heterodimeric transcription factor that is crucial to the cellular response to hypoxia<sup>121</sup>. HIF, a heterodimer composed of an alpha and a beta subunit, the latter being a constitutively-expressed aryl hydrocarbon receptor nuclear translocator<sup>122</sup>. Hypoxia (less than 5% oxygen tension) reduces enzymes prolyl hydroxylase domains activity, resulting in HIF- $\alpha$  accumulation and translocation to the nucleus<sup>123</sup>. HIF- $\alpha$  then dimerizes with HIF- $\beta$  and binds to the hypoxia-response elements of HIF target genes, initiating the following downstream<sup>123</sup>. It is imperative for survival in hypoxic environments that HIFs are activated to regulate a variety of biological processes, such as vascularization, wound healing, pH level modulation, cellular apoptosis<sup>124</sup>.

Emerging evidence shows that unexpected pathological or environmental hypoxia may negatively affect the bone formation and remodeling<sup>125</sup>. The prevalence of poor bone mineral density can be observed in individuals with hypoxia-related disorders such as anemia or chronic obstructive pulmonary disease<sup>126,127</sup>. This situation is especially relevant to fracture healing. A fracture, especially when open or multi-segmental, is commonly complicated by a lack of blood supply to the injured site<sup>128</sup>. This is known as ischemia, and may cause hypoxia, nutrition deficiency, and osteoblast progenitor loss leading to fracture nonunion. In animal models, hypoxia is a common characteristic of fracture sites which correlates with bone cell apoptosis<sup>129,130</sup>. Accordingly, optimal tissue oxygenation promotes fracture healing by maintaining homeostasis, most notably in osteoblasts and osteoclasts.

Osteoblast-mediated mineralization of bone matrix is retarded by hypoxia and completely inhibited by anoxia<sup>131</sup>. In terms of mechanism, hypoxia suppresses not only osteoblast differentiation and activity, but also the transcription factor Runx2 and the PI3K/Akt pathway. This helps to explain why osteoblast progenitors are unable to differentiate into osteoblasts<sup>132–135</sup>. In osteoclasts, intermittent hypoxia exposure significantly promotes osteoclast differentiation and bone resorption, primarily due to the activation of reactive oxidative species<sup>136</sup>. It is interesting, however, that sustained hypoxia prevents osteoclast differentiation due to the induction of apoptosis<sup>137</sup>.

### **1.7 Knowledge gaps, research hypotheses and general aims**

The above studies provide a general picture of the background regarding hypoxia, c-Met, and fracture healing. Hypoxia regulates c-Met expression in various cell lines, especially in cancer cells, but bone cells are seldom studied. Hypoxia also suppresses osteoblast and osteoclast differentiation *in vitro*, suggesting that hypoxia is detrimental to normal bone formation. Analysis of an animal model of fracture repair showed that hypoxia induced by poor blood supply causes interruption of bone progenitor cell differentiation, subsequently leading to fracture nonunion. The relationship between c-Met and bone cells has not been well investigated. HGF/c-Met regulates the normal course of bone formation, particularly osteoblast and osteoclast activity, as demonstrated in the introduction. HGF/c-Met activation promotes osteoblast differentiation, osteoclast migration and bone resorption. Moreover, the literature indicates that osteoblast-induced callus formation and osteoclast-mediated bone remodelling are important contributors to fracture nonunion, which emphasizes the critical role of osteoblasts and osteoclasts in fracture healing.

Given the data presented above, we can summarize the knowledge gaps that exist between hypoxia, bone cells, c-Met, and fracture healing. First, how does c-Met exert its effects on osteoblasts and osteoclasts in fracture healing? Second, does c-Met cause fracture nonunion or delayed union? Third, what is the pattern of expression of c-Met in human fracture nonunion samples? Fourth, does hypoxia impair osteoblast and osteoclast differentiation by regulating the expression of c-Met?



We hypothesize that hypoxia induced by bone fracture results in suppression of c-Met, inhibiting osteoblast-induced bone formation and osteoclast-related callus resorption and contributing to the development of fracture nonunion. In order to answer our research questions, human bone samples obtained from participants with fracture union and nonunion will be collected to determine the expression of c-MET. To determine the effects of c-MET on bone cells, we will generate *c-Met*<sup>fl/fl</sup> mice possessing loxP sites flanking exon 16 of *c-Met* which codes for its catalytic domain. These mice are knockouts once the floxed exon is removed. Since c-Met is critical in development, we are concerned that these mice may not be viable. Thus, we will cross *c-Met*<sup>fl/fl</sup> mice with *Prx1*<sup>cre</sup> mice (to target osteochondral progenitors) or *Ctsk*<sup>cre</sup> mice (to target expression to osteoclasts) and investigate differences in fracture healing following a proximal femur osteotomy. Cell models will be established to explore the mechanism of c-Met in osteogenesis, particularly under hypoxic conditions.

Our current project has three goals: 1) to determine the expression pattern of c-Met as well as bone homeostasis in human fracture non-union samples; 2) to define the fracture healing phenotype in conditional knockout mice; and 3) to determine the role of c-Met in the regulation of osteoblastogenesis and osteoclastogenesis in a hypoxic environment.

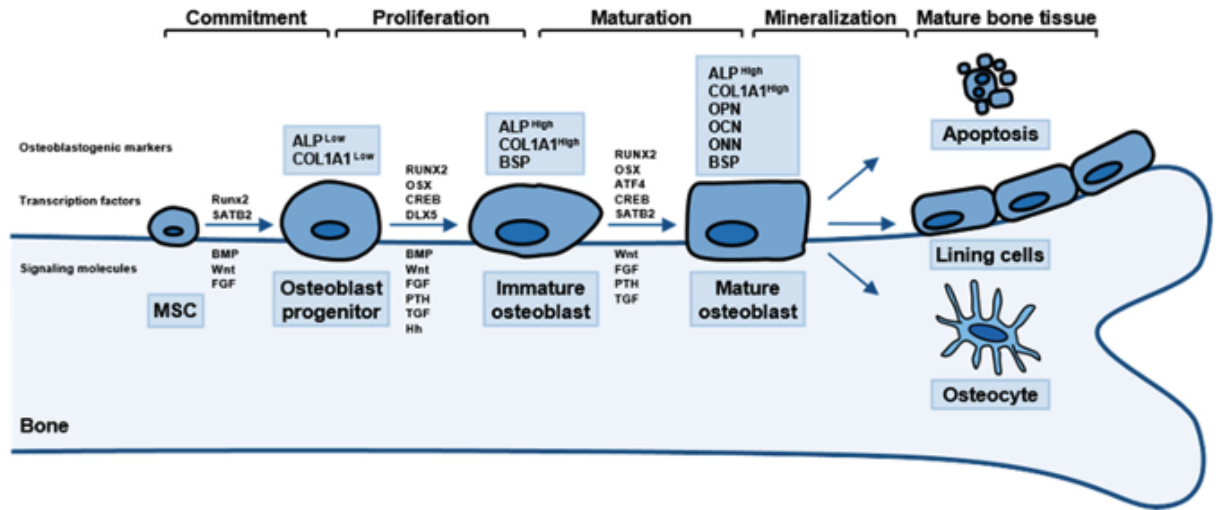


**Figure 1. The procedure of osteoblast differentiation from mesenchymal stem cell to osteoblast progenitor, immature osteoblast, finally differentiating into mature osteoblast.** (Cited Ref.: Amarasekara DS, Kim S, Rho J. Regulation of osteoblast differentiation by cytokine networks. International journal of molecular sciences. 2021;22(6):2851.)

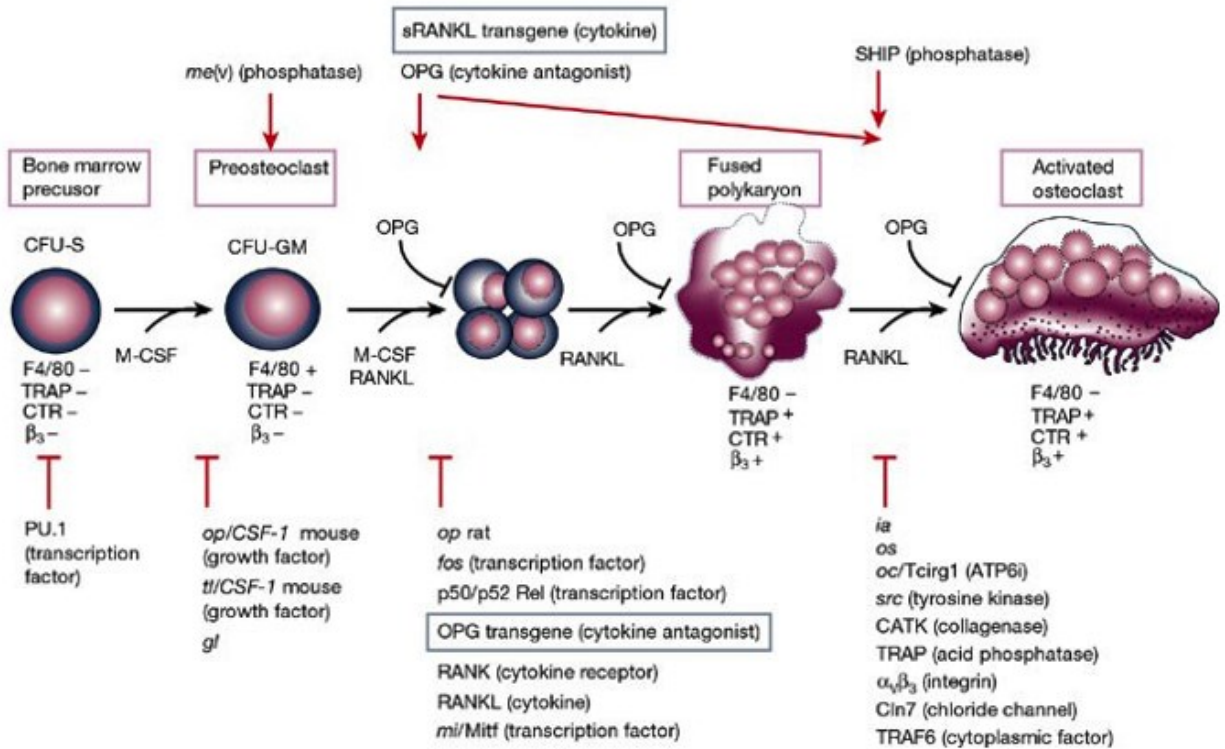


**Figure 2. The procedure of osteoclast differentiation from bone marrow precursor to pre-osteoclast, subsequently differentiating into activated osteoclast (Cited Ref.: Boyle WJ, Simonet WS, Lacey DL. Osteoclast differentiation and activation. Nature. 2003; 423(6937):337-42.).**

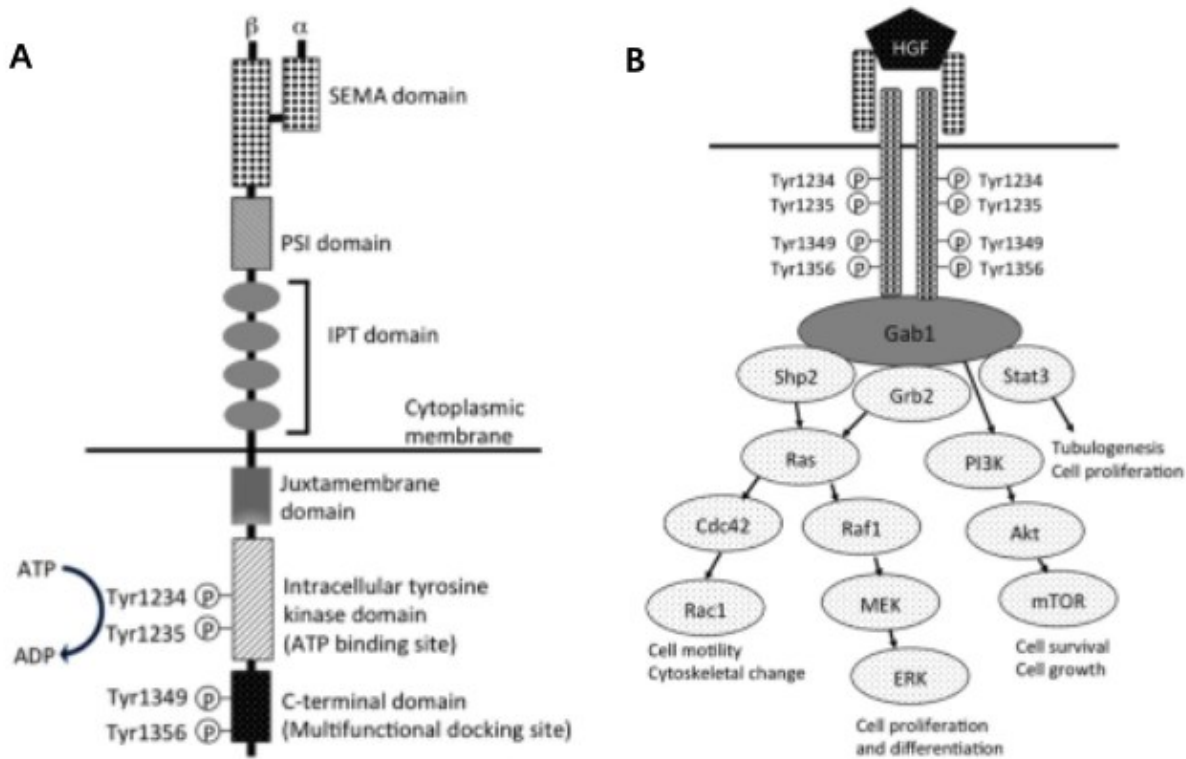


**Figure 3. (A) the molecular structure of c-Met. (B) the Hgf/c-Met system as well as its known downstream signaling pathways. (Cited Ref.: Kato T. Biological roles of hepatocyte growth factor-Met signaling from genetically modified animals. Biomedical reports. 2017;7(6):495-503.)**

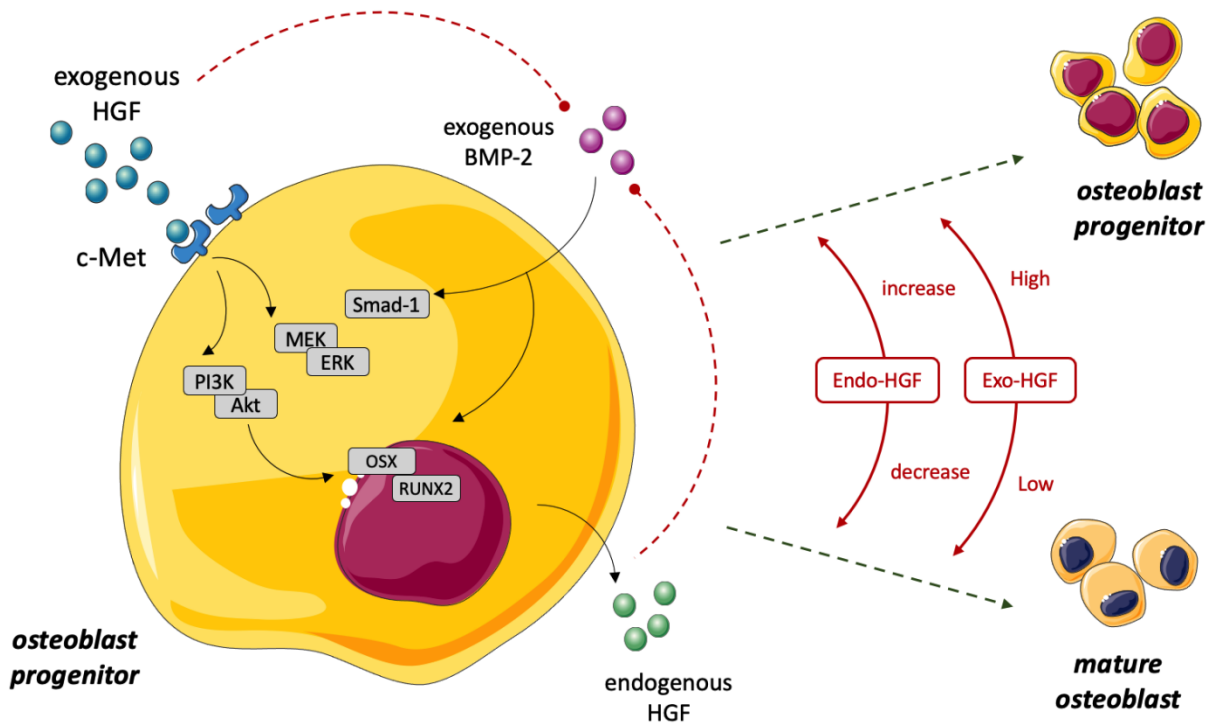


**Figure 4. HGF/c-Met signaling in regulation of osteoblast differentiation.**

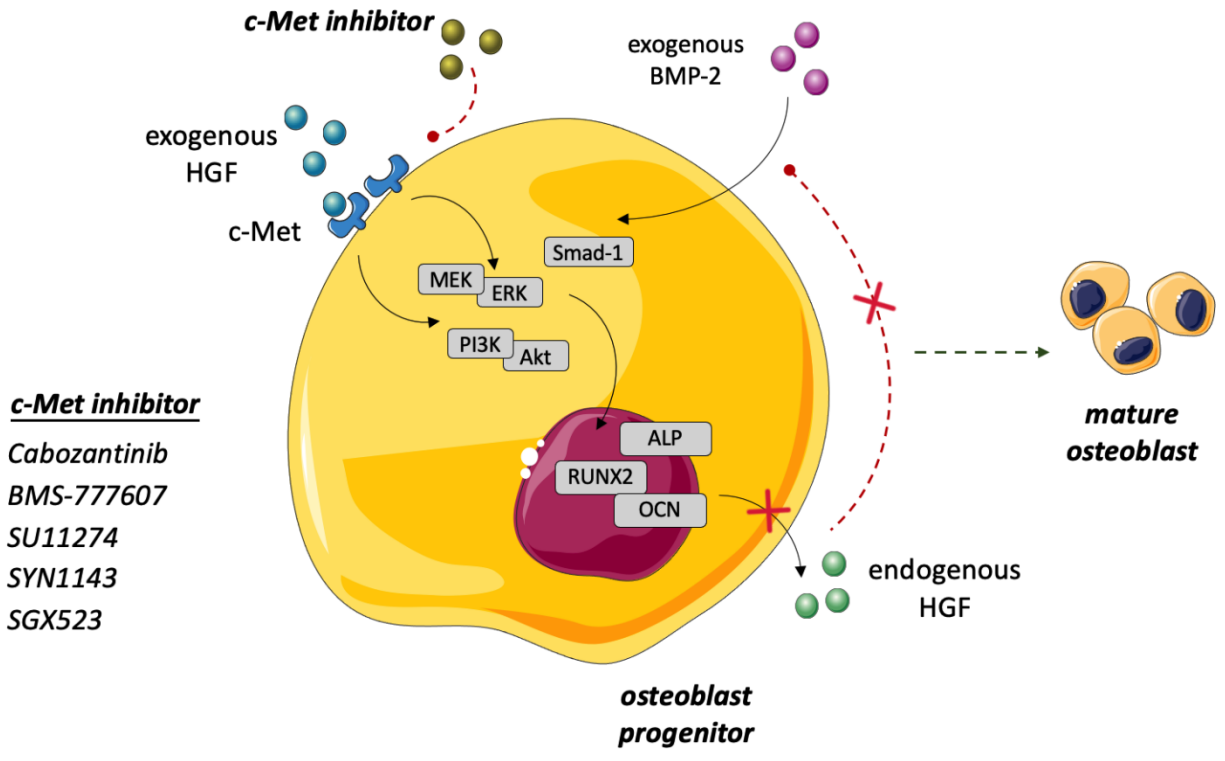


Figure 5. Types of c-Met inhibitors in regulating osteoblast differentiation.

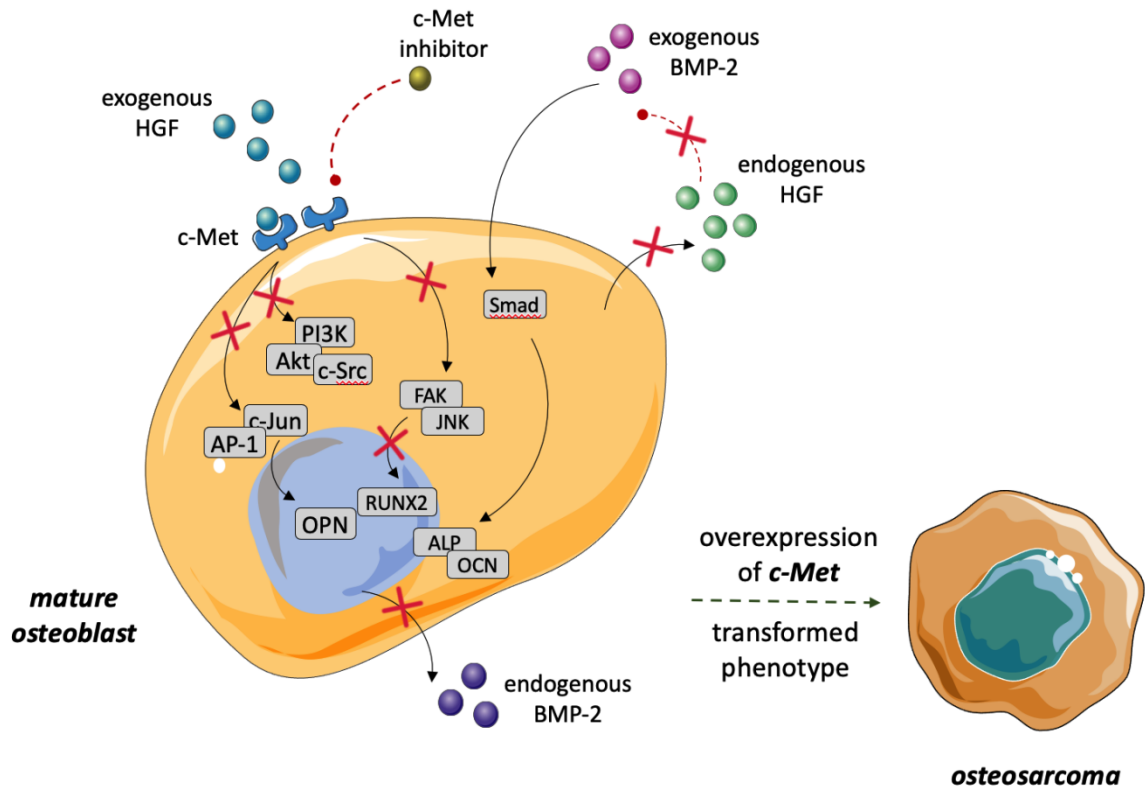


Figure 6. HGF/c-Met system in mature osteoblast regulation.

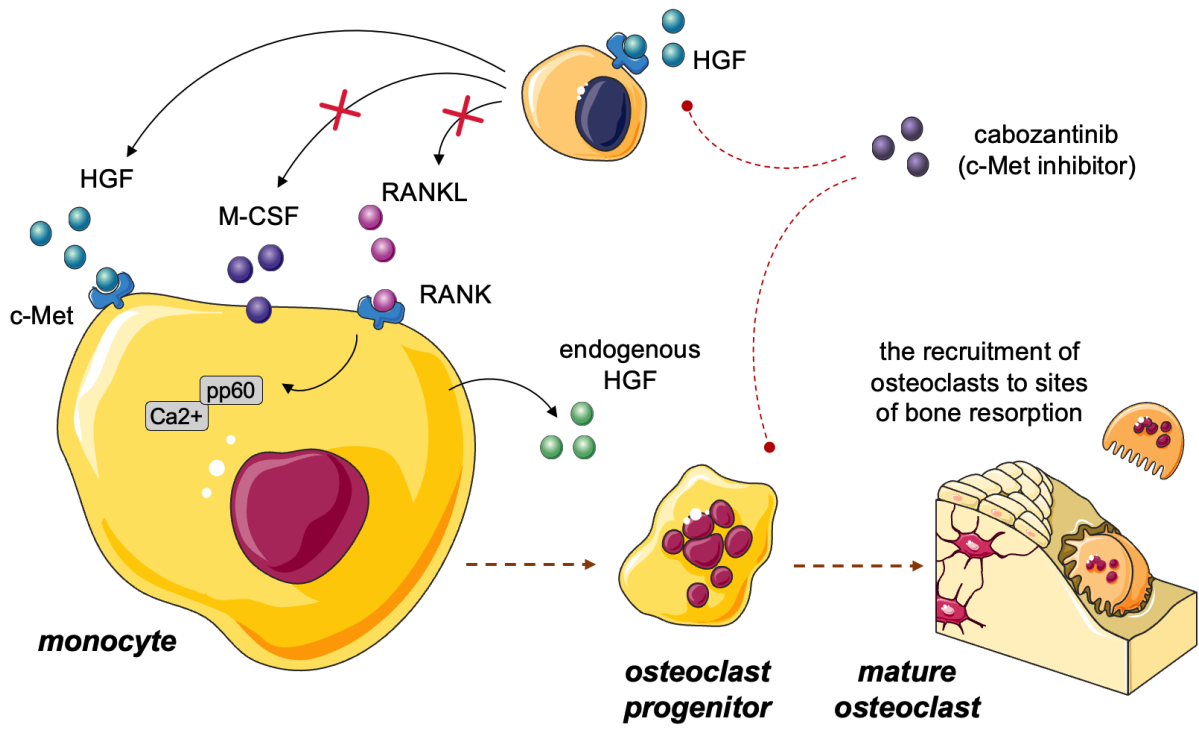


Figure 7. HGF/c-Met system in osteoclast differentiation.



## **CHAPTER 2**

### **c-MET Expression Patterns in Human Fracture Healing**

## 2.1 Abstract

Fracture nonunion is a widely prevalent problem in orthopaedics, and recent studies have explored the efficacy of exogenous HGF or c-Met inhibitors in accelerating fracture healing. Even so, data on c-Met involvement in fracture repair remains obscure, and human fracture nonunion samples have never been examined for c-MET expression. Our research first evaluated the gene and protein expression of c-MET and HGF by histology analysis, quantitative reverse transcription PCR (RT-qPCR), Western blot, and immunofluorescence assay in callus samples obtained from individuals who experienced a femoral neck fracture non-union and required a total hip replacement. We compared this group with individuals who sustained femoral neck fractures which healed but later needed a total hip replacement for reasons such as hip osteoarthritis or femoral head osteonecrosis. Our findings suggest that c-MET is highly expressed in fracture calli but significantly decreased in the fracture nonunion group. The expression of HGF was found to be positively correlated with c-MET expression in callus samples or control bone cubes from the greater trochanter. A decrease in bone metabolism was observed in patients with fracture nonunion when osteoblastic and osteoclastic markers and related genes were measured in serum and bone samples. Thus, we found significant alteration of c-MET in fracture nonunion, along with low osteoblast and osteoclast activity.

## 2.2 Introduction

The human skeleton has amazing regenerative properties, as it is one of the very few organs that can regenerate by partially replacing its cells in their normal orientation and strength<sup>1</sup>. In the event that the fracture is insufficiently immobilized, infection complicates the fracture, surgical intervention fails, or insufficient healing occurs, fracture "nonunion" results<sup>2,7,9</sup>. As previously discussed, fracture nonunion causes significant morbidity including pain and loss of mobility.

Managing fracture nonunion is a significant endeavour for an orthopaedic surgeon, and presents a unique clinical challenge. The success of nonunion treatment depends on the type of nonunion; union must be achieved through optimal stabilization of the fracture<sup>5,7</sup>; likewise, treatment must also augment vascularization of the fracture site and may be achieved via the use of grafts, biomaterials, biological agents, or cells<sup>13</sup>. Ultimately, surgery is the main approach

for nonunion. An operative procedure introducing stabilizing implants restricts mobility at the fracture site assisting the development of fracture union<sup>7,9</sup>.

Despite the success of surgical interventions, some fractures still do not proceed to union causing ongoing pain and suffering. Ultimately, an amputation of the affected limb may be required to restore quality of life. Thus, many researchers are investigating the use of biological agents, which have the potential to enhance the healing process without invasive surgery<sup>13</sup>. Currently, the wide-scale usage of additional biochemical stimuli such as growth factors has gained popularity amongst surgeons. To date, the most widely used method of inducing bone growth is the application of exogenous BMPs<sup>138</sup>. Although BMP2 has the potential to be an effective treatment, its clinical use is waning due to a variety of reported complications<sup>139</sup>. Despite its benefits in producing new bone, BMP2 has many adverse effects (such as ectopic bone formation), mainly because of the high doses used<sup>140</sup>. Alternatives to BMPs include the use of the human parathyroid hormone, applied as teriparatide, which has been proven to be helpful in treating nonunions<sup>141</sup>.

HGF/c-Met signalling has been shown to affect cellular growth, survival, motility, migration, and mitogenesis, as mentioned in the previous section<sup>94</sup>. Cellular activation of the c-MET ligand HGF leads to the proliferation of tissues and the regeneration of tissues<sup>96,98</sup>. To date, several well-established HGF gene therapy technologies have been applied in different disease models. For example, plasmid HGF gene therapy has shown promising results in clinical studies for peripheral arterial occlusive disease and has entered Phase III clinical testing<sup>142</sup>. Adenovirus-HGF (Ad-HGF), a replication defective type 5 adenovirus containing the human HGF gene, induced overexpression of HGF protein in primary myocardial cells, stimulating endothelial cells to grow and migrate<sup>143</sup>.

However, HGF gene technology is still in a preliminary stage of exploration in the treatment of the musculoskeletal system, especially in fracture repair. Observations from a fracture model indicated greater positive immunostaining for HGF and phosphorylated c-Met around the fracture site one day after fracture surgery was performed<sup>144</sup>. In addition, the expression of the BMP receptor 2 was detected in nearby mesenchymal cells. HGF facilitates BMP signalling, and BMP signalling is currently considered to be the underlying mechanism of fracture repair *in vitro*<sup>144</sup>. In a further molecular analysis of human osteoblasts, HGF was shown to induce

BMP-2 expression in a dose-dependent manner through the c-Met receptor/FAK/JNK/Runx2 and p300 signalling pathways. Inhibition of c-Met or siRNA treatment reduced HGF-mediated BMP-2 production<sup>108</sup>. All this data points to a positive role for HGF in fracture healing.

In this regard, it appears that exogenous HGF may be an effective agent in promoting fracture healing in pathological circumstances such as fracture nonunion. After injection of HGF protein in a murine model of fracture repair, the serum expression levels of inflammatory factors such as TNF- $\alpha$ , MCP-1, IL-1 and IL-6 were downregulated, while the levels of p65, I $\kappa$ B kinase- $\beta$  and I $\kappa$ B $\alpha$  as well as endothelial growth factor, BMP-2 receptor and receptor activator of NF- $\kappa$ B ligand in osteoblasts were upregulated in mice. As shown by the results, HGF helped heal injured blood vessels and revascularize tissue-engineered bone<sup>145</sup>. Similarly, in another *in vivo* study, the introduction of human HGF (hHGF) with a haemagglutinating virus of Japan envelope vector enhanced bone healing in rabbit models after an osteotomy. Three weeks after delivery, hHGF expression in bone peaked. As shown by radiography and histology, the hHGF group displayed greater fracture callus and mechanical strength<sup>146</sup>. For targeted HGF interventions, HGF was attached to semisynthetic extracellular matrix-like hydrogel (sECMH) through a tissue engineering method. More new vessels appeared in the defect area after only four weeks, and the bone defect aperture was sealed by mature cortical bone at the eighth week<sup>147</sup>. Other evidence identifies a close connection between HGF/c-Met signalling and fracture repair. For instance, c-Met chemical inhibitors, such as BMS-777607, have also been found to accelerate fracture callus development via osteogenesis<sup>107</sup>.

Undoubtedly, HGF is a highly promising exogenous growth factor for bone regeneration. However, the use of HGF as a therapeutic agent may be limited because HGF at levels exceeding the optimal dose may result in undesirable effects. Despite the fact that no renal or liver toxicity was observed, high doses of HGF may cause mesenchymal cells to proliferate without undergoing osteogenic differentiation, as discussed in the introduction. Thus, we have elected to explore the utility of the c-Met receptor in fracture repair.

Given the evidence presented in the introduction, and the above facts, the following are deduced. i) The suppression of osteoblastic callus formation and osteoclastic bone remodelling is a critical mechanism responsible for the development of fracture nonunion. ii) The HGF/c-Met signalling pathway plays a role in osteogenesis and has been shown to facilitate fracture

healing both *in vitro* and *in vivo*. Thus, we speculate that c-MET is differentially expressed in fracture nonunion bone tissue, resulting in diminished osteoblast-mediated bone formation and osteoclast-driven callus resorption in the secondary stage of fracture healing.

The purpose of this study was primarily to determine the patterns of c-MET expression in human bone tissue that was discarded at the time of joint replacement surgery following internal fixation for femoral neck fractures. An analysis of the fracture callus and its corresponding non-fracture cancellous bone was carried out using histomorphology and microarchitecture analysis. A variety of assays were used to analyse the expression of c-MET and HGF, as well as serum markers for osteoblasts and osteoclasts.

## **2.3 Methods and Materials**

### **2.3.1 Ethical approval**

Ethical approval for all procedures involving human participants was obtained from the ethics board of the First Affiliated Hospital of Guangzhou University of Chinese Medicine and University of Alberta. Informed consent was obtained from all participants involved, and experimental procedures were carried out in accordance with the approved guidelines.

### **2.3.2 Subject enrollment**

A total of ten participants undergoing total hip arthroplasty (THA) for femoral neck fracture at the First Affiliated Hospital of Guangzhou University of Chinese Medicine (Guangzhou, P.R. China) between June 2020 and December 2020 were enrolled in the study. The following medical information was obtained from participants: age, sex, height/weight (BMI), medical history, medication history, family history, and physical examination findings.

### **2.3.3 Inclusion and exclusion criteria**

The inclusion criteria were as follows: 1) male or female, aged 20-55 years old; 2) participants undergoing THA to manage femoral neck fracture or to rescue failure of internal fixation for fracture nonunion or because of femoral head osteonecrosis or arthritis; 3) participants had undergone internal fixation with screws for femoral neck fracture treatment more than five months prior to obtain a sufficient volume of fracture callus; and 4) participants who agreed to participate and completed the informed consent process. The exclusion criteria were as follows:

1) postmenopausal women or subjects >55 years old, participants affected by osteoporosis; 2) participants with pathological femoral neck fracture caused by tumors or osteomyelitis; and 3) participants affected by chronic diseases such as renal failure, pulmonary disease requiring steroid management, rheumatoid arthritis, ankylosing spondylitis or any other diseases that potentially alter bone mass.

#### **2.3.4 Group assignment**

Fracture calluses isolated from participants undergoing THA for fracture nonunion were assigned to the nonunion group (n=5), while calluses obtained from subjects undergoing THA for other reasons, such as femoral head osteonecrosis or arthritis, were assigned to the union group (n=5). Bone tissue was isolated from the greater trochanter of the femur and assigned to the nonunion control (n=5) and union control (n=5) (**Figure 8**).

#### **2.3.5 Pre-surgical data collection**

Subjects underwent a computed tomography (CT) scan of the fracture to enable a three-dimensional reconstruction of the fracture area and the surrounding bone tissue. Fifteen millilitres of blood were collected from each subject for enzyme-linked immunosorbent assays (ELISAs) of osteoblastic markers and osteoclastic markers.

#### **2.3.6 Sample collection**

THA involved a surgical incision over the anterior or lateral aspect of the affected hip. Damaged bone located at the proximal femur was removed, leaving the healthy bone intact. Fracture calli (no less than five pieces) were scraped off the fracture site. Bone cubes (10 mm × 10 mm) were removed from the greater trochanter to match the fracture callus from each individual. Fracture callus and bone cube samples were placed in liquid nitrogen and transferred to a -80 °C freezer for storage before testing (**Figure 9**).

#### **2.3.7 ELISA assay**

The previously collected blood samples were centrifuged to obtain serum for ELISA testing. Serum levels of osteoblastic markers (human bone alkaline phosphatase (BALP), human osteocalcin (OC), human pro-collagen I C-terminal propeptide (PICP), and human osteopontin (OPG)) and human osteoclastic markers (tartrate-resistant acid phosphatase (TRAcP), human C-terminal telopeptide (CTX), and human type I collagen N-telopeptide (NTX)) were

determined by ELISA. The ELISA kits used for the above testing were purchased from Jiangsu Meimian Industrial Co., Ltd. (Zhangjiagang, China).

### **2.3.8 Histomorphometric analysis**

Fracture callus and bone samples were fixed in formalin for 48 h and then decalcified using a 10% ethylenediaminetetraacetic acid (EDTA) soaking solution for approximately three weeks until soft. The samples were then dehydrated by passage through a series of increasing concentrations of ethanol, embedded in paraffin, and sectioned using a microtome (5 µm thick). Sections were prepared and stained by haematoxylin & eosin (H&E) staining to evaluate fracture callus formation, TRAcP staining to detect osteoclastic resorption, ALP staining to show osteoblastic activity and Masson's trichrome staining to show new bone formation and collagen tissue. A TRAcP staining kit (387A) was purchased from Sigma-Aldrich (St. Louis, MO, USA). A safranin O/fast green staining kit (G1053) and Masson's trichrome staining solution (G1006) were purchased from Wuhan Servicebio Technology Co., Ltd. (Wuhan, China).

### **2.3.9 Immunofluorescence**

For immunofluorescence, stored calli and bone cubes were placed in precooled 4% paraformaldehyde (PFA) solution for 4 h. Following decalcification with 0.5 M EDTA at 4 °C with continuous shaking, the samples were dissolved in a solution of 20% sucrose and 2% polyvinylpyrrolidone (PVP). After that, samples were embedded and frozen until testing. The sections were cut using a Leica microtome at a thickness of 20 µm. The prepared sections were permeated with 0.3% Triton X-100 and blocked with 5% BSA before being incubated with primary antibodies. Incubation of the sections with primary antibodies (1:500) against c-Met polyclonal antibody (PA5-85951, Thermo Fisher Scientific, Waltham, MA, USA) and HGF polyclonal antibody (PA5-115354, Thermo Fisher Scientific, Waltham, MA, USA) was performed overnight at 4 °C. After PBS washes, the sections were further incubated with HRP-goat anti-rabbit IgG (111-035-003, Jackson ImmunoResearch Labs, West Grove, PA, USA) and the corresponding secondary antibodies with DyLight® 594 (E032420-01, EarthOx Life Sciences, Burlingame, CA, USA) and DyLight® 488 (E032220-01, EarthOx Life Sciences, Burlingame, CA, USA). Then, 4',6-diamidino-2-phenylindole (DAPI) was used to stain the nuclei.

### **2.3.10 Micro-CT**

The trabecular bone microarchitecture of isolated samples was determined using high-resolution micro-CT (Scanco Medical AG, Zurich, Switzerland). Soft tissue around the samples was removed prior to assessment by a micro-CT machine. Analysis was performed using a 60-kVp X-ray source voltage, a 500  $\mu$ A current, 40 W power, an average of 6 frames, and a 0.5 mm thick aluminium filter for beam hardening. Structural parameters in a square region of interest (ROI) set as 6 mm  $\times$  6 mm were analysed with the program CT analyser (CT-An) in two- and three-dimensional images, including bone volume per tissue volume (BV/TV), number of trabeculae (Tb.N), connectivity density (Conn.Dn) and trabecular thickness (Tb.Th).

### **2.3.11 Western blotting assay**

Bone samples isolated from participants were crushed in liquid nitrogen in a cryotube by shaking with a sterile steel ball. This step was followed by extraction and solubilization of crushed samples in 2% sodium dodecyl sulphate (SDS) for 10 min at 70 °C in a volume corresponding to ten times the tissue wet weight with shaking. Equivalent amounts of extracted proteins were diluted in SDS-sample buffer with 5%  $\beta$ -mercaptoethanol and incubated at 95 °C for 5 min. Samples were then resolved by SDS-PAGE and transferred onto nitrocellulose membranes by electroblotting. Membranes were then blocked with 5% skim milk for 1 h and probed with primary antibodies overnight at 4 °C. Primary antibodies included c-Met (PA5-85951), HGF (PA5-115354), p-ERK1/2 (Thr202/Tyr204), ERK1/2 (Thr202/Tyr204), p-PI3K (Tyr458)/p55 Tyr199, PI3K (C73F8), p-Akt (Ser473) and Akt (C67E7). Membranes were washed and incubated with HRP-conjugated secondary antibodies (Sigma-Aldrich, Castle Hill, Australia) for 1 h. Immunoreactivity detection was performed using the Western Lightning Ultra and ImageQuant LAS 4000 luminescent image analyser. The intensities of the signals were quantified by ImageJ software. C-Met and HGF antibodies were purchased from Thermo Fisher Scientific (Waltham, MA, USA). p-ERK1/2, ERK1/2, p-PI3K, PI3K, p-Akt and Akt were obtained from Cell Signaling Technology (Danvers, MA, USA).

### **2.3.12 RT-qPCR**

Total RNA was isolated from the stored samples using a RNeasy Mini Kit in accordance with the manufacturer's instructions. For RT-qPCR, single-stranded cDNA was reverse tran-



scribed from 2 µg of total RNA using moloney murine leukaemia virus (MMLV) reverse transcriptase with an oligo (dT) primer. PCR was performed using 1 µl of cDNA using the following cycling parameters: 94°C, 40 seconds; 55°C, 40 seconds; 72°C, 40 seconds for 30 cycles with primers designed against the following human sequences: *h-RUNX2* (forward, 5'-GCTTCATTCGCCTCACAAAC-3'; reverse, 5'-GTAGTGACCTGCGGAGATTAAC-3'), *h-Osterix* (forward, 5'-CATTCTGGGCTTGGGTATCT-3'; reverse, 5'-TCACAC-TCCTCGCCCTATT-3'), *h-Osteopontin* (forward, 5'-CATATGATGGCCGAGGTGATAG-3'; reverse, 5'-TCACACTCCTCGCCCTATT-3'), *h-NFATc1* (forward, 5'-TCTGCAACGGGAA-GAGAAAG-3'; reverse, 5'-CACGGCTTACGGTTAGAAAGA-3'), *h-c-FOS* (forward, 5'-GGACTCAAGTCCTTACCTCTTC-3'; reverse, 5'-CCTGGCTCAACATGCTACTA-3'), *h-GAPDH* (forward, 5'-CAAGAGCACAAGAGGAAGAGAG-3'; reverse, 5'-CTACATGG-CAACTGTGAGGAG-3').

### 2.3.13 Statistical analysis

All data shown in this part are presented as the mean ± standard deviation from multiple independent tests. Each test was performed at least three times. Statistical significance was determined by Student's t test or analysis of variance (ANOVA), with *p* less than 0.05 regarded as significant. The normality for all data was measured by Shapiro-Wilk normality testing for the student's t test and ANOVA. The sample size was initially calculated for two experimental groups of 5 union patients and 5 nonunion patients by G\*Power software (Universität Düsseldorf, German), and a significance level of 5% and a statistical test power of 80% were considered.

## 2.4 Results

### 2.4.1 Demographic characteristic of unions and non-unions

This study included five fracture nonunion cases (3 males and 2 females; average age, 44.2 years; range, 37–56 years,) and five fracture union cases (males and 6 females; average age, 46 years; range, 38–54 years). The demographic characteristic of all enrolled cases can be found in **Table 1**.

#### **2.4.2 Osteoblastic and osteoclastic activities in serum are suppressed in fracture nonunion**

The three-dimensional micro-CT images indicate that the trabeculae present in the control bone cube samples were well connected, of normal thickness, and neatly arranged (**Figure 10A**). On the basis of quantitative analysis by microCT, Tb.BV/TV, Tb.Th, and Conn.D of fracture calluses with union and nonunion were reduced when compared to those of the control bone cubes, whereas Tb.Sp was greater (**Figure 10B-F**). In contrast, in the fracture callus samples, the trabeculae were thin and had a disorganized structure with irregular orientation due to the healing process with immature calli (**Figure 10A**). Th.N was higher in the callus of the union group than in any of the other groups but extremely low in the callus of the nonunion group (**Figure 10C**). The results indicate that callus formation was highly activated in the union group. The trabeculae were thicker in the control samples, but there were less trabeculae because of the damage caused by fracture.

Histopathological examination of the fractured samples showed abundant callus around the exiting trabecula, marked by a proliferative fibrous connective tissue response in the union group. In contrast, the nonunion group bone showed loosely filled hematoma tissue and a reduced amount of fibrous tissue. To match fracture calluses, we used bone cubes from the greater trochanter of each group as controls, and only the bone matrix was visible. Adipocytes surrounded the bone matrix, mainly because the samples were taken near the bone marrow cavity (**Figure 10G**).

#### **2.4.3 Failure of endochondral ossification, osteogenesis and resorption activity in human nonunion bone samples**

In histomorphology, enhanced endochondral ossification was detected in the union group by safranin-O staining. The orange to red colour change in bone slides indicates sufficient proteoglycan formation in the fracture site mediated by chondrocytes derived from mesenchymal stem cells. In the nonunion group, low levels of fibrocartilage were observed in the corresponding area (**Figure 11**). Similarly, Masson's trichrome staining, a commonly used method for new callus detection, was used to evaluate the bone samples from both groups. As shown, the red colour representing immature bone, collagen fibres, or osteoids was abundantly detected in the fracture site of the union group, demonstrating the formation of new fracture calli (**Figure 11**). In contrast, no colour change was found in the nonunion group, indicating poor osteogenesis at

the fracture site (**Figure 11**). TRAcP staining is a reliable marker for the identification of multinucleated osteoclasts. Our results show that more TRAcP-positive osteoclast-like cells were observed in the union group, but few were observed in the nonunion group (**Figure 11**). This finding suggests that osteoclast formation is suppressed in the latter group.

#### **2.4.4 Osteoblastic and osteoclastic activities in serum and bones are suppressed in fracture nonunion**

For investigation of the bone metabolism of patients with fracture nonunion, serum concentrations of the human osteoblastic and osteoclastic markers BALP, CTX-1, osteocalcin, PICP, OPG, TRAcP, CTX, and NTX were examined by ELISA. Compared with those in the union group, the osteoblastic and osteoclastic markers in serum were suppressed in the fracture nonunion group, except for OPG, indicating that the activities of osteoblasts and osteoclasts were suppressed in fracture nonunion (**Figure 12A-G**). OPG is largely expressed by osteoblast lineage cells and enable to compete with RANKL so that block the combination of RANKL and RANK. Less osteoclasts may cause less OPG secreted from osteoblasts. The unchanged serum OPG level mainly due to this negative feedback of osteoclasts acting on osteoblast.

RT-qPCR was carried out to measure the osteoblast- and osteoclast-related genes in the fracture callus and bone cubes of the union group and nonunion group. *RUNX2* is a key transcriptional regulator of cell proliferation in osteoblasts at the entry and exit of the cell cycle. *RUNX2* also stimulates osteoblast differentiation by acting downstream of *OSX*. *OPN* is an extracellular structural protein identified in osteoblasts and therefore an organic component of bone. In our study, *RUNX2*, *OSX* and *OPN* were reduced in individuals with nonunion (**Figure 12H and 12I**). In osteoclastogenesis, RANKL signalling is mediated by TRAF6, resulting in autoamplification of *NFATc1*. *c-Fos* mediates intermediate signals downstream of TRAF6. Accordingly, *c-Fos* and *NFATc1* are transcription factors required for osteoclastic differentiation. As demonstrated by our results, *c-FOS* and *NFATc1* levels were less expressed in fracture calluses and bone cubes taken from the nonunion group (**Figure 12K and 12L**).

#### **2.4.5 c-Met and HGF are down-regulated in the human nonunion bone samples**

RT-qPCR was performed on bone samples to determine the expression of the *HGF* and *c-MET* genes in human samples. The results suggested that *HGF* and *c-MET* were highly expressed in the fracture callus compared to the bone cubes in the union group (**Figure 13A and**

**13B**). Since HGF/c-MET signalling is involved in both osteoblastogenesis and osteoclastogenesis<sup>148</sup>, upregulated expression of both genes is linked to a metabolically active tissue repair process with increased osteoblast and osteoclast activity within the fracture callus. Neither gene was expressed in the nonunion group bone samples, indicating that bone regeneration was suppressed (**Figure 13A and 13B**). The ratio of *HGF* versus *c-MET* in bone samples from nonunion across the two kinds of samples in the two groups was not significantly different, revealing a positive correlation between *c-MET* and *HGF* gene expression in certain samples (**Figure 13C and 13D**). The results were further reinforced by a Pearson correlation coefficient among the above samples (**Figure 13E and 13F**).

c-MET and HGF antibodies were used in immunofluorescence to visualize the c-MET receptor and its ligand in human callus and bone specimens. c-MET and HGF primarily manifested in the fracture callus and surface of trabeculae, both of which are responsive to bone modelling and regeneration. Decreased expression of c-MET and HGF was observed in the fracture calli of the nonunion group where there is suppressed bone healing (**Figure 13G**).

In the Western blot assay, c-MET and HGF expression was reduced in fracture calluses of the nonunion group, which was consistent with the outcomes of RT-qPCR and immunofluorescence (**Figure 14A-C**). ERK and PI3K/Akt are two main downstream targets of HGF/c-Met signalling. The phosphorylation of ERK, PI3K and Akt contributes to the bioprocess of fracture repair, specifically cellular proliferation, differentiation, and cell survival. In our present study, the downstream factor ERK was downregulated in the fracture callus of the nonunion group, as demonstrated by the quantitative results (**Figure 14A and 14D**). Notably, the phosphorylation of PI3K and Akt was upregulated in both the fracture calli with union and nonunion, with no significant difference between the results (**Figure 14A and 14E**). This finding suggests that PI3K/Akt may not be involved in fracture non-union. Alternatively, the phosphorylation of these factors may not have altered due to the stability of the disease process.

## 2.5 Discussion

Fracture nonunion is characterized by a persistent unrepaired fracture site and less callus formation<sup>9</sup>. Consistent with this observation, we found, as revealed by Masson's trichrome and H&E staining, we also found reduced new bone formation and more fibrous cartilage noncallus

tissue was observed in the nonunion calli of participants. It is established that fracture nonunion is accompanied by poor vascularization and depressed bone remodelling<sup>7</sup>. Angiogenesis may be deficient in patients with fracture nonunion at the early stage of the disease. An increased degree of ischaemia surrounding a fracture site would thus be predicted to lead to fracture nonunion. In contrast, suppression of osteoblastic and osteoclastic activities are responsible for the late stage of fracture nonunion, since bone reestablishment is the end point of fracture healing<sup>2,4,5</sup>. Our study participants sustained femoral neck fractures more than five months ago. The callus samples obtained from the subjects undergoing THA were in the late stages of fracture healing and consequently showed evidence of depressed bone metabolism. Histomorphological analysis in our study revealed a low number of TRAcP-positive osteoclasts and fewer attached osteoblasts on bone surfaces. Additionally, the inhibition of osteoblastic markers as well as osteoclastic markers supports the above findings from the bone samples. Collectively, our results demonstrate that decreased osteoblast-induced callus formation and decreased osteoclast-mediated bone remodelling were associated with the late stage of fracture nonunion. Note that serum osteoblastic and osteoclastic markers are only used to reflect the status of bone metabolism in nonunions and unions. It is, however, inaccurate to diagnose specific skeletal diseases by using those markers because their changes can be caused by a variety of bone pathogenesis, including fracture nonunion, osteoporosis, osteoarthritis, osteosarcoma<sup>149</sup>.

No definitive research or direct evidence on c-Met receptor on fracture non-union has been published. However, some research indicates that it plays a role in fracture healing, specifically through HGF treatment or inhibition of c-Met<sup>107,144</sup>. An argument may be made over whether c-Met plays a positive or negative role in fracture healing. Injection of exogenous HGF activating the c-Met receptor at the appropriate dose promotes significant fracture healing, supporting the possible beneficial role of c-Met in this disease<sup>144</sup>. There is, however, some evidence suggesting that a c-Met inhibitor, BMS-777607, can also enhance bone regeneration following fracture repair by enhancing the activity of mTORC1<sup>107</sup>. The result of the latter study appears at odds with the claim from the former study. To date, no one has determined the expression of c-MET, (either gene or protein) in fractures with nonunion compared to well healed fractures.

Activation of HGF/c-Met has been demonstrated to promote cellular proliferation and damaged tissue repair in multiple organs<sup>150</sup>. In our present study, fractures in union participants showed high activation of c-MET in bone marrow and fracture calli, indicating that the HGF/c-

MET-mediated tissue repair procedure was triggered. In contrast, extremely low levels of c-MET expression in fracture nonunion callus samples seemed to support the functional importance of c-Met in fracture healing. Contrary to our expectations, it was surprising to find low levels of c-MET expression in control bone cube samples in the fracture nonunion group. Since c-MET expression was reduced in more than just the focal area of nonunion, it was logical to suggest that altered expression of c-Met represented a systemic change in the skeleton. Certainly, there is still confusion regarding whether c-Met is an inducer of fracture healing. Our limited data suggest a downregulation of c-Met expression appears to be closely related to fracture nonunion.

Endogenous HGF secretion is correlated with c-Met expression in skeletal cells. It has been demonstrated that c-Met regulation is only initiated if endogenous HGF levels are low in osteoblast progenitors<sup>103</sup>. Our RT-qPCR and immunofluorescence results showed that HGF expression was positively correlated with c-MET expression in fracture calli and control bone cubes. The findings suggest that *HGF* expression is positively correlated with *c-MET* expression. Nonunion alters not only *c-MET* expression but also endogenous *HGF* secretion. The findings of our study suggest an underlying intrinsic contribution of the HGF/c-MET system in fracture nonunion.

Overall, our study found that participants with fracture nonunion showed less callus formation and bone remodelling, and depressed bone turnover both in serum and bone markers. This finding suggests that deficiency of osteoblasts and osteoclastic activity is one of the prominent features of fracture nonunion in the late stage. In addition, c-Met, which is highly expressed in fracture calli, was decreased not only in the fracture site but also in the control greater trochanter of participants with fracture nonunion. A positive correlation exists between HGF and the expression of c-MET, so HGF is also suppressed in the bone tissues of patients with nonunion. Our findings reveal that the low osteogenesis activity and the low expression of c-Met, are linked to fracture non-union. Their potential mechanism will be explored in the following chapter through the use of transgenic murine models.

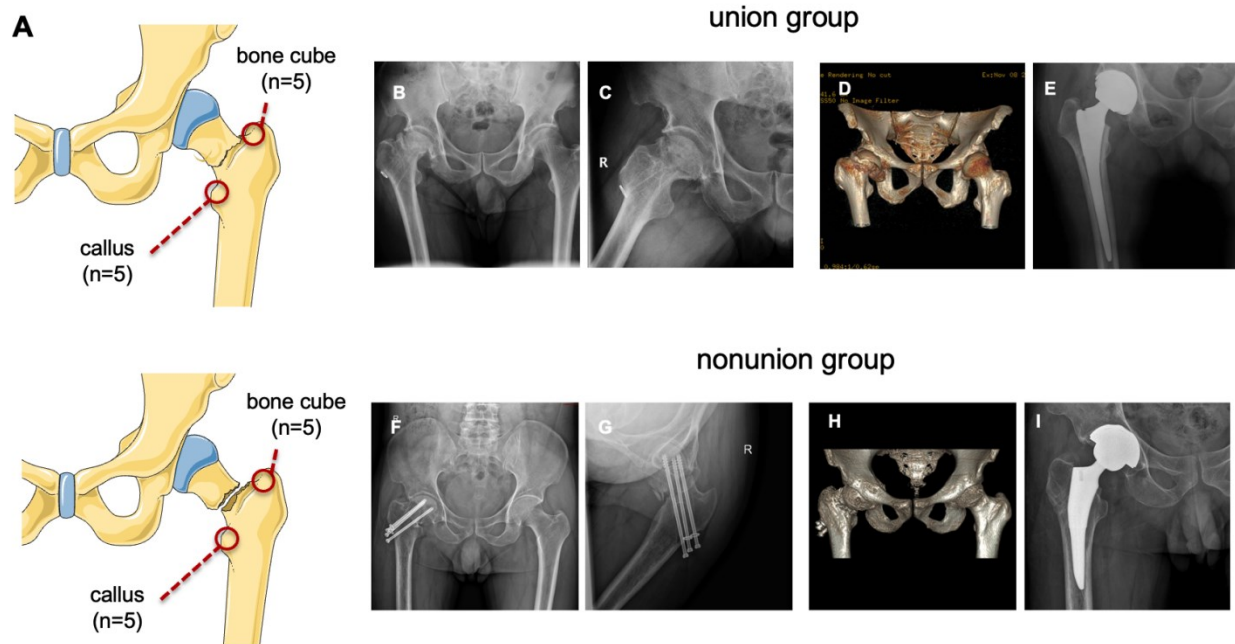


**Figure 8. Group assignment of samples from control volunteers and subjects with nonunion.**

(A) Fracture calli and bone cubes isolated from subjects undergoing total hip arthroplasty (THA) for fracture nonunion were assigned to the nonunion group, while samples obtained from subjects undergoing THA for other reasons, such as femoral head osteonecrosis or arthritis, were assigned to the union group. (B-E) A case of fracture nonunion enrolled in the study. Radiographic images (B and C) and CT images (D) of the hip joint before THA and radiographic images of the hip joint after THA surgery (E) are presented. (F-I) A case of osteonecrosis and hip osteoarthritis enrolled in the study. Radiographic images (F and G) and CT images (H) of the hip joint before THA and radiographic images of the hip joint after THA (I) are presented.

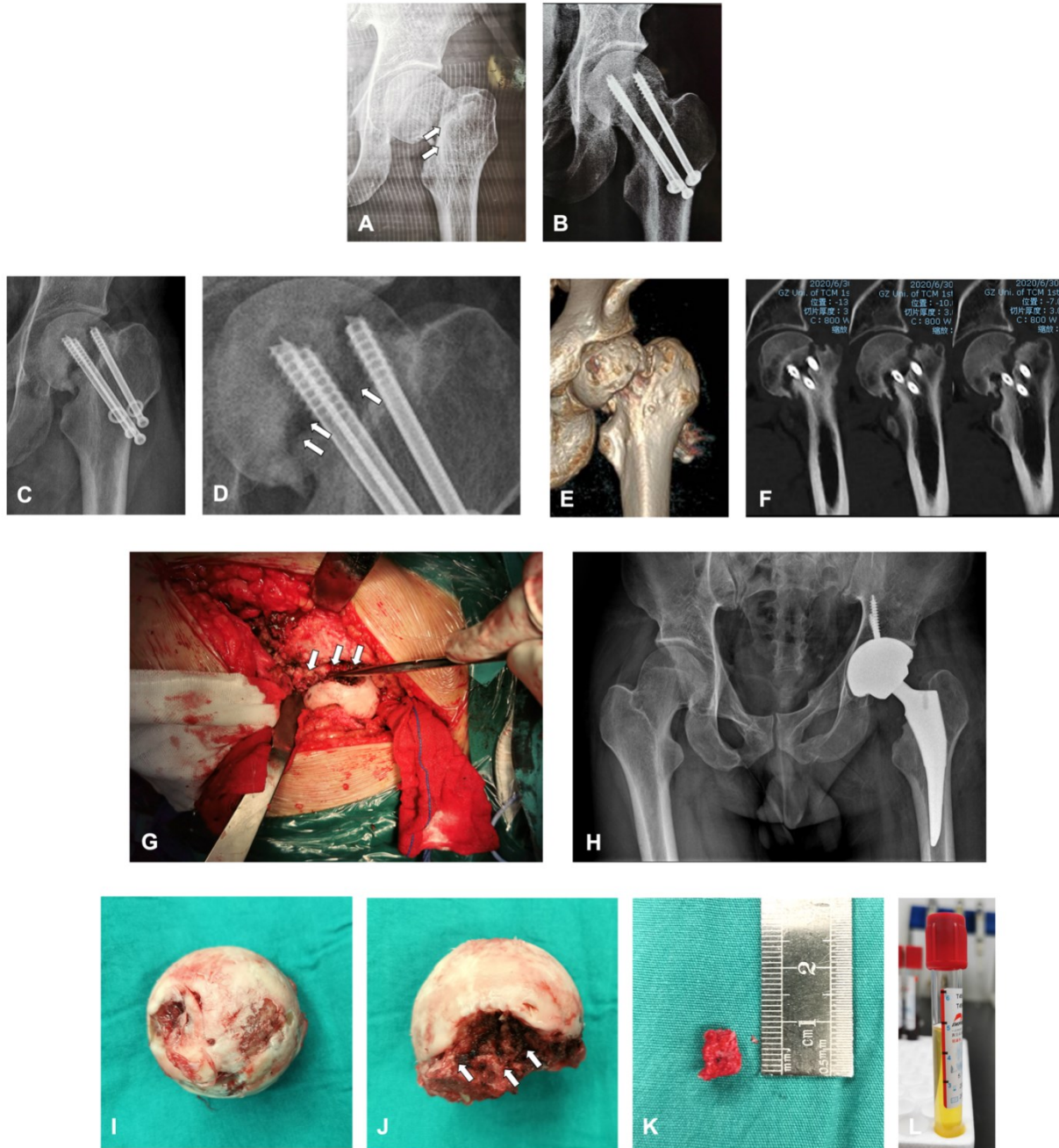


**Figure 9. Samples were collected from control volunteers and patients with nonunion.**

(A) A patient with fracture nonunion who suffered from femoral neck fracture. White arrows point to the fracture gap of the femoral neck. (B) The patient underwent internal fixation surgery. The radiographic image shows the operated hip joint after the preservation surgery. (C-D) The radiographic images show that the fracture of the patients did not show healing for one year after internal fixation. The white arrows point to the nonunion fracture gap of the femoral neck. (E-F) CT images



show discontinued femoral neck in two- and three-dimensional views. **(G)** Total hip arthroplasty (THA) performed on patients with fracture nonunion. THA involves a surgical incision over the anterior or lateral aspect of the affected hip. Fracture calluses were scraped off the fracture site (white arrows). Bone cubes were removed from the greater trochanter to match the fracture callus samples. **(H)** Radiographic image of the surgical hip joint after THA. **(I)** The isolated femoral head. **(J)** Fracture calluses obtained from the bottom of the femoral neck. **(K)** Bone cube from greater trochanter. **(L)** Serum centrifuged from the whole blood of the patient.

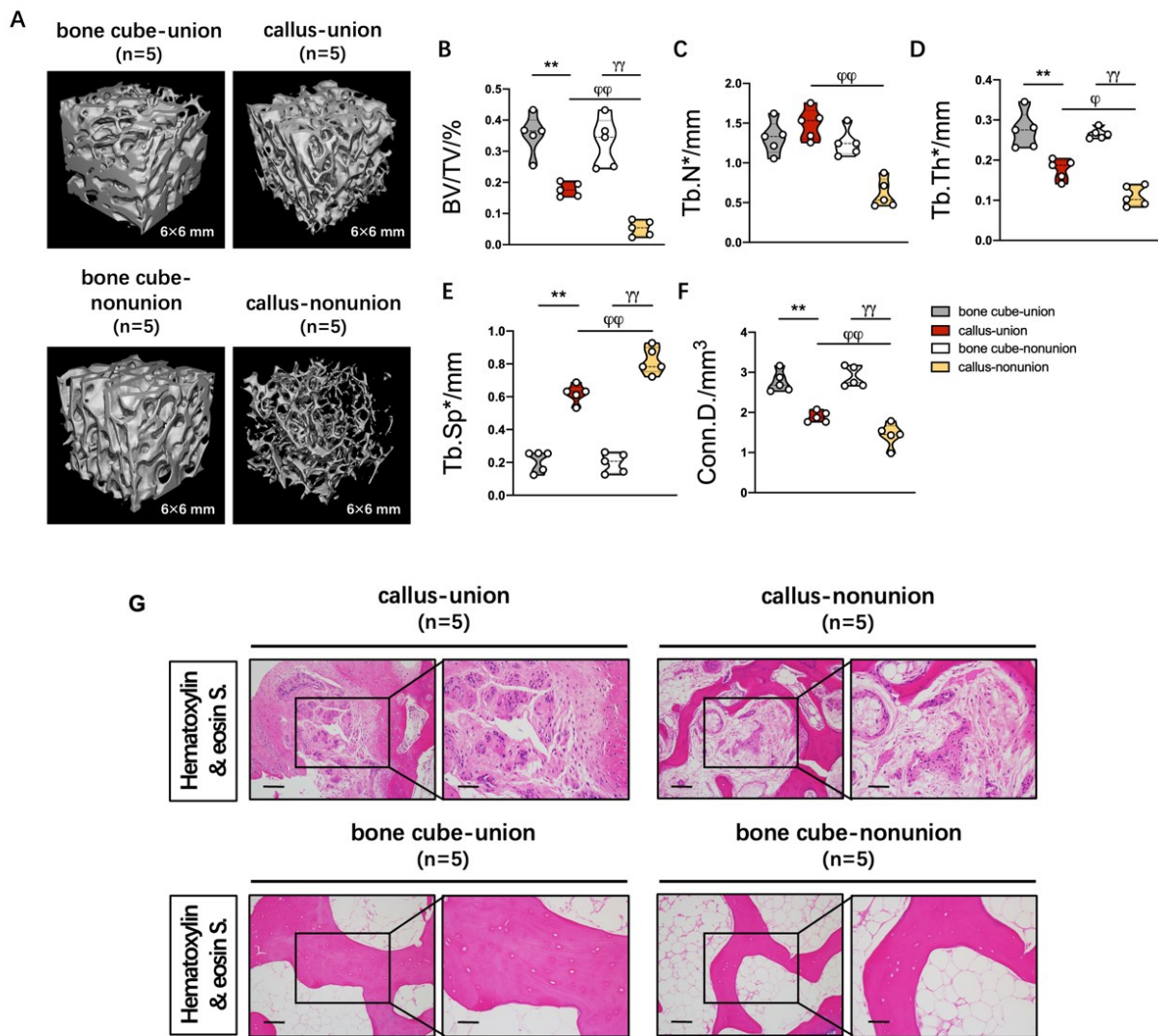


**Figure 10. Morphological changes in fracture calli and control bone cubes obtained from the union group and nonunion group.**

(A) Representative three-dimensional micro-CT images of fracture calli and control bone cubes from the union group and nonunion group (n=5). (B-F) Quantitative analysis of bone volume per tissue volume (BV/TV), number of trabeculae (Tb.N), separation of trabeculae (Tb.Sp), connectivity density (Conn.Dn) and trabecular thickness (Tb.Th) for the micro-CT analysis (n=5). (G) Representative images of H&E staining of fracture calli and control bone cubes from the union group and nonunion group (n=5). Scale bar: 150  $\mu\text{m}$  (left) and 50  $\mu\text{m}$  (right). \*\* $p < 0.01$  versus to

the bone cube of union group.  $\varphi p < 0.05$ ,  $\varphi\varphi p < 0.01$  versus to the fracture callus of union group.  
 $\gamma p < 0.01$  versus to the bone cube of nonunion group.

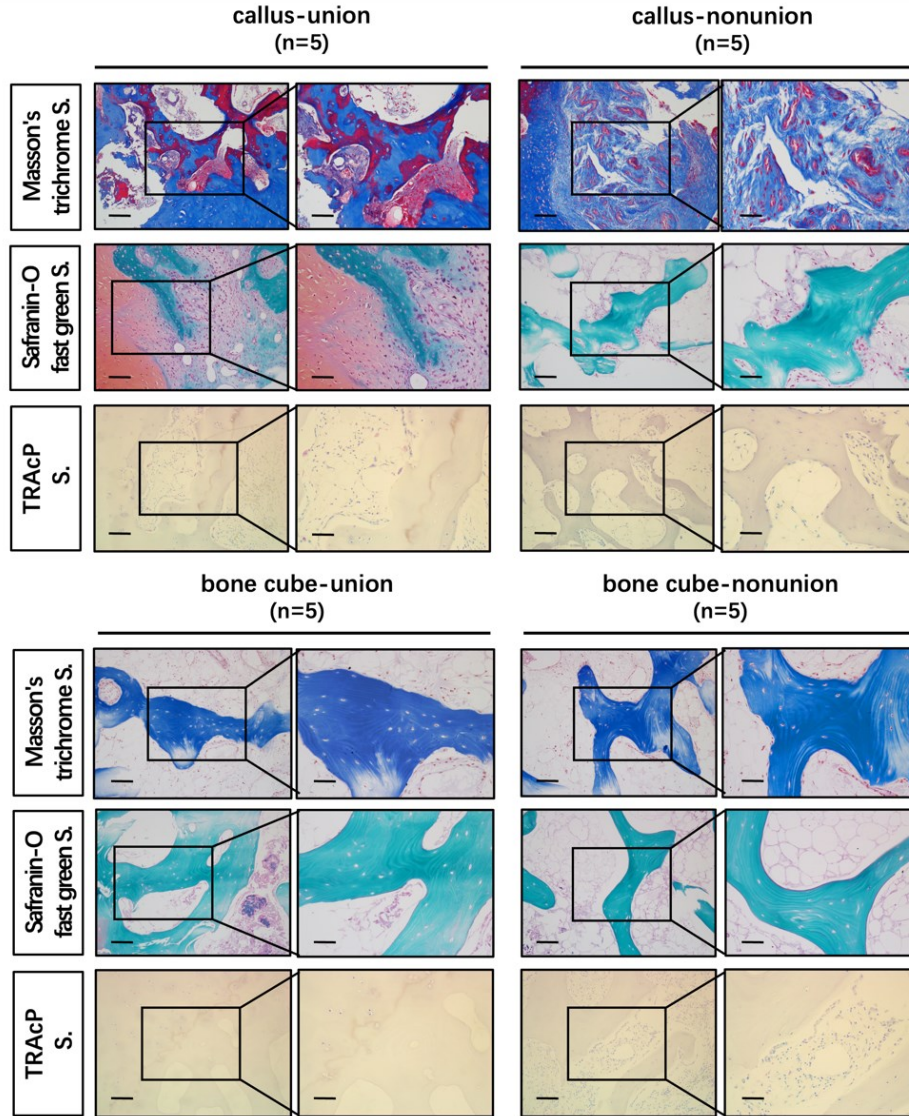


**Figure 11. Safranin O/fast green staining, Masson's trichrome staining and TRAcP staining of fracture calli and bone cubes obtained from the union group and nonunion group.**

(A) Representative three-dimensional micro-CT images of the fracture callus from the union group and nonunion group (n=5). (B) Representative three-dimensional micro-CT images of the control bone cubes from the union group and nonunion group (n=5). Scale bar: 150  $\mu\text{m}$  (left) and 50  $\mu\text{m}$  (right).

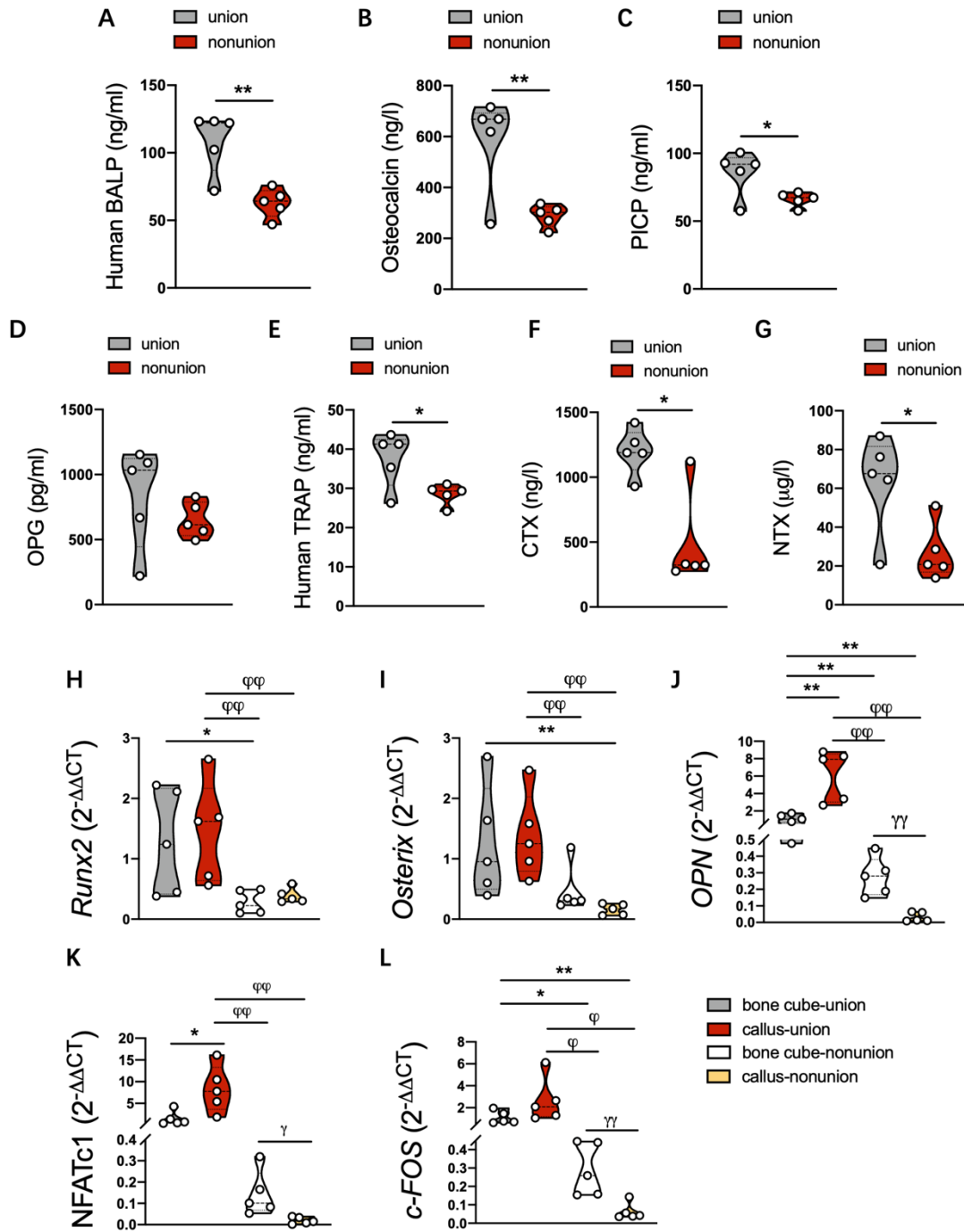


**Figure 12. Osteoblastic and osteoclastic markers and genes expressed in the serum and bone samples of the union group and nonunion group.**

**(A-G)** Quantitative analysis of serum levels of osteoblastic markers (bone alkaline phosphatase (BALP), tartrate-resistant acid phosphatase (TRAcP), C-terminal telopeptide (CTX-1), osteocalcin (OC), pro-collagen I C-terminal propeptide (PICP), and osteoprotegerin (OPG)) and osteoclastic markers (tartrate-resistant acid phosphatase (TRAcP), C-terminal telopeptide (CTX), and type I collagen N-telopeptide (NTX)) in the union group and nonunion group (n=5). **(H-L)** Expression of osteoblast- and osteoclast-related genes, including Runt-related transcription factor 2 (*RUNX2*), *Osterix*, Osteopontin (*OPN*), nuclear factor of activated T cells 1 (*NFATc1*), and *c-Fos*, in the union group and nonunion group (n=5). \* $p < 0.05$ , \*\* $p < 0.01$  versus to the bone cube of union group.  $\phi p < 0.05$ ,  $\phi\phi p < 0.01$  versus to the fracture callus of union group.  $\gamma p < 0.05$ ,  $\gamma\gamma p < 0.01$  versus to the bone cube of nonunion group.

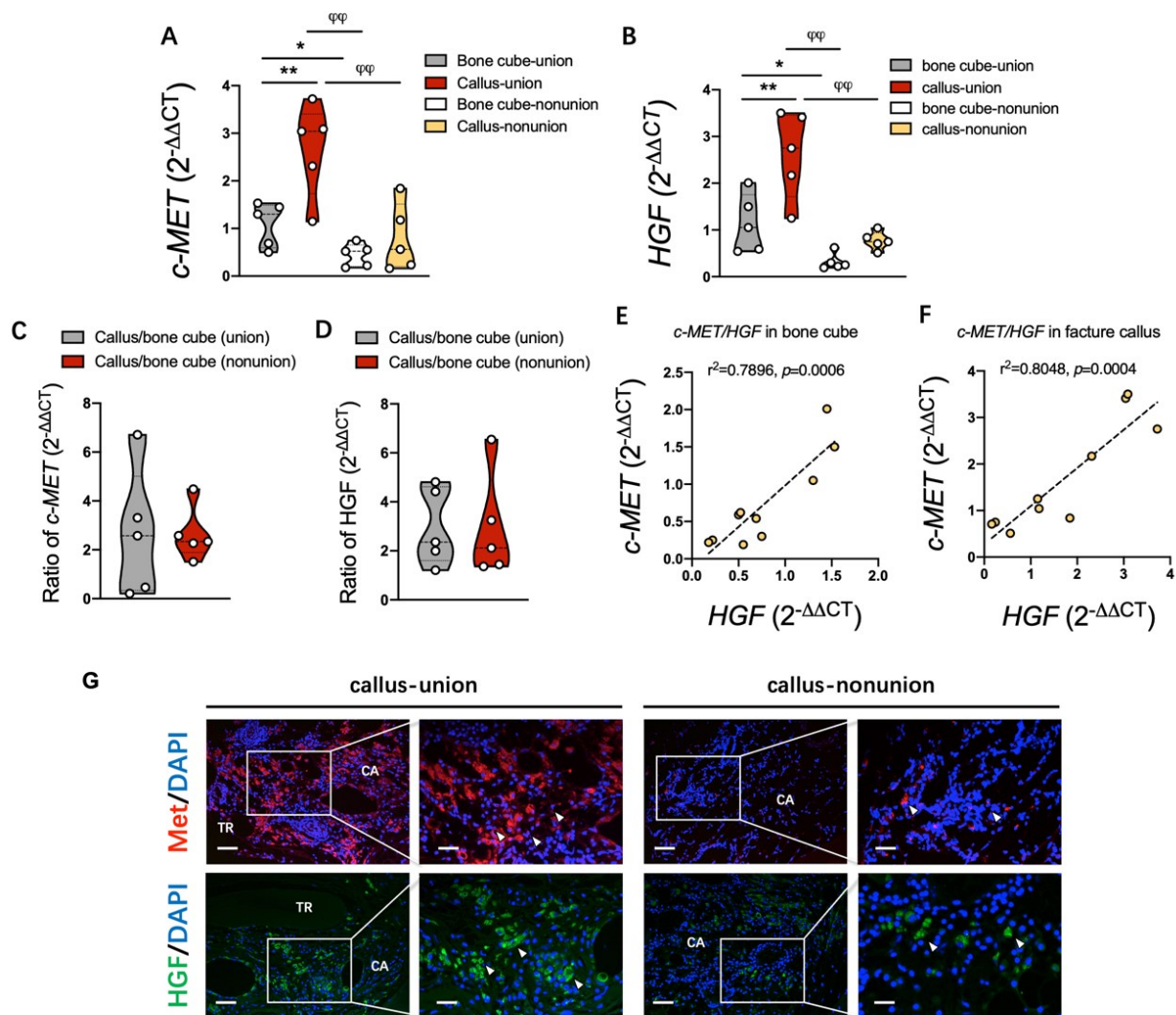


**Figure 13. *c-MET* and *HGF* expression in bone samples of the union group and nonunion group.**

**(A-B)** Quantitative analysis of the gene expression of *c-MET* and *HGF* in bone samples of the union group and nonunion group. **(C-D)** Ratio of *c-MET* and *HGF* gene expression in fracture calluses versus bone cubes in the union group and nonunion group. **(E-F)** Pearson correlation coefficient of the *c-MET* and *HGF* gene expression of fracture calluses and bone cubes in the union group and nonunion group. **(G)** Representative images of immunofluorescence of *c-MET* and *HGF* in the fracture calluses of the union group and nonunion group. In the Pearson correlation coefficient,  $r^2$  is the correlation index of *c-MET* and *HGF* gene expression, and the  $p$  value is the statistical analysis for  $r^2$ . Scale bar: 150  $\mu$ m (left) and 50  $\mu$ m (right). \* $p < 0.05$ , \*\* $p < 0.01$  versus to the

bone cube of union group.  $p < 0.01$  versus to the fracture callus of union group. TR: trabecula, CA: callus, AD: adipocyte, BM: bone marrow.



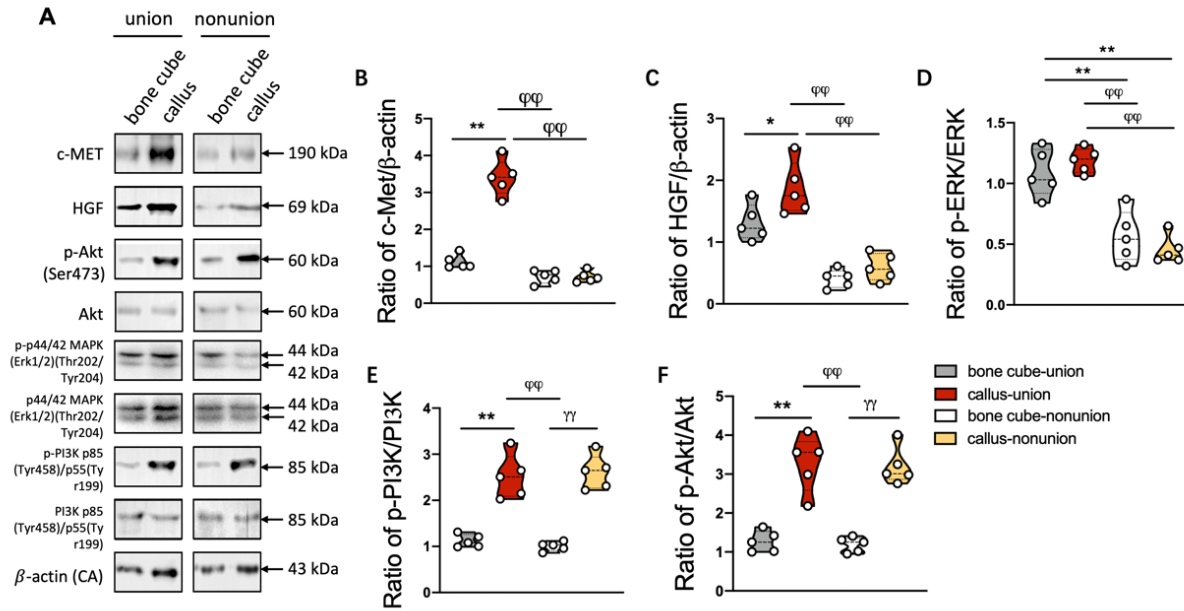


**Figure 14. Protein expression of c-Met, HGF and the downstream signaling factors in fracture calluses and bone cubes of the union group and nonunion group.**

(A) Representative images of Western blot of c-Met, HGF, p-ERK1/2, ERK1/2, p-Akt, Akt, p-PI3K and PI3K in fracture calluses and bone cubes of the union group and nonunion group. (B-F) Quantitative analysis of c-Met, HGF, p-ERK1/2, ERK1/2, p-Akt, Akt, p-PI3K and PI3K. \* $p < 0.05$ , \*\* $p < 0.01$  versus to the bone cube of union group.  $\phi\phi p < 0.01$  versus to the fracture callus of union group.  $\gamma\gamma p < 0.01$  versus to the bone cube of nonunion group.

**Table 1. Demographic characteristic of unions and non-unions.**

	<b>Union (n=5)</b>	<b>Non-union (n=5)</b>
<b>Average age (yr, age range)</b>	44.2 (37–56)	46 (38–54)
<b>Female/Male (n)</b>	3:2	4:1
<b>Average BMI (kg/m<sup>2</sup>)</b>	23.76	22.46
<b>Race/ethnicity</b>	Asian (Chinese)	Asian (Chinese)
<b>Indications for THA (n)</b>		
Fracture non-union	0	5
Osteoarthritis of hip	5	0
Osteonecrosis of femoral head	5	0
<b>Average time for undergoing THA after internal fixation (yr)</b>	2	2.3
<b>Underlying disease (n)</b>		
Renal failure	0	0
Pulmonary disease (requiring steroid management)	0	0
Rheumatoid arthritis	0	0
Ankylosing spondylitis	0	0
Others	0	0
<b>Personal history (n)</b>		
Current smoker	0	0
Drug abuser	0	0
<b>Family history (n)</b>		
Family members with fracture nonunion	0	0

\* BMI: body mass index; THA: total hip arthroplasty

## **CHAPTER 3**

### **The Phenotypes and Expression Changes of *c-Met* in Fracture Model Made by Conditional Knockout *c-Met* Mice**

### 3.1 Abstract

We have previously found decreased c-MET expression and bone cell activity in fracture non-union samples. In order to determine the effect of c-Met on osteoblastogenesis and osteoclastogenesis, we created transgenic mouse model where c-Met is knocked-out in either osteoblasts or osteoclasts. Mice with exon 16 of Met floxed were first created. *c-Met<sup>fl/fl</sup>* mice were crossed next with *Prx1<sup>Cre</sup>* mice or *Ctsk<sup>Cre</sup>* mice to specifically knock out *c-Met* in osteochondral progenitors and osteoclast precursors, respectively. We found that the heterozygous transgenic mice did not show abnormal bone development at birth. However, we found osteopenia and increased bone formation in older *c-Met<sup>fl/fl</sup>*, *Prx1<sup>Cre</sup>* mice and *c-Met<sup>fl/fl</sup>*, *Ctsk<sup>Cre</sup>* mice, respectively. We next used a murine fracture model to study bone repair and identified delayed fracture healing. Specifically, *c-Met<sup>fl/fl</sup>*, *Prx1<sup>Cre</sup>* mice demonstrated reduced callus formation at the fracture site whereas the *c-Met<sup>fl/fl</sup>*, *Ctsk<sup>Cre</sup>* mice exhibited less callus resorption.

### 3.2 Introduction

Targeted deletion of the *c-Met* gene has shed light on the essential roles played by the HGF-Met system in embryogenesis<sup>151</sup>. Deletion of *c-Met* leads to embryonic death between E13 and E16.5<sup>152</sup>. Therefore, a conditional knockout (cKO) murine model is required to study the role of *c-Met*. cKO mice have revealed that the HGF-c-Met system is responsible for regenerating various epithelial sites. In light of this data, we hypothesize the role of HGF-c-Met tissue repair is similar in many organs.

The Cre-loxP system enables a selective knockout of c-Met in specific cells<sup>153,154</sup>. Floxing refers to the addition of lox P sites between a DNA segment of interest so that the region can be deleted upon Cre recombinase mediated recombination. Mice with exon 16 of c-Met floxed were first created. Exon 16 contains an ATP-binding site within a tyrosine kinase domain of c-Met which initiates downstream signalling. ‘Floxed’ c-Met mice were then crossed with Cre recombinase transgenic mice. Examples of *c-Met* cKO mice are presented below.

1) *c-Met* deletion in liver. *Mx<sup>Cre</sup>*, *c-Met<sup>fllox/-</sup>* mice had a normal liver size, although tiny lipid vesicles were observed in their livers after six months of age. Incomplete hepatectomy of these conditional *c-Met<sup>-/-</sup>* mice results in smaller liver regrowth with a decreased growth of

hepatocytes by 60% compared with those of the controls<sup>154</sup>. An injection of chemokine ligands resulted in impaired recovery instead of a decrease in hepatocyte proliferation. Atrophic liver recovery was accompanied by a chronic inflammatory response, excessive osteopontin production, and extensive calcification<sup>153</sup>. Thus, the absence of c-Met specifically in hepatocytes significantly affects liver cell survival and remodelling.

2) *c-Met deletion in lung*. Alveolar epithelial cell type II (AECII)-specific *c-Met*<sup>-/-</sup> mice exhibited abnormal alveolar saccular growth and expanded distal airspaces<sup>155</sup>. Treating these cKO mice with doxycycline resulted in reduced airspace development due to a decline in the number and viability of AECs, narrowed pulmonary arteries, and elevated levels of oxidative stress in AECIIs<sup>156</sup>. This data indicates an important role for the HGF-Met pathway in lung growth, specifically in septum formation. 3) *c-Met deletion in kidney*. Targeted depletion of *c-Met* expression in the renal collecting system did not affect the physical appearance of renal collecting ducts, but nephron number and glomerular hypertrophy were slightly reduced<sup>157</sup>. Tubular cell-specific *c-Met*<sup>-/-</sup> mice (*HoxB7*<sup>Cre</sup>; *c-Met*<sup>fl/fl</sup>) have a reduced ability to regenerate tissue due to excessive nephron damage and extensive interstitial fibrosis<sup>158</sup>. The above quoted literature indicates an important role for c-Met in modulating the function of renal collecting ducts by promoting tissue repair and cellular viability.

Currently, no conditional *c-Met* knock-out mice are available where bone cells have been targeted. During embryonic development, the skeleton is formed through membranous and endochondral ossification<sup>159</sup>. As early as E10 and E12 postcoitum, mesenchymal cells condense to form a structure (mesenchymal condensation) upon which the skeleton is established. Various biological signals guide the mesenchymal cells to differentiate into chondrocytes, which form a cartilage template that can be ossified through endochondral ossification, or osteoblasts through the process of intramembranous ossification<sup>1</sup>. To study the role of c-Met in bone, we needed to create the correct transgenic mouse models using Cre-loxP technology<sup>160</sup>.

In our present study, *Prx1*<sup>cre</sup> mice with targeting of osteochondral progenitors and *Ctsk*<sup>cre</sup> mice with targeting of osteoclast precursors were used to determine the role of *c-Met* in bone cells<sup>161</sup>. *Prx1* is a paired-related homeobox gene that is essential for driving skeletal growth in the limb<sup>162</sup>. *Prx1* recombinase activity is detected in mesenchymal cells throughout embryonic limb bud development, in the lateral plate mesoderm, and in the cranial mesenchyme but not

within the axial skeleton. Cre recombinase activity first appears in the limb buds at 9.5 dpc<sup>163</sup>. By crossing *c-Met*<sup>fl/fl</sup> mice with Prx1 Cre mice, we were able to determine the effect of c-Met on osteoblast progenitors that differentiate into osteoblasts. *Ctsk* is selectively expressed in osteoclasts<sup>164,165</sup>. Transgenic mice expressing *Ctsk*<sup>Cre</sup> recombinase in their long bones, ribs, and calvaria show enhanced Cre activity<sup>166</sup>. *Ctsk*<sup>Cre</sup> activity could be detected in skulls and long bones at E16.5 and P7, in agreement with the appearance and skeletal localization of functionally mature osteoclasts and in vertebrae multinuclear osteoclasts of adult mice<sup>167</sup>. By crossing *c-Met*<sup>fl/fl</sup> mice with *Ctsk*<sup>Cre</sup> mice, we determined changes in osteoclast differentiation when *c-Met* was ablated.

Our aim was to determine whether impaired bone development and possibly spontaneous fracture are observed in c-Met conditional knockout mice, regardless of whether osteoblast progenitors or osteoclast precursors are present. We also wanted to determine whether fracture repair in c-Met conditional knockout mice show delayed healing due to the suppressed activities of osteoblasts and osteoclasts at the fracture site. In this section, *c-Met*<sup>fl/fl</sup> mice possessing loxP sites flanking exon 16 of the c-Met sequence were generated and crossed with the *Prx1*<sup>Cre</sup> mice and the *Ctsk*<sup>Cre</sup> mice to delete c-Met in osteoblast progenitors and osteoclast precursors, respectively. We study the skeletons of these mice shortly after birth and at various time points in the postnatal period. A proximal femoral osteotomy model was performed to study fracture repair. The bone phenotypes were evaluated by micro-CT and histomorphology analysis.

### 3.3 Methods and Materials

#### 3.3.1 Subgroup analysis

c-Met and Hgf gene expression and tissue distribution were evaluated in the bone (femur, tibia, skull, sternum, vertebra) and viscera (heart, liver, lung, kidney and spleen) of wild-type mice. C-Met and HGF expression were evaluated by immunohistochemistry in the tibia of wild-type mice at different ages (3 weeks old, 10 weeks old, 25 weeks old). Alcian Blue-Alizarin Red staining was applied to study the skeletal development of the *c-Met*<sup>fl/fl</sup>, *Prx1*<sup>Cre</sup> mice and the *c-Met*<sup>fl/fl</sup>, *Ctsk*<sup>Cre</sup> mice. Osteoblasts and osteoclasts of the *c-Met*<sup>fl/fl</sup>, *Prx1*<sup>Cre</sup> mice and the *c-Met*<sup>fl/fl</sup>, *Ctsk*<sup>Cre</sup> mice were evaluated by immunohistochemistry. The bone (femur, tibia, skull, sternum, vertebra) and the other organs (heart, liver, lung, kidney and spleen) of these two gene-edited

mice and control mice were evaluated by H&E staining, TRAcP staining and immunohistochemistry. Safranin O/fast green staining, Masson's trichrome staining, TRAcP staining, and ALP immunohistochemistry were performed to evaluate fibrocartilage formation, new callus formation, and osteoclast and osteoblast activity in the murine fracture model.

### 3.3.2 RT-qPCR

RNA was extracted from wild-type bone samples, and RT-qPCR was performed as indicated in **Chapter 2**. Primers were designed against the following mouse sequences: *m-c-Met* (forward, 5'-GGTGC GG TCTCAATATCAGTAG-3'; reverse, 5'-CTCTT-GCGTCATAGCGAACT-3'), *m-Hgf* (forward, 5'-GGACCATGTGAGGGAGATTATG-3'; reverse, 5'-ATACCAGGACGATTTGGGATG-3'), and *m-β-actin* (forward, 5'-GAGGTATCCTGACCCTGAAGTA-3'; reverse, 5'-CACACGCAGCTCATTGTAGA-3').

### 3.3.3 Generation of *c-Met<sup>fl/fl</sup>*, *Prx1<sup>cre</sup>* mice and *c-Met<sup>fl/fl</sup>*, *Ctsk<sup>cre</sup>* mice and phenotype identification

Two types of c-Met conditional-knockout mouse models were generated by crossing the *c-Met<sup>fl/fl</sup>* mice (possessing loxP sites flanking exon 16 of the c-Met sequence) with the *Prx1<sup>cre</sup>* mice and the *Ctsk<sup>cre</sup>* mice to delete *c-Met* in osteoblast progenitors and osteoclast precursors, respectively. *Prx1<sup>cre</sup>* mice mainly express Cre recombinase in osteochondral progenitors that form the early limb bud mesenchyme and a subset of the craniofacial mesenchyme but not the spine or other organs *in vivo*. *c-Met<sup>fl/fl</sup>* mice were created through CRISPR/Cas9 editing by the Shanghai Model Organisms Center, Inc. (Shanghai, China). The strategy of CRISPR/Cas9 editing for conditional knockout of *c-Met* is shown in **Figure 15**. *Prx1<sup>cre</sup>* mice purchased from Jackson Laboratories and *Ctsk<sup>cre</sup>* mice provided by the Shanghai Model Organisms Center, Inc., were crossed with *c-Met<sup>fl/fl</sup>* mice. Mouse breeding from P0 to P2 is demonstrated in **Figure 16**. Ultimately, *c-Met<sup>fl/fl</sup>*, *Prx1<sup>cre</sup>* mice and *c-Met<sup>fl/fl</sup>*, *Ctsk<sup>cre</sup>* mice were obtained, and *c-Met<sup>fl/fl</sup>* mice were assigned as the control mice. All mice were bred and maintained under specific pathogen-free conditions in the Shanghai Model Organisms Center, Inc.. The *c-Met<sup>fl/fl</sup>*, *Prx1<sup>cre</sup>* mice, *c-Met<sup>fl/fl</sup>*, *Ctsk<sup>cre</sup>* mice and their controls were genotyped via PCR on mice tail. Primers were designed as follow: *Met-flox* (forward, 5'-ACCCCTAGAAGCCATCACCT-3'; reverse, 5'-

GTGCCTCAGGGGTGGTAAAG-3'), *Prx1-cre* (forward, 5'-TCGATGCAACGAG-TGATGAG -3'; reverse, 5'-TCCATGAGTGAACGAACCTG-3'), *Ctsk-cre* (forward, 5'-GAGCTGGGGAAACAAAG-3'; reverse, 5'-GGTAGTCCCTCACATCCTCAG-3').

### 3.3.4 Proximal femur osteotomy

A diagram of the proximal femur osteotomy is shown in **Figure 17A**. A 0.5-cm skin incision was cut longitudinally along the femur to expose the proximal femur (**Figure 17B**). The incision was located between the third and lesser trochanters. A 24G needle was inserted into the femur of mice (**Figure 17C**) and the femur was sawed from the bottom to the top until the saw hit the needle, and then, the sawing direction was changed to the top-bottom direction until the osteotomy was complete (**Figure 17D**). After flushing with sterile normal saline, the surgical wound was closed, and the surrounding soft tissue sutured (**Figure 17E**).

### 3.3.5 Alcian Blue-Alizarin Red staining

3 day old *c-Met<sup>fl/fl</sup>*, *Prx1<sup>cre</sup>* mice and *c-Met<sup>fl/fl</sup>*, *Ctsk<sup>cre</sup>* mice were humanely euthanized and stained in Alcian Blue-Alizarin Red solution for 4 h. Then, the mice were placed in 1% potassium hydroxide for 24 to 36 h until the skeleton and muscles were clearly observed. Processed samples were transferred to 50% glycerin for storage or imaging. The mouse skeletons stained purplish red, while the cartilage stained blue.

### 3.3.6 Histological analysis

Mouse samples were dehydrated, embedded in paraffin, and sectioned using a microtome (4 µm thick). Sections were prepared and stained by H&E, TRAcP, safranin O/fast green and Masson's trichrome. For the phenotypic evaluation, quantitative parameters such as the ratio of number of osteoclasts and bone surface (N.Oc/BS), bone volume/tissue volume (BV/TV), and the ratio of osteoblast number and bone surface (N.Ob/BS), were evaluated manually by ImageJ software. Fracture evaluation was undertaken using safranin O/fast green-staining to measure fibrocartilage/tissue volume and Masson's trichrome-staining to measure callus/tissue volume. A square region of interest (ROI) was set at 0.5 mm from the mouse tibia growth plate and image J software was utilised for analysis. In the estimation of fracture healing, a semicircular ROI was set in the haematoma with a radius between the fracture gap and periosteum. A TRAcP staining kit (387A) was purchased from Sigma-Aldrich (St. Louis, MO, USA), and a safranin



O/fast green staining kit (G1053) and Masson's trichrome staining solution (G1006) were purchased from Wuhan Servicebio Technology Co., Ltd. (Wuhan, China).

For immunohistochemistry, samples were decalcified and embedded in paraffin for sectioning. Sections were deparaffinized, rehydrated and incubated with 1% hydrogen peroxide in methanol for 30 min to block endogenous peroxidase activity. Nonspecific binding sites were blocked with goat serum for 60 min at room temperature before incubation with primary antibodies against c-Met (1:500, PA5-85951, Thermo Fisher Scientific, Waltham, MA, USA), HGF (1:1000, PA5-115354, Thermo Fisher Scientific, Waltham, MA, USA) and ALP (1:1000, bs-6292R, Beijing Biosynthesis Biotechnology Co., Ltd., Beijing, China) overnight at 4°C. For detection, sections were incubated with HRP-conjugated secondary antibody (GB23303, Wuhan Servicebio Technology Co., Ltd., Wuhan, China) for 60 min, followed by the addition of liquid DAB substrate. Sections were counterstained with haematoxylin, dehydrated and mounted with fast drying mounting media.

### 3.3.7 Micro-CT

Micro-CT was performed to quantitatively analyse the bone matrix of wild-type mice, *c-Met<sup>fl/fl</sup>*, *Prx1<sup>cre</sup>* mice and *c-Met<sup>fl/fl</sup>*, *Ctsk<sup>cre</sup>* mice as well as the fracture sites of the murine fracture model. The microarchitecture on the trabecular bone of the proximal femur was determined using high-resolution micro-CT (Scanco Medical AG, Zurich, Switzerland). Structural parameters in a square ROI set at 0.5 mm from the tibia growth plate were analysed with the program CT-An in 2- and 3-dimensional images and included bone volume per tissue volume (BV/TV), number of trabeculae (Tb.N), separation of trabeculae (Tb.Sp), connectivity density (Conn.Dn) and trabecular thickness (Tb.Th). For the murine fracture model in gene-edited mice, the whole length of the femur was scanned to identify fracture healing at different time points.

### 3.3.8 Cell line and tissue culture

To investigate the effect of c-Met inhibition on osteoblast differentiation and proliferation, c-Met kinase inhibitor cabozantinib was used to treat the MC3T3 cell lines (an osteoblast precursor cell line derived from *Mus musculus calvaria*). Cellular differentiation was identified by Alizarin Red staining and Alkaline phosphatase staining (Detailed procedure for each staining is indicated in Chapter 4) and cellular proliferation was evaluated by MTT assay, a colorimetric assay for assessing cell metabolic activity. MC3T3 were grown on plates in Alpha Modified

Eagle Medium ( $\alpha$ -MEM) with 10% fetal bovine serum (FBS) until confluent. Cells were cultured in osteogenic induction media ( $\alpha$ -MEM with 10% FBS+10 mM  $\beta$ -glycerophosphate and 50  $\mu$ g/mL ascorbic acid) to stimulate differentiation into osteoblasts for 14 days.

### 3.3.9 Group setting for Alizarin Red staining and ALP staining

Five groups were contained in our project including blank control (MC3T3 without osteogenic inducer), positive control group (MC3T3 plus osteogenic induction media), test group 1 (MC3T3 plus osteogenic induction media and cabozantinib (1 $\mu$ M)), test group 2 (MC3T3 plus osteogenic induction media and cabozantinib (3 $\mu$ M)), test group 3 (MC3T3 plus osteogenic induction media and cabozantinib (5 $\mu$ M)).

### 3.3.10 MTT assay

To evaluate the MC3T3 cells were cultured in a 96-well plate as  $1 \times 10^4$  cells/well. The seeded cells will be treated with cabozantinib (1 $\mu$ M, 3 $\mu$ M, 5 $\mu$ M) for 24, 48 hours. The MC3T3 in the same volume of culture media will be used as control. The culture medium was then removed and 10  $\mu$ L of fresh MTT solution (10  $\mu$ g/L) was added to each well, and the plates were placed in an incubator at 37°C for 4 hours. After that, 150  $\mu$ L DMSO was added to each well and mixed thoroughly to lyse the cells and dissolve the dark blue crystals. After 5 min of dissolution, the absorbance was measured at 570 nm using a microplate reader. Cell proliferation was evaluated by measuring the relative cell viability, comparing the control groups.

### 3.3.11 Statistical analysis

All data shown in this part are presented as the mean  $\pm$  standard deviation from multiple independent tests. Each test was performed at least three times. Statistical significance was determined by Student's t test or ANOVA, with  $p$  less than 0.05 regarded as significant. The normality for all data was measured by Shapiro-Wilk normality testing for the Student's t test and ANOVA. The sample size was initially calculated for two experimental groups of the *c-Met*<sup>fl/fl</sup>, *Prx1*<sup>cre</sup> mice or *c-Met*<sup>fl/fl</sup>, *Ctsk*<sup>cre</sup> mice by G\*Power software (Universität Düsseldorf, German), and a significance level of 5% and a statistical test power of 80% were considered. In Alcian Blue-Alizarin Red staining, the mutant mice and their controls were obtained from same litter. As for the other experiments, the mutant mice and their controls are randomly assigned to each experiment, so they are obtained from different litters. Our subject is to achieve a significance

level of 5% and a statistical test power of 90%, so more than 15 mice for each group are needed in our future work.

### 3.4 Results

#### 3.4.1 c-Met is expressed in the endosteum and highly activated in adult male mice.

Considering that the HGF/c-Met system is ubiquitous in cells and organs, we evaluated the status of c-Met and HGF in the organs and skeletons of wild-type mice. RT-qPCR confirmed that *c-Met* was highly expressed in the liver, viscera and tibia. Similar expression of *Hgf* occurs in these same tissues (**Figure 18A to 18F**). However, calculating the ratio of *c-Met* to *Hgf* gene expression indicated that the proportion of *c-Met* gene expression was much higher in bone tissues, including the tibia, femur, vertebra, sternum, and skull, than in the viscera (**Figure 18C and 18F**). This result suggests that *c-Met* plays a prominent role in the skeletal system.

c-Met and HGF protein levels and locations in bone was further determined by IHC. The data suggest that c-Met is presented in bone endosteum, while HGF is expressed in the bone matrix itself (**Figure 18G**). Since the endosteum represents metabolically active bone tissue where osteoblasts and osteoclasts reside, the c-Met receptor may in fact be more responsible for bone metabolism than its ligand HGF. A description of the expression of c-Met and HGF in different viscera is offered in **Figure 18H**. To investigate the levels of c-Met and HGF in murine bone of various ages, we assessed tibias from mice aged 3 (young), 10 (adult) and 25 (mature) weeks by IHC. As shown in **Figure 19A and 19B**, c-Met is more highly expressed in male mice during their juvenile and adult stages, whereas HGF expression is consistent throughout the lifespan of both sexes, regardless of their age. The bone matrix of mice evaluated by micro-CT is presented in **Figure 19C and 19D**, which indicates that bone volume and the number of trabeculae both increase with age.

#### 3.4.2 Osteoblastic c-Met deficiency resulted in exhaustion of osteoblast differentiation

As c-Met receptor proteins are expressed in the activated endosteum, we hypothesize that c-Met may function as a key regulator of osteoblast and osteoclast differentiation. To test this hypothesis, we developed a conditional knockout *c-Met* mouse model by specifically targeting osteoblast progenitors (*c-Met<sup>fl/fl</sup>, Prx1<sup>cre</sup>*). In **Figure 20A** we show evidence that the CreLox

technology worked for the *c-Met<sup>fl/fl</sup>*, *Prx1<sup>cre</sup>* mice. There was no significant gross appearance of *c-Met<sup>fl/fl</sup>* mice, *c-Met<sup>fl/fl</sup>*, *Prx1<sup>cre</sup>* mice, and *c-Met<sup>fl/-</sup>*, *Prx1<sup>cre</sup>* mice (**Figure 20B**). Staining p3 mutant mice with Alizarin Red-Alcian Blue revealed that the *c-Met<sup>fl/fl</sup>*, *Prx1<sup>cre</sup>* mice exhibit skeletal integrity without evidence of a skeletal dysplasia, such as limb shortening, craniofacial defects and spontaneous fractures (**Figure 20C and 20D**). Conditional knockout of *c-Met* in osteoblast progenitors did not impair normal bone development, as shown by the normal skeletal preparations at p3. Histological analysis of 5-week-old mutant mice revealed a normal tibia bone volume; TRAcP-positive osteoclasts surrounding trabeculae were also unaffected (**Figure 20E and 20F**). Curiously, ALP staining of adult osteoblasts was slightly higher in the *c-Met<sup>fl/fl</sup>*, *Prx1<sup>cre</sup>* mice than in the *c-Met<sup>fl/fl</sup>* control mice (**Figure 20E and 20F**). This finding suggests an increase in osteoblast mineralization despite unchanged osteoblast numbers. A micro-CT scan revealed no difference in bone volume or trabeculae between the *c-Met<sup>fl/fl</sup>*, *Prx1<sup>cre</sup>* mice and the *c-Met<sup>fl/fl</sup>* control mice (**Figure 20G and 20H**).

To assess changes in the bone matrix of *c-Met<sup>fl/fl</sup>*, *Prx1<sup>cre</sup>* mice, we isolated tibial samples from 3-, 10- and 25-week-old mutant mice as well as the *c-Met<sup>fl/fl</sup>* controls for histologic and microarchitecture analysis. By H&E staining, the metaphysis of the proximal tibia showed decreasing bone volume and osteoblast numbers with increasing age (**Figure 21A, 21B, 21C**). ALP expression was higher in younger mice but progressively decreased in older animals (**Figure 21D**). TRAcP staining identified the number of TRAcP-positive osteoclasts was higher in younger mice and lower in adult mice (**Figure 21E**). No significant morphological changes in visceral histology of *c-Met<sup>fl/fl</sup>*, *Prx1<sup>cre</sup>* mice were identified (**Figure 22A and 22B**). The differences noted above suggest that the conditional knockout of *c-Met* in osteoblast progenitors resulted in increased osteoblast ALP expression in newborn mice, but osteoblast numbers decreased in older animals.

To further understand the mechanism of c-Met on osteoblasts, we blocked c-Met in osteoblast progenitor MC3T3 using c-Met kinase activity inhibitor cabozantinib. As demonstrated by Alizarin Red and ALP staining in **Figure 23A**, when c-Met was inhibited in MC3T3, the cells' osteogenesis ability was increased. The antiproliferative activity of cabozantinib at 5 M was in contrast to that of the control group (**Figure 23B**).

### 3.4.3 Osteoclastic *c-Met* deficiency resulted in osteoclast suppression and osteopetrosis.

The skeletons of *c-Met*<sup>fl/fl</sup>, *Ctsk*<sup>cre</sup> mice and their controls were stained with Alizarin Red-Alizarin Blue to evaluate bone development. In **Figure 24A** we show evidence that the CreLox technology worked for the *c-Met*<sup>fl/fl</sup>, *Ctsk*<sup>cre</sup> mice. There was no significant gross appearance of *c-Met*<sup>fl/fl</sup> mice, *c-Met*<sup>fl/fl</sup>, *Ctsk*<sup>cre</sup> mice, and *c-Met*<sup>fl/-</sup>, *Ctsk*<sup>cre</sup> mice (**Figure 24B**). p3 *c-Met*<sup>fl/fl</sup>, *Ctsk*<sup>cre</sup> mice did not display a skeletal dysplasia or spontaneous fractures, which indicated the ablation of *c-Met* in osteoclast precursors did not affect normal bone development (**Figure 24C and 24D**). Histomorphological analysis was performed to determine bone volume and bone cell number. There were no changes in osteoblast numbers or expression levels of ALP in the endosteum of *c-Met*<sup>fl/fl</sup>, *Ctsk*<sup>cre</sup> mice, suggesting that conditional knockout of *c-Met* did not affect osteoblast activity (**Figure 24E and 24F**). However, the proximal tibia of *c-Met*<sup>fl/fl</sup>, *Ctsk*<sup>cre</sup> mice showed more bone trabeculae and significantly fewer TRAcP-positive cells histology (**Figure 24E and 24F**), and micro-CT (**Figure 24G and 24H**).

*c-Met*<sup>fl/fl</sup>, *Ctsk*<sup>cre</sup> mice showed increasing bone matrix formation between young (3-week-old) and adult (25-week-old) mice. *c-Met*<sup>fl/fl</sup>, *Ctsk*<sup>cre</sup> mice also showed increased osteoblast number and ALP expression (**Figure 25A to 25D**). The findings suggest that deletion of *c-Met* in osteoclast precursors significantly impairs osteoclast differentiation, thereby reducing osteoclast-induced bone resorption and increasing bone formation. Interestingly, we still observed a few TRAcP positive cells in the proximal tibia of *c-Met*<sup>fl/fl</sup>, *Ctsk*<sup>cre</sup> mice at each time point (**Figure 25A and 25E**). This finding indicates that osteoclast differentiation is not completely suppressed when *c-Met* is deleted in osteoclast precursors, although underlying mechanism for this observation is unknown. Similarly, the reason for normal bone development in p3 *c-Met*<sup>fl/fl</sup>, *Ctsk*<sup>cre</sup> mice is unclear. No morphological changes in the viscera of mutant mice were observed by H&E staining (**Figure 26A and 26B**).

### 3.4.4 C-Met ablation in osteoblast progenitor and osteoclast progenitor impair fracture healing

A proximal femoral osteotomy was performed in 10-week-old *c-Met*<sup>fl/fl</sup>, *Prx1*<sup>cre</sup> mice, *c-Met*<sup>fl/fl</sup>, *Ctsk*<sup>cre</sup> mice and their respective controls. Three-dimensional micro-CT images of *c-Met*<sup>fl/fl</sup>, *Prx1*<sup>cre</sup> mice showed failure of fracture repair with a discontinuous fracture gap and sporadic callus surrounding the fracture sites (**Figure 27**). Safranin O staining demonstrated

increased fibrocartilage tissue surrounding the fracture gap on day 14 post fracture and continuing to day 28 (**Figure 28A and 27C**). As time progressed, the size of the callus diminished (**Figure 247B**), and fewer TRAcP-positive osteoclasts were detected around the fracture area (**Figure 28E and 28G**). No callus or new bone formation was detected in the fracture gap of the *c-Met<sup>fl/fl</sup>*, *Prx1<sup>cre</sup>* mice by Masson staining (**Figure 28B and 28D**). Due to the occupation of fibrocartilage at the fracture site of the *c-Met<sup>fl/fl</sup>*, *Prx1<sup>cre</sup>* mice instead of any bony tissue, few ALP-positive calluses were observed by ALP immunohistochemistry (**Figure 28F and 28H**). Conditional knockout of c-Met in osteoblast progenitors significantly impaired osteoblast-induced callus formation, thus causing fibrous cartilage tissue to accumulate at fracture sites. The observed reduction in osteoclast activity and numbers may be the effect of knocking-out c-Met in osteoblasts and impairing their function.

*c-Met<sup>fl/fl</sup>*, *Ctsk<sup>cre</sup>* mice showed disorganized calli, nonresorptive woven bone and little lamellar bone formation in the fracture gap, as determined by micro-CT, H&E staining, and Masson's trichrome staining (**Figure 29A and 29B, Figure 29B and 29D**). Safranin-O staining showed the persistence of fibrocartilage in the fracture gap of *c-Met<sup>fl/fl</sup>*, *Ctsk<sup>cre</sup>* mice at day 28 after the osteotomy (**Figure 30A and 30C**). There was no significant difference in ALP expression as demonstrated by ALP immunohistochemistry (**Figure 30F and 30H**). Due to deficiencies of osteoclast number (indicating less osteoclast-induced callus resorption), increased callus generation was observed in the corresponding region, but obviously, the newly developed calluses cannot be successfully resorbed, subsequently leading to failure of lamellar bone formation. Nevertheless, both gene-edited mouse models demonstrated delayed fracture healing.

### 3.5 Discussion

In Chapter 1, we found that human fracture union is characterized by reduced osteoblast and osteoclast numbers and c-Met expression. The conditional knockout of c-Met in murine osteoblast progenitors and osteoclast precursors is a direct approach for analysing the regulatory effects of c-Met on bone cell behaviour *in vivo*. It is also an efficient method to monitor bone development, bone modelling and remodelling when Met is knocked-out in either cell.

Five-week-old *c-Met<sup>fl/fl</sup>*, *Prx1<sup>cre</sup>* mice showed no change in bone volume or osteoblast and osteoclast numbers. Intriguingly, the ALP staining indicates that a targeted knock-out of

Met results in increased ALP secretion into the bone matrix. ALP is an ectoenzyme attached to the osteoblast cell membrane through glycosylphosphatidylinositol. Only a portion of the enzyme is released into the bloodstream, with the remaining part of the enzyme maintained in tissue. The enhanced ALP expression indicates that highly activated osteoblasts or accelerated osteoblast differentiation is triggered by the deletion of *c-Met* in osteoblast progenitors. We also observed an increase in ALP expression and osteoblast number in 3 weeks old *c-Met<sup>fl/fl</sup>, Prx1<sup>cre</sup>* mice, indicating progressively activated osteoblasts. However, ALP staining and osteoblast numbers gradually declined between 10- and 25-week-old mice. Previous *in vitro* studies using c-Met inhibitors has been shown to promote osteogenesis with improved osteoblast differentiation but decreased proliferation<sup>107</sup>. Similarly, in our tissue culture work, c-Met kinase activity inhibitor cabozantinib was found to promote osteogenesis of osteoblast progenitor MC3T3 cell lines but significantly suppress its cellular proliferation. We found that the *c-Met<sup>fl/fl</sup>, Prx1<sup>cre</sup>* mice at three weeks of age showed temporally activated osteoblasts, indicating that c-Met ablation activates cellular differentiation. In contrast, the decline in osteoblast activity in the following weeks indicates a deficit of mature cells, perhaps due to a premature exit of progenitors which did not proliferate. Thus, the bone volume of *c-Met<sup>fl/fl</sup>, Prx1<sup>cre</sup>* mice decreased at a faster rate as the mice aged, leading to osteopenia. Unlike osteoporosis, osteopenia refers to reduced bone formation and less bone matrix. Similarly, adult *c-Met<sup>fl/fl</sup>, Prx1<sup>cre</sup>* mice had slightly fewer TRAcP-positive osteoclasts. Since osteoclasts are partially regulated by osteoblasts through the secretion of M-CSF and RANKL, we hypothesize the reduction in osteoclast number is linked to fewer osteoblasts (**Figure 31**).

Initial investigation of the Hgf/c-Met system revealed that HGF could be localized to territorial matrix surrounding chondrocytes of calcified cartilage and within the deep zone of normal cartilage, accompanied by positive c-MET receptor-staining in these areas<sup>171</sup>. Another study further supported that HGF and c-MET were expressed in human articular cartilage. However, their data suggested that HGF doesn't contribute to cartilage matrix turnover, demonstrated by unchanged anabolic and catabolic gene expression in normal adult articular cartilage<sup>172</sup>. Hence, it is also suspected that murine cartilage may be affected in some way by crossing *c-Met<sup>fl/fl</sup>* mice with *Prx1<sup>cre</sup>* mice.

However, in our work, we have not observed any significant phenotype changes such as cartilage deterioration, chondrocyte apoptosis, or abnormal bone development after *c-Met* ablation. In particular, normal growth plates with chondrocytes have been observed in *c-Met<sup>fl/fl</sup>*, *Prx1<sup>cre</sup>* mice, thus suggesting that *c-Met<sup>fl/fl</sup>*, *Prx1<sup>cre</sup>* mice do not affect growth plate development. Despite the above evidence, we cannot totally exclude the possibility that *c-Met* conditional knockouts interfere with chondrocyte formation as persistent fibrocartilage is existing in the *c-Met<sup>fl/fl</sup>*, *Prx1<sup>cre</sup>* mice after osteotomy. Fracture-related persistent fibrocartilage may be caused by poor endochondral ossification or chondrocyte biofunction changes contributing to overactive chondrification. Therefore, a more detailed validation, such as a PCR assay, is needed to determine if c-Met expression is absent from either chondrocytes or osteoblasts of the *c-Met<sup>fl/fl</sup>*, *Prx1<sup>cre</sup>* mice. We can also further determine the roles of c-Met in osteoblast differentiation with *Osterix* and *Runx2* cre drivers, which could determine these effects on prehypertrophic chondrocytes and mature osteoblasts<sup>161</sup>. By preventing confounding Cre expression leakage in cartilage, we are likely to have a clearer understanding of c-Met in chondrocytes and osteoblasts.

The data from *c-Met<sup>fl/fl</sup>*, *Ctsk<sup>cre</sup>* mice indicate that increased bone matrix was observed between 3 to 25 weeks of age since osteoclastogenesis had been suppressed. The results indicate that ablation of *c-Met* in osteoclast precursors directly attenuates osteoclast differentiation. It has been reported that with the addition of RANKL, HGF can substitute for M-CSF, in promoting osteoclast differentiation<sup>113</sup>. HGF is mainly involved in the migration of precursor cells to the bone surface, cell division and differentiation, and resorption when the cells reach the designated area<sup>173</sup>. The c-Met inhibitor cabozantinib has previously been shown to significantly suppress osteoclast differentiation and osteoclast-induced bone resorption<sup>115</sup>.

Considering c-Met's involvement in biological development and the lethal outcome of knocking out c-Met in mice, it is reasonable to assume that knocking out c-Met would impair embryogenesis and cause failure of tissue growth during the maternal foetal period<sup>151</sup>. For example, altered placental development caused by deletion of *c-Met* contributes to the death of c-Met knockout mice in utero<sup>152</sup>. However, this outcome may not be the case if *c-Met* is only knocked out in specific tissues. As depicted in the introduction, knocking out *c-Met* seldom causes failure of tissue development but generally results in impaired tissue function or failure of tissue regeneration, such as increased liver damage and fibrosis in *c-Met<sup>fl/fl</sup>*, *Alb<sup>cre</sup>* mice<sup>174</sup>, impairment of glucose tolerance and glucose-dependent insulin secretion in *c-Met<sup>fl/fl</sup>*, *RIR<sup>cre</sup>*



mice<sup>175</sup>, and systolic cardiac dysfunction in *c-Met*<sup>fl/fl</sup>, *a-MHC*<sup>cre</sup> mice<sup>176</sup>. In our present study, similarly, conditional knockout of *c-Met* in osteoblast progenitors and osteoclast precursors of mice did not result in observable bone dysplasia and spontaneous fractures. The data suggest that *c-Met* ablation in these cells primarily impairs the regeneration of tissue but does not affect prenatal bone development.

The delayed fracture healing in *c-Met*<sup>fl/fl</sup>, *Prx1*<sup>cre</sup> mice and *c-Met*<sup>fl/fl</sup>, *Ctsk*<sup>cre</sup> mice highlights an important role of c-Met in bone repair (**Figure 32**). As previously discussed, fractures typically heal through the formation of a soft and hard callus, which is followed by remodelling of the callus<sup>4</sup>. Osteoblasts from the periosteum near the fracture gap deposit woven and lamellar bone to overlap the fracture site and provide strong mechanical support<sup>4,25</sup>. Impairment of osteogenesis due to interrupted or depressed osteoblast differentiation would thus delay fracture healing or lead to fracture nonunion<sup>42</sup>. In the *c-Met*<sup>fl/fl</sup>, *Prx1*<sup>cre</sup> mice, the absence of *c-Met* in osteoblast progenitors inhibited the osteoblast differentiation capacity, thereby decreasing the number of mature osteoblasts and suppressing osteogenesis. Thus, the fracture in *c-Met*<sup>fl/fl</sup>, *Prx1*<sup>cre</sup> mice was unable to obtain sufficient lamellar bone support, leading to delayed union. As shown in the histological analysis, the fracture gap showed increasing formation of fibrocartilage with a small callus. The fracture at 28 days post fracture remained un-united. Since osteoclasts dissolve the hard callus at the final stage of fracture repair, enabling the transformation into lamellar bone, an impairment of osteoclast function delays the resorption of the callus. *c-Met*<sup>fl/fl</sup>, *Ctsk*<sup>cre</sup> mice also showed delayed fracture healing. Compared to *c-Met*<sup>fl/fl</sup>, *Prx1*<sup>cre</sup> mice, there was more deposition of callus around the fracture gap between days 14 to 28, but less lamellar bone was deposited. We hypothesize this was due to an inhibition of osteoclast differentiation, leading to less callus resorption by osteoclasts preventing additional bone deposition.

Our data suggest an important role for *c-Met* in fracture repair. Notably, the ablation of c-Met caused different outcomes of osteoblasts and osteoclasts during differentiation. The deletion of c-Met in osteoclast precursors suppresses osteoblastic bone formation and promotes osteoclastic bone resorption. The formation of osteoblasts and mineralization are both activated in the early stages of mouse growth, but they are suppressed in the later stages. Based on current evidence, an underlying mechanism is that c-Met suppression reduces osteoblast progenitor proliferation, resulting in a deficiency of osteoblast progenitor for continued osteoblast development despite the potency of osteoblast differentiation being stimulated. Knockout of c-Met in

both cell lines impaired osteoblast-induced callus formation and osteoclast-mediated callus resorption, ultimately resulting in fracture delayed union. Alternatively, conditional knockout of *c-Met* directly suppressed osteoclast development. Since the conditional knockout of *c-Met* in both osteoblast progenitors and osteoclast precursors did not interrupt normal bone development, we suspect c-Met plays a bigger role in bone modelling and repair.

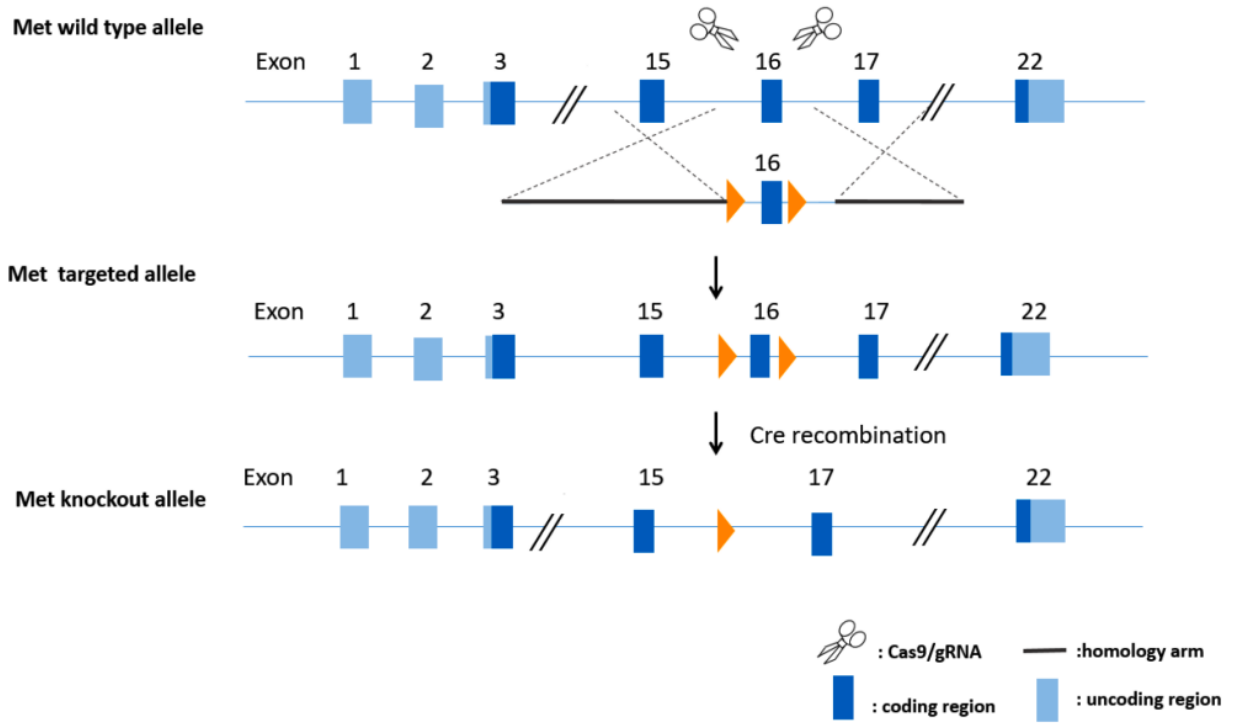
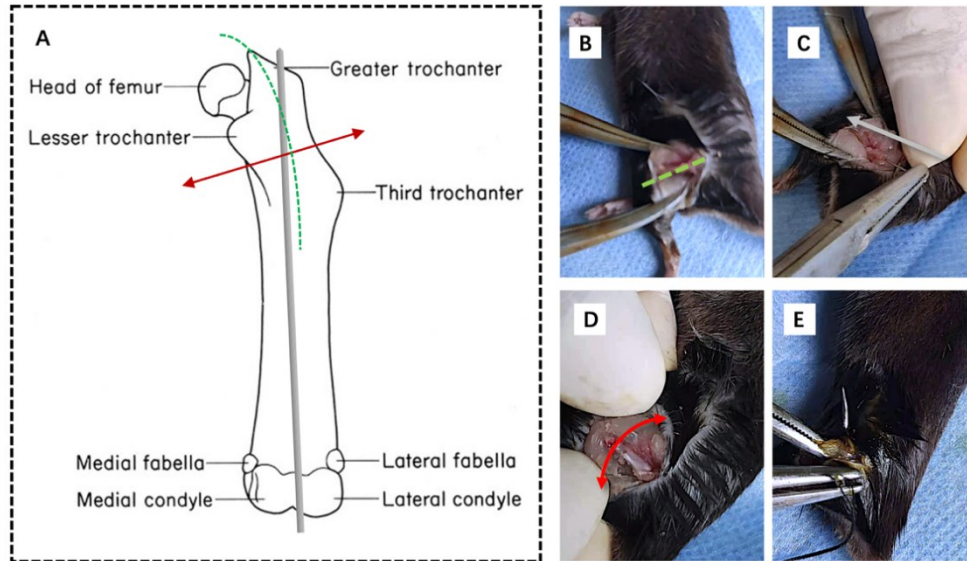


Figure 15. The strategy of CRISPR/Cas9 editing for conditional knockout of *c-Met*.





**Figure 17. The surgical strategy of proximal femur fracture in mice.**

(A) Diagram demonstrating the surgical approach of proximal femur osteotomy. Green line: skin incision direction. Red line: sawing direction. Grey line: direction of needle insertion. (B) A 0.5-cm skin incision was cut longitudinally along the femur to expose the proximal femur. The cutting line was located between the third and lesser trochanters. (C) A 24G needle was first inserted into the femur of the mice. (D) The bone was sawed from the bottom to the top until the saw hit the needle, and then, the sawing direction was changed to the top-bottom until the osteotomy was complete. (E) After flushing with sterile sodium chloride, the surgical wound was closed, and the surrounding soft tissue was sutured.

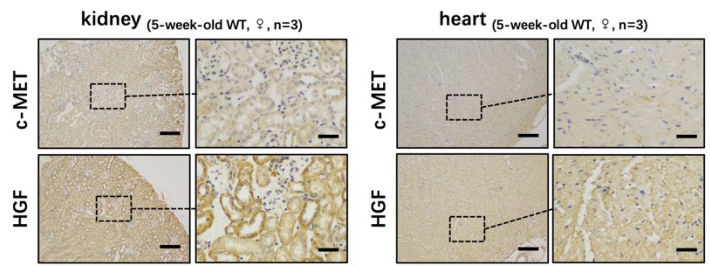
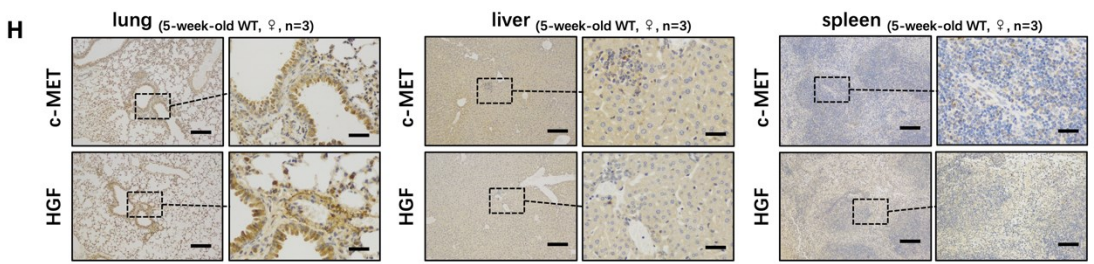
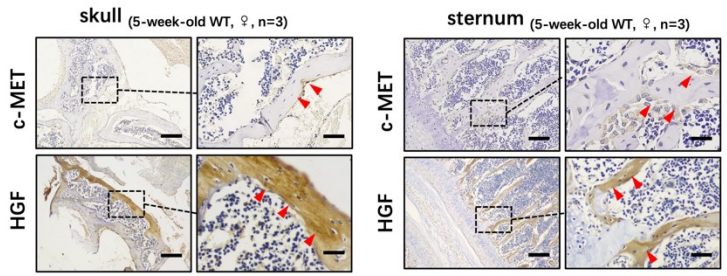
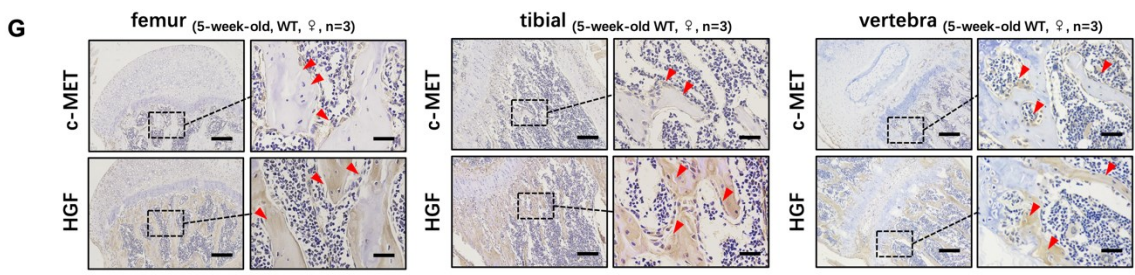
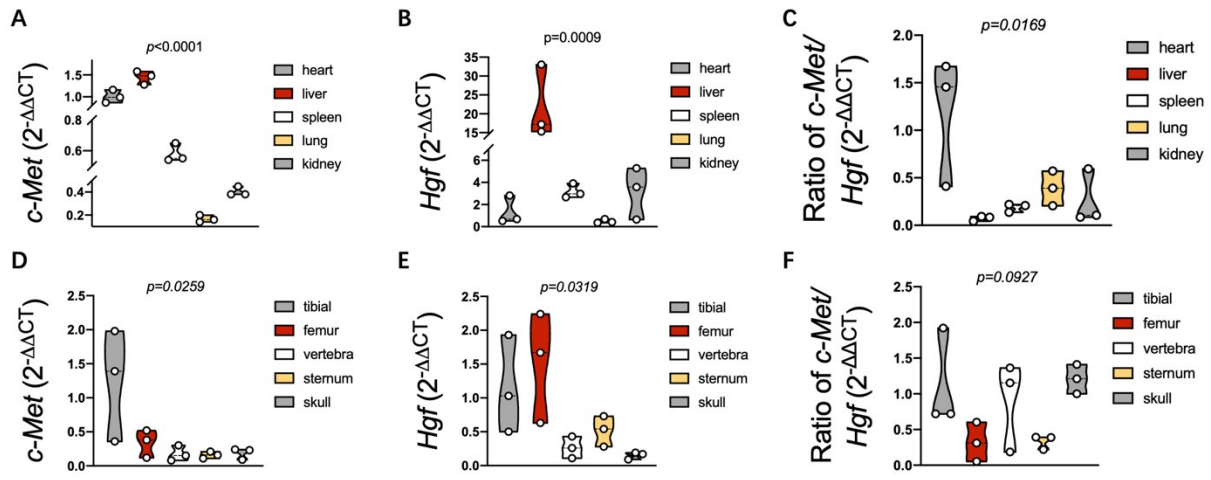


**Figure 18. c-Met and HGF expression in the skeleton and viscera of wild-type mice.**

**(A-B)** Quantitative analysis of *c-Met* and *Hgf* gene expression in the viscera (heart, lung, liver, spleen, kidney) of 5-week-old wild-type mice by RT-qPCR (n=3). **(C)** Ratio of *c-Met* versus *Hgf* in the viscera. **(D-E)** Quantitative analysis of *c-Met* and *Hgf* gene expression in the skeleton (femur, tibia, skull, vertebra, sternum) of 5-week-old wild-type mice by RT-qPCR (n=3). **(F)** Ratio of *c-Met* versus *Hgf* in the skeleton. **(G)** Representative images of immunohistochemistry for c-Met and Hgf expression in the skeleton (femur, tibia, skull, vertebra, sternum) of 5-week-old wild-type mice (n=3). **(H)** Representative images of immunohistochemistry for c-Met and Hgf expression in the viscera (heart, lung, liver, spleen, kidney) of 5-week-old wild-type mice (n=3). Scale bar: 500  $\mu\text{m}$  (left) and 50  $\mu\text{m}$  (right). The RT-qPCR outcomes was presented as  $2^{-\Delta\Delta^{\text{CT}}}$ .

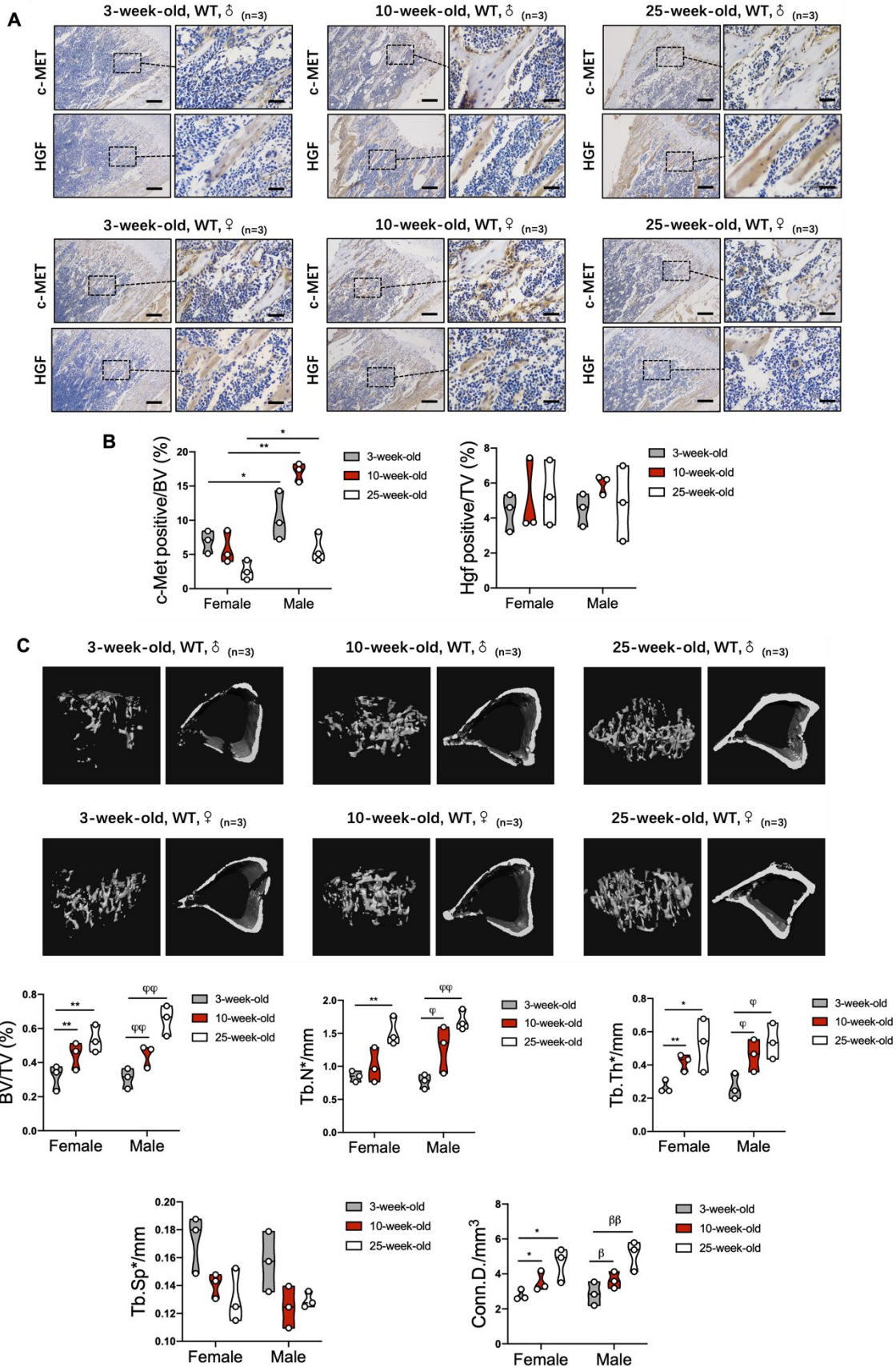




**Figure 19. The distribution of c-Met and Hgf expression in the tibia of wild-type mice.**

**(A)** Representative images of immunohistochemistry for c-Met and Hgf expression at different ages (3, 10 and 25 weeks old) in female and male wild-type mice (n=3). **(B)** Quantitative analysis of the c-Met-positive area and Hgf-positive area/bone volume (BV) at different ages of female and male wild-type mice (n=3). **(C)** Representative micro-CT images of female and male wild-type mice of different ages (n=3). **(D)** Quantitative analysis of bone volume per tissue volume (BV/TV), number of trabeculae (Tb.N), connectivity density (Conn.Dn), separation of trabeculae (Th.Sp) and trabecular thickness (Tb.Th) for the micro-CT analysis (n=3). Scale bar: 500  $\mu\text{m}$  (left) and 50  $\mu\text{m}$  (right). In immunohistochemistry, \* $p < 0.05$ , \*\* $p < 0.01$  versus female mice of the same age. In micro-CT, \* $p < 0.05$ , \*\* $p < 0.01$  versus 3-week-old female mice.  $\Phi p < 0.05$ ,  $\Phi\Phi p < 0.01$  versus 3-week-old male mice.

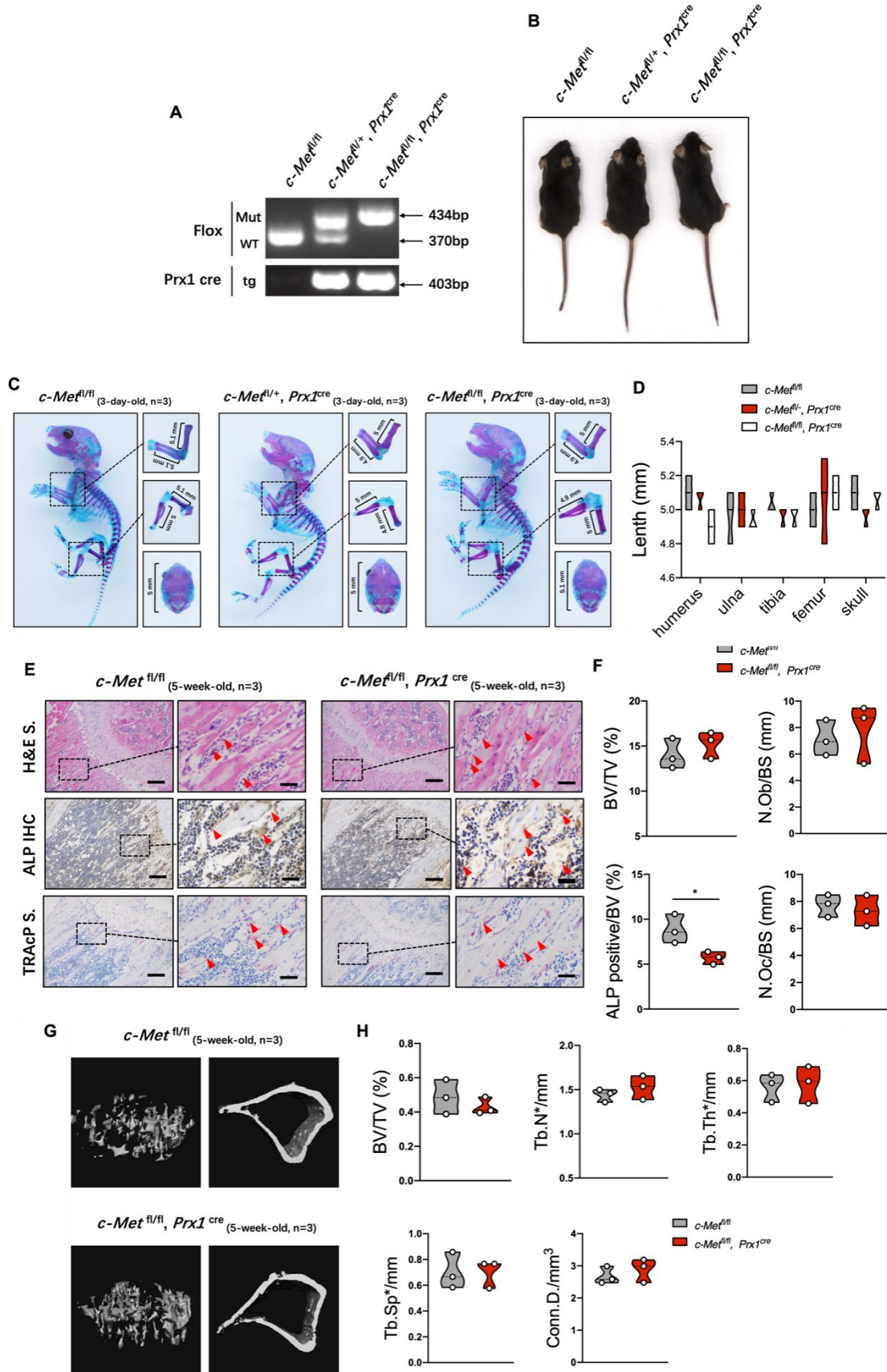


**Figure 20. Phenotype of the *c-Met*<sup>fl/fl</sup>, *Prx1*<sup>cre</sup> mice and the control mice.**

(A) Genotype validation of *c-Met*<sup>fl/fl</sup> mice, *c-Met*<sup>fl/fl</sup>, *Prx1*<sup>cre</sup> mice, and *c-Met*<sup>fl/-</sup>, *Prx1*<sup>cre</sup> mice at 14 days. (B) Gross appearances of *c-Met*<sup>fl/fl</sup> mice, *c-Met*<sup>fl/fl</sup>, *Prx1*<sup>cre</sup> mice, and *c-Met*<sup>fl/-</sup>, *Prx1*<sup>cre</sup> mice (C) Representative images of Alcian Blue-Alizarin Red staining of 3-day-old *c-Met*<sup>fl/fl</sup> mice, *c-Met*<sup>fl/fl</sup>, *Prx1*<sup>cre</sup> mice, and *c-Met*<sup>fl/-</sup>, *Prx1*<sup>cre</sup> mice (n=3). (D) Quantitative analysis of the length of limbs and skull of the 3-day-old *c-Met*<sup>fl/fl</sup> mice, *c-Met*<sup>fl/fl</sup>, *Prx1*<sup>cre</sup> mice, and *c-Met*<sup>fl/-</sup>, *Prx1*<sup>cre</sup> mice (n=3). (E) Representative analysis of H&E staining, TRAcP staining and ALP immunohistochemistry of 5-week-old *c-Met*<sup>fl/fl</sup> and *c-Met*<sup>fl/fl</sup>, *Prx1*<sup>cre</sup> mice (n=3). Red arrows in each image indicate the osteoblasts attaching to the bone surface, ALP-positive area and TRAcP-positive osteoclast-like cells. (F) Quantitative analysis of the bone volume/tissue volume (BV/TV), number of osteoblasts/bone surface (N.Ob/BS), ALP positive area/bone volume (ALP positive/BV) and number of osteoclasts/bone surface (N.Oc/BS) (n=3). (G) Representative micro-CT images of 5-week-old *c-Met*<sup>fl/fl</sup> and *c-Met*<sup>fl/fl</sup>, *Prx1*<sup>cre</sup> mice (n=3). (H) Quantitative analysis of bone volume per tissue volume (BV/TV), number of trabeculae (Tb.N), connectivity density (Conn.Dn), separation of trabeculae (Th.Sp) and trabecular thickness (Tb.Th) for the micro-CT analysis (n=3). Scale bar: 500  $\mu$ m (left) and 50  $\mu$ m (right). \**p* < 0.05 versus the 5-week-old *c-Met*<sup>fl/fl</sup> mice. \*Mut: mutation; WT: wide type; tg: transgene.

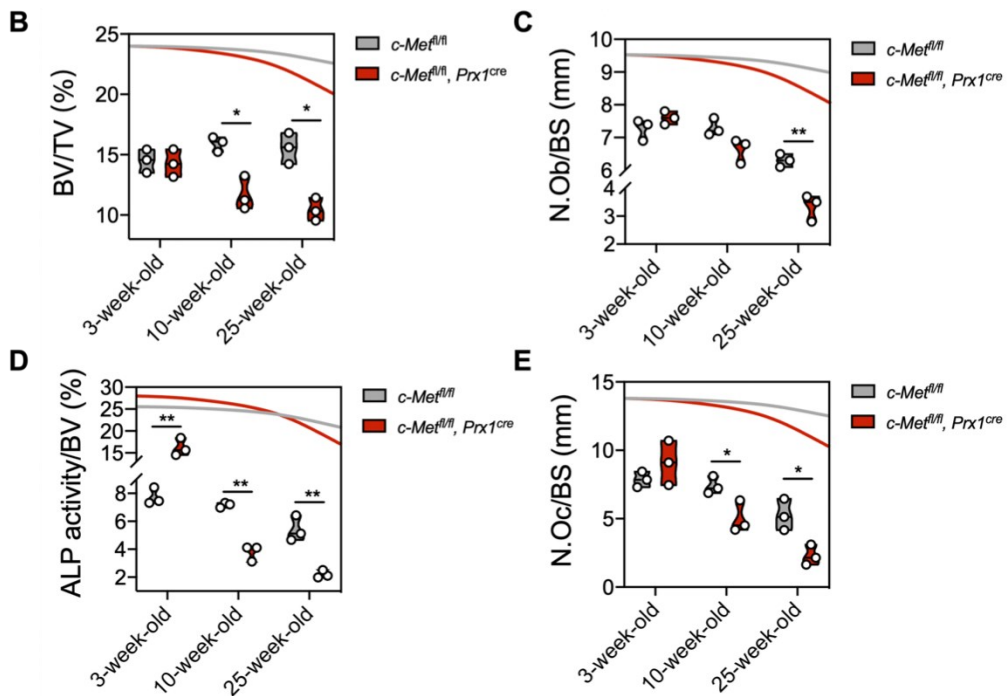
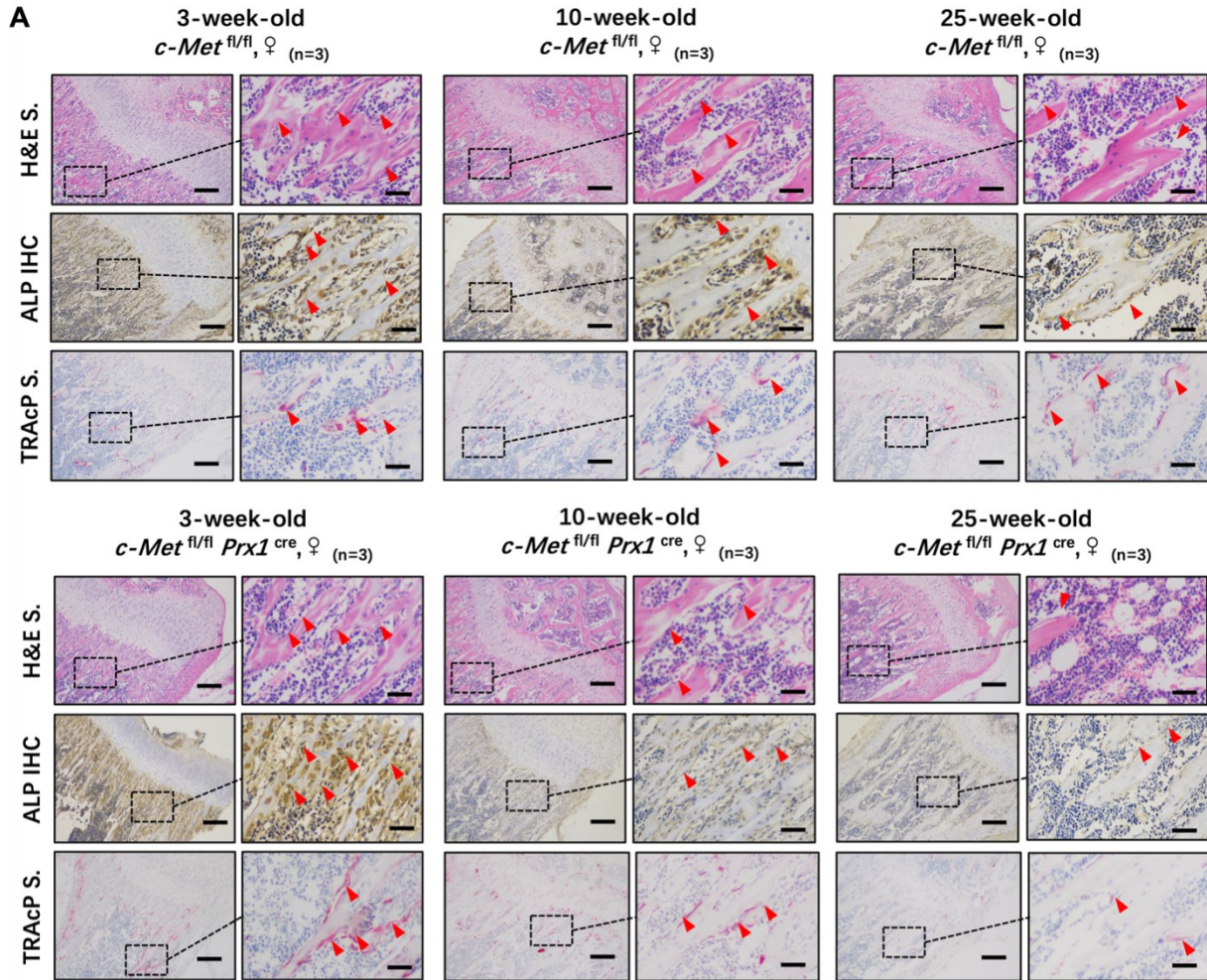


**Figure 21. Osteoblast and osteoclast activities of the *c-Met*<sup>fl/fl</sup>, *Prx1*<sup>cre</sup> mice and the control mice of different ages.**

(A) Representative images of H&E staining, TRAcP staining and ALP immunohistochemistry for the male *c-Met*<sup>fl/fl</sup> and *c-Met*<sup>fl/fl</sup>, *Prx1*<sup>cre</sup> mice at different ages (3, 10 and 25 weeks old) (n=3). Red arrows in each image indicate the osteoblasts attaching to the bone surface, ALP-positive area and TRAcP-positive osteoclast-like cells. (B-E) Quantitative analysis of the bone volume/tissue volume (BV/TV), number of osteoblasts/bone surface (N.Ob/BS), ALP positive area/bone volume (ALP positive/BV) and number of osteoclasts/bone surface (N.Oc/BS) (n=3). Scale bar: 500  $\mu$ m (left) and 50  $\mu$ m (right). \* $p < 0.05$ , \*\* $p < 0.01$  versus the *c-Met*<sup>fl/fl</sup> mice at the relevant age.

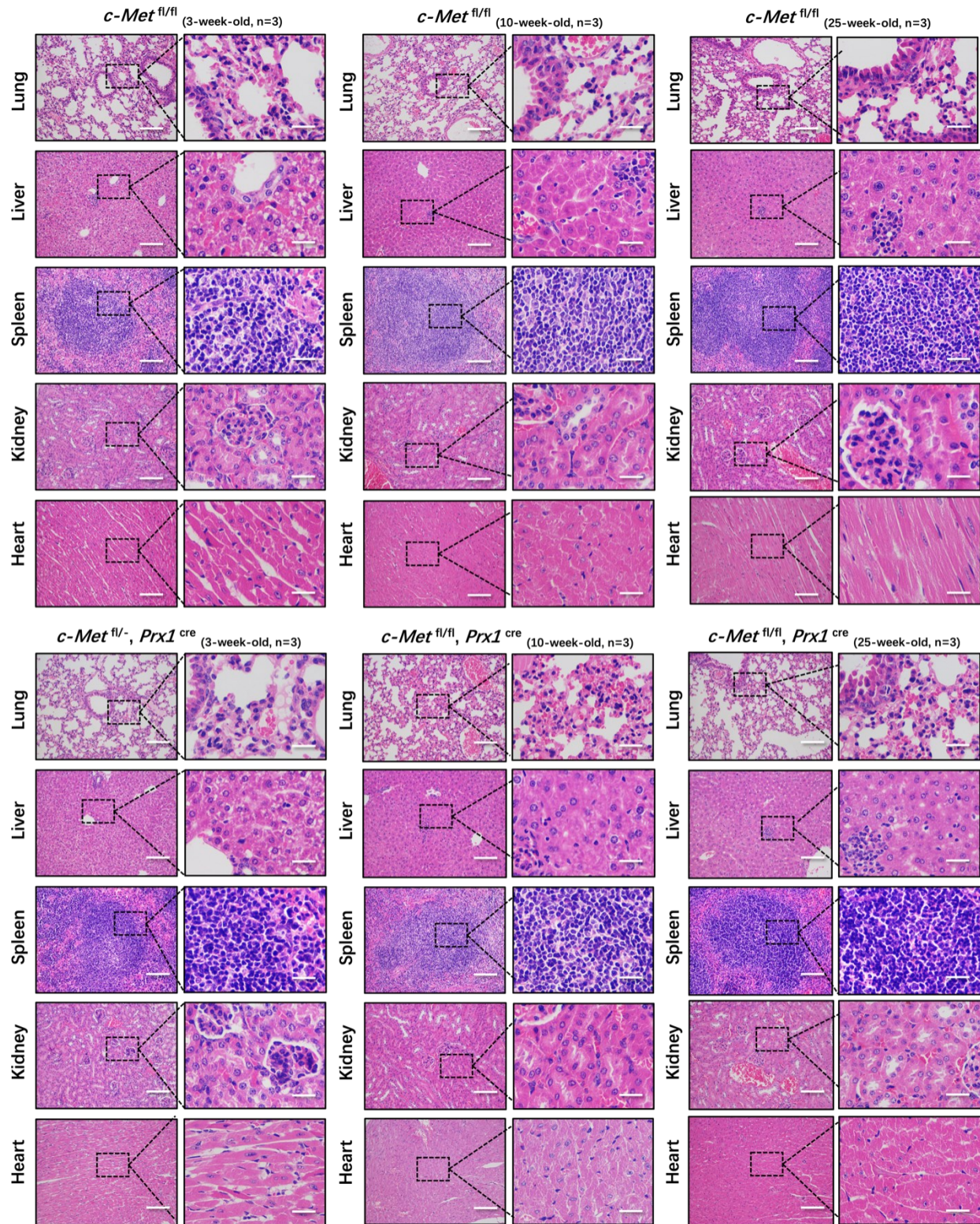
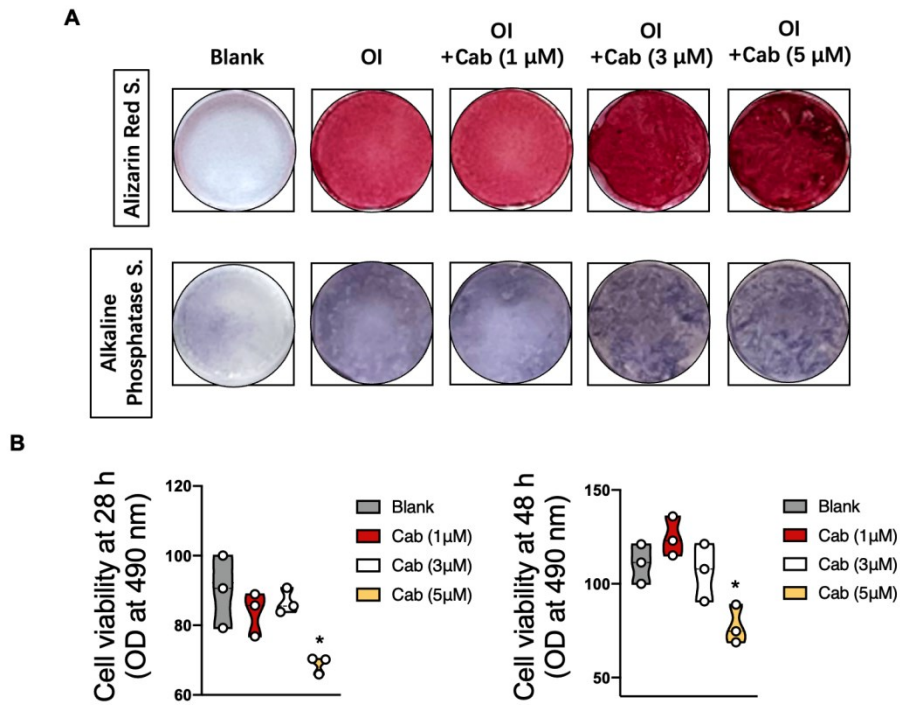


Figure 22. Viscera of the *c-Met*<sup>fl/fl</sup>, *Prx1*<sup>cre</sup> mice and the control mice.

**(A)** Representative images of H&E staining of the viscera (heart, lung, liver, spleen, kidney) of the *c-Met<sup>fl/fl</sup>* and *c-Met<sup>fl/fl</sup>, Prx1<sup>cre</sup>* mice at different ages (3, 10 and 25 weeks old) (n=3). **(B)** Representative images of H&E staining of the viscera (heart, lung, liver, spleen, kidney) of the *c-Met<sup>fl/fl</sup>* and *c-Met<sup>fl/fl</sup>, Prx1<sup>cre</sup>* mice at different ages (3, 10 and 25 weeks old) (n=3). Scale bar: 500  $\mu\text{m}$  (left) and 50  $\mu\text{m}$  (right).



**Figure 23. c-Met kinase activity inhibitor cabozantinib promotes osteogenic differentiation but suppresses proliferation of osteoblast progenitor MC3T3 cell lines.**

**(A)** Representative images of Alizarin Red staining and ALP staining of MC3T3 cell lines when cultured with osteogenic inducer in the present or absent of cabozantinib (1 to 5  $\mu$ M) (n=3). **(B)** Quantitative analysis of MTT assay for the cellular proliferation of MC3T3 with cabozantinib addition (1 to 5  $\mu$ M) (n=3). \* $p < 0.05$  versus the blank group.



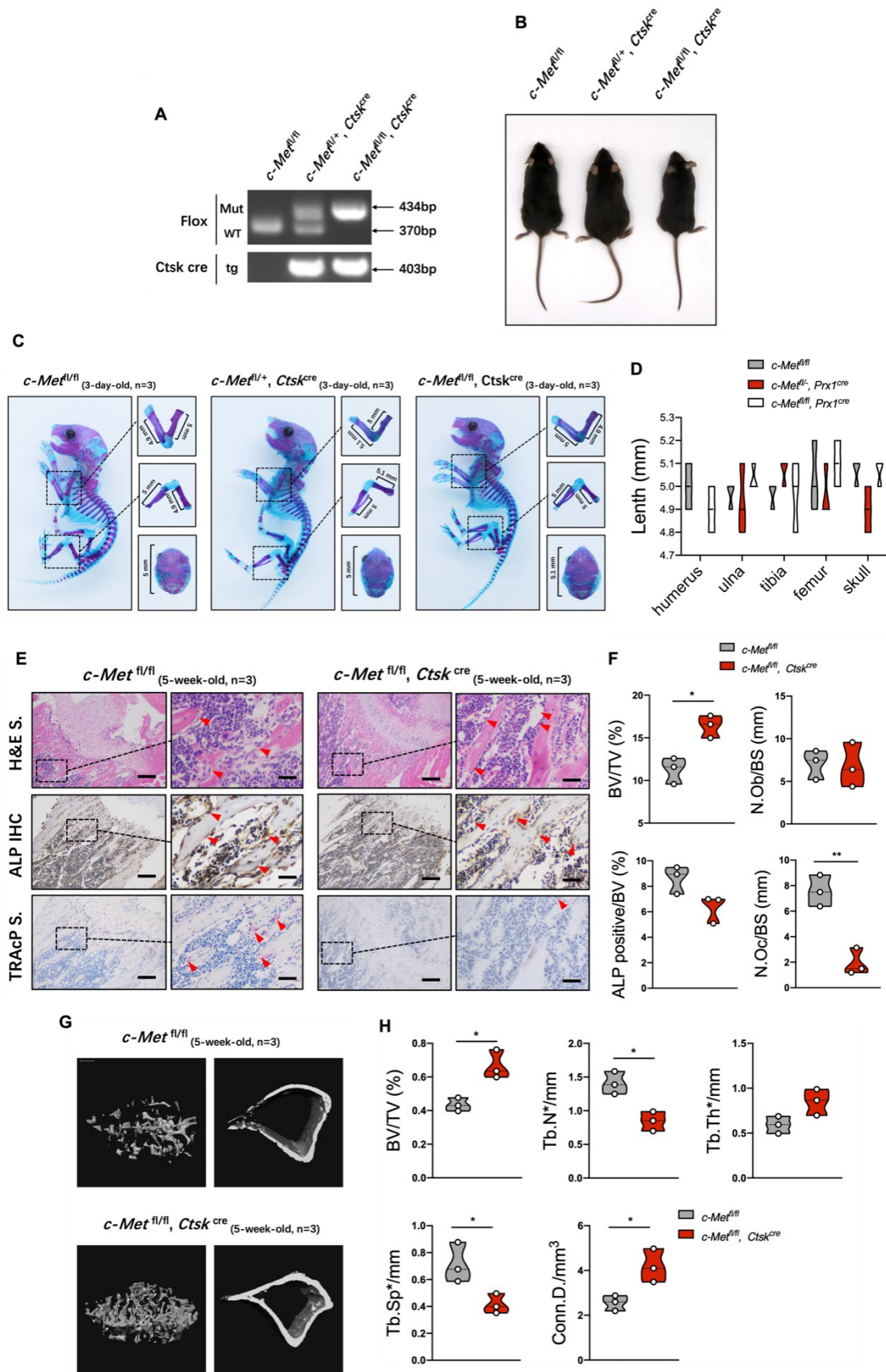


**Figure 24. Phenotype of the *c-Met*<sup>fl/fl</sup>, *Ctsk*<sup>cre</sup> mice and the control mice.**

(A) Genotype validation of *c-Met*<sup>fl/fl</sup> mice, *c-Met*<sup>fl/fl</sup>, *Ctsk*<sup>cre</sup> mice, and *c-Met*<sup>fl/-</sup>, *Ctsk*<sup>cre</sup> mice at 14 days. (B) Gross appearances of *c-Met*<sup>fl/fl</sup> mice, *c-Met*<sup>fl/fl</sup>, *Ctsk*<sup>cre</sup> mice, and *c-Met*<sup>fl/-</sup>, *Ctsk*<sup>cre</sup> mice. (C) Representative images of Alcian Blue-Alizarin Red staining of 3-day-old *c-Met*<sup>fl/fl</sup> mice, *c-Met*<sup>fl/fl</sup>, *Ctsk*<sup>cre</sup> mice, and *c-Met*<sup>fl/-</sup>, *Ctsk*<sup>cre</sup> mice (n=3). (D) Quantitative analysis of the length of limbs and skull of the 3-day-old *c-Met*<sup>fl/fl</sup> mice, *c-Met*<sup>fl/fl</sup>, *Ctsk*<sup>cre</sup> mice, and *c-Met*<sup>fl/-</sup>, *Ctsk*<sup>cre</sup> mice (n=3). (E) Representative analysis of H&E staining, TRAcP staining and ALP immunohistochemistry of 5-week-old *c-Met*<sup>fl/fl</sup> and *c-Met*<sup>fl/fl</sup>, *Ctsk*<sup>cre</sup> mice (n=3). Red arrows in each image indicate the osteoblasts attaching to the bone surface, ALP-positive area and TRAcP-positive osteoclast-like cells. (F) Quantitative analysis of the bone volume/tissue volume (BV/TV), number of osteoblasts/bone surface (N.Ob/BS), ALP positive area/bone volume (ALP positive/BV) and number of osteoclasts/bone surface (N.Oc/BS) (n=3). (G) Representative micro-CT images of the 5-week-old *c-Met*<sup>fl/fl</sup> and *c-Met*<sup>fl/fl</sup>, *Ctsk*<sup>cre</sup> mice (n=3). (H) Quantitative analysis of bone volume per tissue volume (BV/TV), number of trabeculae (Tb.N), connectivity density (Conn.Dn), separation of trabeculae (Th.Sp) and trabecular thickness (Tb.Th) for the micro-CT analysis (n=3). Scale bar: 500  $\mu$ m (left) and 50  $\mu$ m (right). \**p* < 0.05, \*\**p* < 0.01 versus to the 5-week-old *c-Met*<sup>fl/fl</sup> mice. \*Mut: mutation; WT: wide type; tg: transgene.

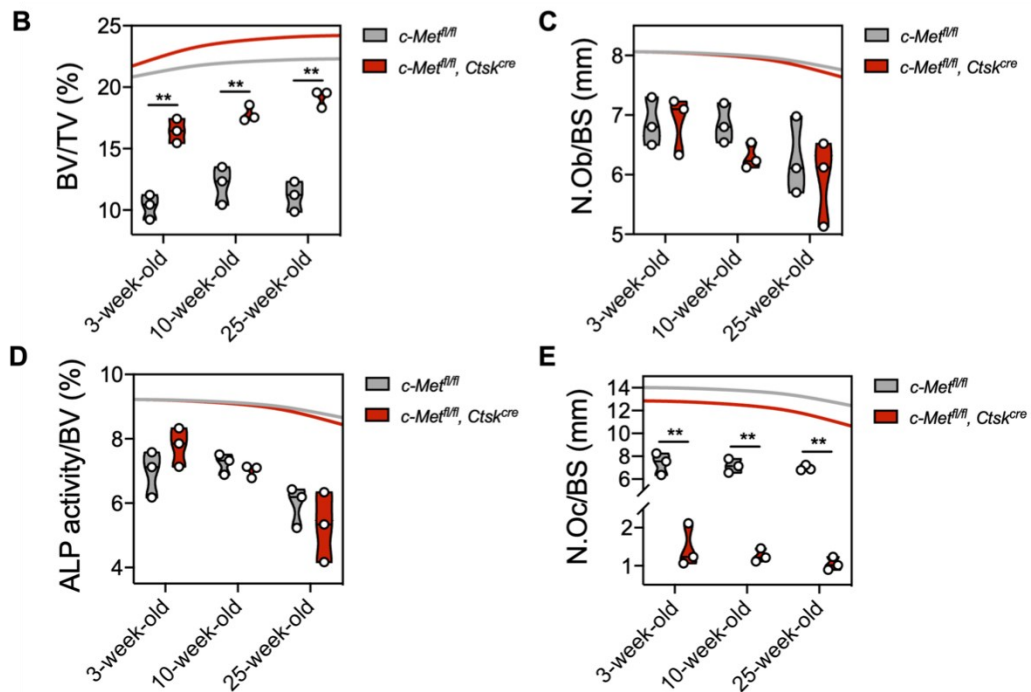
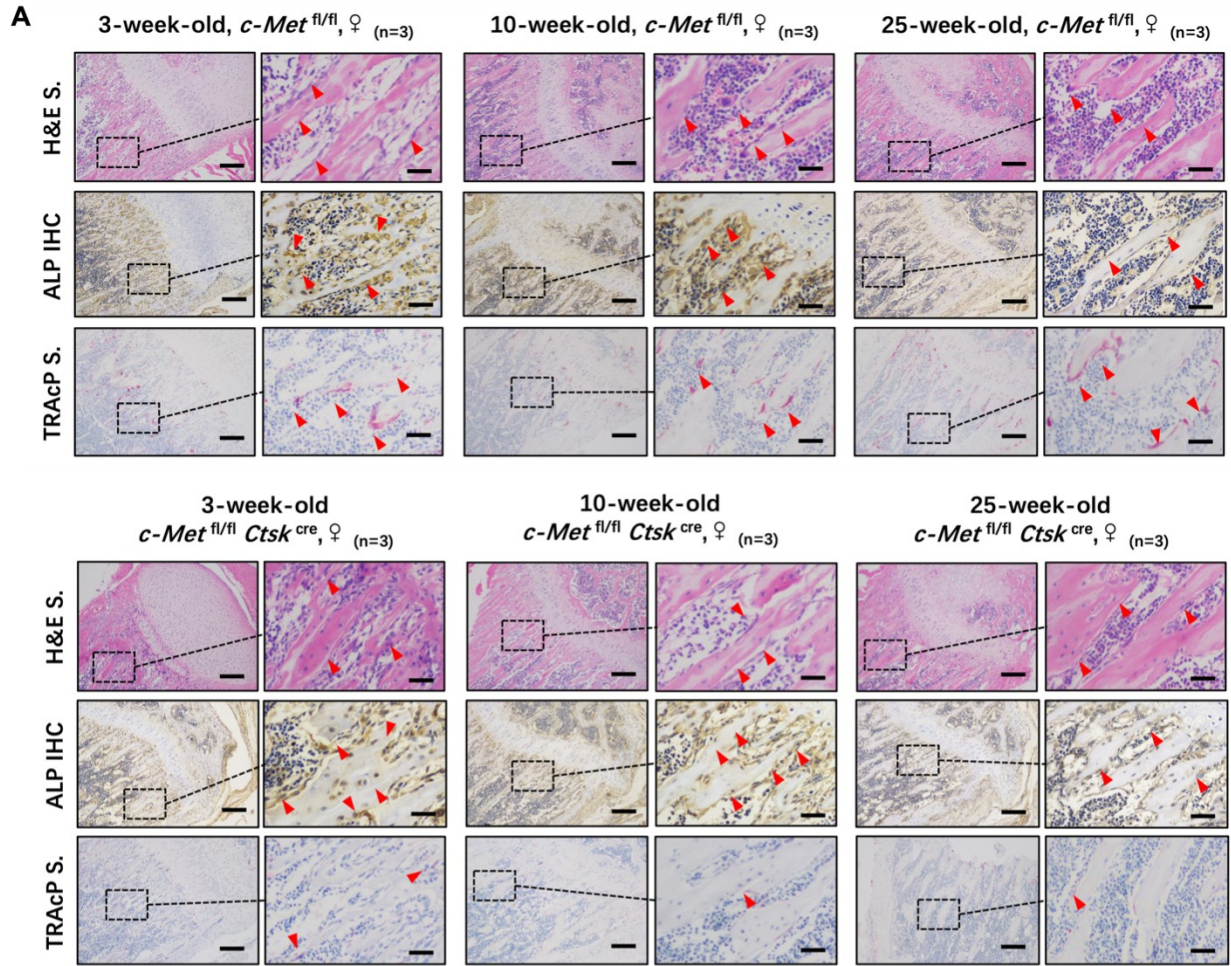


**Figure 25. Osteoblast and osteoclast activities of *c-Met*<sup>fl/fl</sup>, *Ctsk*<sup>cre</sup> mice of different ages and control mice.**

(A) Representative images of H&E staining, TRAcP staining and ALP immunohistochemistry for male *c-Met*<sup>fl/fl</sup> and *c-Met*<sup>fl/fl</sup>, *Ctsk*<sup>cre</sup> mice at different ages (3, 10 and 25 weeks old) (n=3). Red arrows in each image indicate the osteoblasts attaching to the bone surface, ALP-positive area and TRAcP-positive osteoclast-like cells. (B-E) Quantitative analysis of the bone volume/tissue volume (BV/TV), number of osteoblasts/bone surface (N.Ob/BS), ALP positive area/bone volume (ALP positive/BV) and number of osteoclasts/bone surface (N.Oc/BS) (n=3). Scale bar: 500  $\mu$ m (left) and 50  $\mu$ m (right). \*\* $p < 0.01$  versus the *c-Met*<sup>fl/fl</sup> mice at the relevant age.

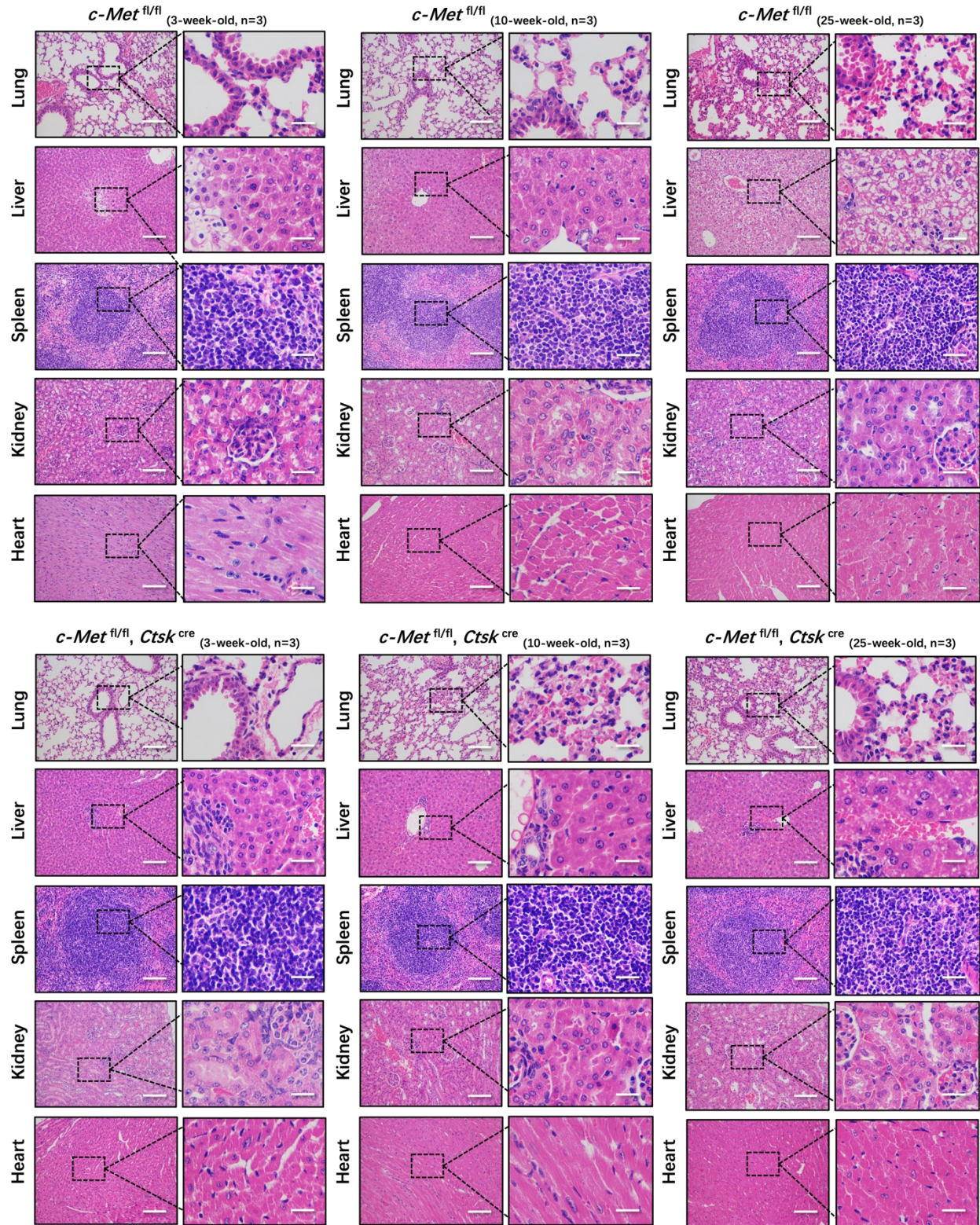
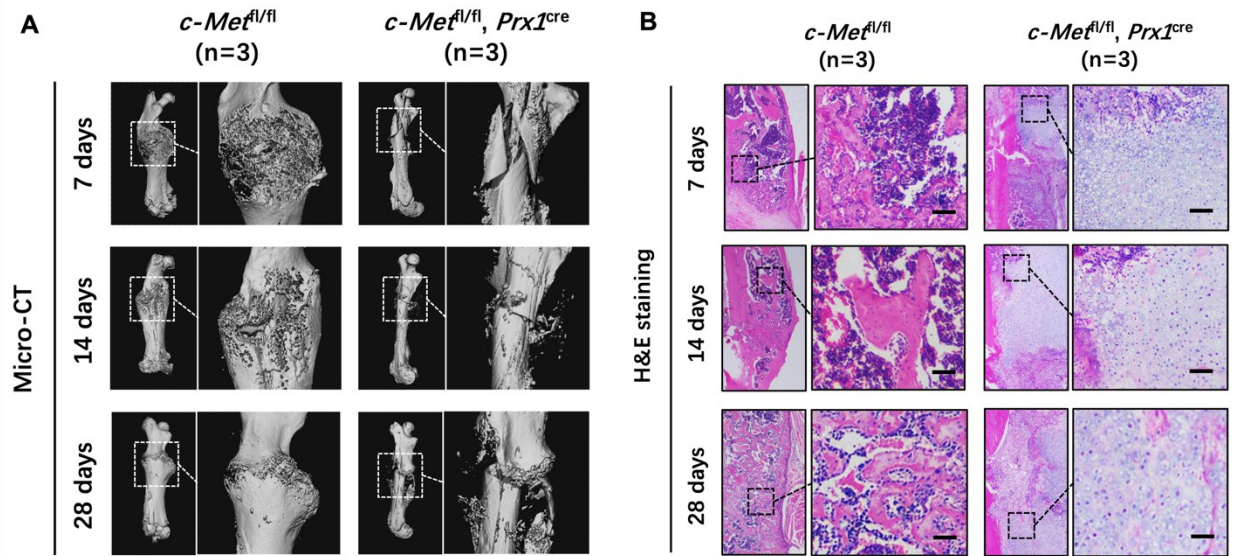


Figure 26. Viscera of the *c-Met*<sup>fl/fl</sup>, *Ctsk*<sup>cre</sup> mice and control mice.

**(A)** Representative images of H&E staining showing the viscera (heart, lung, liver, spleen, kidney) of the *c-Met*<sup>fl/fl</sup> and *c-Met*<sup>fl/fl</sup>, *Ctsk*<sup>cre</sup> mice at different ages (3, 10 and 25 weeks old) (n=3).  
**(B)** Representative images of H&E staining demonstrating the viscera (heart, lung, liver, spleen, kidney) of the *c-Met*<sup>fl/fl</sup> and *c-Met*<sup>fl/fl</sup>, *Ctsk*<sup>cre</sup> mice at different ages (3, 10 and 25 weeks old) (n=3).  
Scale bar: 500  $\mu$ m (left) and 50  $\mu$ m (right).



**Figure 27. Micro-CT and H&E staining of the *c-Met<sup>fl/fl</sup>, Prx1<sup>cre</sup>* mice and the control mice.**

(A) Representative micro-CT images demonstrating fracture healing of the *c-Met<sup>fl/fl</sup>* mice and the *c-Met<sup>fl/fl</sup> Prx1<sup>cre</sup>* mice at 7, 14, and 28 days (n=3). (B) Representative images of H&E staining demonstrating fracture healing and callus formation of the *c-Met<sup>fl/fl</sup>* mice and the *c-Met<sup>fl/fl</sup>, Prx1<sup>cre</sup>* mice at 7, 14, and 28 days (n=3). Scale bar: 50  $\mu$ m.

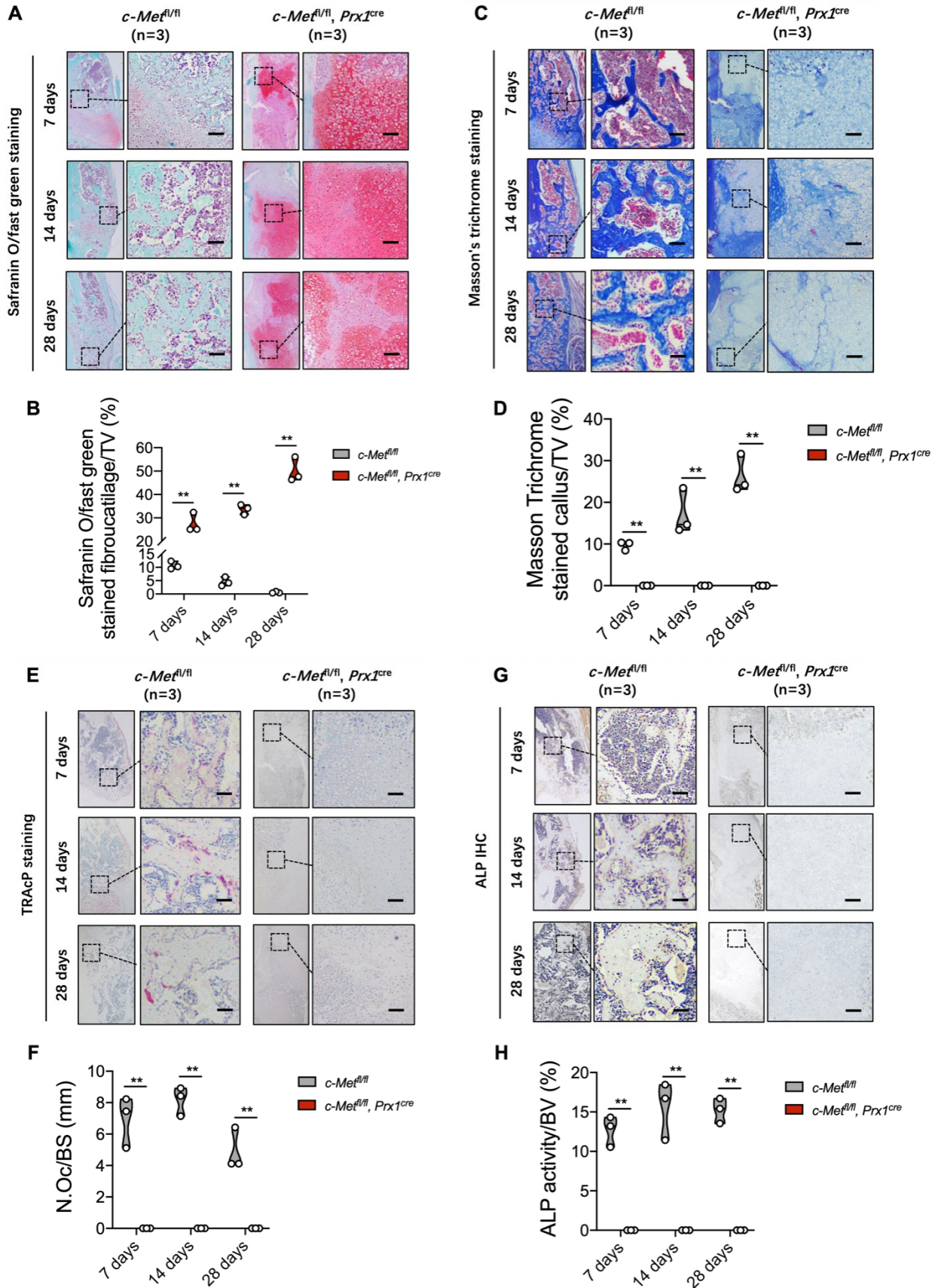




**Figure 28. Safranin O/fast green staining, Masson's trichrome staining, TRAcP staining and ALP immunohistochemistry of the *c-Met*<sup>fl/fl</sup>, *Prx1*<sup>cre</sup> mice and the control mice.**

(A) Representative images of safranin O/fast green staining demonstrating fibrocartilage formation in the *c-Met*<sup>fl/fl</sup> mice and the *c-Met*<sup>fl/fl</sup>, *Prx1*<sup>cre</sup> mice at 7, 14, and 28 days (n=3). (B) Quantitative analysis of safranin O/fast green staining/tissue volume (TV) (n=3). (C) Representative images of Masson's trichrome staining showing callus and collagen formation of the *c-Met*<sup>fl/fl</sup> mice and the *c-Met*<sup>fl/fl</sup>, *Prx1*<sup>cre</sup> mice at 7, 14, and 28 days (n=3). (D) Quantitative analysis of Masson's trichrome staining/TV (n=3). (E) Representative images of TRAcP staining demonstrating osteoclast activity of the *c-Met*<sup>fl/fl</sup> mice and the *c-Met*<sup>fl/fl</sup>, *Prx1*<sup>cre</sup> mice at 7, 14, and 28 days (n=3). (G) Quantitative analysis of TRAcP staining staining/bone surface (BS) (n=3). (F) Representative images of ALP immunohistochemistry demonstrating osteoblast activity of the *c-Met*<sup>fl/fl</sup> mice and the *c-Met*<sup>fl/fl</sup>, *Prx1*<sup>cre</sup> mice at 7, 14, and 28 days (n=3). (H) Quantitative analysis of ALP-positive area/bone volume (TV) (n=3). Scale bar: 50  $\mu$ m. \*\* $p < 0.01$  versus the *c-Met*<sup>fl/fl</sup> mice.

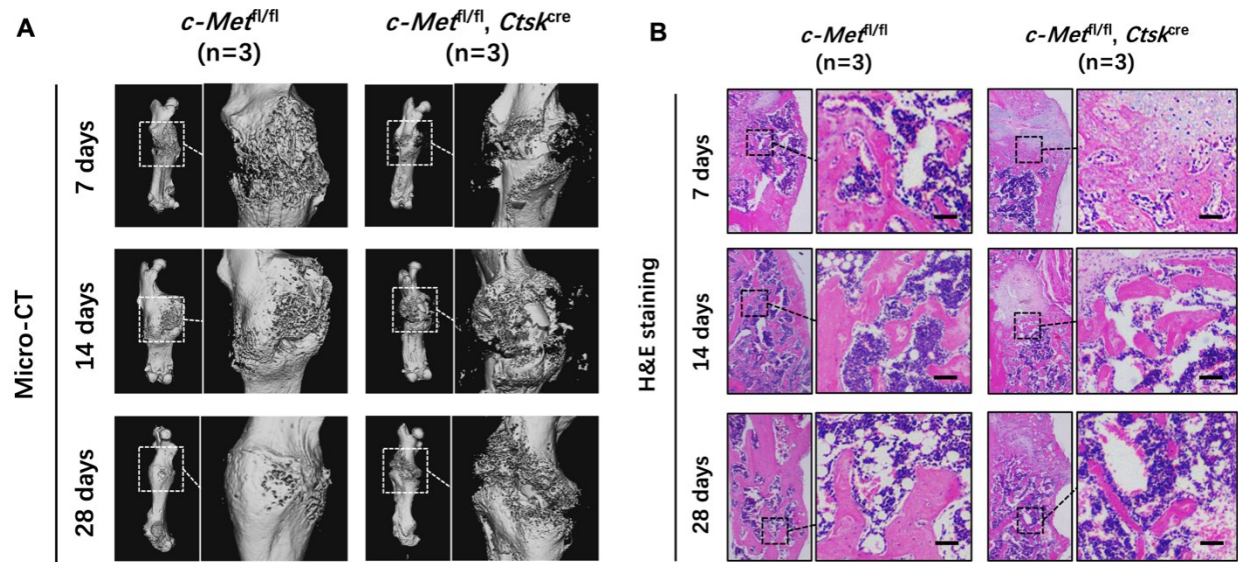


**Figure 29. Fracture healing and callus formation of the *c-Met<sup>fl/fl</sup>, Ctsk<sup>cre</sup>* mice and the control mice.**

**(A)** Representative micro-CT images demonstrating fracture healing of the *c-Met<sup>fl/fl</sup>* mice and the *c-Met<sup>fl/fl</sup>, Ctsk<sup>cre</sup>* mice at 7, 14, and 28 days (n=3). **(B)** Representative images of H&E staining demonstrating fracture healing and callus formation of the *c-Met<sup>fl/fl</sup>* mice and the *c-Met<sup>fl/fl</sup>, Ctsk<sup>cre</sup>* mice at 7, 14, and 28 days (n=3). Scale bar: 50  $\mu$ m.

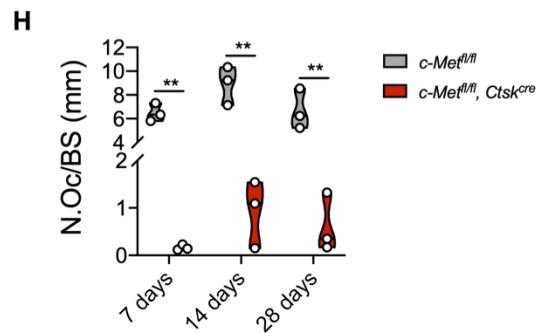
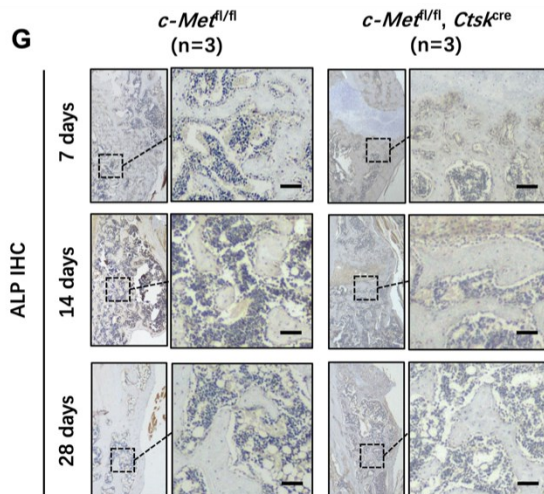
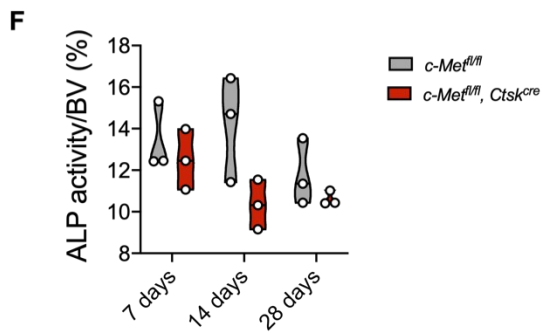
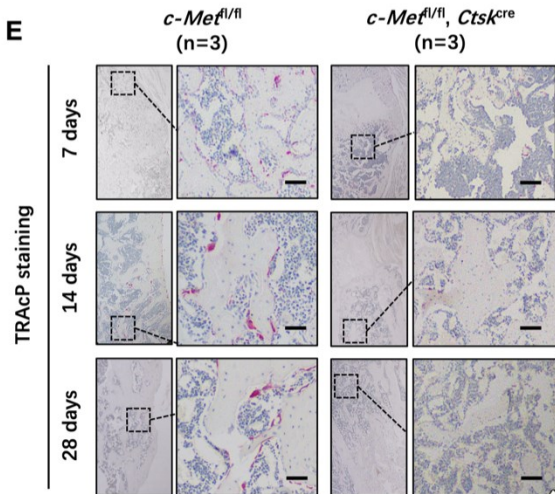
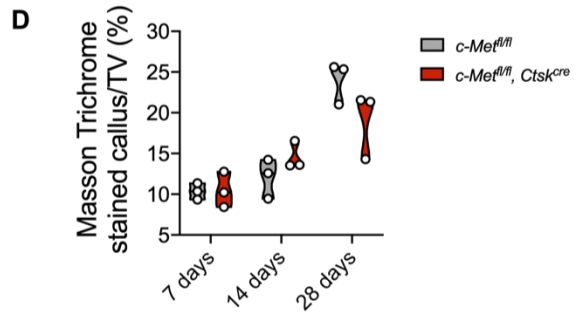
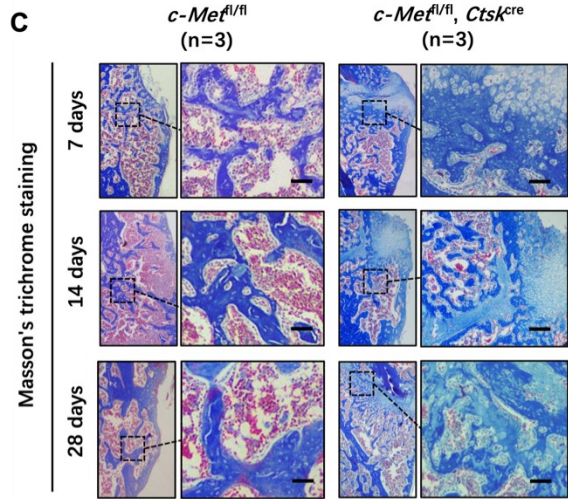
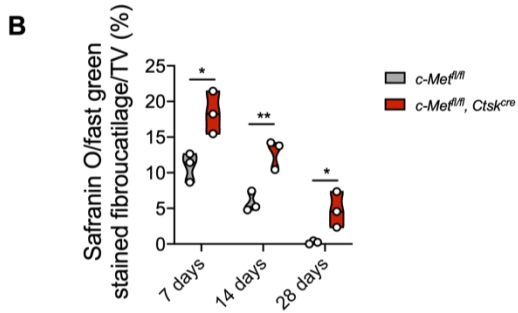
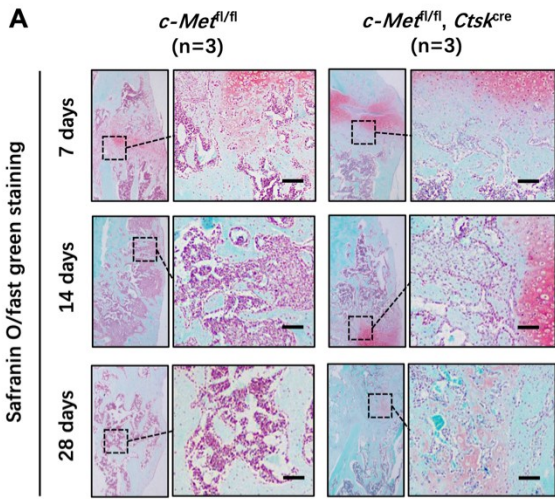


**Figure 30. Safranin O/fast green staining, Masson's trichrome staining, TRAcP staining and ALP immunohistochemistry of the *c-Met*<sup>fl/fl</sup>, *Ctsk*<sup>cre</sup> mice and the control mice.**

(A) Representative images of safranin O/fast green staining demonstrating fibrocartilage formation in the *c-Met*<sup>fl/fl</sup> mice and the *c-Met*<sup>fl/fl</sup>, *Ctsk*<sup>cre</sup> mice at 7, 14, and 28 days (n=3). (B) Quantitative analysis of safranin O/fast green staining/tissue volume (TV) (n=3). (C) Representative images of Masson's trichrome staining showing callus and collagen formation of the *c-Met*<sup>fl/fl</sup> mice and the *c-Met*<sup>fl/fl</sup>, *Ctsk*<sup>cre</sup> mice at 7, 14, and 28 days (n=3). (D) Quantitative analysis of Masson's trichrome staining/TV (n=3). (E) Representative images of TRAcP staining demonstrating osteoclast activity of the *c-Met*<sup>fl/fl</sup> mice and the *c-Met*<sup>fl/fl</sup>, *Ctsk*<sup>cre</sup> mice at 7, 14, and 28 days (n=3). (F) Quantitative analysis of TRAcP staining staining/bone surface (BS) (n=3). (G) Representative images of ALP immunohistochemistry demonstrating osteoblast activity of the *c-Met*<sup>fl/fl</sup> mice and the *c-Met*<sup>fl/fl</sup>, *Ctsk*<sup>cre</sup> mice at 7, 14, and 28 days (n=3). (H) Quantitative analysis of ALP-positive area/bone volume (BV) (n=3). Scale bar: 50  $\mu$ m. \* $p < 0.05$ , \*\* $p < 0.01$  versus the *c-Met*<sup>fl/fl</sup> mice.

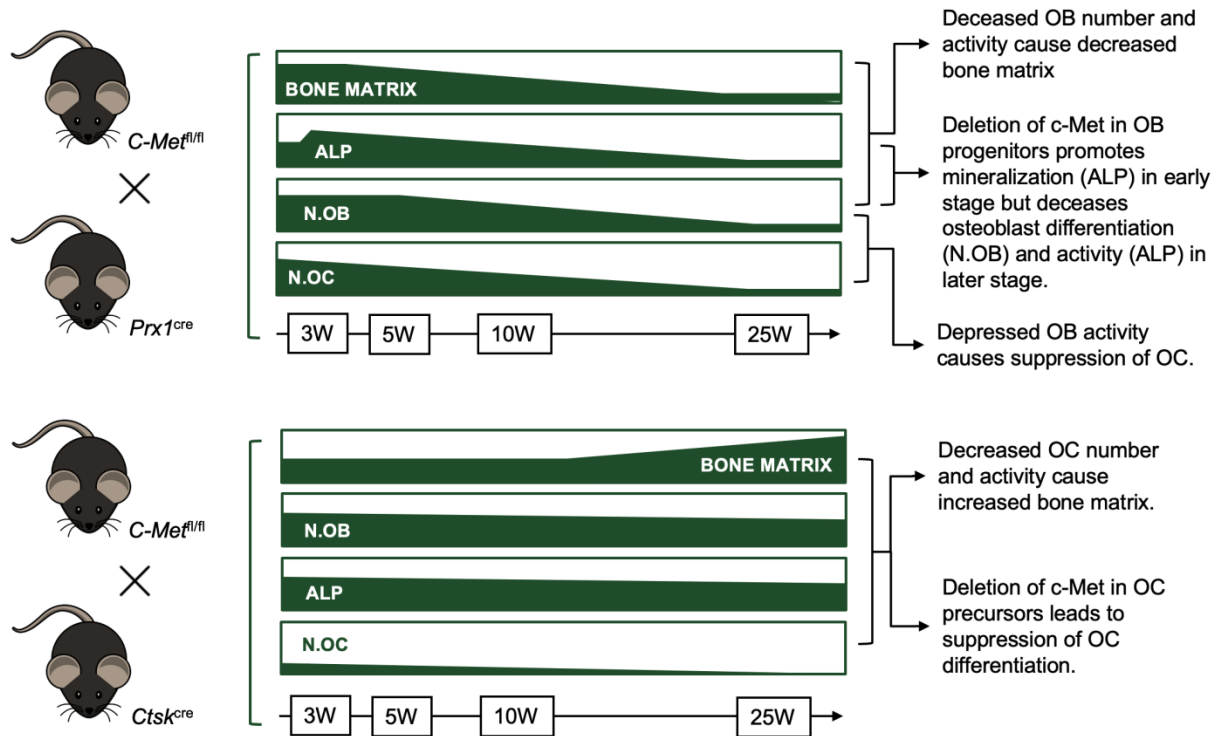


**Figure 31. Summary of trends of bone matrix, ALP expression, number of osteoblasts and osteoclasts in *c-Met<sup>fl/fl</sup>, Prx1<sup>cre</sup>* mice and *c-Met<sup>fl/fl</sup>, Ctsk<sup>cre</sup>* mice from 3-week to 25-week-old.**

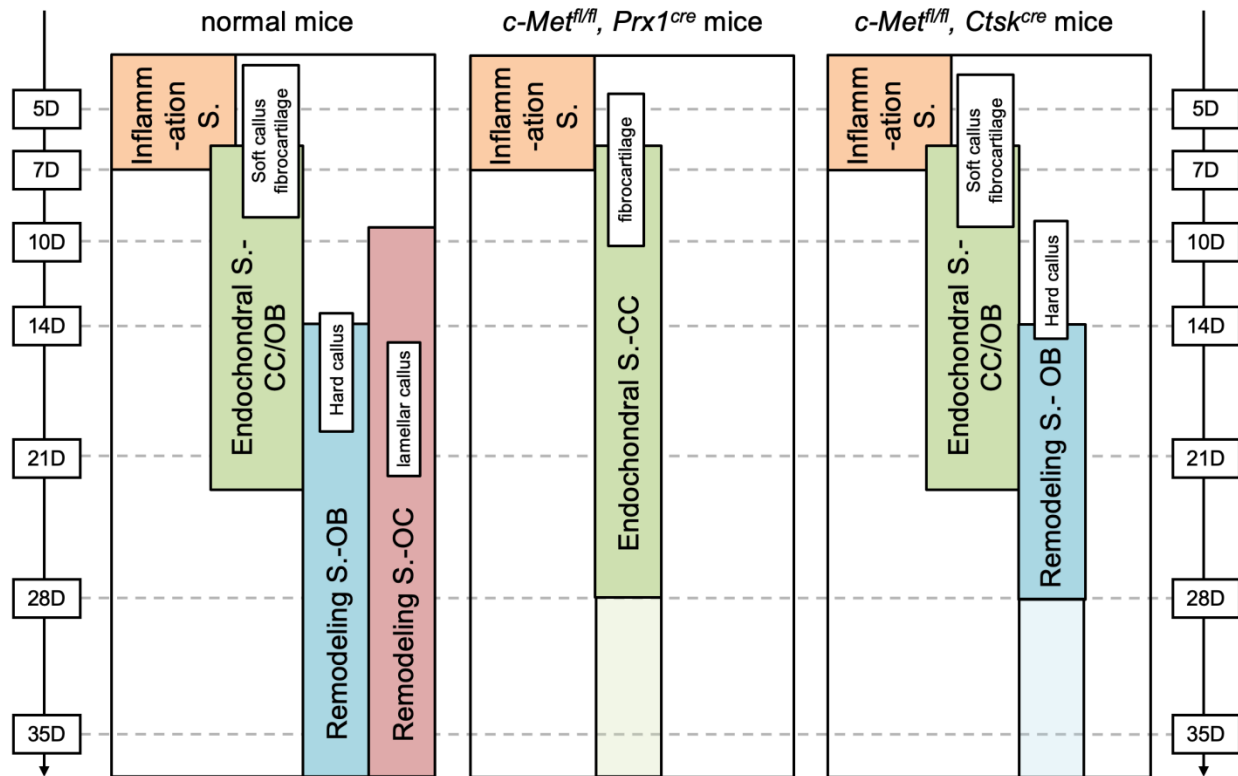


**Figure 32. Stages of fracture healing in normal mice,  $c\text{-Met}^{fl/fl}$ ,  $Prx1^{cre}$  mice and  $c\text{-Met}^{fl/fl}$ ,  $Ctsk^{cre}$  mice after osteotomy.**

Normal fracture healing includes several stages, such as inflammation, endochondral ossification, and bone remodeling. The final one contains hard callus formation and lamellar bone formation. Conditional knockout of  $c\text{-Met}$  in osteoblast progenitors ( $c\text{-Met}^{fl/fl}$ ,  $Prx1^{cre}$  mice) impaired osteoblast-induced callus formation, thus causing fibrous cartilage tissue to accumulate at fracture sites. The observed reduction in osteoclast numbers may be the effect of knocking-out  $c\text{-Met}$  in osteoblasts and impairing their function. In  $c\text{-Met}^{fl/fl}$ ,  $Ctsk^{cre}$  mice, due to deficiencies of osteoclast number, indicating less osteoclast-induced callus resorption, increased callus generation was observed in the corresponding region, but obviously, the newly developed calluses cannot be successfully resorbed, subsequently leading to failure of lamellar bone formation. Nevertheless, both gene-edited mouse models demonstrated delayed fracture healing.

## **CHAPTER 4**

### **The Roles of c-Met in Regulation of Osteoclastogenesis and Osteoblastogenesis Under the Hypoxic Condition**

## 4.1 Abstract

Sustained hypoxia in the musculoskeletal compartment has been reported to suppress osteoblast and osteoclast differentiation. Hypoxia has also been linked to c-Met regulation in salivary gland cancer cells and glioma cells. However, the regulatory effect of hypoxia on c-Met in bone cells is unclear. Here, we incubate osteoblast progenitor MC3T3 cells and osteoclast precursor RAW264.7 cells in hypoxic conditions. Our findings suggest that hypoxia suppresses cellular differentiation and promotes the phosphorylation of c-Met in both MC3T3 and RAW264.7 cell lines. Treatment of the cells using a c-Met kinase inhibitor, carboxantibib, did not restore cellular differentiation under hypoxic conditions. Although hypoxia may stimulate c-Met activation through oxygen deprivation, we were unable to show that activation of c-Met was responsible for the suppression of bone cell differentiation.

## 4.2 Introduction

In cases of fracture, the local blood supply to the bone and periosteum is frequently compromised due to a number of reasons such as the severity of the injury, the process of surgical intervention itself to repair the fracture, and failure of the internal fixation<sup>128</sup>. Ischaemia may indirectly lead to hypoxia, nutrition deficiency, and the loss of a of progenitor cells, which are essential for bone regeneration<sup>129</sup>. It is for these reasons that hypoxia impairs fracture healing and contributes to fracture nonunion<sup>130</sup>.

Although it is not currently possible to monitor local oxygen concentrations at fracture sites in humans, murine tibial fracture models demonstrate that the early fracture phase is characterised by reduced tissue oxygenation at the fracture area<sup>177</sup>. A murine tibial fracture model in which the femoral artery was ligated prior to surgery caused significant hypoxia at the fracture site resulting in apoptosis, delayed osteoblast differentiation, and impaired healing<sup>129</sup>. These results indicate the importance of tissue oxygenation to fracture repair.

A variety of biological processes require appropriate tissue oxygenation for successful fracture healing. Cells require oxygen for aerobic metabolism. Additionally, oxygen is essential for enzyme activity. Active enzymes involved in fracture healing include hydroxylases, oxy-



genases, and cyclooxygenases. The absence of cyclooxygenase 2 activity, for instance, interferes with osteogenic differentiation, thereby impairing bone repair<sup>178</sup>. Finally, the absence of appropriate tissue oxygenation at the fracture tissue impairs collagen synthesis, since oxygen is required for the hydroxylation of both lysine and proline in the collagen triple helix<sup>179</sup>.

Specific to osteoblasts, hypoxic environments reduce the activity of the cells involved in bone formation. The amount of bone formed was significantly reduced after osteoblasts were exposed to low oxygen tensions (2% oxygen). When the oxygen concentration was reduced to 0.2%, bone formation capacity was lost completely<sup>131</sup>. Hypoxia can, therefore, slow osteoblast growth and differentiation, thereby limiting bone formation. An *in vivo* study found that ovariectomized rats exposed to short-term hypoxia were less likely to develop bone than controls<sup>180</sup>. Hypoxia not only inhibits osteoblast differentiation and activity but also expression of the transcription factor Runx2, which is the likely explanation that MSCs' are unable to differentiate into osteoblasts<sup>132,133,134</sup>. Hypoxia also inhibits the PI3K/AKT pathway, a pathway downstream of c-MET signalling which is involved in cellular survival. It is hypothesized that inhibition of PI3K-AKT might account for the reduced osteoblast differentiation in hypoxic conditions<sup>135</sup>.

Regarding enzyme activity in osteoblastogenesis, the expression and activity of the osteoblast enzyme alkaline phosphatase is also decreased in hypoxia, resulting in decreased osteoblast matrix mineralization<sup>131</sup>. Hypoxia-induced inhibition of osteoblast function can also be attributed to reduced pyruvate dehydrogenase and lysyl oxidase enzyme activities<sup>119,131</sup>. In hypoxia, these oxygen-dependent enzymes required for collagen post-translational modifications are reduced, resulting in impaired collagen crosslinking<sup>131</sup>. The release of adenosine triphosphate (ATP) by osteoblasts during hypoxia may also inhibit bone formation while simultaneously stimulating osteoclasts<sup>181</sup>.

In contrast to osteoblasts, osteoclasts are relatively more complex in their response to hypoxia. Initially, hypoxia is known to stimulate an increase in osteoclast activity and proliferation. Specifically, when mouse bone marrow in culture was exposed to 2% oxygen tension, the activity and number of osteoclasts increased rapidly<sup>136</sup>. In addition, oxygen deprivation promoted osteoclast osteoresorption by reducing the cellular oxygen concentration. Resorption pits were formed tenfold more frequently<sup>182</sup>.

However, it is worth noting that this model is based upon a regular "hypoxia-reoxygenation" cycle and quite different from a fracture environment in which continuous hypoxia prevails. Osteoclasts are sensitive to oxygen concentration due to reoxygenation<sup>183</sup>. Increased osteoclast numbers may be related to reactive oxygen species after intermittent hypoxic exposure. In sustained hypoxia, however, osteoclast differentiation and function are inhibited, even causing apoptosis<sup>137</sup>. Interestingly, the mechanism by which hypoxia inhibits osteoclast growth factor (OPG), the decoy receptor for RANKL, is known, but it is not known whether this counteracts the inhibitory effect of hypoxia on osteoclasts<sup>184</sup>.

In order to validate the effect of c-Met inhibition on osteoblast and osteoclast differentiation, cabozantinib was used to treat cells in hypoxia. There are two main ways by which the HGF/c-MET axis is inhibited. Developing monoclonal antibodies (mAbs) that inhibit HGF/c-MET activity and/or c-MET dimerization is one approach. Another approach is the use of small molecule c-MET kinase inhibitors, which block phosphorylation and downstream signaling by targeting activation sites in the receptor's cytoplasm. Cabozantinib is a class II ATP competitor that belongs to the group of kinase inhibitors<sup>185</sup>. Cabozantinib is known to block c-Met signaling efficiently and has been used in multiple cancer treatment trials, for example, thyroid cancer<sup>186</sup>. In our work, we used cabozantinib to treat osteoblast progenitors and osteoclast progenitors in hypoxia environment in order to evaluate the effect of c-Met suppression on osteoblastogenesis and osteoclastogenesis against hypoxia,

Our purpose was to identify whether hypoxia in the musculoskeletal compartment caused by fracture nonunion affects the expression of c-Met in osteoclasts and osteoblasts. We found that inhibition of c-Met in osteoblasts and osteoclasts may disrupt the normal bone metabolic process. In this section, a hypoxic environment with different oxygen densities mimicking fracture nonunion was created to test the differentiation of an osteoblast and osteoclast cell line. The c-Met inhibitor cabozantinib was used to determine whether suppression of c-Met would rescue bone cell differentiation suppressed by hypoxia.

## **4.3 Materials and methods**

### **4.3.1 Cell lines and tissue culture**

MC3T3 cells (an osteoblast precursor cell line derived from *Mus musculus* calvaria, donated by Dr. Fred Berry's Lab, University of Alberta) were grown on plates in alpha modified Eagle's medium ( $\alpha$ -MEM, Sigma-Aldrich, St. Louis, MO, USA) with 10% foetal bovine serum (FBS, Gibco, Carlsbad, CA, USA) until confluent. Cells were cultured in osteogenic induction media,  $\alpha$ -MEM with 10% FBS+10 mM  $\beta$ -glycerophosphate (Sigma-Aldrich, St. Louis, MO, USA) and 50  $\mu$ g/mL ascorbic acid (Sigma-Aldrich, St. Louis, MO, USA), to stimulate differentiation into osteoblasts. RAW264.7 cells (monocyte/macrophage-like cells, Thermo Fisher Scientific, Waltham, MA, USA) were plated on incubation plates with complete  $\alpha$ -MEM to adhere. The next day, the cells were stimulated with medium supplemented with recombinant murine RANK-ligand protein (50 ng/mL, PeproTech, Rocky Hill, NJ, USA).

### **4.3.2 Hypoxic incubation and cabozantinib usage**

Hypoxia was created by an Xvivo System Model X3 (BioSpherix, Parish, NY, USA) or CO<sub>2</sub> Incubator (INCO108med, Memmert GmbH + Co. KG, Schwabach, Germany) with specific chambers that regulated the concentration of oxygen. Prior to incubation, oxygen tensions of 1% and 5% were set to reach stable running conditions. MC3T3 and RAW264.7 cells were seeded in different plates for different assays. After adhesion, cells were either left in the regular incubator containing 5% CO<sub>2</sub> and approximately 20% O<sub>2</sub> or moved to a hypoxic chamber containing 5% CO<sub>2</sub> and 1% O<sub>2</sub>, balanced with nitrogen. The analysis took place at different time points for each type of cell. Cabozantinib (c-Met inhibitor, BMS-907351, Selleck Chemicals LLC, Houston TX 77230 USA), diluted in dimethyl sulfoxide (DMSO), was used at various concentrations (1, 3 and 5  $\mu$ M) to treat MC3T3 and RAW264.7 cells initially incubated at 1% oxygen tension.

### **4.3.3 Alizarin Red staining and ALP staining**

We used Alizarin Red staining and ALP staining to evaluate bone cell differentiation. MC3T3 cells cultured in hypoxic and 20% oxygen tension were fixed with 4% paraformaldehyde (PFA) for 30 min, followed by PBS washing. A 0.2% Alizarin Red Tris HCl (pH: 8.3)

solution (Sigma-Aldrich, St. Louis, MO, USA) was added into the wells and incubated for 5 min.

MC3T3 cells were cultured in the same way for ALP staining. Then, the cells were fixed with 95% ethanol, washed with PBS three times, and stained using the BCIP/NBT Alkaline Phosphatase Color Development Kit (Sigma-Aldrich, St. Louis, MO, USA) in accordance with the manufacturer's instructions.

#### **4.3.4 TRAcP staining**

To determine the osteoclastogenesis of RAW264.7 cells cultured, we used TRAcP staining. RANKL-induced RAW264.7 cells were fixed in 4% PFA and stained using a tartrate resistant acid phosphatase and alkaline phosphatase (TRAP/ALP) stain kit (Wako Pure Chemical Industries, Ltd., Chuo-Ku, Japan). TRAcP<sup>+</sup> multinucleate cells (stained nuclei > three) were counted as osteoclasts using microscopy.

#### **4.3.5 Western blot**

To assess the expression of c-Met and its signalling pathway under hypoxic conditions or treatment with cabozantinib at 1, 3 and 5  $\mu\text{M}$ , we used a Western blot assay to detect protein expression. Pretreated MC3T3 and RAW264.7 cells in each group were lysed in radioimmunoprecipitation assay (RIPA) lysis buffer (Millipore, Billerica, MA, USA), and total protein was extracted. Protein concentrations were measured using a BCA protein assay (Promega, Madison, WI, USA). Equal amounts of cellular protein were separated by sodium dodecyl sulphate (SDS)-polyacrylamide gel electrophoresis and transferred to a polyvinylidene fluoride (PVDF) membrane. Membranes were blocked with 5% skim milk in TBS-T buffer and incubated with the appropriate primary antibodies at 4°C overnight. Antibodies against c-Met, phosphorylated ERK, ERK, phosphorylated JNK, JNK, phosphorylated p38, p38, RUNX2, phosphorylated  $\beta$ -catenin, and  $\beta$ -catenin were purchased from Cell Signaling Technology (Danvers, MA, USA). NFATc1, CTSK and  $\beta$ -actin were purchased from Santa Cruz Biotechnology, Inc. (Dallas, TX, USA). The membranes were incubated with secondary antibodies for 2 h and treated with enhanced chemiluminescence (ECL) reagents (Amersham Pharmacia Biotech, Amersham, United Kingdom). Protein bands were detected by visualizing the blots on a ChemiDoc MP Imaging System (Bio-Rad Laboratories (Canada) Ltd., Mississauga, Canada).

#### 4.3.6 RT-qPCR

To assess the gene expression of *c-Met* and related genes, we used RT-qPCR. RT-qPCR was utilized to evaluate the expression of *Runx2*, *Alp*, *Colla1*, *Sp7*, *Bglap* during osteogenic induction and osteoclast-related gene expression (*Acp5*, *Ctsk*, *Atp6v0a3*, *Nfatc1*, *Dcstamp*) during RANKL-induced osteoclast differentiation. Total RNA was isolated from pretreated MC3T3 and RAW264.7 cells using TRIzol® reagent (Life Technologies, Carlsbad, CA, USA). Next, 1 µg of RNA template was reverse transcribed to single-standard complementary DNA (cDNA) by Moloney murine leukaemia virus reverse transcriptase (M-MLV-RT) with an oligo-dT primer (Promega Corporation, Madison, WI, USA). RT-qPCR was performed using a real-time PCR machine (Applied Biosystems, Warrington, Cheshire, UK). Primers were designed against the following mouse sequences: *m-c-Met* (forward, 5'-GGTGCGGTCTCAATATCAGTAG-3'; reverse, 5'-CTCTTGCGTCATAGCGAACT-3'), *m-Runx2* (forward, 5'-TGGCTTGGGTTTCAGGTTAG-3'; reverse, 5'-GGTTTCTTAGGGTCTTGGAGTG-3'), *m-Alp* (forward, 5'-CTTTCGTAGCAGCAGCAAAC-3'; reverse, 5'-GGAGCGCGTCTTGGATATT-3'), *m-Coll1a1* (forward, 5'-AGACCTGTGTGTTCCCTACT-3'; reverse, 5'-GAATCCATCGGTCATGCTCTC-3'), *m-Sp7* (forward, 5'-TGGAGAGGGAAAGGGATTCT-3'; reverse, 5'-GAAATCTACGAGCAAGGTCTCC-3'), *m-Bglap* (forward, 5'-CTGCCCTAAAGCCAAACTCT-3'; reverse, 5'-AGCTGCTGTGACATCCATAC-3'), *m-Acp5* (forward, 5'-CGCTGACTTCATCATGTCTCT-3'; reverse, 5'-AACACGTCCTCAAAGGTCTC-3'), *m-Nfatc1* (forward, 5'-CCTCTGTGAGTCTTTGGGTTAG-3'; reverse, 5'-ACCACGGCAGGCTTATTT-3'), *m-Ctsk* (forward, 5'-TGACTTCCGCAATCCTTACC-3'; reverse, 5'-GAATCTGTTCGCTAGGCTCTT-3'), *m-Atp6v0a3* (forward, 5'-CGTCTACACTGGCTTCATCTAC-3'; reverse, 5'-TGGGACAGATACTCGTCACT-3'), *m-Dcstamp* (forward, 5'-CTATCTGCTGTATCGGCTCATC-3'; reverse, 5'-CTTGGGTTCCCTTGCTTCTCT-3'), and *m-β-actin* (forward, 5'-GAGGTATCCTGACCCTGAAGTA-3'; reverse, 5'-CACACGCAGCTCATTGTAGA-3').

#### 4.3.7 ELISA assay

To detect levels of intracellular c-Met and secreted HGF in MC3T3 and RAW264.7 cells in a hypoxic environment, we used an ELISA assay to evaluate HGF in the supernatant and c-Met in the lysate. ELISA assays were performed using a mouse HGF and phosphorylation-c-

Met ELISA kit (Jiangsu Meimian Industrial Co., Ltd., Jiangsu, China) according to the manufacturers' instructions.

#### 4.3.8 Statistical analysis

All data shown in this part are presented as the mean  $\pm$  standard deviation from multiple independent tests. Each test was performed at least three times. Statistical significance was determined by Student's t test or ANOVA, with  $p$  less than 0.05 regarded as significant. The normality for all data was measured by Shapiro-Wilk normality testing for the student's t test and ANOVA.

### 4.4 Results

#### 4.4.1 Hypoxia suppresses osteoblast differentiation and increases c-Met phosphorylation

To determine whether hypoxia affects osteoblastogenesis, we exposed MC3T3 cells to oxygen tensions of 1% and 5% during osteogenic differentiation. We evaluated the osteogenic properties of MC3T3 cells in a hypoxic environment using Alizarin Red staining and ALP staining to determine calcium deposition and ALP enzyme activity. The results showed that cells cultured in 5% oxygen tension showed less calcium nodule formation and less ALP production at Day 14 and Day 21 in the differentiation process (**Figure 33A and 33B**), while the 1% oxygen tension group showed almost no osteoblastogenesis, as hardly any calcium nodules were observed, and minimal ALP production was observed during a 21-day incubation (**Figure 33A and 33B**). The findings suggest that hypoxia during MC3T3 incubation significantly suppresses cellular differentiation towards mature osteoblasts.

As determined by Western blot analysis, the expression of c-Met increased threefold during osteogenic induction under normal oxygen tension (20% O<sub>2</sub>) (**Figure 33C and 33D**). Hypoxia (1% and 5% oxygen tensions) did not further promote total c-Met expression (**Figure 33C and 33D**). Nevertheless, the level of phosphorylation of c-Met measured by ELISA was slightly increased (**Figure 33E and 33F**). This result indicates that c-Met activity is slightly enhanced in MC3T3 cells at Day 7, while no changes in HGF in the supernatant were observed. Accord-

ingly, hypoxia appears to regulate the expression of c-Met during osteoblast differentiation. Hypoxia promotes phosphorylation of c-Met, despite no significant change in the total c-Met protein.

Western blot assays show that hypoxia interferes with Runx2 and WNT/ $\beta$ -catenin signaling by suppressing  $\beta$ -catenin phosphorylation and Runx2 (**Figure 34A-34D**). In addition, hypoxia inhibited the phosphorylation of ERK1/2, JNK and p38, which are essential components of MAPK/ERK signalling involved in osteoblast proliferation and differentiation (**Figure 35A and 35B**). Phosphorylation of PI3K and AKT is required for the survival of osteoblasts and was also decreased in hypoxic conditions (**Figure 36A to 36D**). Our findings suggest that hypoxia impairs osteoblastogenesis primarily by blocking RUNX2, MAPK/ERK, Wnt/ $\beta$ -catenin and PI3K/Akt signalling. Hypoxia also inhibited *c-Met*, *Runx2*, *Colla1*, *Alp*, *Sp7* and *Bglap* gene expression, as determined by RT-qPCR (**Figure 37A to 37F**)

#### 4.4.2 Hypoxia inhibits osteoclast differentiation and promotes c-Met phosphorylation

To assess osteoclast differentiation under hypoxia, we exposed RAW264.7 cells (monocytes,  $6 \times 10^3$  cell/well) to 50 ng/mL RANKL at various levels of oxygen tension (20%, 5% and 1%). The differentiation of osteoclasts was identified by tracing these multinuclear cells with TRAcP staining. In our study, we found that RAW264.7 cells began dividing and transformed into mature osteoclasts with multiple TRAcP-positive nuclei after Day 5 (**Figure 38A and 38B**). Comparatively, there were considerably fewer multinuclear cells at the corresponding time point at 5% oxygen tension, and no mature osteoclasts were detected at 1% oxygen tension (**Figure 38A and 38B**). The findings demonstrate that sustained hypoxia significantly suppresses osteoclast differentiation.

Similar to the results in MC3T3 cells, the amount of total c-Met in RAW264.7 cells was drastically increased in response to RANKL (**Figure 38B and 38C**). Although there was no change in c-Met expression under hypoxia, regardless of 1% or 5% oxygen tension, phosphorylation of c-Met was increased (**Figure 38B to 38D**). The results demonstrate that hypoxia can increase c-Met expression and phosphorylation even if total c-Met level remains unchanged. HGF levels in the supernatant during osteoclast differentiation remained unchanged (**Figure 38E**).

Osteoclast differentiation is primarily triggered by RANKL interacting with RANK. RANKL activated the osteoclast transcription factor *Nfatc1* to translocate to the nucleus, and CTSK was secreted as an enzyme in RAW264.7 cells. In the hypoxia-treated RAW264.7 cells, the protein expression of NFATc1 and CTSK and phosphorylation of AKT, as demonstrated by Western blot assays, decreased markedly at Days 5 and 7 (**Figure 39A to 39F**). Moreover, hypoxia reduced the phosphorylation of Jnk and p38 during osteoclast differentiation (**Figure 40A and 40B**). However, c-Met gene expression did not change under hypoxia (**Figure 41A**). Hypoxia also diminished the expression osteoclast-related genes, including *Acp5*, *Ctsk*, *Atp6v0a3*, *Nfatc1*, and *Dcstamp*, as shown by qPCR (**Figure 41B to 41F**). The results of our study suggest that hypoxia inhibits osteoclast differentiation by inhibiting RANKL activation, particularly by downregulating NFATc1 and CTSK expression, as well as MAPK/ERK pathway activation.

#### **4.4.3 Cabozantinib doesn't reverse the suppression of osteoblastogenesis and osteoclastogenesis under hypoxia**

Our observation of increased phosphorylation of c-Met in osteoblasts or osteoclasts differentiated under hypoxia led us to hypothesize that hypoxia inhibits cellular differentiation by activating c-Met expression. To test this hypothesis, we used various concentrations of cabozantinib, a c-Met inhibitor, to treat both osteoblasts and osteoclasts exposed to 1% oxygen tension. As demonstrated by Alizarin Red staining and ALP staining, cabozantinib did not rescue calcium nodule formation in MC3T3 cells under 1% oxygen tension (**Figure 42A**). Cabozantinib significantly suppressed the expression of c-Met in MC3T3 cells cultured in osteogenic-induction medium or when the cells were cultured under hypoxic conditions (**Figure 42B and 42C**). However, cabozantinib gradually increased Runx2 expression and  $\beta$ -catenin phosphorylation to a relatively normal level with increasing dosage (**Figure 43A to 43D**). Additionally, cabozantinib did not change the hypoxia-induced decrease in PI3K/AKT signalling (**Figure 44A to 44D**), ERK1/2 (**Figure 44E and 44F**), JNK, or p38 phosphorylation (**Figure 45A and 45B**). Since inhibition of c-Met failed to reverse the effects of hypoxia on the cells, we suspect that c-Met is not a key target regulator of hypoxia in osteoblast differentiation. Osteoblast differentiation may be affected in part by hyperoxia via RUNX2, the Wnt/ $\beta$ -catenin signaling family, and the MAPK/ERK family but not by c-Met. Cabozantinib promotes RUNX2 expression and activates Wnt/ $\beta$ -catenin signalling, but its effects on osteoblastogenesis promotion are counteracted by hypoxia.



Cabozantinib at concentrations ranging from 1  $\mu$ M to 5  $\mu$ M did not affect the suppression of RANKL-induced osteoclast formation under hypoxia (**Figure 46A and 46B**). Cabozantinib inhibited the expression of c-Met in osteoclasts cultured in hypoxic conditions (**Figure 46C and 46D**). NFATc1, CTSK and AKT were suppressed as a result of hypoxia, and cabozantinib had a plus-inhibitory effect on them; they were suppressed to a much greater extent than with hypoxia (**Figure 47A to 47F**). The same result was also observed in the suppression of JNK and p38 phosphorylation (**Figure 48A and 48B**). Previous *in vitro* works has shown that cabozantinib suppresses osteoclast differentiation in hypoxic conditions; we also observed a reduction of NFATc1 and CTSK in our study. Hyperoxia may not enhance c-Met activity since inhibiting the expression of c-Met with cabozantinib did not restore cellular differentiation.

#### 4.5 Discussion

Tibial shaft and femur neck fractures experience an ongoing hypoxic environment within the fracture site which hinders fracture healing<sup>5,6,29</sup>. Sustained hypoxia disrupts the normal differentiation of osteoblasts and osteoclasts and consequently impairs callus remodelling<sup>131–133,137</sup>. Here, we developed an experimental model that allows us to determine c-Met expression and correlate these levels to cellular growth in hypoxic conditions. MC3T3 differentiation is significantly inhibited by hypoxia, particularly 1% oxygen tension, as shown by a reduction in calcium deposits and decreased ALP expression. Additionally, hypoxia reduces Runx2 protein expression and inhibits  $\beta$ -catenin phosphorylation. The transcription factor, Runx2 induces mesenchymal cells to differentiate into osteoblasts via the regulation of  $\beta$ -catenin activity<sup>37,50,64</sup>. Inhibition of MC3T3 differentiation in our experiments correlated with reduced  $\beta$ -catenin phosphorylation (which indicates decreased  $\beta$ -catenin translocation into the nucleus of osteoblast progenitors) and Runx2 suppression. Hypoxia also suppresses MAPK/ERK signalling which contributes to the proliferation and survival of osteoblast progenitors<sup>85</sup>. Likewise, hypoxia significantly blocked RAW264.7 cell differentiation into multinuclear mature osteoclasts, as revealed by TRAcP staining. TRAcP-positive osteoclast numbers were decreased at 5% oxygen tension, and an even larger decrease was detected at 1% oxygen tension. Hypoxia diminished NFATc1 and CTSK expression, as well as the phosphorylation of p38 and JNK which are key to osteoclast precursor proliferation, differentiation, and survival.

c-Met expression was markedly enhanced during the differentiation of MC3T3 cells and by RANKL in RAW264.7 cells. We suspect that that osteogenic induction and RANKL trigger c-Met receptor activation in the absence of additional HGF. Multiple cell types and cancer cells have been found to differentially express c-Met when hypoxia is present. Glioblastoma, for instance, is known to respond to hypoxia by increasing c-Met expression, which in turn enhances HGF for tumor cell migration<sup>187</sup>. Human salivary gland cancers are prone to metastatic spread due to hypoxia activating the HGF/c-Met system via HIF-1 $\alpha$ <sup>188</sup>. Similarly, hypoxia was found to promote the transcription of c-Met in carcinoma cells from lung (A549), ovarian (SK-OV-3), cervical (SiHa), bone (U2-OS) and liver HepG2 cells<sup>189</sup>. Conversely, in the canine kidney cell line and in the human mammary gland cell line, MET autophosphorylation was drastically diminished by oxygen deprivation but returned to normal within minutes under normoxia<sup>190</sup>. Consequently, it is difficult to predict c-Met expression patterns in specific cell lines since hypoxia may modulate protein or gene expression. In our present study, compared to normal oxygen tension, hypoxia did not modify the expression of total c-Met in either of the two treated cell lines when they were placed in a hypoxic chamber at 1% or 5% oxygen tension. Nonetheless, hypoxia was found to slightly enhance the phosphorylation of c-Met in the lysates of MC3T3 and RAW264.7 cells at later time points by ELISA. Additionally, exogenous HGF was secreted at higher levels in both cell lines when placed in hypoxic environments, indicating a positive correlation between c-Met and HGF.

To further investigate whether the increased phosphorylation of c-Met induced by hypoxia suppresses osteoblast and osteoclast differentiation, we treated both cell lines with a c-Met inhibitor, cabozantinib, and incubated the cells in 1% oxygen. Despite significant reductions in phosphorylation and total levels of c-Met in hypoxic conditions, cabozantinib failed to reverse the suppression of osteoblast and osteoclast differentiation. Thus, we infer the following conclusion based on these findings. First, the changes in c-Met expression induced by hypoxia have no bearing on the differentiation of bone cells. Second, inhibiting c-Met did not reverse the suppressive effect of hypoxia on cellular differentiation. Third, hypoxia suppresses osteoblast and osteoclast differentiation not through c-Met but via signaling pathways, such as RUNX2, Wnt/ $\beta$ -catenin, NFATc1 and CTSK. Fourth, the increase in active c-Met induced by hypoxia may not affect the actual behavior of cells.

In the previous chapter, conditional knockout mice showed that c-Met regulates osteoblast and osteoclast activity *in vivo*. Here we found that the change in c-Met activity induced by hypoxia does not contribute to osteoblast and osteoclast differentiation. Therefore, we conclude that c-Met is a molecular driver of bone cell differentiation, independent of hypoxia. Further research is needed to determine the mechanism by which c-Met regulates osteoblast-induced callus formation and osteoclast-induced bone remodelling in fracture repair.

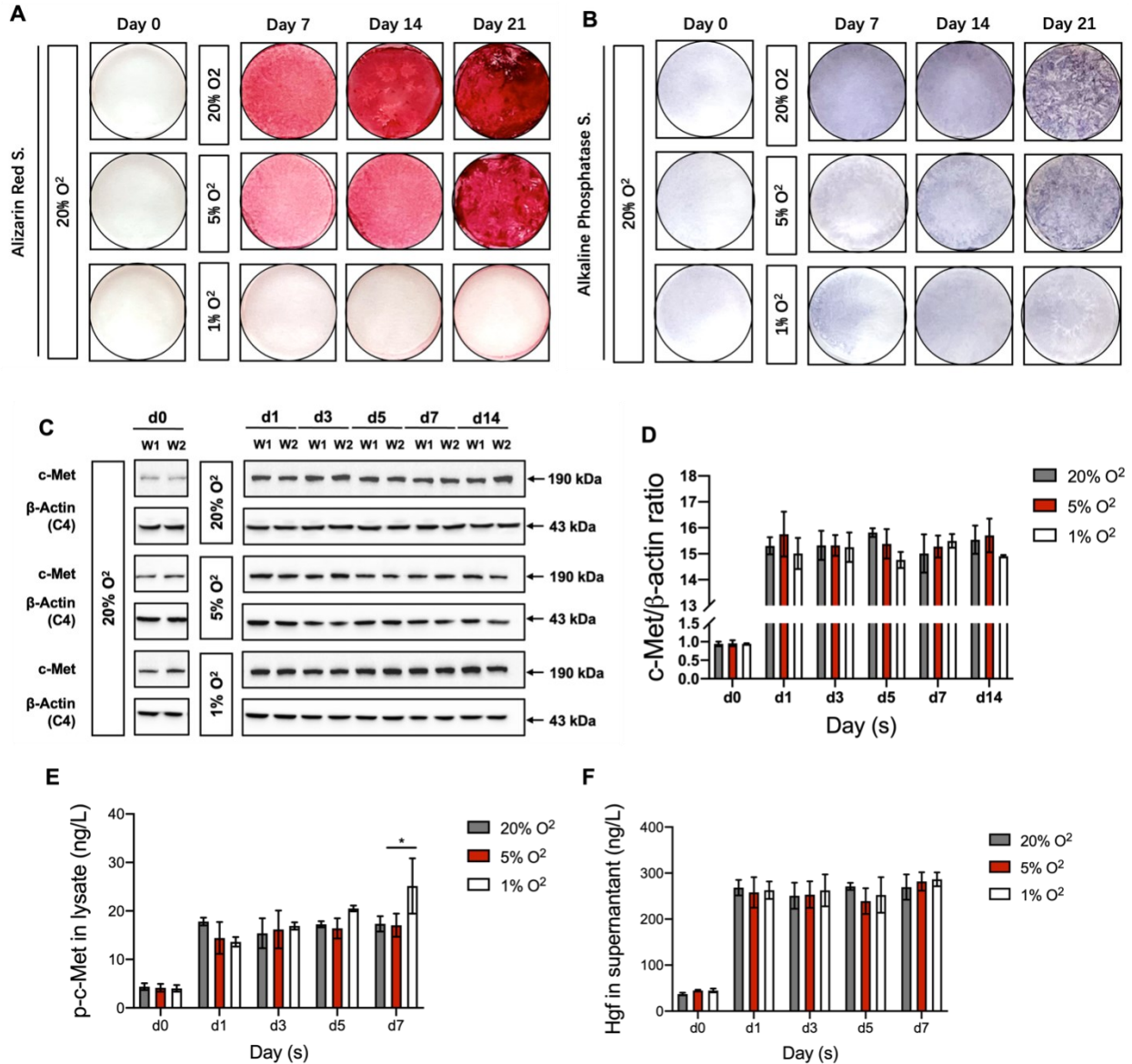


**Figure 33. Hypoxia regulates osteoblast differentiation and c-Met/HGF expression.**

(A) Representative images of Alizarin Red staining showing osteoclast differentiation in 20%, 5% and 1% oxygen tension from Day 0 to Day 21 (n=3). (B) Representative images of ALP staining demonstrating osteoclast differentiation in 20%, 5% and 1% oxygen tension from Day 0 to Day 21 (n=3). (C) Representative Western blot images showing c-Met protein expression in 20%, 5% and 1% oxygen tension from Day 0 to Day 14 (n=3).  $\beta$ -actin was set as the loading control. (D) Quantitative analysis of c-Met expression (n=3). (E) Quantitative analysis of ELISAs for the lysate phosphorylation of c-Met in 20%, 5% and 1% oxygen tension from Day

0 to Day 21 (n=3). (F) Quantitative ELISAs for the supernatant HGF in 20%, 5% and 1% oxygen tension from Day 0 to Day 21 (n=3). \* $p < 0.05$  versus the 20% oxygen group at each time point.

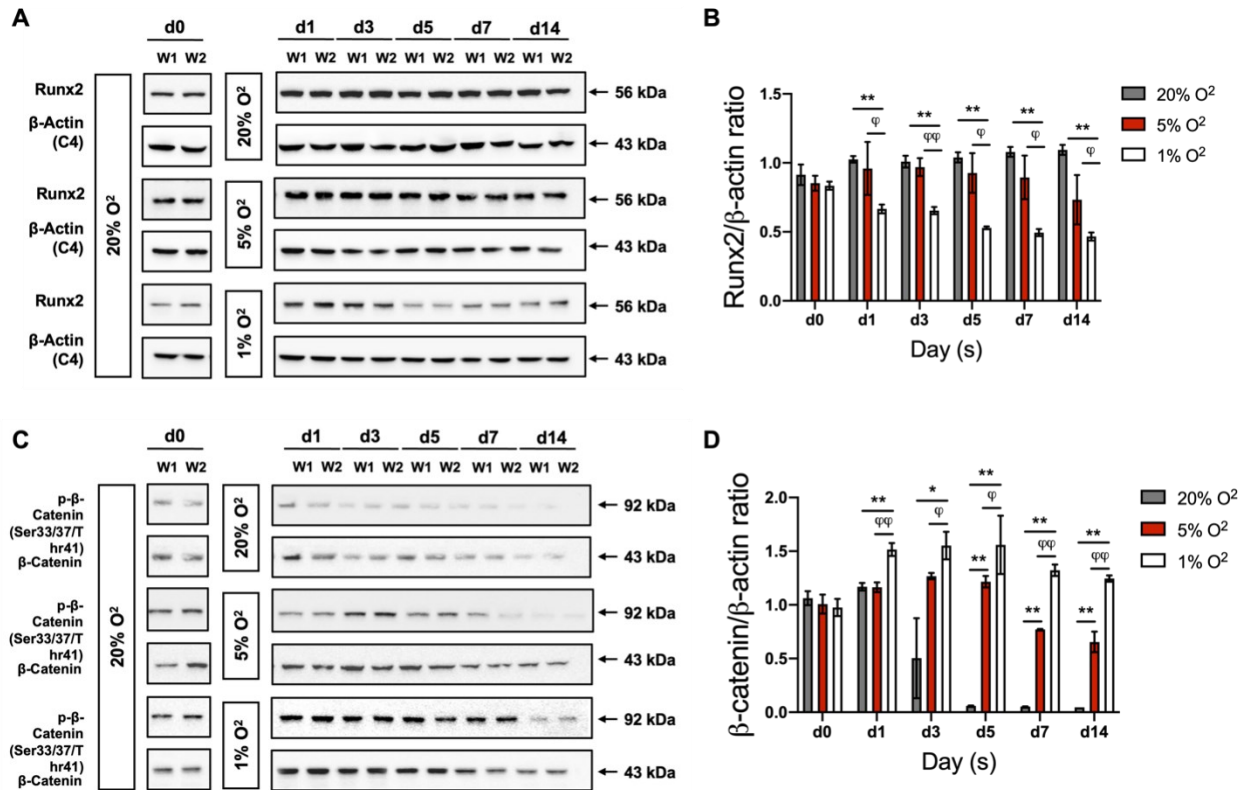


**Figure 34. Hypoxia regulates RUNX2 and  $\beta$ -catenin in osteoblast differentiation.**

(A) Representative Western blot images showing RUNX2 protein expression in 20%, 5% and 1% oxygen tension from Day 0 to Day 14 (n=3). (B) Quantitative analysis of RUNX2 expression (n=3). (C) Representative Western blot images showing  $\beta$ -catenin protein expression in 20%, 5% and 1% oxygen tension from Day 0 to Day 14 (n=3). (D) Quantitative analysis of  $\beta$ -catenin expression (n=3).  $\beta$ -actin was set as the loading control. \* $p < 0.05$ , \*\* $p < 0.01$  versus the 20% oxygen group at each time point.  $\phi p < 0.05$ ,  $\phi\phi p < 0.01$  versus the 5% oxygen group at each time point.

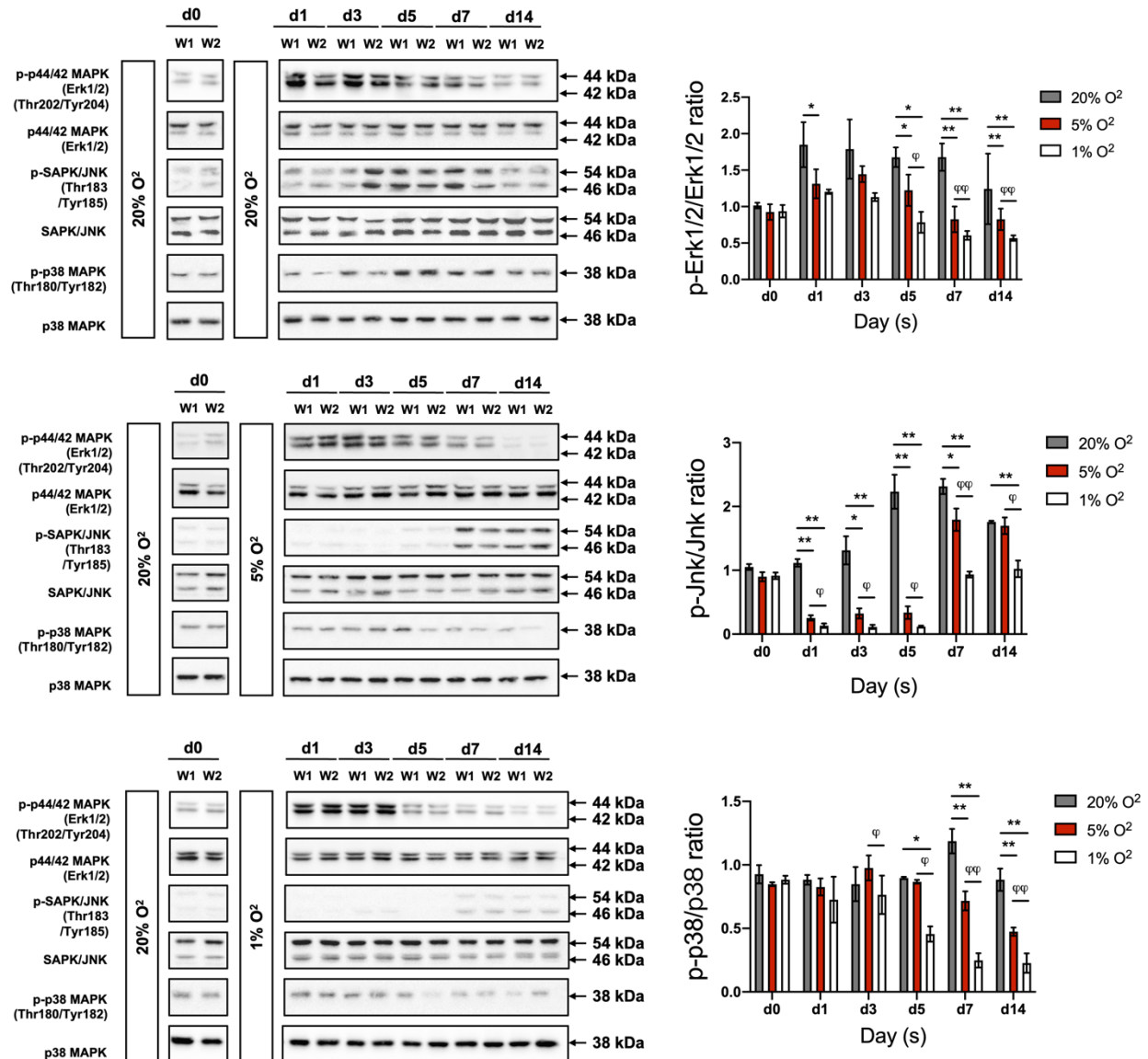


**Figure 35. Hypoxia regulates MAPK/Erk signalling in osteoblast differentiation.**

(A) Representative Western blot images showing the phosphorylation of ERK1/2, JNK and p38 in 20%, 5% and 1% oxygen tension from Day 0 to Day 14 (n=3). (B) Quantitative analysis of the phosphorylation of ERK1/2, JNK and p38 (n=3). ERK1/2, JNK and p38 were used as the loading controls. \* $p < 0.05$ , \*\* $p < 0.01$  versus the 20% oxygen group at each time point.  $\phi p < 0.05$ ,  $\phi\phi p < 0.01$  versus the 5% oxygen group at each time point.

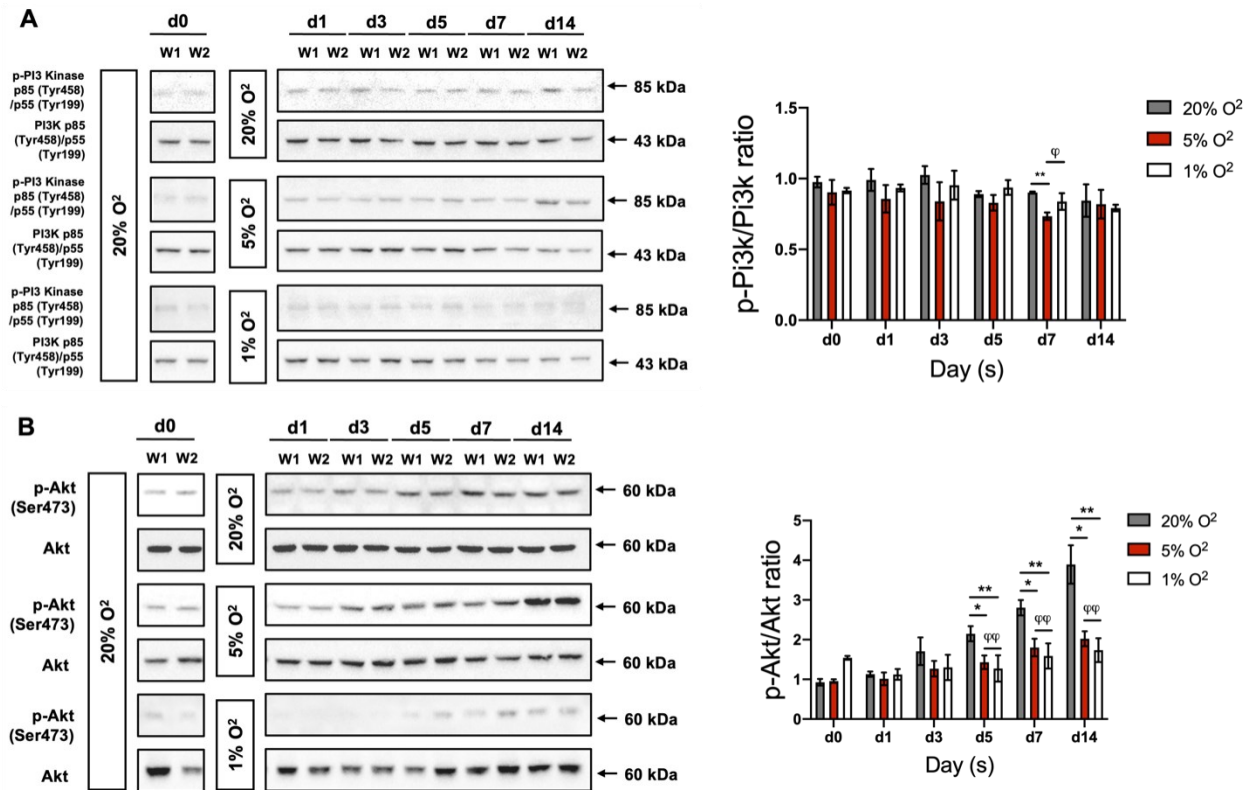


**Figure 36. Hypoxia regulates PI3K/AKT signalling in osteoblast differentiation.**

(A) Representative Western blot images showing the phosphorylation of PI3K and AKT in 20%, 5% and 1% oxygen tension from Day 0 to Day 14 (n=3). (B) Quantitative analysis of the expression of phosphorylated PI3K and AKT (n=3). PI3K and AKT were set as the loading controls. \* $p < 0.05$ , \*\* $p < 0.01$  versus the 20% oxygen group at each time point.  $\phi p < 0.05$ ,  $\phi\phi p < 0.01$  versus the 5% oxygen group at each time point.



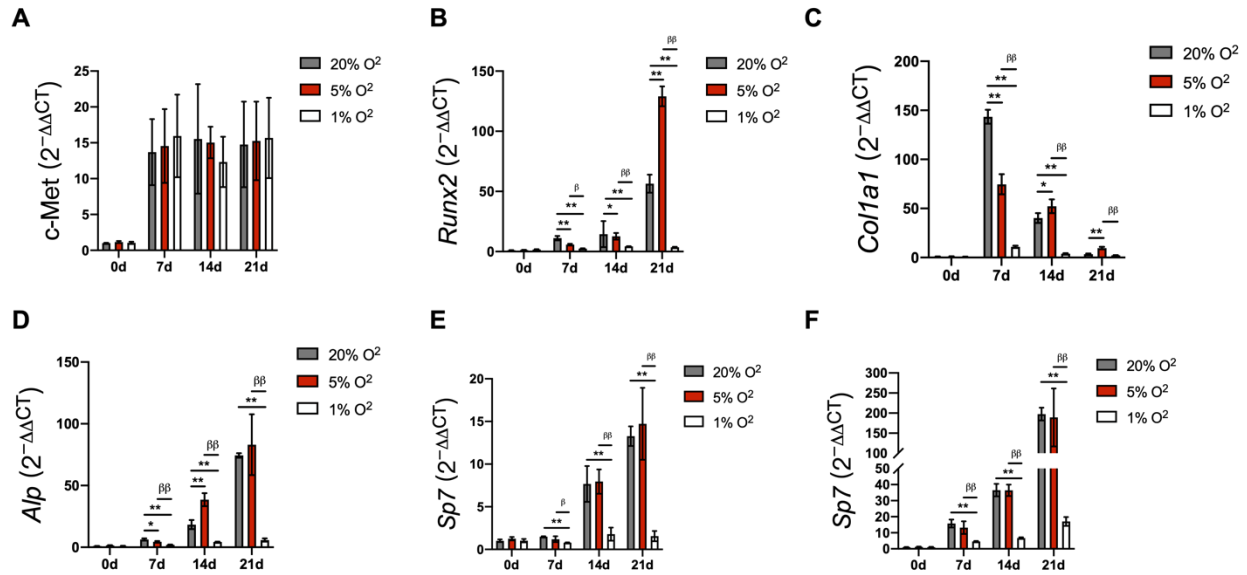


**Figure 37. Hypoxia regulates *c-Met* and osteoblast-related genes during osteoblast differentiation.**

(A-F) Quantitative analysis of the gene expression of *c-Met*, *Runx2*, *Col1a1*, *Alp*, *Sp7*, and *Bglap* in 20%, 5% and 1% oxygen tension from Day 0 to Day 14 (n=3).  $\beta$ -actin was set as the control.  $*p < 0.05$ ,  $**p < 0.01$  versus the 20% oxygen group at each time point.  $\beta p < 0.05$ ,  $\beta\beta p < 0.01$  versus the 5% oxygen group at each time point.

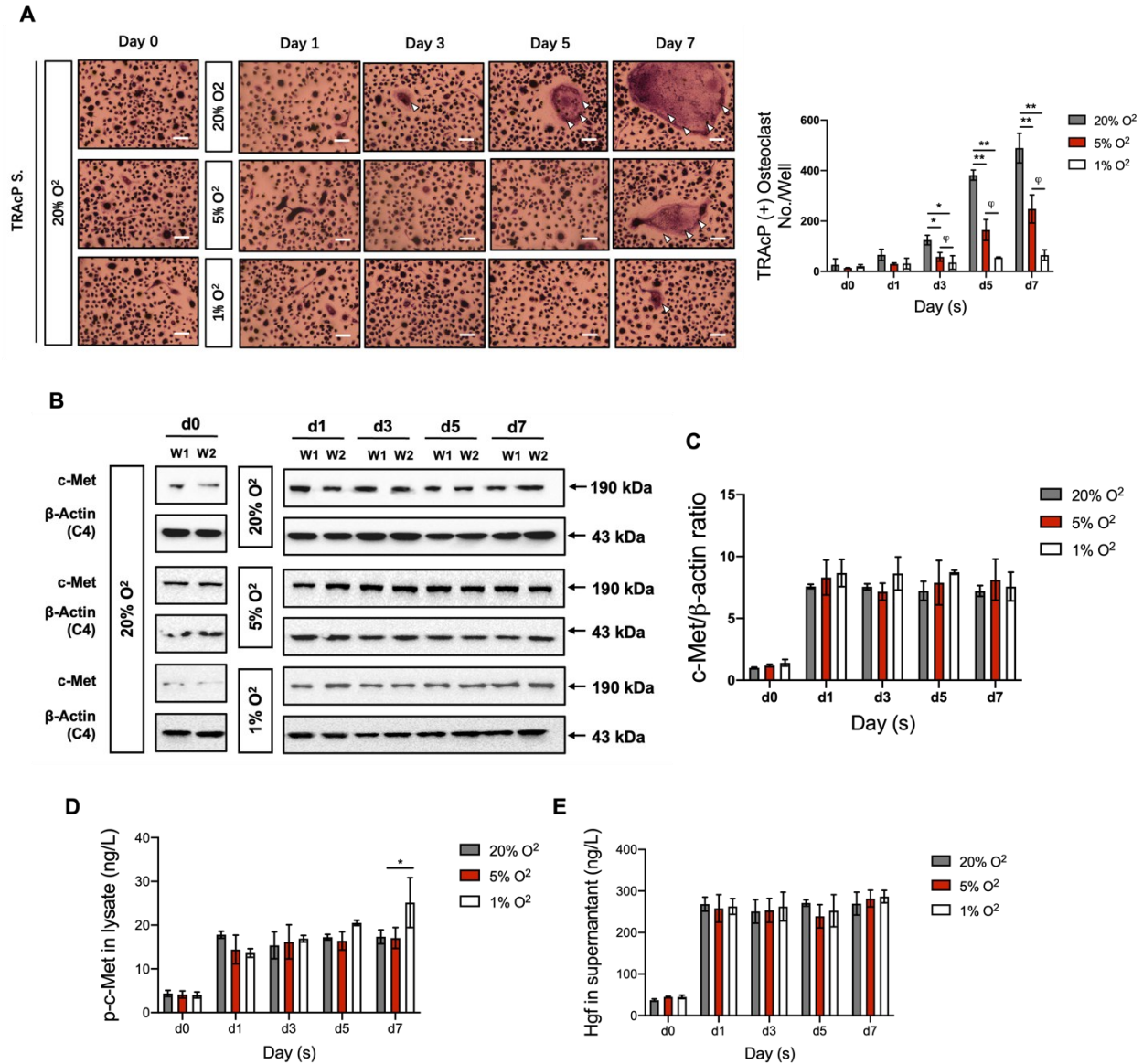


**Figure 38. Hypoxia regulates osteoclast differentiation and c-Met/HGF expression.**

(A) Representative images of TRAcP staining showing osteoclast differentiation in 20%, 5% and 1% oxygen tension from Day 0 to Day 21 (n=3). (B) Representative Western blot images showing c-Met protein expression in 20%, 5% and 1% oxygen tension from Day 0 to Day 7 (n=3). (C) Quantitative analysis of c-Met expression (n=3).  $\beta$ -actin was set as the loading control. (D) Quantitative ELISAs for the lysate phosphorylation of c-Met in 20%, 5% and 1% oxygen tension from Day 0 to Day 21 (n=3). (E) Quantitative ELISAs for the supernatant HGF in 20%, 5% and 1% oxygen tension from Day 0 to Day 21 (n=3). \* $p < 0.05$ , \*\* $p < 0.01$  versus the

20% oxygen group at each time point.  $p < 0.05$ ,  $p < 0.01$  versus the 5% oxygen group at each time point.

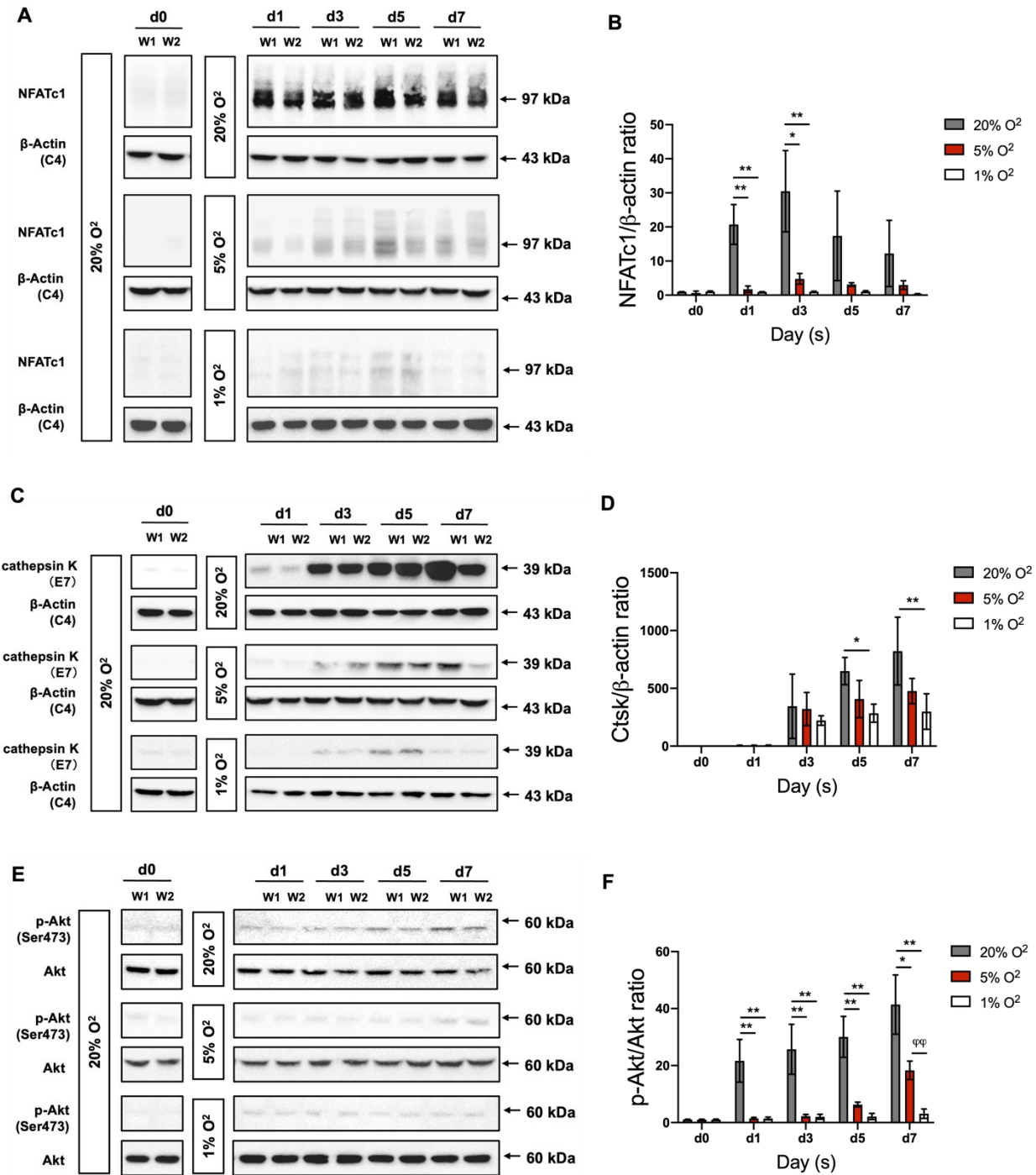


**Figure 39. Hypoxia regulates NFAT1, CTSK and AKT in osteoclast differentiation.**

(A) Representative Western blot images showing NFATc1 expression under 20%, 5% and 1% oxygen tension from Day 0 to Day 7 (n=3). (B) Quantitative analysis of NFATc1 expression (n=3). (C) Representative Western blot images showing CTSK protein expression in 20%, 5%

and 1% oxygen tension from Day 0 to Day 7 (n=3). (D) Quantitative analysis of CTSK expression (n=3). (E) Representative Western blot images showing the phosphorylation of AKT in 20%, 5% and 1% oxygen tension from Day 0 to Day 7 (n=3). (F) Quantitative analysis of AKT phosphorylation (n=3).  $\beta$ -actin and AKT were set as the loading controls. \* $p < 0.05$ , \*\* $p < 0.01$  versus the 20% oxygen group at each time point.  $\Phi p < 0.05$ ,  $\Phi\Phi p < 0.01$  versus the 5% oxygen group at each time point.

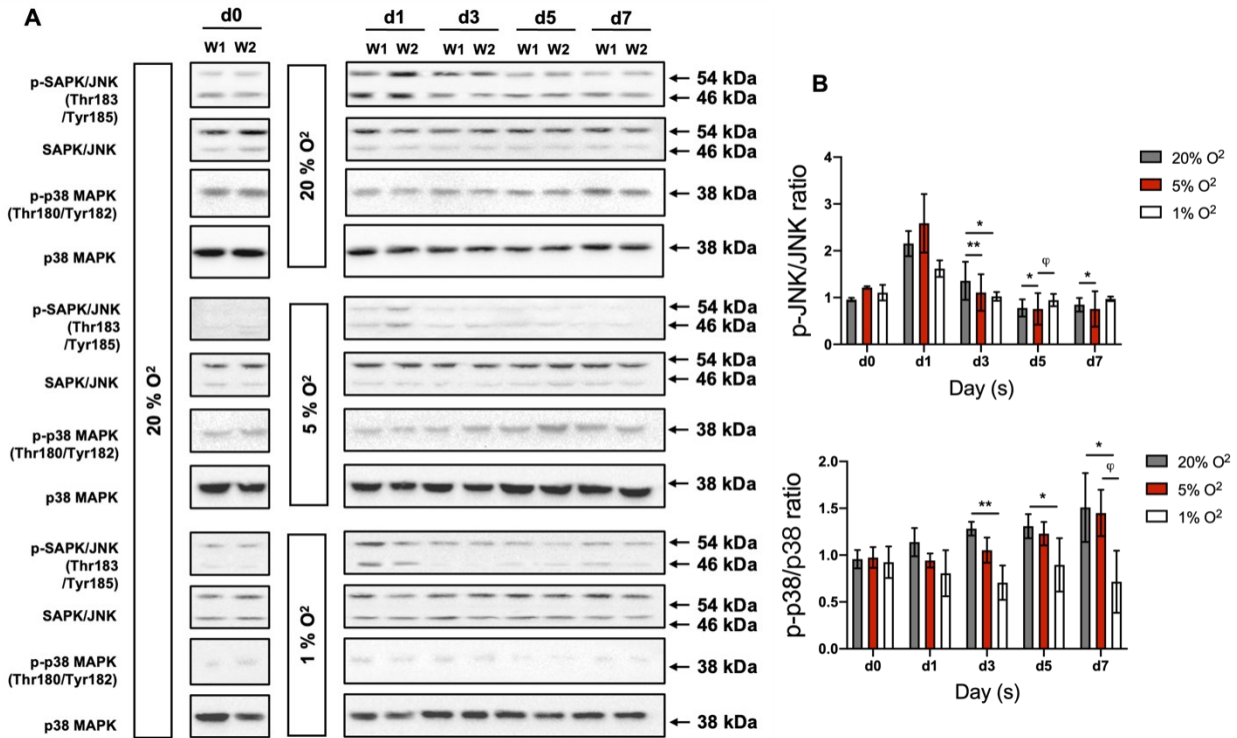


**Figure 40. Hypoxia regulates JNK and p38 in osteoclast differentiation.**

(A) Representative Western blot images showing the phosphorylation of JNK and p38 in 20%, 5% and 1% oxygen tension from Day 0 to Day 7 (n=3). (B) Quantitative analysis of phosphorylation of JNK and p38 expression (n=3). JNK and p38 were set as the loading controls. \* $p < 0.05$ , \*\* $p < 0.01$  versus the 20% oxygen group at each time point.  $\phi p < 0.05$ ,  $\phi\phi p < 0.01$  versus the 5% oxygen group at each time point.

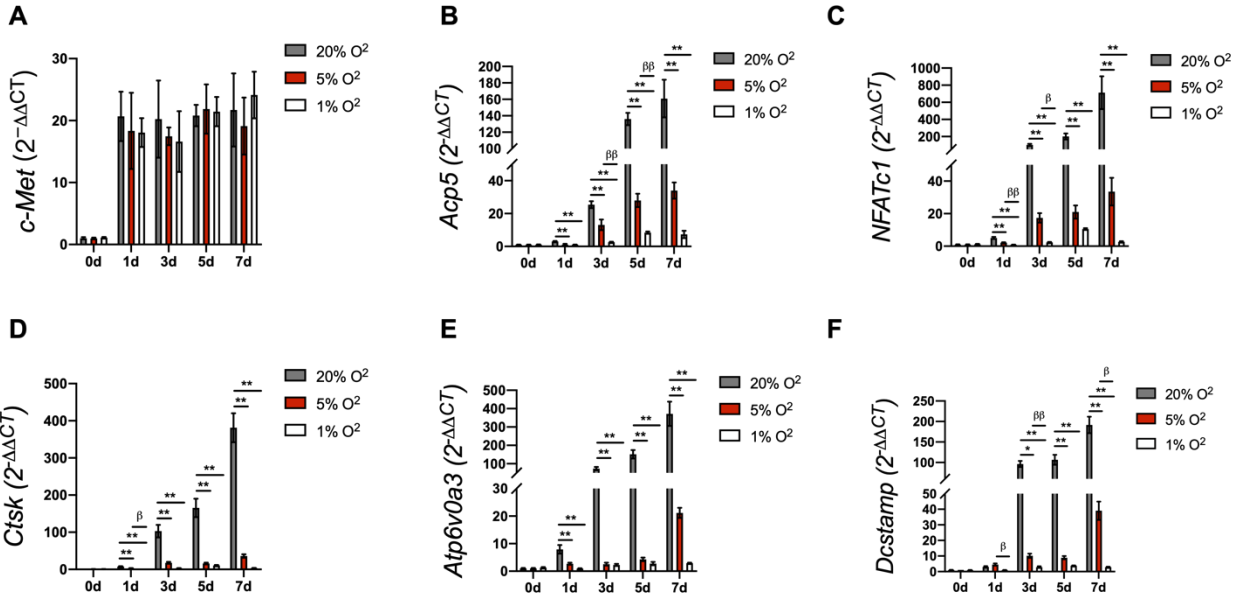


**Figure 41. Hypoxia regulates *c-Met* and osteoclast-related genes during osteoclast differentiation.**

(A-F) Quantitative analysis of the gene expression of *c-Met*, *Acp5*, *NFATc1*, *Ctsk*, *Atp6v0a3* and *Dcstamp* in 20%, 5% and 1% oxygen tension from Day 0 to Day 7 (n=3).  $\beta$ -actin was set as the control. \* $p < 0.05$ , \*\* $p < 0.01$  versus the 20% oxygen group at each time point.  $\beta$  $p < 0.05$ ,  $\beta\beta$  $p < 0.01$  versus the 5% oxygen group at each time point.

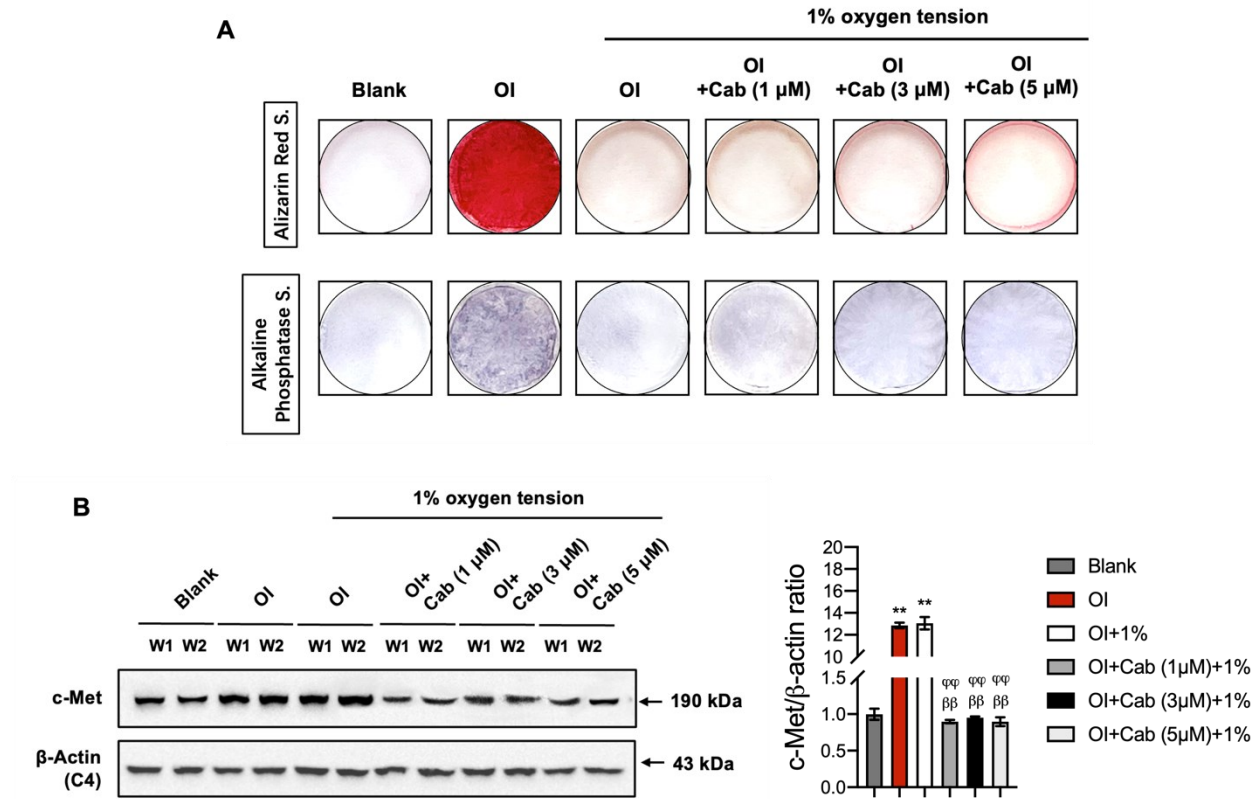


**Figure 42. Cabozantinib regulates osteoblast differentiation and c-Met expression.**

(A) Representative images of Alizarin Red staining and ALP staining showing osteoclast differentiation in addition to various concentrations of cabozantinib (n=3). (B) Representative Western blot images showing c-Met protein expression in addition to various concentrations of cabozantinib (n=3). (C) Quantitative analysis of c-Met expression (n=3).  $\beta$ -actin was set as the loading control.  $**p < 0.01$  versus to the blank group.  $\beta\beta p < 0.01$  versus to the OI group.  $\phi\phi p < 0.01$  versus to the OI group+1%.



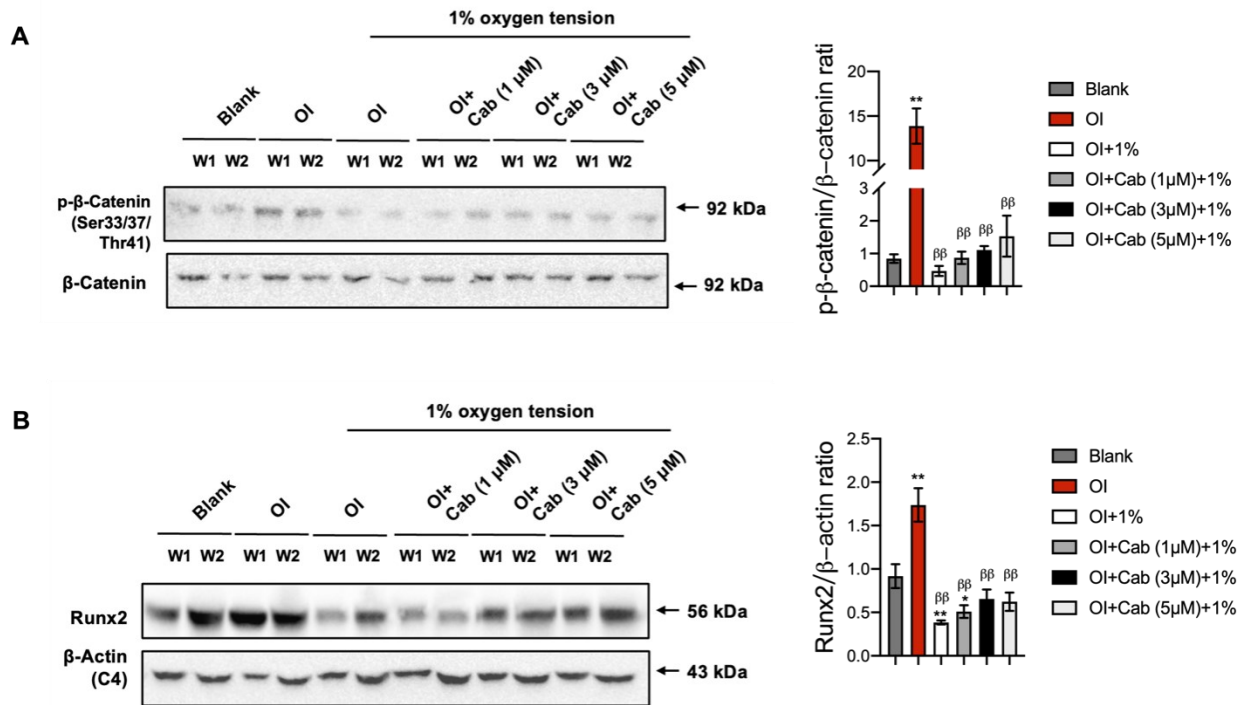


**Figure 43. Cabozantinib regulates RUNX2 and  $\beta$ -catenin in osteoblast differentiation.**

(A) Representative Western blot images showing RUNX2 protein expression with various concentrations of cabozantinib (n=3). (B) Quantitative analysis of RUNX2 expression (n=3). (C) Representative Western blot images showing  $\beta$ -catenin protein expression with various concentrations of cabozantinib (n=3). (D) Quantitative analysis of  $\beta$ -catenin expression (n=3).  $\beta$ -actin and  $\beta$ -catenin were used as the loading controls.  $**p < 0.01$  versus the blank group.  $\beta\beta p < 0.01$  versus the OI group.

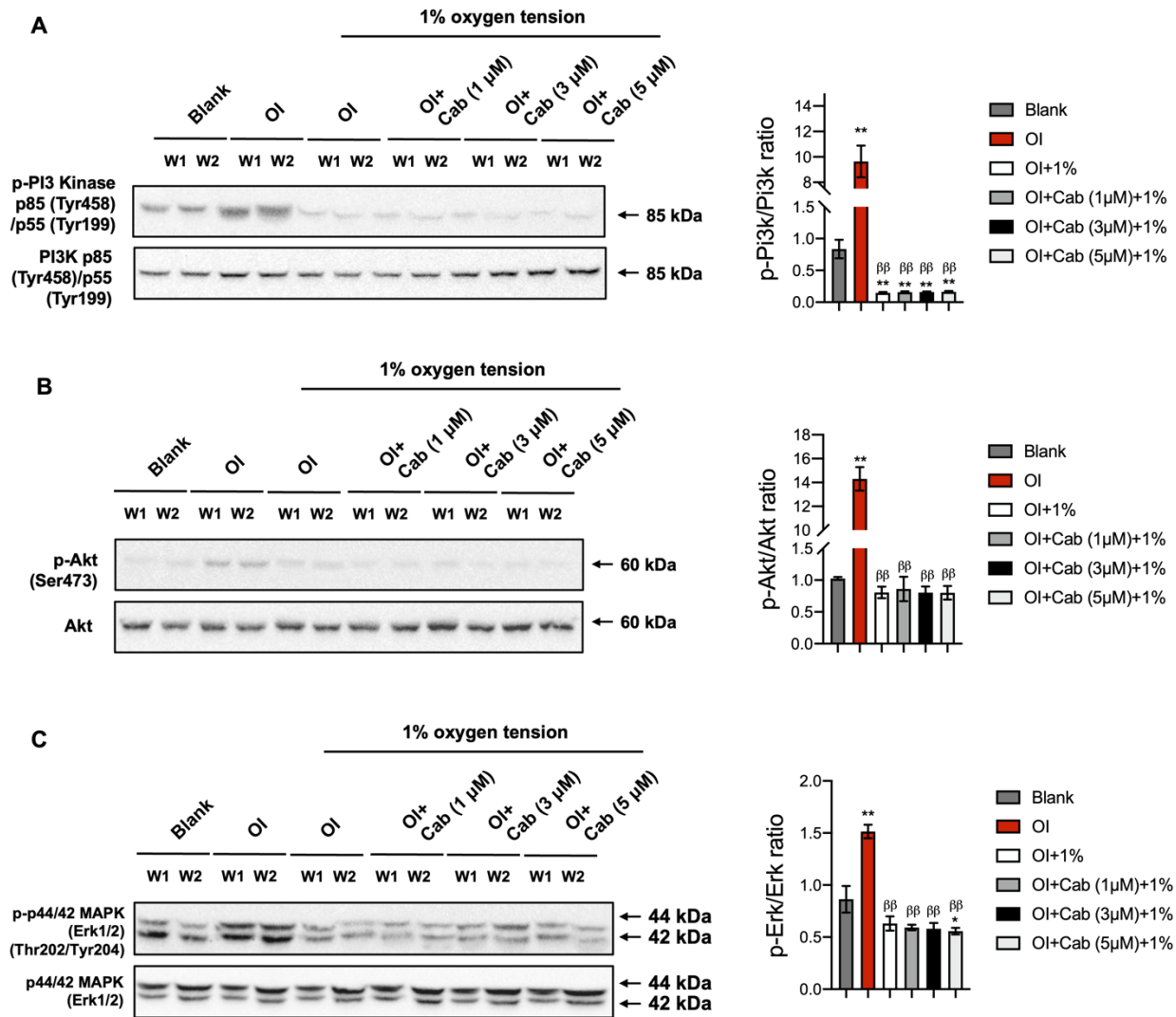


**Figure 44. Cabozantinib regulates the phosphorylation of AKT and PI3K and ERK1/2 signalling in osteoblast differentiation.**

(A) Representative Western blot images showing the phosphorylation of AKT with various concentrations of cabozantinib (n=3). (B) Quantitative analysis of AKT phosphorylation (n=3). (A) Representative Western blot images showing the phosphorylation of PI3K with various concentrations of cabozantinib (n=3). (B) Quantitative analysis of phosphorylation of PI3K (n=3). (C) Representative Western blot images showing the phosphorylation of ERK1/2 with various concentrations of cabozantinib (n=3). (D) Quantitative analysis of ERK1/2 phosphorylation (n=3). PI3K, AKT, and ERK1/2 were set as the loading controls. \*\* $p < 0.01$  versus the blank group.  $\beta\beta p < 0.01$  versus the OI group.

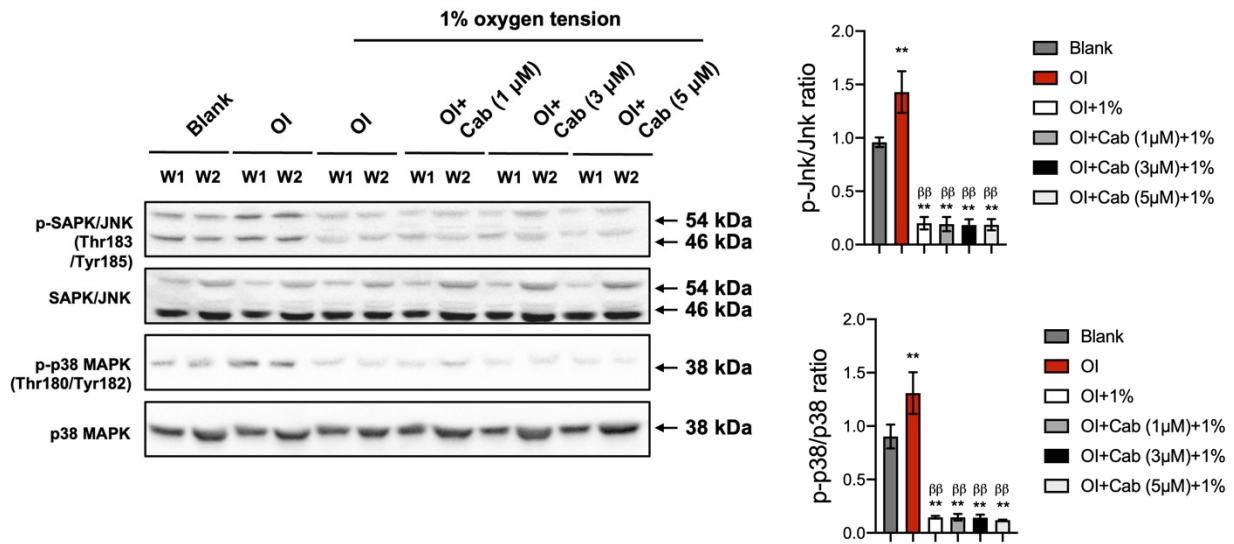


**Figure 45. Cabozantinib regulates the phosphorylation of MAPK signalling (JNK and p38) in osteoblast differentiation.**

(A) Representative Western blot images showing the phosphorylation of JNK and p38 with various concentrations of cabozantinib (n=3). (B) Quantitative analysis of the phosphorylation of JNK and p38 (n=3). JNK and p38 were set as the loading controls. \*\* $p < 0.01$  versus the blank group.  $\beta\beta p < 0.01$  versus the OI group.

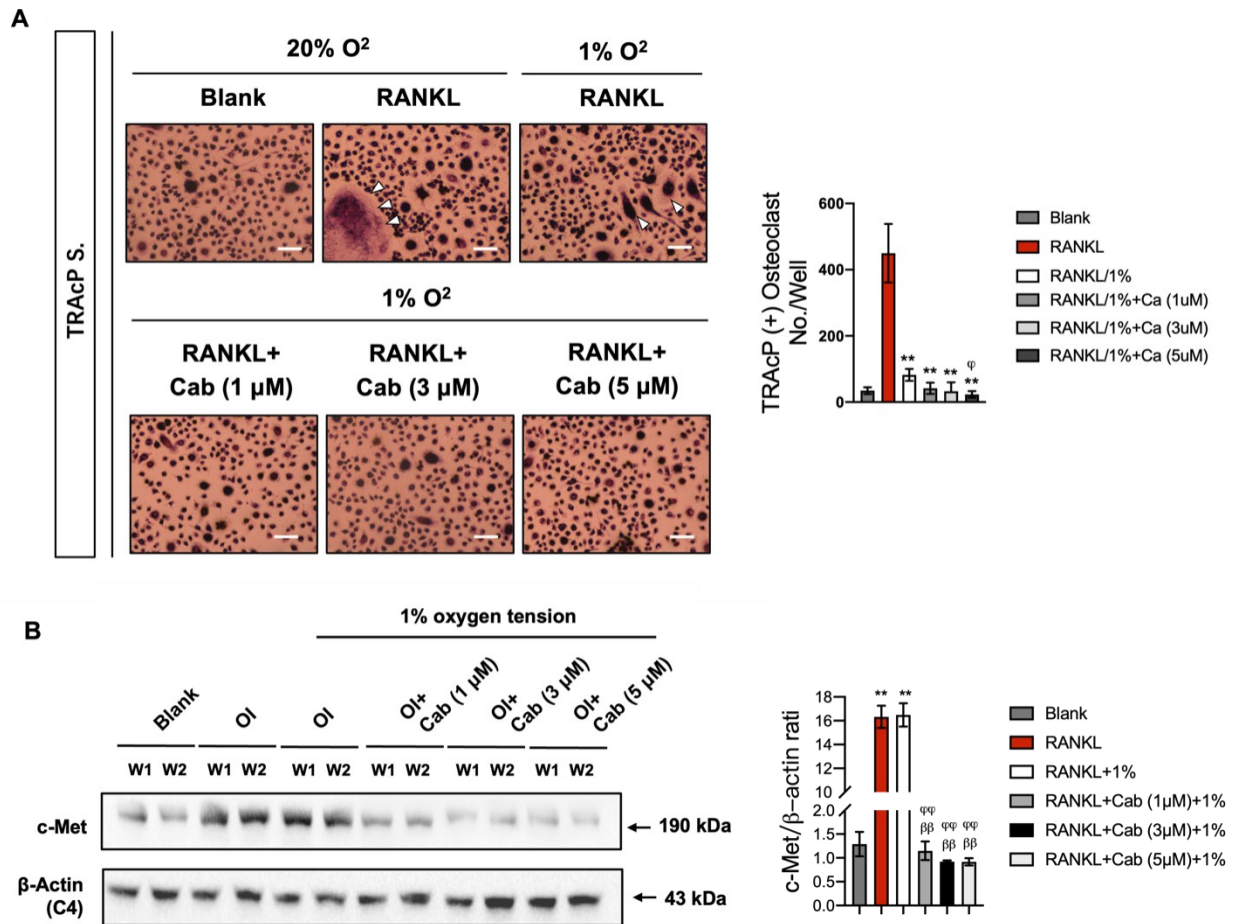


**Figure 46. Hypoxia regulates osteoclast differentiation and c-Met protein expression.**

(A) Representative images of TRAcP staining showing osteoclast differentiation with various concentrations of cabozantinib (n=3). (B) Quantitative analysis of TRAcP-positive osteoclasts with various concentrations of cabozantinib (n=3). (C) Representative Western blot images showing c-Met protein expression with various concentrations of cabozantinib (n=3). (D) Quantitative analysis of c-Met expression (n=3).  $\beta$ -actin was set as the loading control.  $**p < 0.01$  versus the blank group.  $\beta\beta p < 0.01$  versus the RANKL group.  $\phi p < 0.05$  versus the RANKL group+1%.

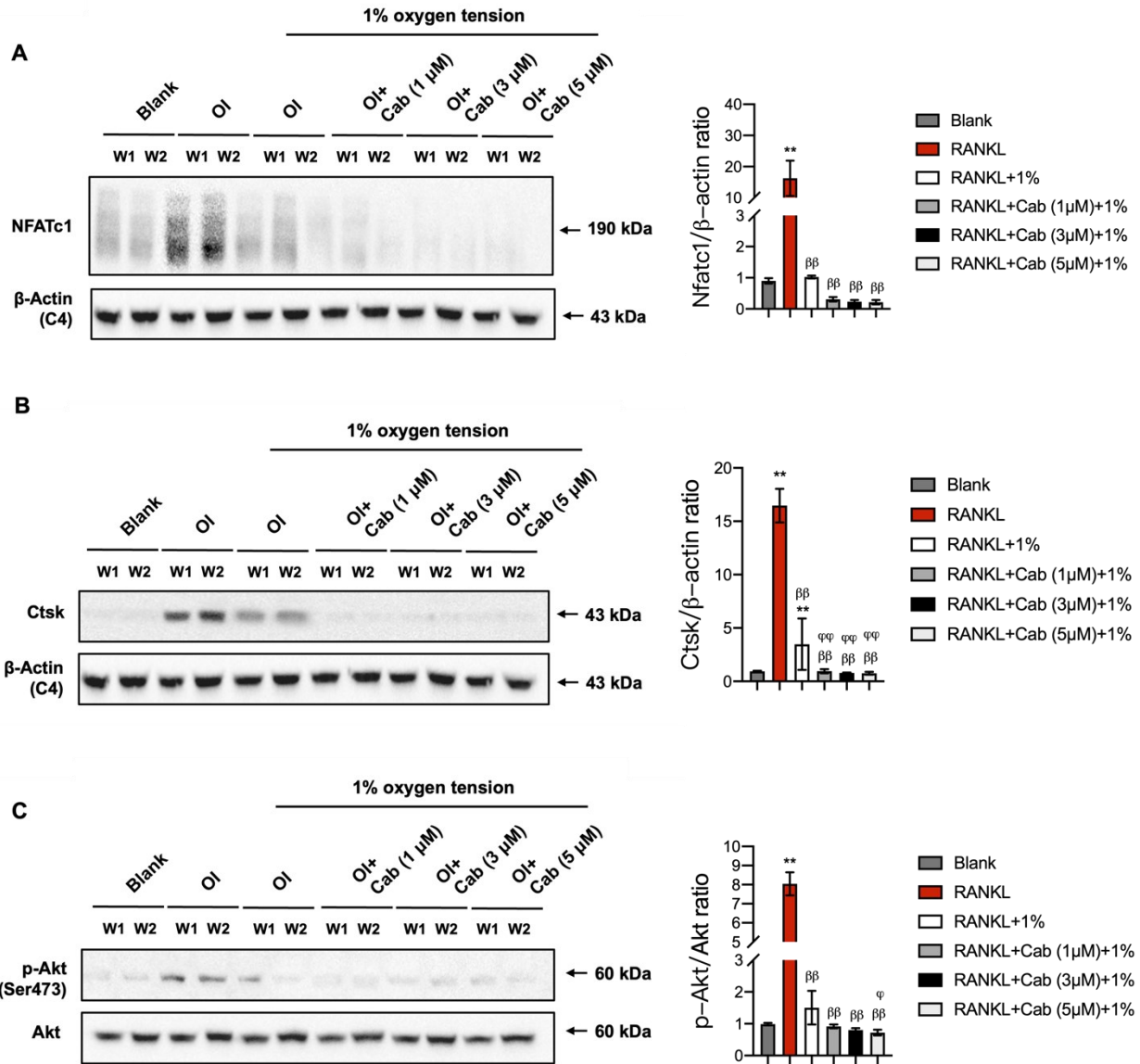


**Figure 47. Cabozantinib regulates NFATc1, CTSK and AKT signalling in osteoclast differentiation.**

(A) Representative Western blot images showing NFATc1 with various concentrations of cabozantinib (n=3). (B) Quantitative analysis of NFATc1 (n=3). (C) Representative Western blot images showing CTSK protein expression with various concentrations of cabozantinib (n=3). (D) Quantitative analysis of CTSK expression (n=3). (E) Representative Western blot images showing the phosphorylation of AKT with various concentrations of cabozantinib (n=3).

(F) Quantitative analysis of AKT phosphorylation (n=3).  $\beta$ -actin and AKT were set as the loading controls. **\*\*** $p < 0.01$  versus the blank group.  **$\beta\beta$**  $p < 0.01$  versus the RANKL group.  **$\phi$**  $p < 0.05$ ,  **$\phi\phi$**  $p < 0.01$  versus the RANKL group+1%.

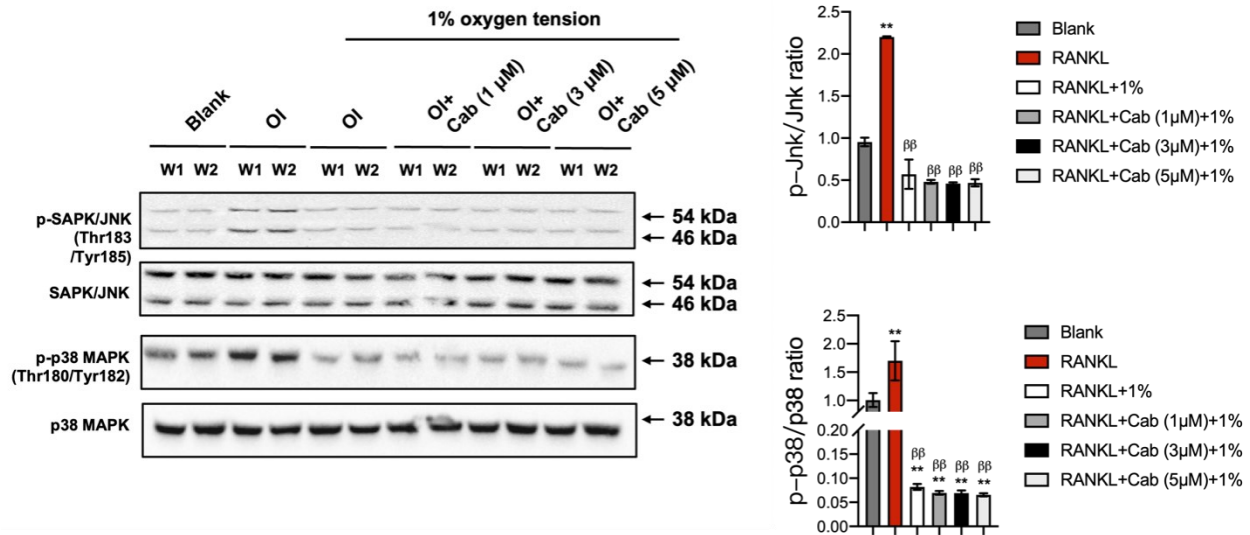


**Figure 48. Cabozantinib regulates MAPK signalling (JNK and p38) in osteoclast differentiation.**

(A) Representative Western blot images showing phosphorylation of JNK and p38 with various concentrations of cabozantinib (n=3). (B) Quantitative analysis of the phosphorylation of JNK and p38 (n=3). JNK and p38 were set as the loading controls.  $**p < 0.01$  versus the blank group.  $\beta\beta p < 0.01$  versus the RANKL group.

## **CHAPTER 5**

### **Summary and general discussion**



The HGF/c-Met axis is an important biological systems that is extensively expressed and functions in almost every organ and tissue<sup>191,192</sup>. This pathway is involved in a variety of biological processes, including cell proliferation, cell motility, evasion of apoptosis, epithelial-to-mesenchymal transition, and angiogenesis<sup>193-196</sup>. Intriguingly, the earliest studies of HGF/c-Met in bone homeostasis were initiated from bone metastasis. It is suggested that the pathway also regulates breast and prostate cancer invasion and metastasis<sup>197,198</sup>. Research has since shown that HGF/c-Met plays a role in bone metastasis, as c-Met is highly expressed in these metastatic lesions<sup>199,200</sup>. During the process of bone metastasis, stromal cells, including fibroblasts and pericytes, secrete HGF to activate the c-Met receptor in tumour cells. Tumour cells in turn induce growth factors that promote osteoblast and osteoclast differentiation<sup>148</sup>. c-Met is expressed in osteoblasts and osteoclasts, and activated by HGF<sup>111</sup>. c-Met mRNA levels are significantly increased during osteoclast differentiation but remain high in osteoblasts<sup>115</sup>.

As we demonstrated in the Chapter one, many studies have attempted to dissect the role of HGF/c-Met in bone homeostasis. Nevertheless, the precise mechanism is exceedingly complex and difficult to understand. There is often confusion over whether it is HGF or c-Met that drives the biological process or if they both do. There is further debate about HGF's distinct mechanism from c-Met. As mentioned in the Chapter one, HGF is an exogenous secreted protein; therefore, its actual effect is dosage dependent. Therefore, our search for a molecular factor with more stable regulatory effect on osteoblastogenesis and osteoclastogenesis finally led us to identify c-Met.

Fracture nonunion is a complicated process that presents major treatment challenges to orthopaedic surgeons<sup>9,42</sup>. The late stage process is characterized by depressed osteoblastic and osteoclastic activity, along with a failure of fracture healing<sup>2-4</sup>. The work here is the first to studying c-Met in the context of fracture nonunion in order to provide insights into the receptor's role in osteoblast and osteoclast regulation. Our present study is the first to identify c-Met expression in fracture nonunion and show that c-Met is highly expressed in human fracture callus tissue. Moreover, we observed that c-Met expression was downregulated in both fracture callus and the control bone of patients with fracture nonunion, indicating that the suppression of c-Met is not exclusively localized to the fracture tissue. A key discussion point to consider is whether individuals with genetic polymorphisms predisposing to changes in c-MET receptor activity

may be more prone to suffer a nonunion following fracture. Large scale population studies correlating polymorphisms in c-MET to fracture repair would be required to answer this question. The second interesting observation we made was that osteoblastic and osteoclastic markers were nearly suppressed in serum and bone samples, which suggests that fracture nonunion correlates with low bone metabolic activity.

To investigate the relationships between c-Met and bone cells, we generated two types of transgenic mice, *c-Met<sup>fl/fl</sup>, Prx1<sup>cre</sup>* mice and *c-Met<sup>fl/fl</sup>, Ctsk<sup>cre</sup>* mice. C-Met conditional knockout mice offer numerous advantages. This model allows us to identify the skeletal phenotype in the presence or absence of osteoblast progenitor and osteoclast precursor c-Met activity. The conditional knockout of c-Met enables us to exclude interference from HGF and focus on c-Met itself. Our results show that ablation of c-Met in osteoblast progenitors and osteoclast precursors suppresses osteoblastogenesis and osteoclastogenesis, respectively, in postnatal bone development but has seemingly little effect on fetal bone development. Following proximal femoral fracture surgery, fracture healing was significantly delayed with less callus formation in the *c-Met<sup>fl/fl</sup>, Prx1<sup>cre</sup>* mice or callus resorption in the *c-Met<sup>fl/fl</sup>, Ctsk<sup>cre</sup>* mice. The results emphasize the important role of c-Met in bone repair rather than in bone development, and c-Met may serve as a molecular driver for osteoblast and osteoclast differentiation.

Since hypoxia induced by poor vascularization is important in the genesis of fracture nonunion, we determined whether hypoxia suppresses osteoblast and osteoclast differentiation through the regulation c-Met. Although we observed increased c-Met phosphorylation in hypoxic conditions, we found that the suppression of bone cell differentiation cannot be explained by c-Met activity. It is likely that the enhancement of c-Met is caused by hypoxia as a natural bioresponse and does not lead to a change in cellular differentiation.

Our current project suffers from several limitations:

- 1) In Chapter two, we calculated the sample size at a pre-experimental stage for two experimental groups of human and animal studies by G\*Power software. Our sample size was determined by a significance level of 5% and a statistical test power of 80%. However, a relatively small number of samples may limit the applicability of our results, despite the significant findings. In human study, fracture nonunion is a common complication occurring in multiple areas of bone or joints, especially in tibial fractures. However, owing to the limitations of the

surgical approach and medical guidance, we were unable to obtain enough samples from patients with tibial fractures. Thus, we selected patients with femoral neck fractures so that we could examine their calluses and control samples when they were undergoing hip arthroplasty. In any case, we are still considering the possibility of expanding our sample sizes by a longer-term collaboration with the Chinese surgical team. A larger sample size of conditional knockout mice will also be obtained through the breeding of more mice. Taken all together, we would like to achieve a final statistical test power that is greater than 90%.

2) Additionally, the inclusion criteria for human subjects are ranging from 20 to 55 to exclude adolescents with immature skeletons and elderly patients with fragile bones. It is mainly due to a lack of appropriate subjects that fit our criteria so that the age range is quite variable. Our conclusion may be more confident if we increased our sample size and performed statistical analysis by dividing different age groups.

3) We determined that c-Met is a promoter of osteoblast and osteoclast differentiation. Nevertheless, the mechanism of c-Met used to explain the observed phenotypes of mice originates from prior research. For *in vitro* validation of the c-Met mechanism, we did not isolate primary cells from gene-edited mice. Therefore, there is a lack of direct evidence supporting our conclusion about the regulatory effect of c-Met on bone homeostasis.

4) Even though several downstream pathways of c-Met, such as MAPK/ERK and PI3K/Akt, have been identified, the precise target of c-Met in specific bone cells remains unclear. We must therefore perform RNA-seq on bone samples from gene-edited mice to identify the molecular factors that might be differentially expressed when c-Met is deleted.

5) The outcome of fracture healing can be affected by multiple factors, such as inflammation, immunology, angiogenesis at the initial phase of haematoma and granulation tissue formation, or endochondral ossification at the beginning of soft callus formation. In fracture healing, we focused solely on bone regeneration with osteoblasts and osteoclasts, neglecting to consider the possibility that c-Met may be related to other factors, chondrocyte in fibrocartilage formation or endothelial cells in vessel formation.

6) Osteotomy surgery was performed only on male mutant mice and their controls in Chapter 4. This is mainly because men are more prone to nonunion than women as demonstrated by epidemiology study<sup>11</sup>. Young men (<40 years of age) are more prone to high energy injuries

than women, although osteoporotic fractures occur equally in elderly patients of both sexes<sup>201</sup>. Furthermore, in our work, the levels of *c-Met* expression in wild-type mice are higher and more dynamic, which will lead to more significant results. Nevertheless, our future studies will also include female mice to exclude the effect of estrogen that regulates bone homeostasis.

7) In Chapter 4, only cell lines of osteoblast progenitors and osteoclast precursors are utilized to validate the regulatory effect of hypoxia on cellular differentiation and biofunctions. Primary osteoblasts and osteoclasts are able to closely resemble the parental tissue, bone. However, primary cells are much more difficult to be isolated from the corresponding tissue and also at a higher risk of contamination than cell lines. Moreover, primary osteoblasts and osteoclasts suffer from a shorter lifespan because the growth of cells exhausts substrate and nutrients. Nevertheless, our future work may include further analysis of the c-Met mechanism using primary osteoblasts and osteoclasts isolated from mice's skulls and bone marrows. Despite these limitations, our results provide us with future directions for our upcoming research.

To summarize, our project first identifies the expression of c-MET in late-stage fracture nonunion, then predicts its possible biological properties, which have not been revealed in previous research. This finding suggests that c-MET may be a potential target for late-stage fracture non-union therapy. Non-unions are rarely diagnosed and treated in their early stages, because there is insufficient medical monitoring after the fracture. Thus, exploring the target therapy for late stage non-union is of great importance to orthopedic practice. Furthermore, the dysregulation of c-MET is found not only at fracture sites, but also in control bone cubes, suggesting that c-MET is depressed consistently in fracture nonunion patients. Our data indicate that the option of c-MET gene therapy through human circulation is viable, not just limited to nonunion focal areas.

A more detailed mechanism study was performed through a functional knockout of *c-Met* in mice and various *in vivo* studies were performed in order to determine if osteoblast and osteoclast differentiation changes in those mutant mice. Also noteworthy is that the conditional knockout c-Met mice in osteoblast progenitors and osteoclast precursors were created for the first time by crossing flox mice with *Prx1* cre mice and *Ctsk* cre mice and haven't been observed in previous studies. Currently, only a few knockout mice have been applied in fracture healing study. For example, *Trpv1* knockout mice had an obvious fracture gap with unresorbed soft-

callus 4 weeks post-fracture. The number of osteoclasts was reduced in the *Trpv1* knockout fracture callus, and osteoclast formation and resorption activity were also impaired *in vitro*<sup>202</sup>. In contrast, *Cathepsin K* deletion accelerated bone healing and remodeling with increased callus opacity and bridging at days 28 and 42 post-fracture<sup>203</sup>. Fractures in *Ep1* knockout mice had an earlier appearance of TRAcP-positive osteoclasts, accelerated bone remodeling, and an earlier return to normal bone morphometry<sup>204</sup>. However, the above mice models are all general knock-out instead of conditional knockout in specific cell types and they failed to declare the different roles of osteoblasts and osteoclasts in fracture healing. In our work, by using *c-Met*<sup>fl/fl</sup>, *Prx1*<sup>cre</sup> mice and *c-Met*<sup>fl/fl</sup>, *Ctsk*<sup>cre</sup> mice, we creatively demonstrated that *c-Met* plays a dynamic role in osteoblast-mediated callus formation and osteoclast-mediated callus resorption in fracture models via proximal femur osteotomy.

Finally, we evaluated the effect of hypoxia, a critical factor hampering normal fracture healing, on c-Met regulation during osteoblast and osteoclast differentiation. Based on our study, c-Met is an independent factor in the regulation of bone cells, that is unaffected by hypoxia. By eliminating the potential relationship between hypoxia and c-Met, we can deduce a broader picture of the promoter of c-Met regulation in fracture non-union, which is promising to be presented in our future work.

## Reference

- (1) Salhotra, A.; Shah, H. N.; Levi, B.; Longaker, M. T. Mechanisms of Bone Development and Repair. *Nat. Rev. Mol. Cell Biol.* **2020**, *21* (11), 696–711. <https://doi.org/10.1038/s41580-020-00279-w>.
- (2) Einhorn, T. A.; Gerstenfeld, L. C. Fracture Healing: Mechanisms and Interventions. *Nat. Rev. Rheumatol.* **2015**, *11* (1), 45–54. <https://doi.org/10.1038/nrrheum.2014.164>.
- (3) Panteli, M.; Pountos, I.; Jones, E.; Giannoudis, P. V. Biological and Molecular Profile of Fracture Non-Union Tissue: Current Insights. *J. Cell. Mol. Med.* **2015**, *19* (4), 685–713. <https://doi.org/10.1111/jcmm.12532>.
- (4) Bahney, C. S.; Zondervan, R. L.; Allison, P.; Theologis, A.; Ashley, J. W.; Ahn, J.; Miclau, T.; Marcucio, R. S.; Hankenson, K. D. Cellular Biology of Fracture Healing. *J. Orthop. Res. Off. Publ. Orthop. Res. Soc.* **2019**, *37* (1), 35–50. <https://doi.org/10.1002/jor.24170>.
- (5) Hak, D. J.; Fitzpatrick, D.; Bishop, J. A.; Marsh, J. L.; Tilp, S.; Schnettler, R.; Simpson, H.; Alt, V. Delayed Union and Nonunions: Epidemiology, Clinical Issues, and Financial Aspects. *Injury* **2014**, *45 Suppl 2*, S3-7. <https://doi.org/10.1016/j.injury.2014.04.002>.
- (6) Nicholson, J. A.; Makaram, N.; Simpson, A.; Keating, J. F. Fracture Nonunion in Long Bones: A Literature Review of Risk Factors and Surgical Management. *Injury* **2021**, *52 Suppl 2*, S3–S11. <https://doi.org/10.1016/j.injury.2020.11.029>.
- (7) Reahl, G. B.; Gerstenfeld, L.; Kain, M. Epidemiology, Clinical Assessments, and Current Treatments of Nonunions. *Curr. Osteoporos. Rep.* **2020**, *18* (3), 157–168. <https://doi.org/10.1007/s11914-020-00575-6>.
- (8) Bell, A.; Templeman, D.; Weinlein, J. C. Nonunion of the Femur and Tibia: An Update. *Orthop. Clin. North Am.* **2016**, *47* (2), 365–375. <https://doi.org/10.1016/j.ocl.2015.09.010>.

- (9) Nauth, A.; Lee, M.; Gardner, M. J.; Brinker, M. R.; Warner, S. J.; Tornetta, P.; Leucht, P. Principles of Nonunion Management: State of the Art. *J. Orthop. Trauma* **2018**, *32 Suppl 1*, S52–S57. <https://doi.org/10.1097/BOT.0000000000001122>.
- (10) Outcomes of Patients With Nonunion After Open Tibial Shaft Fractures With or Without Soft Tissue Coverage Procedures - PubMed <https://pubmed.ncbi.nlm.nih.gov/33252441/> (accessed 2021 -10 -26).
- (11) Zura, R.; Xiong, Z.; Einhorn, T.; Watson, J. T.; Ostrum, R. F.; Prayson, M. J.; Della Rocca, G. J.; Mehta, S.; McKinley, T.; Wang, Z.; Steen, R. G. Epidemiology of Fracture Nonunion in 18 Human Bones. *JAMA Surg.* **2016**, *151* (11), e162775. <https://doi.org/10.1001/jamasurg.2016.2775>.
- (12) George, M. D.; Baker, J. F.; Leonard, C. E.; Mehta, S.; Miano, T. A.; Hennessy, S. Risk of Nonunion with Nonselective NSAIDs, COX-2 Inhibitors, and Opioids. *J. Bone Joint Surg. Am.* **2020**, *102* (14), 1230–1238. <https://doi.org/10.2106/JBJS.19.01415>.
- (13) Kostenuik, P.; Mirza, F. M. Fracture Healing Physiology and the Quest for Therapies for Delayed Healing and Nonunion: THERAPIES FOR DELAYED/NON-UNION FRACTURES. *J. Orthop. Res.* **2017**, *35* (2), 213–223. <https://doi.org/10.1002/jor.23460>.
- (14) Rupp, M.; Popp, D.; Alt, V. Prevention of Infection in Open Fractures: Where Are the Pendulums Now? *Injury* **2020**, *51 Suppl 2*, S57–S63. <https://doi.org/10.1016/j.injury.2019.10.074>.
- (15) Thevendran, G.; Wang, C.; Pinney, S. J.; Penner, M. J.; Wing, K. J.; Younger, A. S. E. Nonunion Risk Assessment in Foot and Ankle Surgery: Proposing a Predictive Risk Assessment Model. *Foot Ankle Int.* **2015**, *36* (8), 901–907. <https://doi.org/10.1177/1071100715577789>.
- (16) Zura, R.; Braid-Forbes, M. J.; Jeray, K.; Mehta, S.; Einhorn, T. A.; Watson, J. T.; Della Rocca, G. J.; Forbes, K.; Steen, R. G. Bone Fracture Nonunion Rate Decreases with Increasing Age: A Prospective Inception Cohort Study. *Bone* **2017**, *95*, 26–32. <https://doi.org/10.1016/j.bone.2016.11.006>.

- (17) Lavery, L. A.; Lavery, D. C.; Green, T.; Hunt, N.; La Fontaine, J.; Kim, P. J.; Wukich, D. Increased Risk of Nonunion and Charcot Arthropathy After Ankle Fracture in People With Diabetes. *J. Foot Ankle Surg. Off. Publ. Am. Coll. Foot Ankle Surg.* **2020**, *59* (4), 653–656. <https://doi.org/10.1053/j.jfas.2019.05.006>.
- (18) Loi, F.; Córdova, L. A.; Pajarinen, J.; Lin, T.; Yao, Z.; Goodman, S. B. Inflammation, Fracture and Bone Repair. *Bone* **2016**, *86*, 119–130. <https://doi.org/10.1016/j.bone.2016.02.020>.
- (19) Ekegren, C. L.; Edwards, E. R.; de Steiger, R.; Gabbe, B. J. Incidence, Costs and Predictors of Non-Union, Delayed Union and Mal-Union Following Long Bone Fracture. *Int. J. Environ. Res. Public. Health* **2018**, *15* (12), E2845. <https://doi.org/10.3390/ijerph15122845>.
- (20) Tzioupis, C.; Giannoudis, P. V. Prevalence of Long-Bone Non-Unions. *Injury* **2007**, *38* Suppl 2, S3-9. [https://doi.org/10.1016/s0020-1383\(07\)80003-9](https://doi.org/10.1016/s0020-1383(07)80003-9).
- (21) Tian, R.; Zheng, F.; Zhao, W.; Zhang, Y.; Yuan, J.; Zhang, B.; Li, L. Prevalence and Influencing Factors of Nonunion in Patients with Tibial Fracture: Systematic Review and Meta-Analysis. *J. Orthop. Surg.* **2020**, *15* (1), 377. <https://doi.org/10.1186/s13018-020-01904-2>.
- (22) Rupp, M.; Biehl, C.; Budak, M.; Thormann, U.; Heiss, C.; Alt, V. Diaphyseal Long Bone Nonunions - Types, Aetiology, Economics, and Treatment Recommendations. *Int. Orthop.* **2018**, *42* (2), 247–258. <https://doi.org/10.1007/s00264-017-3734-5>.
- (23) Cottrell, J. A.; Turner, J. C.; Arinzech, T. L.; O'Connor, J. P. The Biology of Bone and Ligament Healing. *Foot Ankle Clin.* **2016**, *21* (4), 739–761. <https://doi.org/10.1016/j.fcl.2016.07.017>.
- (24) Coates, B. A.; McKenzie, J. A.; Buettmann, E. G.; Liu, X.; Gontarz, P. M.; Zhang, B.; Silva, M. J. Transcriptional Profiling of Intramembranous and Endochondral Ossification after Fracture in Mice. *Bone* **2019**, *127*, 577–591. <https://doi.org/10.1016/j.bone.2019.07.022>.
- (25) Marsell, R.; Einhorn, T. A. The Biology of Fracture Healing. *Injury* **2011**, *42* (6), 551–555. <https://doi.org/10.1016/j.injury.2011.03.031>.



- (26) Hinton, R. J.; Jing, Y.; Jing, J.; Feng, J. Q. Roles of Chondrocytes in Endochondral Bone Formation and Fracture Repair. *J. Dent. Res.* **2017**, *96* (1), 23–30. <https://doi.org/10.1177/0022034516668321>.
- (27) Runyan, C. M.; Gabrick, K. S. Biology of Bone Formation, Fracture Healing, and Distraction Osteogenesis. *J. Craniofac. Surg.* **2017**, *28* (5), 1380–1389. <https://doi.org/10.1097/SCS.00000000000003625>.
- (28) Kolar, P.; Schmidt-Bleek, K.; Schell, H.; Gaber, T.; Toben, D.; Schmidmaier, G.; Perka, C.; Buttgerit, F.; Duda, G. N. The Early Fracture Hematoma and Its Potential Role in Fracture Healing. *Tissue Eng. Part B Rev.* **2010**, *16* (4), 427–434. <https://doi.org/10.1089/ten.TEB.2009.0687>.
- (29) Kolar, P.; Gaber, T.; Perka, C.; Duda, G. N.; Buttgerit, F. Human Early Fracture Hematoma Is Characterized by Inflammation and Hypoxia. *Clin. Orthop.* **2011**, *469* (11), 3118–3126. <https://doi.org/10.1007/s11999-011-1865-3>.
- (30) Gibon, E.; Lu, L.; Goodman, S. B. Aging, Inflammation, Stem Cells, and Bone Healing. *Stem Cell Res. Ther.* **2016**, *7*, 44. <https://doi.org/10.1186/s13287-016-0300-9>.
- (31) Danoff, J. R.; Aurégan, J.-C.; Coyle, R. M.; Burky, R. E.; Rosenwasser, M. P. Augmentation of Fracture Healing Using Soft Callus. *J. Orthop. Trauma* **2016**, *30* (3), 113–118. <https://doi.org/10.1097/BOT.0000000000000481>.
- (32) Schindeler, A.; McDonald, M. M.; Bokko, P.; Little, D. G. Bone Remodeling during Fracture Repair: The Cellular Picture. *Semin. Cell Dev. Biol.* **2008**, *19* (5), 459–466. <https://doi.org/10.1016/j.semcdb.2008.07.004>.
- (33) Maes, C.; Kobayashi, T.; Selig, M. K.; Torrekens, S.; Roth, S. I.; Mackem, S.; Carmeliet, G.; Kronenberg, H. M. Osteoblast Precursors, but Not Mature Osteoblasts, Move into Developing and Fractured Bones along with Invading Blood Vessels. *Dev. Cell* **2010**, *19* (2), 329–344. <https://doi.org/10.1016/j.devcel.2010.07.010>.
- (34) Fazzalari, N. L. Bone Fracture and Bone Fracture Repair. *Osteoporos. Int. J. Establ. Result Coop. Eur. Found. Osteoporos. Natl. Osteoporos. Found. USA* **2011**, *22* (6), 2003–2006. <https://doi.org/10.1007/s00198-011-1611-4>.

- (35) Wang, T.; Zhang, X.; Bikle, D. D. Osteogenic Differentiation of Periosteal Cells During Fracture Healing. *J. Cell. Physiol.* **2017**, *232* (5), 913–921. <https://doi.org/10.1002/jcp.25641>.
- (36) Oryan, A.; Monazzah, S.; Bigham-Sadegh, A. Bone Injury and Fracture Healing Biology. *Biomed. Environ. Sci. BES* **2015**, *28* (1), 57–71. <https://doi.org/10.3967/bes2015.006>.
- (37) Komori, T. Regulation of Proliferation, Differentiation and Functions of Osteoblasts by Runx2. *Int. J. Mol. Sci.* **2019**, *20* (7), E1694. <https://doi.org/10.3390/ijms20071694>.
- (38) Komori, T. Regulation of Osteoblast Differentiation by Transcription Factors. *J. Cell. Biochem.* **2006**, *99* (5), 1233–1239. <https://doi.org/10.1002/jcb.20958>.
- (39) Kylmaoja, E.; Nakamura, M.; Tuukkanen, J. Osteoclasts and Remodeling Based Bone Formation. *Curr. Stem Cell Res. Ther.* **2016**, *11* (8), 626–633. <https://doi.org/10.2174/1574888x10666151019115724>.
- (40) Udagawa, N.; Koide, M.; Nakamura, M.; Nakamichi, Y.; Yamashita, T.; Uehara, S.; Kobayashi, Y.; Furuya, Y.; Yasuda, H.; Fukuda, C.; Tsuda, E. Osteoclast Differentiation by RANKL and OPG Signaling Pathways. *J. Bone Miner. Metab.* **2021**, *39* (1), 19–26. <https://doi.org/10.1007/s00774-020-01162-6>.
- (41) Ono, T.; Nakashima, T. Recent Advances in Osteoclast Biology. *Histochem. Cell Biol.* **2018**, *149* (4), 325–341. <https://doi.org/10.1007/s00418-018-1636-2>.
- (42) Ding, Z.; Lin, Y.; Gan, Y.; Tang, T. Molecular Pathogenesis of Fracture Nonunion. *J. Orthop. Transl.* **2018**, *14*, 45–56. <https://doi.org/10.1016/j.jot.2018.05.002>.
- (43) Kazmers, N. H.; McKenzie, J. A.; Shen, T. S.; Long, F.; Silva, M. J. Hedgehog Signaling Mediates Woven Bone Formation and Vascularization during Stress Fracture Healing. *Bone* **2015**, *81*, 524–532. <https://doi.org/10.1016/j.bone.2015.09.002>.
- (44) Shapiro, F. Bone Development and Its Relation to Fracture Repair. The Role of Mesenchymal Osteoblasts and Surface Osteoblasts. *Eur. Cell. Mater.* **2008**, *15*, 53–76. <https://doi.org/10.22203/ecm.v015a05>.

- (45) Martínez-Reina, J.; García-Rodríguez, J.; Mora-Macías, J.; Domínguez, J.; Reina-Romo, E. Comparison of the Volumetric Composition of Lamellar Bone and the Woven Bone of Calluses. *Proc. Inst. Mech. Eng. [H]* **2018**, *232* (7), 682–689. <https://doi.org/10.1177/0954411918784085>.
- (46) Walmsley, G. G.; Ransom, R. C.; Zielins, E. R.; Leavitt, T.; Flacco, J. S.; Hu, M. S.; Lee, A. S.; Longaker, M. T.; Wan, D. C. Stem Cells in Bone Regeneration. *Stem Cell Rev. Rep.* **2016**, *12* (5), 524–529. <https://doi.org/10.1007/s12015-016-9665-5>.
- (47) Guppy, K. H.; Chan, P. H.; Prentice, H. A.; Norheim, E. P.; Harris, J. E.; Brara, H. S. Does the Use of Preoperative Bisphosphonates in Patients with Osteopenia and Osteoporosis Affect Lumbar Fusion Rates? Analysis from a National Spine Registry. *Neurosurg. Focus* **2020**, *49* (2), E12. <https://doi.org/10.3171/2020.5.FOCUS20262>.
- (48) Garg, P.; Mazur, M. M.; Buck, A. C.; Wandtke, M. E.; Liu, J.; Ebraheim, N. A. Prospective Review of Mesenchymal Stem Cells Differentiation into Osteoblasts. *Orthop. Surg.* **2017**, *9* (1), 13–19. <https://doi.org/10.1111/os.12304>.
- (49) Chen, Q.; Shou, P.; Zheng, C.; Jiang, M.; Cao, G.; Yang, Q.; Cao, J.; Xie, N.; Velletri, T.; Zhang, X.; Xu, C.; Zhang, L.; Yang, H.; Hou, J.; Wang, Y.; Shi, Y. Fate Decision of Mesenchymal Stem Cells: Adipocytes or Osteoblasts? *Cell Death Differ.* **2016**, *23* (7), 1128–1139. <https://doi.org/10.1038/cdd.2015.168>.
- (50) Komori, T. Runx2, an Inducer of Osteoblast and Chondrocyte Differentiation. *Histochem. Cell Biol.* **2018**, *149* (4), 313–323. <https://doi.org/10.1007/s00418-018-1640-6>.
- (51) Takarada, T.; Hinoi, E.; Nakazato, R.; Ochi, H.; Xu, C.; Tsuchikane, A.; Takeda, S.; Karsenty, G.; Abe, T.; Kiyonari, H.; Yoneda, Y. An Analysis of Skeletal Development in Osteoblast-Specific and Chondrocyte-Specific Runt-Related Transcription Factor-2 (Runx2) Knockout Mice. *J. Bone Miner. Res. Off. J. Am. Soc. Bone Miner. Res.* **2013**, *28* (10), 2064–2069. <https://doi.org/10.1002/jbmr.1945>.
- (52) Komori, T. Molecular Mechanism of Runx2-Dependent Bone Development. *Mol. Cells* **2020**, *43* (2), 168–175. <https://doi.org/10.14348/molcells.2019.0244>.
- (53) Eriksen, E. F. Cellular Mechanisms of Bone Remodeling. *Rev. Endocr. Metab. Disord.* **2010**, *11* (4), 219–227. <https://doi.org/10.1007/s11154-010-9153-1>.

- (54) Moon, Y. J.; Yun, C.-Y.; Choi, H.; Kim, J. R.; Park, B.-H.; Cho, E.-S. Osterix Regulates Corticalization for Longitudinal Bone Growth via Integrin B3 Expression. *Exp. Mol. Med.* **2018**, *50* (7), 1–11. <https://doi.org/10.1038/s12276-018-0119-9>.
- (55) Tang, J.; Xie, J.; Chen, W.; Tang, C.; Wu, J.; Wang, Y.; Zhou, X.-D.; Zhou, H.-D.; Li, Y.-P. Runt-Related Transcription Factor 1 Is Required for Murine Osteoblast Differentiation and Bone Formation. *J. Biol. Chem.* **2020**, *295* (33), 11669–11681. <https://doi.org/10.1074/jbc.RA119.007896>.
- (56) Nusse, R.; Clevers, H. Wnt/ $\beta$ -Catenin Signaling, Disease, and Emerging Therapeutic Modalities. *Cell* **2017**, *169* (6), 985–999. <https://doi.org/10.1016/j.cell.2017.05.016>.
- (57) Karner, C. M.; Long, F. Wnt Signaling and Cellular Metabolism in Osteoblasts. *Cell. Mol. Life Sci. CMLS* **2017**, *74* (9), 1649–1657. <https://doi.org/10.1007/s00018-016-2425-5>.
- (58) Teufel, S.; Hartmann, C. Wnt-Signaling in Skeletal Development. *Curr. Top. Dev. Biol.* **2019**, *133*, 235–279. <https://doi.org/10.1016/bs.ctdb.2018.11.010>.
- (59) Duan, P.; Bonewald, L. F. The Role of the Wnt/ $\beta$ -Catenin Signaling Pathway in Formation and Maintenance of Bone and Teeth. *Int. J. Biochem. Cell Biol.* **2016**, *77* (Pt A), 23–29. <https://doi.org/10.1016/j.biocel.2016.05.015>.
- (60) van Tienen, F. H. J.; Laemans, H.; van der Kallen, C. J. H.; Smeets, H. J. M. Wnt5b Stimulates Adipogenesis by Activating PPAR $\gamma$ , and Inhibiting the Beta-Catenin Dependent Wnt Signaling Pathway Together with Wnt5a. *Biochem. Biophys. Res. Commun.* **2009**, *387* (1), 207–211. <https://doi.org/10.1016/j.bbrc.2009.07.004>.
- (61) Jullien, N.; Maudinet, A.; Leloutre, B.; Ringe, J.; Häupl, T.; Marie, P. J. Downregulation of ErbB3 by Wnt3a Contributes to Wnt-Induced Osteoblast Differentiation in Mesenchymal Cells. *J. Cell. Biochem.* **2012**, *113* (6), 2047–2056. <https://doi.org/10.1002/jcb.24076>.
- (62) Christodoulides, C.; Laudes, M.; Cawthorn, W. P.; Schinner, S.; Soos, M.; O’Rahilly, S.; Sethi, J. K.; Vidal-Puig, A. The Wnt Antagonist Dickkopf-1 and Its Receptors Are Coordinately Regulated during Early Human Adipogenesis. *J. Cell Sci.* **2006**, *119* (0 12), 2613–2620. <https://doi.org/10.1242/jcs.02975>.

- (63) Pinzone, J. J.; Hall, B. M.; Thudi, N. K.; Vonau, M.; Qiang, Y.-W.; Rosol, T. J.; Shaughnessy, J. D. The Role of Dickkopf-1 in Bone Development, Homeostasis, and Disease. *Blood* **2009**, *113* (3), 517–525. <https://doi.org/10.1182/blood-2008-03-145169>.
- (64) Gaur, T.; Lengner, C. J.; Hovhannisyann, H.; Bhat, R. A.; Bodine, P. V. N.; Komm, B. S.; Javed, A.; van Wijnen, A. J.; Stein, J. L.; Stein, G. S.; Lian, J. B. Canonical WNT Signaling Promotes Osteogenesis by Directly Stimulating Runx2 Gene Expression. *J. Biol. Chem.* **2005**, *280* (39), 33132–33140. <https://doi.org/10.1074/jbc.M500608200>.
- (65) Wu, L.; Wei, Q.; Lv, Y.; Xue, J.; Zhang, B.; Sun, Q.; Xiao, T.; Huang, R.; Wang, P.; Dai, X.; Xia, H.; Li, J.; Yang, X.; Liu, Q. Wnt/ $\beta$ -Catenin Pathway Is Involved in Cadmium-Induced Inhibition of Osteoblast Differentiation of Bone Marrow Mesenchymal Stem Cells. *Int. J. Mol. Sci.* **2019**, *20* (6), 1519. <https://doi.org/10.3390/ijms20061519>.
- (66) Wu, M.; Chen, G.; Li, Y.-P. TGF- $\beta$  and BMP Signaling in Osteoblast, Skeletal Development, and Bone Formation, Homeostasis and Disease. *Bone Res.* **2016**, *4* (1), 1–21. <https://doi.org/10.1038/boneres.2016.9>.
- (67) Gomez-Puerto, M. C.; Iyengar, P. V.; García de Vinuesa, A.; ten Dijke, P.; Sanchez-Duffhues, G. Bone Morphogenetic Protein Receptor Signal Transduction in Human Disease. *J. Pathol.* **2019**, *247* (1), 9–20. <https://doi.org/10.1002/path.5170>.
- (68) Kamiya, N.; Mishina, Y. New Insights on the Roles of BMP Signaling in Bone – A Review of Recent Mouse Genetic Studies. *BioFactors Oxf. Engl.* **2011**, *37* (2), 75–82. <https://doi.org/10.1002/biof.139>.
- (69) Zou, M.-L.; Chen, Z.-H.; Teng, Y.-Y.; Liu, S.-Y.; Jia, Y.; Zhang, K.-W.; Sun, Z.-L.; Wu, J.-J.; Yuan, Z.-D.; Feng, Y.; Li, X.; Xu, R.-S.; Yuan, F.-L. The Smad Dependent TGF- $\beta$  and BMP Signaling Pathway in Bone Remodeling and Therapies. *Front. Mol. Biosci.* **2021**, *8*, 593310. <https://doi.org/10.3389/fmolb.2021.593310>.
- (70) Murakami, K.; Etlinger, J. D. Role of SMURF1 Ubiquitin Ligase in BMP Receptor Trafficking and Signaling. *Cell. Signal.* **2019**, *54*, 139–149. <https://doi.org/10.1016/j.cellsig.2018.10.015>.

- (71) Zhao, M.; Qiao, M.; Harris, S. E.; Oyajobi, B. O.; Mundy, G. R.; Chen, D. Smurf1 Inhibits Osteoblast Differentiation and Bone Formation in Vitro and in Vivo. *J. Biol. Chem.* **2004**, *279* (13), 12854–12859. <https://doi.org/10.1074/jbc.M313294200>.
- (72) Guo, Y.; Wang, M.; Zhang, S.; Wu, Y.; Zhou, C.; Zheng, R.; Shao, B.; Wang, Y.; Xie, L.; Liu, W.; Sun, N.; Jing, J.; Ye, L.; Chen, Q.; Yuan, Q. Ubiquitin-specific Protease USP34 Controls Osteogenic Differentiation and Bone Formation by Regulating BMP2 Signaling. *EMBO J.* **2018**, *37* (20), e99398. <https://doi.org/10.15252/embj.201899398>.
- (73) Feng, X.; Teitelbaum, S. L. Osteoclasts: New Insights. *Bone Res.* **2013**, *1* (1), 11–26. <https://doi.org/10.4248/BR201301003>.
- (74) Boyce, B. F. Advances in the Regulation of Osteoclasts and Osteoclast Functions. *J. Dent. Res.* **2013**, *92* (10), 860–867. <https://doi.org/10.1177/0022034513500306>.
- (75) Ross, F. P. M-CSF, c-Fms, and Signaling in Osteoclasts and Their Precursors. *Ann. N. Y. Acad. Sci.* **2006**, *1068*, 110–116. <https://doi.org/10.1196/annals.1346.014>.
- (76) Krysinska, H.; Hoogenkamp, M.; Ingram, R.; Wilson, N.; Tagoh, H.; Laslo, P.; Singh, H.; Bonifer, C. A Two-Step, PU.1-Dependent Mechanism for Developmentally Regulated Chromatin Remodeling and Transcription of the c-Fms Gene. *Mol. Cell. Biol.* **2007**, *27* (3), 878–887. <https://doi.org/10.1128/MCB.01915-06>.
- (77) Mun, S. H.; Park, P. S. U.; Park-Min, K.-H. The M-CSF Receptor in Osteoclasts and Beyond. *Exp. Mol. Med.* **2020**, *52* (8), 1239–1254. <https://doi.org/10.1038/s12276-020-0484-z>.
- (78) Hodge, J. M.; Collier, F. M.; Pavlos, N. J.; Kirkland, M. A.; Nicholson, G. C. M-CSF Potently Augments RANKL-Induced Resorption Activation in Mature Human Osteoclasts. *PLoS One* **2011**, *6* (6), e21462. <https://doi.org/10.1371/journal.pone.0021462>.
- (79) Hanada, R.; Hanada, T.; Sigl, V.; Schramek, D.; Penninger, J. M. RANKL/RANK-beyond Bones. *J. Mol. Med. Berl. Ger.* **2011**, *89* (7), 647–656. <https://doi.org/10.1007/s00109-011-0749-z>.
- (80) Sundaram, K.; Nishimura, R.; Senn, J.; Youssef, R. F.; London, S. D.; Reddy, S. V. RANK Ligand Signaling Modulates the Matrix Metalloproteinase-9 Gene Expression

- during Osteoclast Differentiation. *Exp. Cell Res.* **2007**, *313* (1), 168–178.  
<https://doi.org/10.1016/j.yexcr.2006.10.001>.
- (81) Wada, T.; Nakashima, T.; Hiroshi, N.; Penninger, J. M. RANKL-RANK Signaling in Osteoclastogenesis and Bone Disease. *Trends Mol. Med.* **2006**, *12* (1), 17–25.  
<https://doi.org/10.1016/j.molmed.2005.11.007>.
- (82) Novack, D. V. Role of NF-KB in the Skeleton. *Cell Res.* **2011**, *21* (1), 169–182.  
<https://doi.org/10.1038/cr.2010.159>.
- (83) Jung, Y.; Kim, H.; Min, S. H.; Rhee, S. G.; Jeong, W. Dynein Light Chain LC8 Negatively Regulates NF-KB through the Redox-Dependent Interaction with I $\kappa$ B $\alpha$ . *J. Biol. Chem.* **2008**, *283* (35), 23863–23871. <https://doi.org/10.1074/jbc.M803072200>.
- (84) Boyce, B. F.; Xiu, Y.; Li, J.; Xing, L.; Yao, Z. NF-KB-Mediated Regulation of Osteoclastogenesis. *Endocrinol. Metab.* **2015**, *30* (1), 35–44.  
<https://doi.org/10.3803/EnM.2015.30.1.35>.
- (85) Plotnikov, A.; Zehorai, E.; Procaccia, S.; Seger, R. The MAPK Cascades: Signaling Components, Nuclear Roles and Mechanisms of Nuclear Translocation. *Biochim. Biophys. Acta* **2011**, *1813* (9), 1619–1633. <https://doi.org/10.1016/j.bbamcr.2010.12.012>.
- (86) Lee, K.; Seo, I.; Choi, M. H.; Jeong, D. Roles of Mitogen-Activated Protein Kinases in Osteoclast Biology. *Int. J. Mol. Sci.* **2018**, *19* (10), 3004.  
<https://doi.org/10.3390/ijms19103004>.
- (87) Wagner, E. F.; Matsuo, K. Signalling in Osteoclasts and the Role of Fos/AP1 Proteins. *Ann. Rheum. Dis.* **2003**, *62 Suppl 2*, ii83-85.  
[https://doi.org/10.1136/ard.62.suppl\\_2.ii83](https://doi.org/10.1136/ard.62.suppl_2.ii83).
- (88) Huang, H.; Chang, E.-J.; Ryu, J.; Lee, Z. H.; Lee, Y.; Kim, H.-H. Induction of C-Fos and NFATc1 during RANKL-Stimulated Osteoclast Differentiation Is Mediated by the P38 Signaling Pathway. *Biochem. Biophys. Res. Commun.* **2006**, *351* (1), 99–105.  
<https://doi.org/10.1016/j.bbrc.2006.10.011>.
- (89) Cong, Q.; Jia, H.; Li, P.; Qiu, S.; Yeh, J.; Wang, Y.; Zhang, Z.-L.; Ao, J.; Li, B.; Liu, H. P38 $\alpha$  MAPK Regulates Proliferation and Differentiation of Osteoclast Progenitors

- and Bone Remodeling in an Aging-Dependent Manner. *Sci. Rep.* **2017**, *7*, 45964. <https://doi.org/10.1038/srep45964>.
- (90) Kim, J. H.; Kim, N. Regulation of NFATc1 in Osteoclast Differentiation. *J. Bone Metab.* **2014**, *21* (4), 233–241. <https://doi.org/10.11005/jbm.2014.21.4.233>.
- (91) Zhao, Q.; Wang, X.; Liu, Y.; He, A.; Jia, R. NFATc1: Functions in Osteoclasts. *Int. J. Biochem. Cell Biol.* **2010**, *42* (5), 576–579. <https://doi.org/10.1016/j.biocel.2009.12.018>.
- (92) Shao, Z.; Pan, H.; Tu, S.; Zhang, J.; Yan, S.; Shao, A. HGF/c-Met Axis: The Advanced Development in Digestive System Cancer. *Front. Cell Dev. Biol.* **2020**, *8*, 801. <https://doi.org/10.3389/fcell.2020.00801>.
- (93) Silva Paiva, R.; Gomes, I.; Casimiro, S.; Fernandes, I.; Costa, L. C-Met Expression in Renal Cell Carcinoma with Bone Metastases. *J. Bone Oncol.* **2020**, *25*, 100315. <https://doi.org/10.1016/j.jbo.2020.100315>.
- (94) Zambelli, A.; Biamonti, G.; Amato, A. HGF/c-Met Signalling in the Tumor Microenvironment. *Adv. Exp. Med. Biol.* **2021**, *1270*, 31–44. [https://doi.org/10.1007/978-3-030-47189-7\\_2](https://doi.org/10.1007/978-3-030-47189-7_2).
- (95) Yap, T. A.; de Bono, J. S. Targeting the HGF/c-Met Axis: State of Play. *Mol. Cancer Ther.* **2010**, *9* (5), 1077–1079. <https://doi.org/10.1158/1535-7163.MCT-10-0122>.
- (96) Noriega-Guerra, H.; Freitas, V. M. Extracellular Matrix Influencing HGF/c-MET Signaling Pathway: Impact on Cancer Progression. *Int. J. Mol. Sci.* **2018**, *19* (11), E3300. <https://doi.org/10.3390/ijms19113300>.
- (97) Chen, H.-T.; Tsou, H.-K.; Chang, C.-H.; Tang, C.-H. Hepatocyte Growth Factor Increases Osteopontin Expression in Human Osteoblasts through PI3K, Akt, c-Src, and AP-1 Signaling Pathway. *PLoS ONE* **2012**, *7* (6), e38378. <https://doi.org/10.1371/journal.pone.0038378>.
- (98) Nakamura, T.; Sakai, K.; Nakamura, T.; Matsumoto, K. Hepatocyte Growth Factor Twenty Years on: Much More than a Growth Factor. *J. Gastroenterol. Hepatol.* **2011**, *26 Suppl 1*, 188–202. <https://doi.org/10.1111/j.1440-1746.2010.06549.x>.



- (99) Fu, R.; Jiang, S.; Li, J.; Chen, H.; Zhang, X. Activation of the HGF/c-MET Axis Promotes Lenvatinib Resistance in Hepatocellular Carcinoma Cells with High c-MET Expression. *Med. Oncol. Northwood Lond. Engl.* **2020**, *37* (4), 24. <https://doi.org/10.1007/s12032-020-01350-4>.
- (100) Dai, R.; Li, J.; Fu, J.; Chen, Y.; Wang, R.; Zhao, X.; Luo, T.; Zhu, J.; Ren, Y.; Cao, J.; Qian, Y.; Li, N.; Wang, H. The Tyrosine Kinase C-Met Contributes to the pro-Tumorigenic Function of the P38 Kinase in Human Bile Duct Cholangiocarcinoma Cells. *J. Biol. Chem.* **2012**, *287* (47), 39812–39823. <https://doi.org/10.1074/jbc.M112.406520>.
- (101) D'ippolito, G.; Schiller, P. C.; Perez-stable, C.; Balkan, W.; Roos, B. A.; Howard, G. A. Cooperative Actions of Hepatocyte Growth Factor and 1,25-Dihydroxyvitamin D3 in Osteoblastic Differentiation of Human Vertebral Bone Marrow Stromal Cells. *Bone* **2002**, *31* (2), 269–275. [https://doi.org/10.1016/S8756-3282\(02\)00820-7](https://doi.org/10.1016/S8756-3282(02)00820-7).
- (102) Kawasaki, T.; Niki, Y.; Miyamoto, T.; Horiuchi, K.; Matsumoto, M.; Aizawa, M.; Toyama, Y. The Effect of Timing in the Administration of Hepatocyte Growth Factor to Modulate BMP-2-Induced Osteoblast Differentiation. *Biomaterials* **2010**, *31* (6), 1191–1198. <https://doi.org/10.1016/j.biomaterials.2009.10.048>.
- (103) Qian Wen; Shimeng Zhang; Xialin Du; Ruining Wang; Yanfen Li; Honglin Liu; Shengfeng Hu; Chaoying Zhou; Xinying Zhou; Li Ma. The Multiplicity of Infection-Dependent Effects of Recombinant Adenovirus Carrying HGF Gene on the Proliferation and Osteogenic Differentiation of Human Bone Marrow Mesenchymal Stem Cells. *Int. J. Mol. Sci.* **2018**, *19* (3), 734. <https://doi.org/10.3390/ijms19030734>.
- (104) Standal, T.; Abildgaard, N.; Fagerli, U.-M.; Stordal, B.; Hjertner, Ø.; Borset, M.; Sundan, A. HGF Inhibits BMP-Induced Osteoblastogenesis: Possible Implications for the Bone Disease of Multiple Myeloma. *Blood* **2007**, *109* (7), 3024–3030. <https://doi.org/10.1182/blood-2006-07-034884>.
- (105) Shibasaki, S.; Kitano, S.; Karasaki, M.; Tsunemi, S.; Sano, H.; Iwasaki, T. Blocking C-Met Signaling Enhances Bone Morphogenetic Protein-2-Induced Osteoblast Differentiation. *FEBS Open Bio* **2015**, *5* (1), 341–347. <https://doi.org/10.1016/j.fob.2015.04.008>.

- (106) Kim, J.-W.; Lee, M. N.; Jeong, B.-C.; Oh, S.-H.; Kook, M.-S.; Koh, J.-T. Chemical Inhibitors of C-Met Receptor Tyrosine Kinase Stimulate Osteoblast Differentiation and Bone Regeneration. *Eur. J. Pharmacol.* **2017**, *806*, 10–17.  
<https://doi.org/10.1016/j.ejphar.2017.03.032>.
- (107) Wang, R.; Xu, X.; Li, Y.; Li, J.; Yao, C.; Wu, R.; Jiang, Q.; Shi, D. A C-Met Chemical Inhibitor Promotes Fracture Healing through Interacting with Osteogenic Differentiation via the MTORC1 Pathway. *Exp. Cell Res.* **2019**, *381* (1), 50–56.  
<https://doi.org/10.1016/j.yexcr.2019.03.037>.
- (108) Tsai, S.-Y.; Huang, Y.-L.; Yang, W.-H.; Tang, C.-H. Hepatocyte Growth Factor-Induced BMP-2 Expression Is Mediated by c-Met Receptor, FAK, JNK, Runx2, and P300 Pathways in Human Osteoblasts. *Int. Immunopharmacol.* **2012**, *13* (2), 156–162.  
<https://doi.org/10.1016/j.intimp.2012.03.026>.
- (109) Abed, E.; Bouvard, B.; Martineau, X.; Jouzeau, J.-Y.; Reboul, P.; Lajeunesse, D. Elevated Hepatocyte Growth Factor Levels in Osteoarthritis Osteoblasts Contribute to Their Altered Response to Bone Morphogenetic Protein-2 and Reduced Mineralization Capacity. *Bone* **2015**, *75*, 111–119. <https://doi.org/10.1016/j.bone.2015.02.001>.
- (110) Patanè, S.; Avnet, S.; Coltella, N.; Costa, B.; Sponza, S.; Olivero, M.; Vigna, E.; Naldini, L.; Baldini, N.; Ferracini, R.; Corso, S.; Giordano, S.; Comoglio, P. M.; Di Renzo, M. F. *MET* Overexpression Turns Human Primary Osteoblasts into Osteosarcomas. *Cancer Res.* **2006**, *66* (9), 4750–4757. <https://doi.org/10.1158/0008-5472.CAN-05-4422>.
- (111) Grano, M.; Galimi, F.; Zambonin, G.; Colucci, S.; Cottone, E.; Zallone, A. Z.; Comoglio, P. M. Hepatocyte Growth Factor Is a Coupling Factor for Osteoclasts and Osteoblasts in Vitro. *Proc. Natl. Acad. Sci.* **1996**, *93* (15), 7644–7648.  
<https://doi.org/10.1073/pnas.93.15.7644>.
- (112) Sato, T.; Hakeda, Y.; Yamaguchi, Y.; Mano, H.; Tezuka, K.-I.; Matsumoto, K.; Nakamura, T.; Mori, Y.; Yoshizawa, K.; Sumitani, K.; Kodama, H.; Kumegawa, M. Hepatocyte Growth Factor Is Involved in Formation of Osteoclast-like Cells Mediated by

- Clonal Stromal Cells (MC3T3-G2/PA6). *J. Cell. Physiol.* **1995**, *164* (1), 197–204. <https://doi.org/10.1002/jcp.1041640124>.
- (113) Adamopoulos, I. E.; Xia, Z.; Lau, Y. S.; Athanasou, N. A. Hepatocyte Growth Factor Can Substitute for M-CSF to Support Osteoclastogenesis. *Biochem. Biophys. Res. Commun.* **2006**, *350* (2), 478–483. <https://doi.org/10.1016/j.bbrc.2006.09.076>.
- (114) Gaasch, J. A.; Bolwahn, A. B.; Suzanne Lindsey, J. Hepatocyte Growth Factor-Regulated Genes in Differentiated RAW 264.7 Osteoclast and Undifferentiated Cells. *Gene* **2006**, *369*, 142–152. <https://doi.org/10.1016/j.gene.2005.10.036>.
- (115) Fioramonti, M.; Santini, D.; Iuliani, M.; Ribelli, G.; Manca, P.; Papapietro, N.; Spiezia, F.; Vincenzi, B.; Denaro, V.; Russo, A.; Tonini, G.; Pantano, F. Cabozantinib Targets Bone Microenvironment Modulating Human Osteoclast and Osteoblast Functions. *Oncotarget* **2017**, *8* (12), 20113–20121. <https://doi.org/10.18632/oncotarget.15390>.
- (116) Sheffield, P. J. Measuring Tissue Oxygen Tension: A Review. *Undersea Hyperb. Med. J. Undersea Hyperb. Med. Soc. Inc* **1998**, *25* (3), 179–188.
- (117) De Santis, V.; Singer, M. Tissue Oxygen Tension Monitoring of Organ Perfusion: Rationale, Methodologies, and Literature Review. *Br. J. Anaesth.* **2015**, *115* (3), 357–365. <https://doi.org/10.1093/bja/aev162>.
- (118) Zepeda, A. B.; Pessoa, A.; Castillo, R. L.; Figueroa, C. A.; Pulgar, V. M.; Farías, J. G. Cellular and Molecular Mechanisms in the Hypoxic Tissue: Role of HIF-1 and ROS. *Cell Biochem. Funct.* **2013**, *31* (6), 451–459. <https://doi.org/10.1002/cbf.2985>.
- (119) Arnett, T. R. Acidosis, Hypoxia and Bone. *Arch. Biochem. Biophys.* **2010**, *503* (1), 103–109. <https://doi.org/10.1016/j.abb.2010.07.021>.
- (120) Reyes, J. G.; Farias, J. G.; Henríquez-Olavarrieta, S.; Madrid, E.; Parraga, M.; Zepeda, A. B.; Moreno, R. D. The Hypoxic Testicle: Physiology and Pathophysiology. *Oxid. Med. Cell. Longev.* **2012**, *2012*, 929285. <https://doi.org/10.1155/2012/929285>.
- (121) McGettrick, A. F.; O'Neill, L. A. J. The Role of HIF in Immunity and Inflammation. *Cell Metab.* **2020**, *32* (4), 524–536. <https://doi.org/10.1016/j.cmet.2020.08.002>.

- (122) Semenza, G. L. Targeting HIF-1 for Cancer Therapy. *Nat. Rev. Cancer* **2003**, *3* (10), 721–732. <https://doi.org/10.1038/nrc1187>.
- (123) Déry, M.-A. C.; Michaud, M. D.; Richard, D. E. Hypoxia-Inducible Factor 1: Regulation by Hypoxic and Non-Hypoxic Activators. *Int. J. Biochem. Cell Biol.* **2005**, *37* (3), 535–540. <https://doi.org/10.1016/j.biocel.2004.08.012>.
- (124) Fallah, J.; Rini, B. I. HIF Inhibitors: Status of Current Clinical Development. *Curr. Oncol. Rep.* **2019**, *21* (1), 6. <https://doi.org/10.1007/s11912-019-0752-z>.
- (125) Johnson, R. W.; Schipani, E.; Giaccia, A. J. HIF Targets in Bone Remodeling and Metastatic Disease. *Pharmacol. Ther.* **2015**, *150*, 169–177. <https://doi.org/10.1016/j.pharmthera.2015.02.002>.
- (126) Ramachandran, K.; Mani, S. K.; Gopal, G. K.; Rangasami, S. Prevalence of Bone Mineral Density Abnormalities and Factors Affecting Bone Density in Patients with Chronic Obstructive Pulmonary Disease in a Tertiary Care Hospital in Southern India. *J. Clin. Diagn. Res. JCDR* **2016**, *10* (9), OC32–OC34. <https://doi.org/10.7860/JCDR/2016/22464.8551>.
- (127) Valderrábano, R. J.; Lui, L.-Y.; Lee, J.; Cummings, S. R.; Orwoll, E. S.; Hoffman, A. R.; Wu, J. Y.; Osteoporotic Fractures in Men (MrOS) Study Research Group. Bone Density Loss Is Associated With Blood Cell Counts. *J. Bone Miner. Res. Off. J. Am. Soc. Bone Miner. Res.* **2017**, *32* (2), 212–220. <https://doi.org/10.1002/jbmr.3000>.
- (128) Walters, G.; Pountos, I.; Giannoudis, P. V. The Cytokines and Micro-Environment of Fracture Haematoma: Current Evidence. *J. Tissue Eng. Regen. Med.* **2018**, *12* (3), e1662–e1677. <https://doi.org/10.1002/term.2593>.
- (129) Lu, C.; Miclau, T.; Hu, D.; Marcucio, R. S. Ischemia Leads to Delayed Union during Fracture Healing: A Mouse Model. *J. Orthop. Res. Off. Publ. Orthop. Res. Soc.* **2007**, *25* (1), 51–61. <https://doi.org/10.1002/jor.20264>.
- (130) Lu, C.; Saless, N.; Wang, X.; Sinha, A.; Decker, S.; Kazakia, G.; Hou, H.; Williams, B.; Swartz, H. M.; Hunt, T. K.; Miclau, T.; Marcucio, R. S. The Role of Oxygen during Fracture Healing. *Bone* **2013**, *52* (1), 220–229. <https://doi.org/10.1016/j.bone.2012.09.037>.

- (131) Utting, J. C.; Robins, S. P.; Brandao-Burch, A.; Orriss, I. R.; Behar, J.; Arnett, T. R. Hypoxia Inhibits the Growth, Differentiation and Bone-Forming Capacity of Rat Osteoblasts. *Exp. Cell Res.* **2006**, *312* (10), 1693–1702.  
<https://doi.org/10.1016/j.yexcr.2006.02.007>.
- (132) Ontiveros, C.; Irwin, R.; Wiseman, R. W.; McCabe, L. R. Hypoxia Suppresses Runx2 Independent of Modeled Microgravity. *J. Cell. Physiol.* **2004**, *200* (2), 169–176.  
<https://doi.org/10.1002/jcp.20054>.
- (133) Park, J. H.; Park, B. H.; Kim, H. K.; Park, T. S.; Baek, H. S. Hypoxia Decreases Runx2/Cbfa1 Expression in Human Osteoblast-like Cells. *Mol. Cell. Endocrinol.* **2002**, *192* (1–2), 197–203. [https://doi.org/10.1016/s0303-7207\(02\)00036-9](https://doi.org/10.1016/s0303-7207(02)00036-9).
- (134) Salim, A.; Nacamuli, R. P.; Morgan, E. F.; Giaccia, A. J.; Longaker, M. T. Transient Changes in Oxygen Tension Inhibit Osteogenic Differentiation and Runx2 Expression in Osteoblasts. *J. Biol. Chem.* **2004**, *279* (38), 40007–40016.  
<https://doi.org/10.1074/jbc.M403715200>.
- (135) Zou, W.; Yang, S.; Zhang, T.; Sun, H.; Wang, Y.; Xue, H.; Zhou, D. Hypoxia Enhances Glucocorticoid-Induced Apoptosis and Cell Cycle Arrest via the PI3K/Akt Signaling Pathway in Osteoblastic Cells. *J. Bone Miner. Metab.* **2015**, *33* (6), 615–624.  
<https://doi.org/10.1007/s00774-014-0627-1>.
- (136) Arnett, T. R.; Gibbons, D. C.; Utting, J. C.; Orriss, I. R.; Hoebertz, A.; Rosendaal, M.; Meghji, S. Hypoxia Is a Major Stimulator of Osteoclast Formation and Bone Resorption. *J. Cell. Physiol.* **2003**, *196* (1), 2–8. <https://doi.org/10.1002/jcp.10321>.
- (137) Ma, Z.; Yu, R.; Zhao, J.; Sun, L.; Jian, L.; Li, C.; Liu, X. Constant Hypoxia Inhibits Osteoclast Differentiation and Bone Resorption by Regulating Phosphorylation of JNK and IκBα. *Inflamm. Res. Off. J. Eur. Histamine Res. Soc. Al* **2019**, *68* (2), 157–166.  
<https://doi.org/10.1007/s00011-018-1209-9>.
- (138) Conway, J. D.; Shabtai, L.; Bauernschub, A.; Specht, S. C. BMP-7 versus BMP-2 for the Treatment of Long Bone Nonunion. *Orthopedics* **2014**, *37* (12), e1049-1057.  
<https://doi.org/10.3928/01477447-20141124-50>.

- (139) James, A. W.; LaChaud, G.; Shen, J.; Asatrian, G.; Nguyen, V.; Zhang, X.; Ting, K.; Soo, C. A Review of the Clinical Side Effects of Bone Morphogenetic Protein-2. *Tissue Eng. Part B Rev.* **2016**, *22* (4), 284–297. <https://doi.org/10.1089/ten.teb.2015.0357>.
- (140) Hashimoto, K.; Kaito, T.; Furuya, M.; Seno, S.; Okuzaki, D.; Kikuta, J.; Tsukazaki, H.; Matsuda, H.; Yoshikawa, H.; Ishii, M. In Vivo Dynamic Analysis of BMP-2-Induced Ectopic Bone Formation. *Sci. Rep.* **2020**, *10* (1), 4751. <https://doi.org/10.1038/s41598-020-61825-2>.
- (141) Canintika, A. F.; Dilogio, I. H. Teriparatide for Treating Delayed Union and Nonunion: A Systematic Review. *J. Clin. Orthop. Trauma* **2020**, *11* (Suppl 1), S107–S112. <https://doi.org/10.1016/j.jcot.2019.10.009>.
- (142) Iyer, S. R.; Annex, B. H. Therapeutic Angiogenesis for Peripheral Artery Disease. *JACC Basic Transl. Sci.* **2017**, *2* (5), 503–512. <https://doi.org/10.1016/j.jac-bts.2017.07.012>.
- (143) Ha, X.; Yuan, B.; Li, Y.; Lao, M.; Wu, Z. Gene Therapy for Pathological Scar with Hepatocyte Growth Factor Mediated by Recombinant Adenovirus Vector. *Sci. China C Life Sci.* **2003**, *46* (3), 320–327. <https://doi.org/10.1360/03yc9034>.
- (144) Imai, Y.; Terai, H.; Nomura-Furuwatari, C.; Mizuno, S.; Matsumoto, K.; Nakamura, T.; Takaoka, K. Hepatocyte Growth Factor Contributes to Fracture Repair by Upregulating the Expression of BMP Receptors. *J. Bone Miner. Res.* **2005**, *20* (10), 1723–1730. <https://doi.org/10.1359/JBMR.050607>.
- (145) Giannopoulou, M.; Dai, C.; Tan, X.; Wen, X.; Michalopoulos, G. K.; Liu, Y. Hepatocyte Growth Factor Exerts Its Anti-Inflammatory Action by Disrupting Nuclear Factor- $\kappa$ B Signaling. *Am. J. Pathol.* **2008**, *173* (1), 30–41. <https://doi.org/10.2353/ajpath.2008.070583>.
- (146) Matsubara, H.; Tsuchiya, H.; Watanabe, K.; Takeuchi, A.; Tomita, K. Percutaneous Nonviral Delivery of Hepatocyte Growth Factor in an Osteotomy Gap Promotes Bone Repair in Rabbits: A Preliminary Study. *Clin. Orthop.* **2008**, *466* (12), 2962–2972. <https://doi.org/10.1007/s11999-008-0493-z>.

- (147) Liu, P.; Guo, L.; Huang, L.; Zhao, D.; Zhen, R.; Hu, X.; Yuan, X. Effect of Semisynthetic Extracellular Matrix-like Hydrogel Containing Hepatocyte Growth Factor on Repair of Femoral Neck Defect in Rabbits. *Int. J. Clin. Exp. Med.* **2015**, *8* (5), 7374–7380.
- (148) Whang, Y. M.; Jung, S. P.; Kim, M.-K.; Chang, I. H.; Park, S. I. Targeting the Hepatocyte Growth Factor and C-Met Signaling Axis in Bone Metastases. *Int. J. Mol. Sci.* **2019**, *20* (2), E384. <https://doi.org/10.3390/ijms20020384>.
- (149) Seibel, M. J. Biochemical Markers of Bone Turnover Part I: Biochemistry and Variability. *Clin. Biochem. Rev. Aust. Assoc. Clin. Biochem.* **2005**, *26* (4), 97–122.
- (150) Frisch, R. N.; Curtis, K. M.; Aenlle, K. K.; Howard, G. A. Hepatocyte Growth Factor and Alternative Splice Variants - Expression, Regulation and Implications in Osteogenesis and Bone Health and Repair. *Expert Opin. Ther. Targets* **2016**, *20* (9), 1087–1098. <https://doi.org/10.1517/14728222.2016.1162293>.
- (151) Miyazawa, K.; Tsubouchi, H.; Naka, D.; Takahashi, K.; Okigaki, M.; Arakaki, N.; Nakayama, H.; Hirono, S.; Sakiyama, O.; Takahashi, K. Molecular Cloning and Sequence Analysis of cDNA for Human Hepatocyte Growth Factor. *Biochem. Biophys. Res. Commun.* **1989**, *163* (2), 967–973. [https://doi.org/10.1016/0006-291x\(89\)92316-4](https://doi.org/10.1016/0006-291x(89)92316-4).
- (152) Uehara, Y.; Minowa, O.; Mori, C.; Shiota, K.; Kuno, J.; Noda, T.; Kitamura, N. Placental Defect and Embryonic Lethality in Mice Lacking Hepatocyte Growth Factor/Scatter Factor. *Nature* **1995**, *373* (6516), 702–705. <https://doi.org/10.1038/373702a0>.
- (153) Huh, C.-G.; Factor, V. M.; Sánchez, A.; Uchida, K.; Conner, E. A.; Thorgeirsson, S. S. Hepatocyte Growth Factor/c-Met Signaling Pathway Is Required for Efficient Liver Regeneration and Repair. *Proc. Natl. Acad. Sci. U. S. A.* **2004**, *101* (13), 4477–4482. <https://doi.org/10.1073/pnas.0306068101>.
- (154) Borowiak, M.; Garratt, A. N.; Wüstefeld, T.; Strehle, M.; Trautwein, C.; Birchmeier, C. Met Provides Essential Signals for Liver Regeneration. *Proc. Natl. Acad. Sci. U. S. A.* **2004**, *101* (29), 10608–10613. <https://doi.org/10.1073/pnas.0403412101>.

- (155) Yamamoto, H.; Yun, E. J.; Gerber, H.-P.; Ferrara, N.; Whitsett, J. A.; Vu, T. H. Epithelial-Vascular Cross Talk Mediated by VEGF-A and HGF Signaling Directs Primary Septae Formation during Distal Lung Morphogenesis. *Dev. Biol.* **2007**, *308* (1), 44–53. <https://doi.org/10.1016/j.ydbio.2007.04.042>.
- (156) Calvi, C.; Podowski, M.; Lopez-Mercado, A.; Metzger, S.; Misono, K.; Malinina, A.; Dikeman, D.; Poonyagariyon, H.; Ynalvez, L.; Derakhshandeh, R.; Le, A.; Merchant, M.; Schwall, R.; Neptune, E. R. Hepatocyte Growth Factor, a Determinant of Airspace Homeostasis in the Murine Lung. *PLoS Genet.* **2013**, *9* (2), e1003228. <https://doi.org/10.1371/journal.pgen.1003228>.
- (157) Ishibe, S.; Karihaloo, A.; Ma, H.; Zhang, J.; Marlier, A.; Mitobe, M.; Togawa, A.; Schmitt, R.; Czyczk, J.; Kashgarian, M.; Geller, D. S.; Thorgeirsson, S. S.; Cantley, L. G. Met and the Epidermal Growth Factor Receptor Act Cooperatively to Regulate Fetal Nephron Number and Maintain Collecting Duct Morphology. *Dev. Camb. Engl.* **2009**, *136* (2), 337–345. <https://doi.org/10.1242/dev.024463>.
- (158) Ma, H.; Saenko, M.; Opuko, A.; Togawa, A.; Soda, K.; Marlier, A.; Moeckel, G. W.; Cantley, L. G.; Ishibe, S. Deletion of the Met Receptor in the Collecting Duct Decreases Renal Repair Following Ureteral Obstruction. *Kidney Int.* **2009**, *76* (8), 868–876. <https://doi.org/10.1038/ki.2009.304>.
- (159) Horton, W. A. Skeletal Development: Insights from Targeting the Mouse Genome. *Lancet Lond. Engl.* **2003**, *362* (9383), 560–569. [https://doi.org/10.1016/S0140-6736\(03\)14119-0](https://doi.org/10.1016/S0140-6736(03)14119-0).
- (160) Kim, H.; Kim, M.; Im, S.-K.; Fang, S. Mouse Cre-LoxP System: General Principles to Determine Tissue-Specific Roles of Target Genes. *Lab. Anim. Res.* **2018**, *34* (4), 147–159. <https://doi.org/10.5625/lar.2018.34.4.147>.
- (161) Elefteriou, F.; Yang, X. Genetic Mouse Models for Bone Studies--Strengths and Limitations. *Bone* **2011**, *49* (6), 1242–1254. <https://doi.org/10.1016/j.bone.2011.08.021>.
- (162) Lu, M. F.; Cheng, H. T.; Lacy, A. R.; Kern, M. J.; Argao, E. A.; Potter, S. S.; Olson, E. N.; Martin, J. F. Paired-Related Homeobox Genes Cooperate in Handplate and



- Hindlimb Zeugopod Morphogenesis. *Dev. Biol.* **1999**, *205* (1), 145–157.  
<https://doi.org/10.1006/dbio.1998.9116>.
- (163) Logan, M.; Martin, J. F.; Nagy, A.; Lobe, C.; Olson, E. N.; Tabin, C. J. Expression of Cre Recombinase in the Developing Mouse Limb Bud Driven by a Prxl Enhancer. *Genes. N. Y. N* **2002**, *33* (2), 77–80. <https://doi.org/10.1002/gene.10092>.
- (164) Saftig, P.; Hunziker, E.; Wehmeyer, O.; Jones, S.; Boyde, A.; Rommerskirch, W.; Moritz, J. D.; Schu, P.; von Figura, K. Impaired Osteoclastic Bone Resorption Leads to Osteopetrosis in Cathepsin-K-Deficient Mice. *Proc. Natl. Acad. Sci. U. S. A.* **1998**, *95* (23), 13453–13458. <https://doi.org/10.1073/pnas.95.23.13453>.
- (165) Drake, F. H.; Dodds, R. A.; James, I. E.; Connor, J. R.; Debouck, C.; Richardson, S.; Lee-Rykaczewski, E.; Coleman, L.; Rieman, D.; Barthlow, R.; Hastings, G.; Gowen, M. Cathepsin K, but Not Cathepsins B, L, or S, Is Abundantly Expressed in Human Osteoclasts. *J. Biol. Chem.* **1996**, *271* (21), 12511–12516.  
<https://doi.org/10.1074/jbc.271.21.12511>.
- (166) Chiu, W. S. M.; McManus, J. F.; Notini, A. J.; Cassady, A. I.; Zajac, J. D.; Davey, R. A. Transgenic Mice That Express Cre Recombinase in Osteoclasts. *Genes. N. Y. N* **2004**, *39* (3), 178–185. <https://doi.org/10.1002/gene.20041>.
- (167) Nakamura, T.; Imai, Y.; Matsumoto, T.; Sato, S.; Takeuchi, K.; Igarashi, K.; Harada, Y.; Azuma, Y.; Krust, A.; Yamamoto, Y.; Nishina, H.; Takeda, S.; Takayanagi, H.; Metzger, D.; Kanno, J.; Takaoka, K.; Martin, T. J.; Chambon, P.; Kato, S. Estrogen Prevents Bone Loss via Estrogen Receptor Alpha and Induction of Fas Ligand in Osteoclasts. *Cell* **2007**, *130* (5), 811–823. <https://doi.org/10.1016/j.cell.2007.07.025>.
- (168) Wang, L.; You, X.; Lotinun, S.; Zhang, L.; Wu, N.; Zou, W. Mechanical Sensing Protein PIEZO1 Regulates Bone Homeostasis via Osteoblast-Osteoclast Crosstalk. *Nat. Commun.* **2020**, *11* (1), 282. <https://doi.org/10.1038/s41467-019-14146-6>.
- (169) Taniguchi, Y.; Kawata, M.; Ho Chang, S.; Mori, D.; Okada, K.; Kobayashi, H.; Sugita, S.; Hosaka, Y.; Inui, H.; Taketomi, S.; Yano, F.; Ikeda, T.; Akiyama, H.; Mills, A. A.;

- Chung, U.-I.; Tanaka, S.; Kawaguchi, H.; Saito, T. Regulation of Chondrocyte Survival in Mouse Articular Cartilage by P63. *Arthritis Rheumatol. Hoboken NJ* **2017**, *69* (3), 598–609. <https://doi.org/10.1002/art.39976>.
- (170) Bruce, S. J.; Butterfield, N. C.; Metzis, V.; Town, L.; McGlenn, E.; Wicking, C. Inactivation of Patched1 in the Mouse Limb Has Novel Inhibitory Effects on the Chondrogenic Program. *J. Biol. Chem.* **2010**, *285* (36), 27967–27981. <https://doi.org/10.1074/jbc.M109.091785>.
- (171) Pfander, D.; Cramer, T.; Weseloh, G.; Pullig, O.; Schuppan, D.; Bauer, M.; Swoboda, B. Hepatocyte Growth Factor in Human Osteoarthritic Cartilage. *Osteoarthritis Cartilage* **1999**, *7* (6), 548–559. <https://doi.org/10.1053/joca.1999.0259>.
- (172) Bau, B.; McKenna, L. A.; Soeder, S.; Fan, Z.; Pecht, A.; Aigner, T. Hepatocyte Growth Factor/Scatter Factor Is Not a Potent Regulator of Anabolic and Catabolic Gene Expression in Adult Human Articular Chondrocytes. *Biochem. Biophys. Res. Commun.* **2004**, *316* (4), 984–990. <https://doi.org/10.1016/j.bbrc.2004.03.001>.
- (173) Fuller, K.; Owens, J.; Chambers, T. J. The Effect of Hepatocyte Growth Factor on the Behaviour of Osteoclasts. *Biochem. Biophys. Res. Commun.* **1995**, *212* (2), 334–340. <https://doi.org/10.1006/bbrc.1995.1974>.
- (174) Factor, V. M.; Seo, D.; Ishikawa, T.; Kaposi-Novak, P.; Marquardt, J. U.; Andersen, J. B.; Conner, E. A.; Thorgeirsson, S. S. Loss of C-Met Disrupts Gene Expression Program Required for G2/M Progression during Liver Regeneration in Mice. *PloS One* **2010**, *5* (9), e12739. <https://doi.org/10.1371/journal.pone.0012739>.
- (175) Roccisana, J.; Reddy, V.; Vasavada, R. C.; Gonzalez-Pertusa, J. A.; Magnuson, M. A.; Garcia-Ocaña, A. Targeted Inactivation of Hepatocyte Growth Factor Receptor C-Met in Beta-Cells Leads to Defective Insulin Secretion and GLUT-2 Downregulation without Alteration of Beta-Cell Mass. *Diabetes* **2005**, *54* (7), 2090–2102. <https://doi.org/10.2337/diabetes.54.7.2090>.
- (176) Arechederra, M.; Carmona, R.; González-Nuñez, M.; Gutiérrez-Uzquiza, A.; Bragado, P.; Cruz-González, I.; Cano, E.; Guerrero, C.; Sánchez, A.; López-Novoa, J. M.;

- Schneider, M. D.; Maina, F.; Muñoz-Chápuli, R.; Porras, A. Met Signaling in Cardiomyocytes Is Required for Normal Cardiac Function in Adult Mice. *Biochim. Biophys. Acta* **2013**, *1832* (12), 2204–2215. <https://doi.org/10.1016/j.bbadis.2013.08.008>.
- (177) Lu, C.; Rollins, M.; Hou, H.; Swartz, H. M.; Hopf, H.; Miclau, T.; Marcucio, R. S. Tibial Fracture Decreases Oxygen Levels at the Site of Injury. *Iowa Orthop. J.* **2008**, *28*, 14–21.
- (178) Zhang, X.; Schwarz, E. M.; Young, D. A.; Puzas, J. E.; Rosier, R. N.; O’Keefe, R. J. Cyclooxygenase-2 Regulates Mesenchymal Cell Differentiation into the Osteoblast Lineage and Is Critically Involved in Bone Repair. *J. Clin. Invest.* **2002**, *109* (11), 1405–1415. <https://doi.org/10.1172/JCI15681>.
- (179) Kivirikko, K. I.; Prockop, D. J. Enzymatic Hydroxylation of Proline and Lysine in Procollagen. *Proc. Natl. Acad. Sci. U. S. A.* **1967**, *57* (3), 782–789. <https://doi.org/10.1073/pnas.57.3.782>.
- (180) Wang, G.; Wang, J.; Sun, D.; Xin, J.; Wang, L.; Huang, D.; Wu, W.; Xian, C. J. Short-Term Hypoxia Accelerates Bone Loss in Ovariectomized Rats by Suppressing Osteoblastogenesis but Enhancing Osteoclastogenesis. *Med. Sci. Monit. Int. Med. J. Exp. Clin. Res.* **2016**, *22*, 2962–2971. <https://doi.org/10.12659/msm.899485>.
- (181) ATP is a potent stimulator of the activation and formation of rodent osteoclasts. - Search Results <https://pubmed.ncbi.nlm.nih.gov/?term=ATP+is+a+potent+stimulator+of+the+activation+and+formation+of+rodent+osteoclasts.&size=200> (accessed 2021 -10 -26).
- (182) Utting, J. C.; Flanagan, A. M.; Brandao-Burch, A.; Orriss, I. R.; Arnett, T. R. Hypoxia Stimulates Osteoclast Formation from Human Peripheral Blood. *Cell Biochem. Funct.* **2010**, *28* (5), 374–380. <https://doi.org/10.1002/cbf.1660>.
- (183) Knowles, H. J. Hypoxic Regulation of Osteoclast Differentiation and Bone Resorption Activity. *Hypoxia Auckl. NZ* **2015**, *3*, 73–82. <https://doi.org/10.2147/HP.S95960>.
- (184) Shirakura, M.; Tanimoto, K.; Eguchi, H.; Miyauchi, M.; Nakamura, H.; Hiyama, K.; Tanimoto, K.; Tanaka, E.; Takata, T.; Tanne, K. Activation of the Hypoxia-Inducible

- Factor-1 in Overloaded Temporomandibular Joint, and Induction of Osteoclastogenesis. *Biochem. Biophys. Res. Commun.* **2010**, *393* (4), 800–805.  
<https://doi.org/10.1016/j.bbrc.2010.02.086>.
- (185) Puccini, A.; Marín-Ramos, N. I.; Bergamo, F.; Schirripa, M.; Lonardi, S.; Lenz, H.-J.; Loupakis, F.; Battaglin, F. Safety and Tolerability of C-MET Inhibitors in Cancer. *Drug Saf.* **2019**, *42* (2), 211–233. <https://doi.org/10.1007/s40264-018-0780-x>.
- (186) Cabanillas, M. E.; de Souza, J. A.; Geyer, S.; Wirth, L. J.; Menefee, M. E.; Liu, S. V.; Shah, K.; Wright, J.; Shah, M. H. Cabozantinib As Salvage Therapy for Patients With Tyrosine Kinase Inhibitor-Refractory Differentiated Thyroid Cancer: Results of a Multicenter Phase II International Thyroid Oncology Group Trial. *J. Clin. Oncol. Off. J. Am. Soc. Clin. Oncol.* **2017**, *35* (29), 3315–3321.  
<https://doi.org/10.1200/JCO.2017.73.0226>.
- (187) Eckerich, C.; Zapf, S.; Fillbrandt, R.; Loges, S.; Westphal, M.; Lamszus, K. Hypoxia Can Induce C-Met Expression in Glioma Cells and Enhance SF/HGF-Induced Cell Migration. *Int. J. Cancer* **2007**, *121* (2), 276–283. <https://doi.org/10.1002/ijc.22679>.
- (188) Hara, S.; Nakashiro, K.-I.; Klosek, S. K.; Ishikawa, T.; Shintani, S.; Hamakawa, H. Hypoxia Enhances C-Met/HGF Receptor Expression and Signaling by Activating HIF-1alpha in Human Salivary Gland Cancer Cells. *Oral Oncol.* **2006**, *42* (6), 593–598.  
<https://doi.org/10.1016/j.oraloncology.2005.10.016>.
- (189) Pennacchietti, S.; Michieli, P.; Galluzzo, M.; Mazzone, M.; Giordano, S.; Comoglio, P. M. Hypoxia Promotes Invasive Growth by Transcriptional Activation of the Met Protooncogene. *Cancer Cell* **2003**, *3* (4), 347–361. [https://doi.org/10.1016/s1535-6108\(03\)00085-0](https://doi.org/10.1016/s1535-6108(03)00085-0).
- (190) Mekki, M. S.; Mougel, A.; Vinchent, A.; Paquet, C.; Copin, M.-C.; Leroy, C.; Kherrouche, Z.; Bonte, J.-P.; Melnyk, O.; Vicogne, J.; Tulasne, D. Hypoxia Leads to Decreased Autophosphorylation of the MET Receptor but Promotes Its Resistance to Tyrosine Kinase Inhibitors. *Oncotarget* **2018**, *9* (43), 27039–27058.  
<https://doi.org/10.18632/oncotarget.25472>.

- (191) Organ, S. L.; Tsao, M.-S. An Overview of the C-MET Signaling Pathway. *Ther. Adv. Med. Oncol.* **2011**, *3* (1\_suppl), S7–S19. <https://doi.org/10.1177/1758834011422556>.
- (192) Zhang, Y.; Xia, M.; Jin, K.; Wang, S.; Wei, H.; Fan, C.; Wu, Y.; Li, X.; Li, X.; Li, G.; Zeng, Z.; Xiong, W. Function of the C-Met Receptor Tyrosine Kinase in Carcinogenesis and Associated Therapeutic Opportunities. *Mol. Cancer* **2018**, *17* (1), 45. <https://doi.org/10.1186/s12943-018-0796-y>.
- (193) Safaie Qamsari, E.; Safaei Ghaderi, S.; Zarei, B.; Dorostkar, R.; Bagheri, S.; Jadidi-Niaragh, F.; Somi, M. H.; Yousefi, M. The C-Met Receptor: Implication for Targeted Therapies in Colorectal Cancer. *Tumour Biol. J. Int. Soc. Oncodevelopmental Biol. Med.* **2017**, *39* (5), 1010428317699118. <https://doi.org/10.1177/1010428317699118>.
- (194) Hughes, P. E.; Rex, K.; Caenepeel, S.; Yang, Y.; Zhang, Y.; Broome, M. A.; Kha, H. T.; Burgess, T. L.; Amore, B.; Kaplan-Lefko, P. J.; Moriguchi, J.; Werner, J.; Damore, M. A.; Baker, D.; Choquette, D. M.; Harmange, J.-C.; Radinsky, R.; Kendall, R.; Dussault, I.; Coxon, A. In Vitro and In Vivo Activity of AMG 337, a Potent and Selective MET Kinase Inhibitor, in MET-Dependent Cancer Models. *Mol. Cancer Ther.* **2016**, *15* (7), 1568–1579. <https://doi.org/10.1158/1535-7163.MCT-15-0871>.
- (195) Kuang, W.; Deng, Q.; Deng, C.; Li, W.; Shu, S.; Zhou, M. Hepatocyte Growth Factor Induces Breast Cancer Cell Invasion via the PI3K/Akt and P38 MAPK Signaling Pathways to up-Regulate the Expression of COX2. *Am. J. Transl. Res.* **2017**, *9* (8), 3816–3826.
- (196) Leung, E.; Xue, A.; Wang, Y.; Rougerie, P.; Sharma, V. P.; Eddy, R.; Cox, D.; Condeelis, J. Blood Vessel Endothelium-Directed Tumor Cell Streaming in Breast Tumors Requires the HGF/C-Met Signaling Pathway. *Oncogene* **2017**, *36* (19), 2680–2692. <https://doi.org/10.1038/onc.2016.421>.
- (197) Parr, C.; Watkins, G.; Mansel, R. E.; Jiang, W. G. The Hepatocyte Growth Factor Regulatory Factors in Human Breast Cancer. *Clin. Cancer Res. Off. J. Am. Assoc. Cancer Res.* **2004**, *10* (1 Pt 1), 202–211. <https://doi.org/10.1158/1078-0432.ccr-0553-3>.
- (198) Tate, A.; Isotani, S.; Bradley, M. J.; Sikes, R. A.; Davis, R.; Chung, L. W. K.; Edlund, M. Met-Independent Hepatocyte Growth Factor-Mediated Regulation of Cell Adhesion

- in Human Prostate Cancer Cells. *BMC Cancer* **2006**, *6*, 197.  
<https://doi.org/10.1186/1471-2407-6-197>.
- (199) Previdi, S.; Maroni, P.; Matteucci, E.; Broggin, M.; Bendinelli, P.; Desiderio, M. A. Interaction between Human-Breast Cancer Metastasis and Bone Microenvironment through Activated Hepatocyte Growth Factor/Met and Beta-Catenin/Wnt Pathways. *Eur. J. Cancer Oxf. Engl. 1990* **2010**, *46* (9), 1679–1691.  
<https://doi.org/10.1016/j.ejca.2010.02.036>.
- (200) Varkaris, A.; Corn, P. G.; Gaur, S.; Dayyani, F.; Logothetis, C. J.; Gallick, G. E. The Role of HGF/c-Met Signaling in Prostate Cancer Progression and c-Met Inhibitors in Clinical Trials. *Expert Opin. Investig. Drugs* **2011**, *20* (12), 1677–1684.  
<https://doi.org/10.1517/13543784.2011.631523>.
- (201) Mills, L. A.; Aitken, S. A.; Simpson, A. H. R. W. The Risk of Non-Union per Fracture: Current Myths and Revised Figures from a Population of over 4 Million Adults. *Acta Orthop.* **2017**, *88* (4), 434–439. <https://doi.org/10.1080/17453674.2017.1321351>.
- (202) He, L.-H.; Liu, M.; He, Y.; Xiao, E.; Zhao, L.; Zhang, T.; Yang, H.-Q.; Zhang, Y. TRPV1 Deletion Impaired Fracture Healing and Inhibited Osteoclast and Osteoblast Differentiation. *Sci. Rep.* **2017**, *7*, 42385. <https://doi.org/10.1038/srep42385>.
- (203) Gentile, M. A.; Soung, D. Y.; Horrell, C.; Samadfam, R.; Drissi, H.; Duong, L. T. Increased Fracture Callus Mineralization and Strength in Cathepsin K Knockout Mice. *Bone* **2014**, *66*, 72–81. <https://doi.org/10.1016/j.bone.2014.04.032>.
- (204) Zhang, M.; Ho, H.; Sheu, T.; Breyer, M. D.; Flick, L. M.; Jonason, J. H.; Awad, H. A.; Schwarz, E. M.; O’Keefe, R. J. EP1(-/-) Mice Have Enhanced Osteoblast Differentiation and Accelerated Fracture Repair. *J. Bone Miner. Res. Off. J. Am. Soc. Bone Miner. Res.* **2011**, *26* (4), 792–802. <https://doi.org/10.1002/jbmr.272>.